



**UNIVERSITY OF INSUBRIA**

Department of Science and High Technology

COMO

Ph.D. Course in Environmental Sciences

# **Variability of ecosystem exposure: integration of dynamic fate models**

*Melissa MORSELLI*

Supervisor: *Prof. Antonio DI GUARDO*

December 2014



**«Le vent se lève!...  
il faut tenter de vivre»**

(Paul Valéry, Le cimetière marin)

***To my Family,  
with Love***



# Table of contents

<b>Chapter 1. Introduction</b>	5
1.1 Models in ecological risk assessment	5
1.2 Limits of current approaches and new challenges	9
1.3 Aims of the work and thesis structure	13
1.4 Summary of results	18
1.5 References	23
Acknowledgements	28
<b>Chapter 2. Paper I</b>	29
Integration of a dynamic organism model into the DynA Model: Development and application to the case of DDT in Lake Maggiore, Italy	
Supporting information	38
<b>Chapter 3. Paper II</b>	60
Evaluating the temporal variability of concentrations of POPs in a glacier-fed stream food chain using a combined modeling approach	
Supporting information	70
<b>Chapter 4. Paper III</b>	95
Theoretically exploring direct and indirect chemical effects across ecological and exposure scenarios using mechanistic fate and effects modelling	
Supporting information	106
<b>Chapter 5. Paper IV</b>	126
Importance of ecological dynamics in predicting chemical exposure in ecological risk assessment	
Supporting information	155

<b>Chapter 6. Paper V</b>	184
Combined effects of intra- and interspecific interactions and pyrene on <i>Daphnia magna</i> populations	
Supporting information	209
<b>Chapter 7. Paper VI</b>	221
Investigating the need for complex vs. simple scenarios to improve predictions of aquatic ecosystem exposure with the SoilPlus model	
Supporting information	231
<b>Chapter 8. Paper VII</b>	243
Modelling the temporal uptake of semi-volatile organic chemicals in plants using an ecologically realistic scenario	
Supporting information	270

# Chapter 1. Introduction

## 1.1 Models in ecological risk assessment

Predicting ecosystem exposure to chemicals represents a complex task in ecotoxicology and ecological risk assessment (ERA). Exposure assessment generally implies the evaluation of the concentration of a specific chemical in the main environmental media (air, soil, water, sediment) and in organisms representing a food source for other organisms (predators) by secondary poisoning (EC, 2003). This results in a *predicted exposure concentration (PEC)* for each environmental compartment, which is compared to a *predicted no-effect concentration (PNEC)*, deriving from effect assessment, to provide a quantitative estimation (*risk quotient, RQ*) of the level of risk posed by the investigated substance to a certain trophic level of the ecosystem (EC, 2003):

$$RQ = PEC / PNEC$$

The calculation of *RQ* is an iterative process, which involves the continuous refinement of such ratio when further information or testing are required and should be carried out until a final conclusion regarding the environmental risks can be reached. Reasonably, the relevance of such estimate relies on the accuracy of *PEC* and *PNEC* estimates.

The estimation of environmental exposure is performed by means of (1) experimental monitoring and/or (2) predictive modelling. Both approaches have advantages and disadvantages and the choice of a particular approach needs to be based on a case by-case-evaluation. Monitoring is crucial, for example, when the contamination levels of known and unknown chemicals in a certain area must be investigated, and when the evolution of such contamination needs to be followed in time. However, monitoring data represent single points in space and time and provide “snapshots” of reality and little opportunity for extrapolation to reconstruct spatial and temporal patterns. Moreover, they

represent an *a posteriori* approach, reflecting a contamination that has already happened and leaving no chances of intervention (EC, 2013). In contrast, models are an *a priori* approach, which allow the investigation of the environmental fate of a chemical before its use or emission and the prediction of concentrations in the different compartments. Moreover, models can also be employed to (1) interpret monitoring data, since they are based on relationships between physical-chemical properties and environmental characteristics with chemical partitioning and distribution in the environment and (2) as a support tool when planning new monitoring campaigns, providing information, for example, on when and where concentrations in a certain compartment are expected to be the highest. On the other hand, models need experimental data for their calibration and validation and the proper predictive approach must be carefully selected for each specific situation, in order to avoid misleading calculations or interpretations (EC, 2013). This implies that, whenever possible, a combination of the two approaches (i.e., monitoring + modelling) would be desirable (EC, 2003; EC, 2013).

Nowadays, multimedia fate models (MFMs) are widely employed to evaluate chemical fate in the environment and therefore ecosystem exposure, since they represent a good compromise between ease of implementation and predictive ability (EC, 2013). Such models generally provide a picture of the behaviour of the investigated chemical in the main environmental compartments (air, water, soil, sediment) starting from data concerning emission, physical-chemical properties and environmental characteristics (Mackay, 2001; Mackay and Mackay, 2007). Among MFMs, the “Mackay-type” multimedia box models (Mackay, 2001) and derived approaches are among the most commonly used (Hollander et al., 2007). In such models, environmental compartments are seen as a number of *boxes*, characterized by a well-mixed internal mass and, therefore, by uniform chemical distribution throughout. Such compartments may be continuous (e.g., water) or consist of a number of particles that are not in contact with each other, although residing in the same phase (e.g., atmospheric particles or biota in water). “Mackay-type” multimedia box models rely on the concept of fugacity, introduced by G. N. Lewis in 1901 as a more convenient thermodynamic

equilibrium criterion than chemical potential and later adopted by Mackay for chemical mass balance calculations (Mackay, 1979; Mackay and Paterson, 1981). After these first, pioneering works, a number of multimedia box models were soon developed and applied to a number of scenarios (Mackay et al., 1983; 1996a; 1996b) and a tiered strategy was also proposed with the main aim of encouraging standardization in the investigation of the fate of substances and in the calculation of PECs (Mackay et al., 1996c); in the tiered-strategy, 3 of the 5 steps involve the use of modelling tools, to first deduce the general features of chemical behaviour in a generic environment and, subsequently, to investigate chemical fate at regional and local scales.

Apart from the spatial scale, models can also be distinguished into *steady-state* approaches, which ignore the temporal variability of chemical emission and environmental characteristics (e.g., compartment temperature, air or water fluxes, biota abundance, etc.), and *unsteady-state* models, developed to investigate exposure concentrations in response to changes in discharge and environmental properties, and therefore capable of providing a picture of exposure variability with time (e.g., on a daily or hourly basis). While steady-state models are better suited to simulate situations in which chemical emission does not significantly vary during the simulation period (e.g., sewage treatment plant discharges), dynamic ones are better suited to handle episodic discharges, such as pulse emissions (e.g., pesticides within the FOCUS groundwater and surface-water models) (FOCUS 2000, 2001) or chemical mass movements caused by environmental phenomena such as runoff after a rainfall event (EC, 2013; Di Guardo and Hermens, 2013). Examples of steady-state models are the evaluative model EQC (Mackay et al., 1996a) and the regional model ChemCAN (Mackay et al., 1996b), while to unsteady-state approaches belong, for example, the SoilFug model (Di Guardo et al., 1994), developed to investigate the fate of pesticides at field scale in agricultural basins, and the DynA Model (Di Guardo et al., 2006), a dynamic surface water-sediment model accounting for time-varying chemical emissions, water and sediment properties; examples of more recent unsteady-state models are SoilPlus (Ghirardello et al., 2010), developed to investigate the fate of organic chemicals in layered air-litter-soil systems, AirFug (Morselli et al., 2011) and

AirPlus (Morselli et al., 2012), 2 air-soil models integrating some aspects of more complex physically-based models to account for the dynamics of the atmospheric compartment.

From a regulatory point of view, the European Union System for the Evaluation of Substances (EUSES; EC, 2004) is currently the reference support tool for the evaluation of the risk posed by industrial chemicals to humans and environment and represents the implementation of the Technical Guidance Document on Risk Assessment in support of Commission Directive 93/67/EEC on Risk Assessment for New Notified Substances (EC, 2003). The comprehensive modelling framework EUSES includes 7 different modules, one of which (“distribution module”) allows the calculation of the concentrations in the relevant environmental compartments (air, surface water, marine water, sediment, soil and groundwater) at the appropriate spatial scale (EC, 2004). Regional-scale fate calculations in EUSES are based on a recent version of the steady-state modelling approach SimpleBox (Den Hollander and Van de Meent, 2004).

## **1.2 Limits of current approaches and new challenges**

The main limitation of the EUSES modelling framework lies in the assumption of steady-state concerning chemical emission and environmental characteristics; more specifically, emission rates are assumed to be constant in time and temporal variations in flow rates, temperatures and partition coefficients are disregarded (EC, 2004). Moreover, simulations are run in generalized local and regional scenarios. All these assumptions imply that EUSES predicts space- and time- averaged concentrations of chemical substances in non-existing hypothetical exposure situations (EC, 2013). If on one hand such assumptions answer the need for systematic treatment of substances in a fair and equitable way, on the other hand they limit the environmental and ecological realism and relevance of exposure predictions (De Laender et al., 2014). For example, emissions are only seldom constant; they usually vary in space, creating a complex exposure pattern, and in time, even at short time scales, allowing less time than required for the establishment of a steady state. Concerning environmental heterogeneity, it must be remarked that EUSES was designed with a number of hard-coded static environmental parameters simulating an ideal region located in the Netherlands and is therefore not suitable to derive specific information on chemical fate for other European regions (e.g., mountainous regions or zones characterized by different climatic conditions). This issue is partially overcome, in regulatory models for pesticide fate in groundwater and surface water (FOCUS 2000, 2001), by the possibility of running simulations with regionally-based scenarios, selecting for example combinations of weather, soil and cropping data representative of different European conditions (EC, 2013).

A recent opinion of three scientific committees of the European Commission (EC, 2013) tried to address the increasing need for realism and relevance of ERA procedures and identified a number of new challenges in both the exposure and the effect fields. Moreover, a recent publication (Di Guardo and Hermens, 2013) listed and extensively discussed all the raised issues in exposure assessment. A summary of the suggested challenges is reported in Table 1.

**Table 1.** Overview of the suggested challenges and growing needs in exposure assessment (modified from Di Guardo and Hermens, 2013)

<p><b>BIOAVAILABILITY AND INTERNAL EXPOSURE</b></p>	<ul style="list-style-type: none"> <li>■ Exposure dynamics in biota: need for more detailed studies on kinetic aspects of the rate limiting steps</li> <li>■ Internal exposure: need for research and new concepts for chemicals other than those which act by narcosis</li> </ul>
<p><b>MONITORING DATA</b></p>	<ul style="list-style-type: none"> <li>■ Need for data for chemical mixtures, metabolites and nanoparticles</li> <li>■ Ecological variability of scenarios: need for spatially- and temporally-resolved data</li> <li>■ Need for harmonization and availability (open-access) of data (and metadata) for evaluation of quality and possible use</li> <li>■ Need for peer-review of physical-chemical properties and environmental half-lives</li> <li>■ Need for improvement of the current environmental scenarios (including mass transfer coefficients, MTCs) to describe realistic ecological conditions (e.g. variability of conditions in time and space)</li> <li>■ Need for temporal and spatial patterns of chemical emissions</li> <li>■ Need for datasets of model evaluation purposes</li> </ul>
<p><b>IMPROVEMENT AND CHALLENGES OF MODELLING APPROACHES</b></p>	<ul style="list-style-type: none"> <li>■ Need for modelling approaches for the prediction of sorption, bioavailability and bioaccumulation of polar and ionized chemicals and nanomaterials</li> <li>■ Need for dynamic and spatially-explicit models, to reconstruct the variability of environmental exposure</li> <li>■ Need for model application to realistic scenarios, to reflect the amplitude of ecological variability of conditions</li> <li>■ Need for specific organism parameters (and their change with time) to unfold the differences among organisms and to extend the applicability of bioaccumulation models in aquatic and terrestrial systems</li> <li>■ Need for dynamic bioaccumulation models, especially accounting for ecological variation in the food web path of chemicals</li> <li>■ Need for integration between exposure and effect models, to account for risk evaluation beyond individual level and move to populations and communities</li> </ul>

With respect to improvements in modelling approaches, there is a strong need to estimate bioavailable concentrations, here defined as the freely-dissolved chemical concentrations (e.g., in water), which therefore determine the amount of chemical available for uptake by organisms. In

aquatic environments, bioavailable concentrations are known to vary in space and time in response to changes in primary producers biomass (algae and/or macrophytes) (Taylor et al., 1991; Berglund et al., 2001; Leistra et al., 2003), particulate organic carbon (POC) and/or dissolved organic carbon (DOC) concentrations in water (Schwarzenbach, 1993), and to the presence of high concentrations of sorbing materials (organic matter or soot) in sediment (Gustafsson et al., 1997). Therefore, predictive fate models should be able to account for such variability and to capture the complexity of exposure related to environmental and ecological heterogeneity; this can be accomplished by developing and using spatially-explicit dynamic (unsteady-state) models including compartments and/or sub-compartments capable of describing environmental phases such as primary producers, POC and DOC.

The complexity and variety of ecosystems implies the need for modelling tools capable of predicting the extent of concentration changes in time and space, to better characterize organism responses which may vary according to their life cycle and contribute to short- and long-term effects on ecosystems (EC, 2013). Temporal changes are related, for example, to chemical emission patterns (e.g., seasonal, pulse, event-driven) and meteorology (temperature, precipitations, wind speed, and direction) (Di Guardo and Hermens, 2013). This variability was shown to be significant especially in mobile phases such as air, where rapid changes in semi-volatile organic contaminant concentrations, mainly related to atmospheric dynamics (e.g., planetary boundary layer height and wind speed), were measured in different environmental contexts (e.g., Gasic et al., 2009). As a consequence, a number of modelling approaches tried to incorporate atmospheric dynamics (e.g., Ma et al., 2003; Hansen et al., 2004; Sehili and Lammel, 2007; Morselli et al., 2011; 2012) and the need for exposure monitoring at shorter time scales and with higher temporal frequency was highlighted. Also spatial changes can be related to both emission variability and environmental heterogeneity (e.g., organic carbon content in soil and sediment, POC/DOC concentrations in water, etc.). Historically, this issue has been partially addressed by means of scale discretization, moving from larger-scale models to site-specific ones. However, this simple acting on model scales could

hide important variations in environmental properties, which could in turn lead to misleading exposure predictions. A possible, more complete, answer could be an increase of detail in horizontal discretization of model domains, therefore moving from large homogeneous regions or sites, with standard or averaged properties, to more spatially explicit models, also with the help of GIS tools (Di Guardo and Hermens, 2013). Moreover, the adoption of a vertical discretization of compartments (i.e., layered air, water, soil, and sediment) could help to better describe chemical movement in them and therefore to capture concentration variability (e.g., Ghirardello et al., 2010). A further challenge is represented by the introduction of more realism in bioaccumulation models, predictive tools designed to evaluate the concentrations that a chemical could reach in an organism (aquatic or terrestrial) starting from its concentrations in the main environmental media (i.e., water, sediment, air, soil) (EC, 2013) and in organisms representing a food source for the investigated organism. For such purposes, fully dynamic models should be developed and adopted, for both aquatic and terrestrial environments (Di Guardo and Hermens, 2013), in order to capture the exposure variability deriving not only from emission dynamics, but also from changes in organism properties (e.g., volume, lipid fraction, feeding rate, etc.) during their life cycle and in environmental and ecological parameters (e.g., temperature, precipitations, biomass of primary producers, etc.). The parameterization of such modelling approaches reasonably require specific information concerning environmental and ecological aspects and realistic, dynamic scenarios, should be built for both calibration and “validation” purposes.

A full integration of exposure modelling approaches improved as described above with proper effect assessment tools would be the final step and allow carrying out *ad hoc* simulations to evaluate and characterize risk in a more thorough and realistic fashion with respect to the currently adopted risk assessment procedures.

### **1.3 Aims of the work and thesis structure**

The present Ph.D. project was conceived with the aim of addressing some of the emerging challenges concerning exposure modelling for ecological risk assessment purposes. More in detail, the main specific objectives of this work were:

1. Developing and applying integrated multimedia fate-bioaccumulation models for predicting exposure variability in different dynamic aquatic environments, in order to investigate the influence of environmental and ecological dynamics on PECs and bioaccumulation in organisms
2. Developing and applying a dynamic, spatially-explicit, model for shallow-water environments, capable of accounting for temporal and spatial variability of emissions and compartment properties and accounting for the role of primary producers (macrophytes and phytoplankton), POC and DOC dynamics in affecting bioavailable concentrations

As an answer to Objective 1, two works were undertaken. In the first one, resulted in a published manuscript (*Paper I*) constituting *Chapter 2* of this thesis, the integration between an existing dynamic MFM for water-sediment systems (DynA Model; Di Guardo et al., 2006) and a new dynamic bioaccumulation model (Single Organism) was presented. This integrated modelling approach (EcoDynA) was developed with the aim of investigating temporal variability in bioaccumulation resulting not only from emission or environmental changes, but also from organism properties dynamics (e.g., volume, lipid fraction, feeding rate, lipid fraction in food, etc.). The application of EcoDynA to a case study concerning p,p'-DDT bioaccumulation by Lake Maggiore whitefish and the comparison between predicted and measured concentrations in fish allowed appreciating the added value of simulating organism dynamics with respect to adopt single,

static values for the different properties and the consequent improved model performance. In the second work (*Paper II, Chapter 3*), the EcoDynA model was applied to a scenario characterized by a high temporal variability of environmental properties (the glacier-fed stream Frodolfo, Italian Alps) to investigate the influence of such changes on bioaccumulation of some persistent organic pollutants (PCB 70, PCB 101 and p,p'-DDE) by macroinvertebrate individuals representative of 3 trophic levels (collectors, scrapers and predators). The first step of this work consisted in the calculation of bioavailable concentration profiles of the investigated chemicals on an hourly basis. For this purpose, a hydrological module for EcoDynA was first developed; such module, based on a simple temperature-index model, allowed the estimation of the hourly water contributions deriving from ice and snow melt to the Frodolfo stream discharge, and therefore to predict hourly discharge values for the whole simulation year. Afterwards, basing on previously measured chemical concentrations in ice and snow, chemical loadings and concentrations in stream water were calculated. The second step implied the application of the EcoDynA model to estimate bioaccumulation in the investigated organisms, and comparisons between model predictions and experimental observations were performed. Results indicated a satisfying model performance, but a strong need from an accurate model parameterization, especially concerning organism properties and their changes with time. Moreover, such modelling approach appeared as a valuable tool for investigating the occurrence and magnitude of peak exposure events, as well as the amplitude of exposure variations in response to environmental heterogeneity (e.g., day/night cycles in discharge, especially in the glacier ablation period).

*Chapter 4* and *5* include works developed within the context of the recently approved European Chemical Industry Council-Long-range Research Initiative (CEFIC-LRI) 3-year project “ChimERA: An integrated modelling tool for ecological risk assessment”. Such project has the main aim of developing an integrated exposure and effect ecosystem model (ChimERA) which could be used as a support tool for performing ERA in aquatic environments.

In *Paper III (Chapter 4)*, simulations performed by a fugacity-based fate model and a differential equation-based ecosystem model were presented, with the aim of theoretically exploring how direct and indirect effects on invertebrate shallow pond communities can vary in response to changes in exposure and ecological scenarios (here defined as the variables potentially influencing chemical fate and exposure, and the ones determining effects at the ecosystem level, respectively). For this purpose, the EcoDyna model was modified by adding a new water sub-compartment representing DOC and by neglecting the organism compartment, while phytoplankton was assumed to contribute to POC. Results showed that the combination of a dynamic fate model and a food-web/food-chain model allows evaluating chemical availability together with the resulting population-level effects in an ecosystem context.

*Paper IV (Chapter 5)* addressed the development and application of the dynamic, spatially-explicit ChimERA fate and exposure sub-model, including not only POC/DOC dynamics, but also the ones of rooted macrophytes, which have been proven to be highly effective in influencing chemical bioavailability in shallow-water environments. In the manuscript, the implementation of the macrophyte compartment was described and the results of a local sensitivity analysis and the comparison between model predictions and observations for 4 case studies were presented. Moreover, the model was also applied to an illustrative spatially-explicit scenario, in order to show its capability in predicting both temporal and spatial exposure variations. The implementation of the phytoplankton compartment and model application to scenarios representative of different European conditions is the object of an ongoing work (Di Guardo et al., *in preparation*), which was not included in the thesis since further efforts are required.

Last, *Chapter 6 to 8* collect manuscripts for which only minor work from this Ph.D. project was required. More in detail, *Paper V (Chapter 6)*, concerning experiments to assess the contribution of intraspecific (competition) and interspecific interactions (competition and predation) to chemical effects on *Daphnia magna* populations, involved the use of the same fate model described in *Chapter 4*, properly parameterized, to assess the fate of the tested chemical (pyrene) in the

experimental vessels and to verify the potential influence of the algae used as a food source for *D. magna* individuals on bioavailable concentrations. For *Paper VI (Chapter 7)*, presenting the development and application of a spatially-explicit version of the SoilPlus model (Ghirardello et al., 2010) help was provided with manuscript writing and revision. Finally, in *Paper VII (Chapter 8)*, introducing a new modelling approach for the prediction of organic chemicals uptake by terrestrial vegetation, most of the work concerned model coding (using Microsoft Visual Basic 6.0) of transport processes and numerical solution and sensitivity analysis.

In summary, the present Ph.D. thesis was grounded on the following manuscripts:

### **Main works**

***Paper I.*** Infantino, A.; Morselli, M.; Di Guardo, A. Integration of a dynamic organism model into the DynA Model: Development and application to the case of DDT in Lake Maggiore, Italy. *Sci. Total Environ.* **2013**, *454–455*, 358–365.

***Paper II.*** Morselli, M.; Semplice, M.; Villa, S.; Di Guardo, A. Evaluating the temporal variability of concentrations of POPs in a glacier-fed stream food chain using a combined modeling approach. *Sci. Total Environ.* **2014**, *493*, 571–579.

***Paper III.*** De Laender, F.; Morselli, M.; Baveco, H.; Van den Brink, P.J.; Di Guardo, A. Theoretically exploring direct and indirect chemical effects across ecological and exposure scenarios using mechanistic fate and effects modelling. *Environ. Int.* **2015**, *74*, 181–190.

***Paper IV.*** Morselli, M.; Semplice, M.; De Laender, F.; Van den Brink, P.J.; Di Guardo, A. Importance of ecological dynamics in predicting chemical exposure in ecological risk assessment. *Submitted to Environ. Sci. Technol.*

## **Further works**

**Paper V.** Viaene, K.P.J.; De Laender, F.; Rico, A.; Van den Brink, P.J.; Di Guardo, A.; Morselli, M.; Janssen, C.R. Combined effects of intra- and interspecific interactions and pyrene on *Daphnia magna* populations. *Submitted to Environ. Toxicol. Chem.*

**Paper VI.** Ghirardello, D.; Morselli, M.; Otto, S.; Zanin, G.; Di Guardo, A. Investigating the need for complex vs. simple scenarios to improve predictions of aquatic ecosystem exposure with the SoilPlus model. *Environ. Pollut.* **2014**, *184*, 502–510.

**Paper VII.** Terzaghi, E.; Morselli, M.; Semplice, M.; Cerabolini, B.; Jones, K.C.; Di Guardo, A. Modelling the temporal uptake of semi-volatile organic chemicals in plants using an ecologically realistic scenario. *Draft to be submitted to Environ. Sci. Technol.*

## **1.4 Summary of results**

### **Paper I**

The Single Organism (SO) model was developed to investigate the influence of temporal dynamics of aquatic organism properties on their exposure to organic chemicals in water. SO was then integrated with an existing dynamic surface-water model (DynA), to form the coupled water-bioaccumulation model EcoDynA. In order to evaluate the model performance, the results produced by EcoDynA were compared to the p,p'-DDT concentrations measured in specimens of whitefish of different age and sex caught in Lake Maggiore after the discovery of a DDT spill. The comparison showed a good agreement. Other satisfying results were obtained comparing model results with p,p'-DDT concentration values measured in another species of whitefish which were available in the literature. A preliminary sensitivity analysis confirmed that accounting for dynamics of parameters such as organism lipid fraction and feeding rate is necessary to obtain accurate exposure predictions.

### **Paper II**

Falling snow acts as an efficient scavenger of contaminants from the atmosphere and, accumulating on the ground surface, behaves as a temporary storage reservoir; during snow aging and metamorphosis, contaminants may concentrate and be subject to pulsed release during intense snow melt events. In high-mountain areas, firn and ice play a similar role. The consequent concentration peaks in surface waters can pose a risk to high-altitude ecosystems, since snow and ice melt often coincide with periods of intense biological activity. In such situations, the role of dynamic models can be crucial when assessing environmental behavior of contaminants and their accumulation patterns in aquatic organisms. In the present work, a dynamic fate modeling approach was combined to a hydrological module capable of estimating water discharge and snow/ice melt contributions on an hourly basis, starting from hourly air temperatures. The model was applied to

the case study of the Frodolfo glacier-fed stream (Italian Alps), for which concentrations of a number of persistent organic pollutants (POPs), such as polychlorinated biphenyl (PCBs) and p,p'-dichlorodiphenyldichloroethylene (p,p'-DDE) in stream water and four macroinvertebrate groups were available. Considering the uncertainties in input data, results showed a satisfying agreement for both water and organism concentrations. This study showed the model adequacy for the estimation of pollutant concentrations in surface waters and bioaccumulation in aquatic organisms, as well as its possible role in assessing the consequences of climate change on the cycle of POPs.

### **Paper III**

Predicting ecosystem response to chemicals is a complex problem in ecotoxicology and a challenge for risk assessors. The variables potentially influencing chemical fate and exposure define the exposure scenario while the variables determining effects at the ecosystem level define the ecological scenario. In absence of any empirical data, the objective of this paper is to present simulations by a fugacity-based fate model and a differential equation-based ecosystem model to theoretically explore how direct and indirect effects on invertebrate shallow pond communities vary with changing ecological and exposure scenarios. These simulations suggest that direct and indirect effects are larger in mesotrophic systems than in oligotrophic systems. In both trophic states, interaction strength (quantified using grazing rates) was suggested a more important driver for the size and recovery from direct and indirect effects than immigration rate. In general, weak interactions led to smaller direct and indirect effects. For chemicals targeting mesozooplankton only, indirect effects were common in (simple) food-chains but rare in (complex) food-webs. For chemicals directly affecting microzooplankton, the dominant zooplankton group in the modelled community, indirect effects occurred both in food-chains and food-webs. We conclude that the choice of the ecological and exposure scenarios in ecotoxicological modelling efforts needs to be justified because of its influence on the prevalence and magnitude of the predicted effects. Overall, more work needs to be done to empirically test the theoretical expectations formulated here.

## **Paper IV**

In currently used approaches for ecological risk assessment (ERA), exposure is generally modelled assuming steady-state in emissions and environmental properties and neglecting the potential role of ecological dynamics in affecting bioavailable concentrations. In order to investigate the potential influence of ecological scenario and emission dynamics on predicted exposure levels, the spatially-resolved dynamic model "ChimERA fate" was developed, incorporating macrophyte biomass and particulate/dissolved organic carbon dynamics into a water-sediment system. A comparison between model output and experimental observations for four case studies allowed verifying the implementation of the macrophyte compartment and assessing model performance, which was generally satisfying. Illustrative runs showed the potential spatio-temporal variability of bioavailable concentrations of two chemicals after a pulsed emission in a system composed of a pond and its inflow/outflow streams: biomass dynamics caused variations in concentrations of a factor of 2-3 during the simulation period, and of orders of magnitude in space (along the stream-pond system). Given the increased level of ecological realism, ChimERA fate could represent a vital tool for the identification of those environmental and ecological conditions where risk is expected to be highest (e.g., emissions associated with low biomass/POC/DOC levels).

## **Paper V**

Species interactions are often suggested as an important factor when assessing the effects of chemicals on higher levels of biological organisation. Nevertheless, the contribution of intraspecific (competition) and interspecific interactions (competition and predation) to chemical effects on populations is often overlooked. In the current study, *Daphnia magna* populations were initiated with different levels of intra- and interspecific competition and predation and exposed to two pyrene pulses. Generalized linear models were used to test which of these factors significantly explained population size and structure at different time points. Pyrene had a negative effect on total population densities, with effects being more pronounced on smaller *D. magna* individuals. Among

all species interactions tested, predation had the largest negative effect on population densities. Predation and high initial intraspecific competition were shown to interact antagonistically with pyrene exposure. This was attributed to differences in population structure prior to pyrene exposure and pyrene-induced reduced feeding by *Chaoborus* sp. larvae. The current study provides empirical evidence that species interactions within and between populations can alter the response of aquatic populations to chemical exposure, suggesting complex interactions between the underlying mechanisms.

## **Paper VI**

A spatially-explicit version of the recent multimedia fate model SoilPlus was developed and applied to predict the runoff of three pesticides in a small agricultural watershed in north-eastern Italy. In order to evaluate model response to increasing spatial resolution, a tiered simulation approach was adopted, also using a dynamic model for surface water (DynA model), to predict the fate of pesticides in runoff water and sediment, and concentrations in river water. Simulation outputs were compared to water concentrations measured in the basin. Results showed that a high spatial resolution and scenario complexity improved model predictions of metolachlor and terbuthylazine in runoff to an acceptable performance ( $R^2 = 0.64-0.70$ ). The importance was also shown of a field-based database of properties (i.e. soil texture and organic carbon, rainfall and water flow, pesticides half-life in soil) in reducing the distance between predicted and measured surface water concentrations and its relevance for risk assessment.

## **Paper VII**

A new dynamic vegetation model was developed to simulate the fate of organic compounds in the air/plant/litter/soil system. Key features of the model are the double-layered air compartment (planet boundary layer, PBL and residual layer) interacting dynamically with vegetation and multilayered litter/soil compartments. Vegetation can represent both monospecific and multispecific

forest. Leaf biomass is dynamically calculated employing two important ecological parameters (LAI and SLA), while stem and root biomass are assumed constant over time. The model was used to investigate the air compartment structure and meteorological variability in influencing PAH air-leaf exchanges, simulating a broadleaf wood located in Northern Italy (Como). Modelled leaf concentrations showed a satisfying agreement with measured one. Leaves appeared to act as a “filter” but also as a “dispenser” of air contaminants in response to meteorological parameters and emission changes. A preliminary sensitivity analysis showed that air concentrations are most affected by emission, PBL height and wind speed, while for leaf concentrations  $K_{OW}$ , air temperature and SLA are also important. Illustrative simulations were then performed for PCB 52 and PCB 153 to show the influence of leaves biomass on air concentrations in realistic forest conditions in terms of air residence time, wind speed and domain size.

## 1.5 References

Berglund, O.; Larsson, P.; Ewald, G.; Okla, L. Influence of trophic status on PCB distribution in lake sediment and biota. *Environ. Pollut.* **2001**, *82* (4), 199–210.

De Laender, F., van den Brink P. J., Janssen C.R., Di Guardo, A. The ChimERA project: coupling mechanistic exposure and effect models into an integrated platform for ecological risk assessment. *Environ. Sci. Pollut. Res.* **2014**, *21*, 6263–6267.

Den Hollander, H. A.; van de Meent, D. *Model parameters and equations used in Simplebox 3.0*. Report No. 601200 003. National Institute of Public Health and the Environment (RIVM): Bilthoven, the Netherlands, 2004.

Di Guardo, A.; Calamari, D.; Zanin, G.; Consalter, A.; Mackay, D. A fugacity model of pesticide runoff to surface water: development and validation. *Chemosphere* **1994**, *28* (3), 511–531.

Di Guardo, A.; Ferrari, C.; Infantino, A. Development of a Dynamic Aquatic Model (DynA Model): Estimating temporal emissions of DDT to Lake Maggiore (N. Italy). *Environ. Sci. Pollut. R.* **2006**, *13* (1), 50–58.

Di Guardo, A.; Hermens, J. L. M. Challenges for exposure prediction in ecological risk assessment. *Integr. Environ. Assess. Manag.* **2013**, *9* (3), e4–e14.

EC (European Commission), 2003. *Technical guidance document on risk assessment*; 2nd ed; EUR 20418 EN/2; European Chemical Bureau, Joint Research Centre: Ispra, Italy, 2003; [http://echa.europa.eu/documents/10162/16960216/tgdpart2\\_2ed\\_en.pdf](http://echa.europa.eu/documents/10162/16960216/tgdpart2_2ed_en.pdf).

EC (European Commission), 2004. *European Union System for the Evaluation of Substances 2.0 (EUSES 2.0)*. Background report 601900005/2004. National Institute of Public Health and the Environment (RIVM): Bilthoven, the Netherlands, 2004;  
<http://www.pbl.nl/sites/default/files/cms/publicaties/601900005.pdf>.

EC (European Commission), 2013. *Addressing the new challenges for risk assessment*. Opinion adopted in March 2013. SCHER (Scientific Committee on Health and Environmental Risks), SCENIHR (Scientific Committee on Emerging and Newly Identified Health Risks), SCCS (Scientific Committee on Consumer Safety);  
[http://ec.europa.eu/health/scientific\\_committees/consumer\\_safety/docs/sccs\\_o\\_131.pdf](http://ec.europa.eu/health/scientific_committees/consumer_safety/docs/sccs_o_131.pdf).

FOCUS, 2000. *FOCUS groundwater scenarios in the EU review of active substances*. Report of the FOCUS Groundwater Scenarios Workgroup, EC Document Reference Sanco/321/2000 rev.2, 202pp.

FOCUS, 2001. *FOCUS surface water scenarios in the EU evaluation process under 91/414/EEC*. Report of the FOCUS Working Group on Surface Water Scenarios, EC Document Reference SANCO/4802/2001-rev.2. 245 pp.

Gasic, B.; Moeckel, C.; MacLeod, M.; Brunner, J.; Scheringer, M.; Jones, K. C.; Hungerbühler, K. Measuring and modeling short-term variability of PCBs in air and characterization of urban source strength in Zurich, Switzerland. *Environ. Sci. Technol.* **2009**, *43*, 769–776.

Ghirardello, D.; Morselli, M.; Semplice, M.; Di Guardo, A. A dynamic model of the fate of organic chemicals in a multilayered air/soil system: Development and illustrative application. *Environ. Sci. Technol.* **2010**, *44*, 9010–9017.

Gustafsson, O.; Haghseta, F.; Chan, C.; MacFarlane, J.; Gschwend, P.M. Quantification of the dilute sedimentary soot phase: Implications for PAH speciation and bioavailability. *Environ. Sci. Technol.* **1997**, *31*, 203–209.

Hansen, K. M.; Christensen, J. H.; Brandt, J.; Frohn, L. M.; Geels, C. Modeling atmospheric transport of  $\alpha$ -hexachlorocyclohexane in the Northern Hemisphere with a 3-D dynamical model: DEHM-POP. *Atmos. Chem. Phys.* **2004**, *4*, 1125–1137.

Hollander, A.; Sauter, F.; den Hollander, H.; Huijbregts, M.; Ragas, A.; van de Meent, D. Spatial variance in multimedia mass balance models: Comparison of LOTOS-EUROS and SimpleBox for PCB-153. *Chemosphere* **2007**, *68*, 1318–1326.

Leistra, M.; Zweers, A. J.; Warinton, J. S.; Crum, S. J. H.; Hand, L. H.; Beltman, W. H. J.; Maund, S. J. Fate of the insecticide lambda-cyhalothrin in ditch enclosures differing in vegetation density. *Pest. Manag. Sci.* **2003**, *60*, 75–84.

Ma, J.; Daggupaty, S.; Harner, T.; Li, Y. Impacts of lindane usage in the Canadian prairies on the Great Lakes ecosystem. 1. Coupled atmospheric transport model and modeled concentrations in air and soil. *Environ. Sci. Technol.* **2003**, *37*, 3774–3781.

Mackay, D. Finding fugacity feasible. *Environ. Sci. Technol.* **1979**, *13*, 1218–1223.

Mackay, D.; Paterson, S. Calculating fugacity. *Environ. Sci. Technol.* **1981**, *5*, 1006–1014.

Mackay, D.; Joy, M.; Paterson, S. A Quantitative Water, Air, Sediment Interaction (QWASI) fugacity model for describing the fate of chemicals in lakes. *Chemosphere* **1983**, *12*, 981–997.

Mackay, D.; Di Guardo, A.; Paterson, S.; Cowan, C. E. Evaluating the environmental fate of a variety of types of chemicals using the EQC Model. *Environ. Toxicol. Chem.* **1996a**, *15*, 1627–1637.

Mackay, D.; Di Guardo, A.; Paterson, S.; Kicsi, G.; Cowan, C. E.; Kane, D. M. Assessment of chemical fate in the environment using evaluative, regional and local-scale models: Illustrative application to chlorobenzene and linear alkylbenzene sulfonates. *Environ. Toxicol. Chem.* **1996b**, *15*, 1638–1648.

Mackay, D.; Di Guardo, A.; Paterson, S.; Kicsi, G.; Cowan, C. E. Assessing the fate of new and existing chemicals: a five stage process. *Environ. Toxicol. Chem.* **1996c**, *15*, 1618–1626.

Mackay, D. *Multimedia environmental models: the fugacity approach*. 2nd ed. Lewis Publishers: Boca Raton, 2001.

Mackay, D.; Mackay, N. Mathematical models of chemical transport and fate. In *Ecological risk assessment*; Suter, G. W. II, Ed. CRC Press: Boca Raton, 2007.

Morselli, M.; Ghirardello, D.; Semplice, M.; Di Guardo, A. Modeling short-term variability of semivolatile organic chemicals in air at a local scale: An integrated modeling approach. *Environ. Pollut.* **2011**, *159*, 1406–1412.

Morselli, M.; Ghirardello, D.; Semplice, M.; Raspa, G.; Di Guardo, A. Integration of an atmospheric dispersion model with a dynamic multimedia fate model: Development and illustration. *Environ. Pollut.* **2012**, *164*, 182–187.

Schwarzenbach, R. P.; Gschwend, P. M.; Imboden, D. M. *Environmental Organic Chemistry*; Wiley: New York, 1993.

Sehili, A. M.; Lammel, G. Global fate and distribution of polycyclic aromatic hydrocarbons emitted from Europe and Russia. *Atmos. Environ.* **2007**, *41*, 8301–8315.

Taylor, W. B.; Carey, J.H.; Lean, D. R. S.; McQueen, D. I. Organochlorine concentrations in the plankton of lakes in southern Ontario and their relationship to plankton biomass. *Can. J. Fish. Aquat. Sci.* **1991**, *48*, 1960–1966.

## ***Acknowledgements (Ringraziamenti)***

Il primo, sentito ringraziamento lo rivolgo al prof. Antonio Di Guardo, per avermi offerto questa grande opportunità di crescita, sia scientifica che personale. In questi anni ho potuto approfondire le tematiche che avevo iniziato a conoscere durante la tesi specialistica e ho avuto la possibilità di esplorarne di nuove, misurandomi con sfide ed imprevisti che tanto mi hanno spaventata quanto entusiasmata. Ho avuto l'opportunità di collaborare con diversi gruppi di ricerca, italiani e di altri paesi europei, di presentare i miei lavori a congressi internazionali e di conoscere realtà universitarie estere. Tutto questo è entrato a far parte di un bagaglio il cui valore reputo inestimabile. Grazie!

Un doveroso ringraziamento va ai miei colleghi di lavoro e ricerca: ad Elisa, compagna di avventure, disavventure e scrivania, a Matteo, per il suo supporto scientifico e morale, al sempre presente Davide: carissimo, tanto continuo ad imparare dagli anni trascorsi spalla a spalla...

Grazie alle mie amiche lontane ma vicine, Annalisa, Aurora e Samanta, che sempre si preoccupano per la mia incolumità... :-)

Il mio più grande e profondo ringraziamento va alla mia Famiglia: grazie mamma e papà, per il vostro supporto fisico, economico e morale e perché credete in me ogni volta che intraprendo un nuovo viaggio. A Elisa, mia sorella: ovunque tu sia, ti sento sempre vicina e partecipe di ogni mia azione e decisione.

Fabio, so che non ami i ringraziamenti. Ma io non posso non esserti grata... Ci siamo conosciuti all'inizio di questa mia esperienza di dottorato e abbiamo vissuto gli ultimi tre anni avvicinandoci sempre più. Mi sei stato accanto sempre, in ogni modo. Nella quotidianità, anche in occasione di workshop e congressi: hai capito quanto fosse importante per me senza che fossi io a chiedertelo. Mi hai fatto capire che ogni cosa bella, se condivisa con la persona giusta, lo è ancora di più. Ora, oltre alla tua presenza, mi stai donando anche la gioia di una nuova vita, che cresce in me giorno dopo giorno: se vuoi non ti ringrazio, ma permettimi di ringraziare la vita, il caso, qualsiasi cosa abbia fatto sì che quel giorno di settembre le nostre strade si incrociassero...

## **Chapter 2. Paper I**

# **Integration of a dynamic organism model into the DynA Model: Development and application to the case of DDT in Lake Maggiore, Italy**

Alfonso Infantino<sup>1</sup>, Melissa Morselli<sup>1</sup> and Antonio di Guardo<sup>1\*</sup>

<sup>1</sup>Department of Science and High Technology, University of Insubria, Via Valleggio, 11, 22100  
Como CO, Italy

\*Corresponding author

*Science of the Total Environment* **2013**, 454-455, 358–365





## Integration of a dynamic organism model into the DynA Model: Development and application to the case of DDT in Lake Maggiore, Italy

Alfonso Infantino, Melissa Morselli, Antonio Di Guardo \*

Department of Science and High Technology, University of Insubria, Via Valleggio, 11, 22100 Como CO, Italy

### HIGHLIGHTS

- An integrated single organism–water–sediment dynamic model was developed.
- The model was applied to investigate p,p'-DDT bioaccumulation in whitefish.
- Comparisons with measured data revealed good model performance.
- Results highlighted the importance of ecological parameter dynamics.

### ARTICLE INFO

#### Article history:

Received 18 January 2013

Received in revised form 8 March 2013

Accepted 8 March 2013

Available online 3 April 2013

#### Keywords:

Dynamic bioaccumulation model

Coregonid

Lake Maggiore

Fugacity

DDT

### ABSTRACT

The Single Organism (SO) model was developed to investigate the influence of temporal dynamics of aquatic organism properties on their exposure to organic chemicals in water. SO was then integrated with an existing dynamic surface-water model (DynA), to form the coupled water-bioaccumulation model EcoDynA. In order to evaluate the model performance, the results produced by EcoDynA were compared to the p,p'-DDT concentrations measured in specimens of whitefish of different age and sex caught in Lake Maggiore after the discovery of a DDT spill. The comparison showed a good agreement. Other satisfying results were obtained comparing model results with p,p'-DDT concentration values measured in another species of whitefish which were available in the literature. A preliminary sensitivity analysis confirmed that accounting for dynamics of parameters such as organism lipid fraction and feeding rate is necessary to obtain accurate exposure predictions.

© 2013 Elsevier B.V. All rights reserved.

### 1. Introduction

The evaluation of the impact of pollutants in aquatic ecosystems is a formidable challenge that needs the improvement of modelling tools to understand distribution, bioavailability, and biological effects of single chemicals and mixtures. Traditionally, static models assuming constant transport rates among media were developed to investigate the fate of chemicals characterized by high persistence in the environment and the presence of long-term effects (Mackay, 2001). However, the classic steady-state approach is not suitable for modelling the exposure to less persistent chemicals (such as pesticides) or to persistent chemicals deriving from spills or characterized by fluctuating concentrations depending on seasonal variability of environmental parameters. This variability in exposure concentrations results in effects which are difficult to evaluate according to the standard ecotoxicological paradigm, which compares a predicted environmental concentration (PEC) with a predicted no-effect concentration (PNEC), both obtained or derived from a steady exposure. Reinert et al. (2002) and later

Ashauer et al. (2006) reviewed approaches and models that may be used to predict effects on aquatic organisms resulting from time-varying exposure to pesticides. However, there is a need for dynamic fate models capable of predicting concentrations and mass distributions resulting from a chemical emission into a realistic and changing environment. An example of a dynamic fate model for aquatic systems is the Dynamic Aquatic Model (DynA Model) (Di Guardo et al., 2006; Infantino et al., 2008), a surface water model in which not only the chemical emission, but also the properties of environmental compartments (volumes, capacities, etc.) can vary with time. In the past years, some dynamic bioaccumulation models accounting for a certain dynamics of organism life cycles were developed for several organisms (van Beusekom et al., 2006; Patwa et al., 2007). For example, in the model by Patwa et al. (2007), volume and lipid variation were introduced as well as spatially different feeding habitats. More recently, the importance of lipid dynamics in determining bioaccumulation patterns (De Laender et al., 2010a) and the sensitivity of dynamic bioaccumulation model predictions to ecological parameters (Gobas and Arnot, 2010; Nfon et al., 2011) were shown. It is now well recognized that a more accurate definition of ecological data, such as food web structure and ecosystem functions, contributes to a reduction of predicted

\* Corresponding author. Tel.: +39 031 2386480; fax: +39 031 2386449.  
E-mail address: [antonio.diguardo@uninsubria.it](mailto:antonio.diguardo@uninsubria.it) (A. Di Guardo).

concentration uncertainty (De Laender et al., 2009, 2010b). Therefore, one of the new challenges of dynamic models lies in the implementation of time-varying ecological parameters (e.g., life style, egestion rate, feeding rate, assimilation rate, and specific diet matrix for each life stage) for the estimation of bioaccumulation in aquatic organisms (Borgà et al., 2004; De Laender et al., 2009).

The contamination by DDTs in Lake Maggiore (Italy) offered the possibility to study the dynamic behavior of such contaminants in a large lake. Lake Maggiore is the second largest and deepest lake in Italy. During routine monitoring of contamination in fish from Lake Maggiore in 1995, DDT was found at levels well exceeding the average contamination measured in the previous years (Ceschi et al., 1996). Therefore, in 1998, an international project was started to monitor concentrations in a number of media such as water, sediment, fish, precipitation, etc. (CIPAI, 1999, 2002, 2003, 2004, 2005). The source of the contamination was identified in a chemical plant which discharged DDTs in the Toce River, a tributary of the lake (Di Guardo et al., 2006). On this topic, a number of publications appeared in the past years (e.g., Di Guardo et al., 2006; Bettinetti et al., 2006, 2010, 2012; Volta et al., 2009) which indicate that Lake Maggiore, unlike most European lakes, is probably far from the steady state for DDTs; although DDT synthesis ended in 1996, a possible additional loading coming from the Toce River watershed or due to sediment resuspension during floods may still influence chemical concentrations in the lake (Di Guardo et al., 2006; Bettinetti et al., 2012).

In the present work, a new bioaccumulation model (Single Organism) accounting for the dynamics of ecological parameters was developed and integrated with the surface water–sediment model DynA (Di Guardo et al., 2006) to form the water-bioaccumulation model EcoDynA. The results produced by EcoDynA were first compared to p,p'-DDT concentrations measured in whitefish sampled in 1997/1998, and then compared to measured values available in the literature for specimens of another species of whitefish sampled in 2003 (Volta et al., 2009).

## 2. Materials and Methods

### 2.1. Sample Collection and Analysis

Samples of whitefish (pollan) (*Coregonus* sp., hybrid form deriving from *C. wartmanni coeruleus* Fatio, 1890 and *C. schinzi helveticus* Fatio, 1890, common Italian name "lavarello") were caught in Lake Maggiore (Fig. S1) using different types of nets (in order to obtain fishes of different sizes) in December 1997 and January 1998. Fish samples were frozen and kept at  $-30^{\circ}\text{C}$  until analyses for DDT compounds. Analyses were performed on 24 individuals (10 males and 14 females, aged 2 to 6 years); the analyzed tissues were portions of fish fillet, obtained according EPA method 823-R-95-007 (US EPA, 1995). Samples were freeze dried and extracted in hexane/acetone (9:1) with a Soxtec apparatus (VELP Scientifica) for 6 h. A portion of the extracted fraction was used for the determination of extractable lipids. Extracts were then digested with sulphuric acid (on Extrelut columns, Merck) for 4 h, in order to remove the lipid fraction. Samples were then eluted and purified on silica gel chromatography. The elution solvent was a mixture of hexane and toluene (65:35). The eluted fraction was concentrated in a rotary evaporator and then evaporated with a gentle flux of nitrogen. Internal standards ( $^{13}\text{C}_{12}$  p,p'-DDT and  $^{13}\text{C}_{12}$  p,p'-DDE, CIL, Boston, MA, USA) were added at extraction time to monitor recovery and quantify the chemicals. The analysis was performed using GC-MS (HP 6890-5972a) (electron impact ionization, selected ion monitoring mode). The column was a 50-m long SGE BP10 (0.22-mm internal diameter, 25-mm phase thickness).

### 2.2. Quality Assurance/Quality Control (QA/QC)

Recoveries were checked at the method development stage and were of  $88 \pm 10\%$ . The extraction efficiency was  $>95\%$  and it was

measured using the labelled standards spiked to the dry samples. During routine analysis the labelled internal standards were added to the samples just after extraction, and therefore no additional recovery correction was performed on results. The method detection limit was set to  $0.5 \text{ ng g}^{-1}$  for all compounds and corresponded to the lower concentration of the calibration curve when an average extracted weight of 2 g (d.w.) was assumed. Procedural blanks were included every five samples. The analyzed compounds were never detected in blanks. No significant degradation of DDT to DDD was observed, since  $^{13}\text{C}$ -labelled standards were used as internal standards and only DDT and DDE were monitored in the samples (Foreman and Gates, 1997). Method reproducibility was checked by routinely analyzing a certified fish sample obtained during a previous laboratory inter-calibration. Results were within 12% of the certified values.

### 2.3. Coregonid Age Estimation

The age of the whitefish specimens was determined by counting the number of translucent or opaque rings in otoliths. A few scales of otoliths were taken just above the lateral line, cleaned with a solution of KOH and counted with an optical microscope. March 1st was assumed as transition date between age  $n$  and  $n + 1$ .

### 2.4. The DynA Model

The DynA Model (Di Guardo et al., 2006; Infantino et al., 2008) is a fugacity-based model developed to predict the fate of organic chemicals in a dynamic water–sediment system. DynA is dynamic not only in terms of chemical discharge, which may be discontinuous over time (to simulate, for example, a single spill in a lake or a pesticide application in a rice paddy), but also in terms of some environmental parameters (e.g., temperature and water fluxes). More specifically, it requires as input data daily values of parameters such as temperature, water inflow and outflow, and water depth. Additional details regarding the model formulation are available in Di Guardo et al. (2006), while an evaluation of the model performance in a rice-field scenario can be found in Infantino et al., 2008.

### 2.5. Statistical Analyses and Software Employed

The statistical analyses were performed with SigmaStat version 3.0. The Single Organism model and the integrated version, EcoDynA, were coded using Microsoft Visual Basic 6.0.

### 2.6. Model Parameterization

In the present work, EcoDynA was run to investigate p,p'-DDT bioaccumulation in 2- to 4-year old whitefish of two different species, "lavarello" whitefish and *Coregonus macrophthalmus* Nüsslin, 1882 (common Italian name: "bondella"), in Lake Maggiore. Simulations results were compared with the concentrations presented in this work for "lavarello" (see 3.1) and in Volta et al. (2009) for "bondella". Both these species are pelagic and mainly zooplanktivorous, although some differences must be remarked: "lavarello" grows more rapidly than "bondella", especially during the first year of life, and reaches higher dimensions. During the winter, when feeding rate generally reduces for both species, "bondella" leaves its strict zooplanktivorous habits in favor of other types of food (e.g., Oligochaetes, Isopoda, burbot or whitefish eggs); a similar behavior can be attributed also to "lavarello", but for this whitefish it is less pronounced. Moreover, while for "lavarello" spawning occurs in the first meters of water, "bondella" spawns at higher depths (Berg and Grimaldi, 1965). In order to investigate the influence of physiological parameters in determining bioaccumulation, dynamic profiles of fish volume, lipid fraction and feeding rate were built, combining information available in the

literature (Berg and Grimaldi, 1965; CIP AIS, 2002, 2003, 2004, 2005; Volta et al., 2009) with measurements presented in the present work (see 3.4).

Given the pelagic nature of whitefish, EcoDynA was parameterized considering epilimnion only, as suggested by Bettinetti et al. (2006). A constant water compartment depth of 25 m was assumed (equivalent to the measured epilimnion depth during stratification months), while a shallow sediment layer was used as a proxy of the metalimnion. Additionally, water inflow and outflow rates were constant (CIP AIS, 1998, 2000, 2001). A complete list of the values adopted for environmental parameters, with corresponding references, can be found in Table S1. For both “lavarello” and “bondella” simulations, a constant emission to the water compartment was used in order to recreate a water-dissolved p,p'-DDT concentration of about 0.2 ng L<sup>-1</sup>, which was the steady-state concentration assumed in Di Guardo et al. (2006) and also the average concentration measured in Lake Maggiore epilimnion (CIP AIS, 2003, 2004, 2005). Since the focus of this study was not to detail the dynamics of DDT input to the lake, but rather to develop a dynamic organism model, we decided to match the available concentrations in water and to show the influence of some factors (such as POC dynamic) on their variability. More details on the recent DDT contamination can be found in the literature mentioned in the introduction. A variable profile of particulate organic carbon (POC) was also adopted, in order to simulate the possible effect of phytoplankton in sequestering the chemical; such profile was built starting from the POC measures performed in Lake Maggiore in 1997 (CIP AIS, 1998). p,p'-DDT physical-chemical properties are listed in Table S2.

### 3. Results and Discussion

#### 3.1. DDT Concentrations in “Lavarello” Whitefish

Among the DDT compounds detected in whitefish, p,p'-DDE was found in concentrations up to 10 times higher than p,p'-DDT and p,p'-DDD ones (Table S3). This is probably due to the longer metabolic half-life of DDE in fish and to a possible accumulation of the metabolically-converted DDE from the previously accumulated DDT (Kwong et al., 2008). Considering the uncertainty related to this process, it was decided to restrict our modelling attempts to p,p'-DDT only. Lipid-normalized concentrations for male and female whitefish are shown in Fig. S2. Replicates (number in brackets) were available for female fishes of age 2 (3), 4 (4) and male fishes of age 2 (5), 3 (3), 4 (5). For the other ages, a single sample was available, and standard error was not calculated. The lipid-normalized concentrations varied from 500 to 2000 ng g<sup>-1</sup> lipid weight (l.w.); the high variability observed did not allow perceiving a statistically significant correlation between DDT levels and age classes, despite an increasing trend of average concentrations with age can be noticed in both female and male fishes in this work and in Volta et al. (2009). The p,p'-DDT concentrations measured in “lavarello” specimens were a factor of about 2–2.5 higher than the concentrations measured in “bondella” whitefish caught in Lake Maggiore in 2003 by Volta and co-workers (2009). Since p,p'-DDT water concentrations are available from 2002, it can be only hypothesized that this discrepancy can be due to higher p,p'-DDT water concentrations in the years preceding 1997/1998 than in the ones before 2003.

#### 3.2. Development of the Single Organism Model

Single Organism is a dynamic model based on the fugacity concept (Mackay, 2001) developed to simulate the bioaccumulation of organic chemicals by a single aquatic organism. Its mass balance description is similar to the one of Clark et al. (1990), Gobas (1993) and Campfens and Mackay (1997), but some organism dynamics are included. In SO, the aquatic organism grows with time and its volume changes following

specific age growth rates. Thus, the model incorporates not only volume variation, but also variations of other parameters, such as ventilation rates and ingestion rate, which are linked to the volume by means of allometric equations (Gobas et al., 1988). In addition, SO simulates the seasonal variations in other organism properties such as the body lipid content or feeding rate. In order to simulate organism volume variation with time, the model uses a linear growth rate as default equation. If the aquatic organism of interest is a fish, the model provides three possible calculation routines to describe volume variation: linear growth, the von Bertalanffy equation (von Bertalanffy, 1938), and a user-defined equation. The linear growth equation can be used when the available information is just the growth rate for a single life stage or when the length/weight measured data are best fitted by linear regression. The von Bertalanffy growth model allows describing individual fish growth as a function of time. The mathematical equation is an exponential growth function, expressed as:

$$V_{org}(t) = \alpha * (1 - e^{-\beta(t)}) \quad (1)$$

where  $V_{org}$  is the fish volume (m<sup>3</sup>) at time  $t$  and  $\alpha$  (fish volume at  $t \rightarrow \infty$ ) and  $\beta$  are the regression coefficients. Commonly, this model is used to fit length or weight measurements in order to estimate empirically  $\alpha$  and  $\beta$  coefficients. Therefore, the growth rate  $k_G$  (fraction of body volume per unit time) for each time step can be calculated from Eq. (1) as follows:

$$k_G(t) = \alpha * \beta * (e^{-\beta(t)}) \quad (2)$$

As a third option, the model can be run using a user-derived function, if available (such as for “lavarello” whitefish, as shown later).

The rate at which the chemical is absorbed via gills is expressed by the uptake rate constant  $k_I$ , which has units of L kg<sup>-1</sup> d<sup>-1</sup>.

In this model,  $k_I$  is calculated from the equation:

$$\frac{1}{k_I} = \left(1000 * \sigma_F * \frac{V_{org}}{Q_W}\right) + \left(1000 * \sigma_F * \frac{V_{org}}{Q_L} * \frac{1}{K_{ow}}\right) \quad (3)$$

where 1000 is a unit conversion factor allowing the conversion of  $V_{org}$  from m<sup>3</sup> to L,  $\sigma_F$  is the fish density (assumed as 1 kg L<sup>-1</sup>) and  $Q_W$  and  $Q_L$  (L d<sup>-1</sup>) represent the transport rates in water and lipid phases (Gobas, 1993). The water transport parameter  $Q_W$  is estimated from  $V_{org}$  (Gobas et al., 1988):

$$Q_W = 88.3 * 1000 * V_{org}^{0.6} \quad (4)$$

while the lipid-phase transport parameter,  $Q_L$ , is considered as  $1/100 * Q_W$ .

The depuration rate ( $k_2$ ) (d<sup>-1</sup>) is calculated from the bioconcentration factor (BCF) according to equation proposed by Mackay and Fraser (2000):

$$k_2 = \frac{k_1}{BCF} \quad (5)$$

The BCF is expressed as  $\sigma_{org} * K_{OW}$ , where  $\sigma_{org}$  is the organism lipid fraction.

These kinetic parameters ( $k_1$ ,  $k_2$ ,  $Q_W$ ,  $Q_L$ ) are updated as the organism volume changes with time.

Food uptake is usually the most important bioaccumulation pathway by which hydrophobic and persistent organic chemicals may accumulate in aquatic organism such as fish or macroinvertebrates. In the modelling exercises presented in this work, the food source is assumed at equilibrium with water and its lipid fraction ( $\sigma_{food}$ ) constant with time. However, it should be considered that since  $\sigma_{food}$  can change with the season, the fugacity capacity for food ( $Z_{food}$ ) could show a seasonal

trend, too. The food ingestion rate ( $G_a$ ,  $m^3 h^{-1}$ ) depends on body weight variations, as shown by the following equation:

$$Ga(t) = \frac{Vorg(t) * FR}{24} \quad (6)$$

where  $FR$  (fraction of body volume per day) is the feeding rate. When data are available, a  $FR$  trend with time can be specified. Alternatively,  $FR$  can be assumed as constant during the entire life cycle.

The loss of chemical via metabolism is calculated from the rate constant  $k_M$  ( $d^{-1}$ ) which, which is obtained from the metabolic half-life  $T_M$  (d):

$$k_M(t) = \frac{\ln 2}{T_M} \quad (7)$$

All these transport and transformation processes are computed by means of  $D$  values ( $mol Pa^{-1} h^{-1}$ ), which are listed in Table 1.

### 3.3. The EcoDynA Model

The integrated model EcoDynA was created adding the new dynamic compartment representing the aquatic organism, and therefore a new mass balance equation, to the original DynA Model (Di Guardo et al., 2006) (Fig. 1).

In EcoDynA, the dynamic chemical behavior in the three compartments (organism, water and sediment) is described by a system of three 1st-order ordinary differential equations (ODEs), one for each compartment, which is solved numerically using a modified 5th-order adaptive, implicit Runge–Kutta method (ESDIRK5(4)) (Semplice et al., 2012). The ODEs, representing the variation of residue moles with time are:

$$dmolORG/dt = a + b * molWAT - c * molORG \quad (8)$$

$$dmolWAT/dt = d + e * molORG + g * molSED - h * molWAT \quad (9)$$

$$dmolSED/dt = i + j * molWAT - k * molSED \quad (10)$$

where  $molORG$ ,  $molWAT$  and  $molSED$  represent the moles present in the three compartments at a certain time, while each coefficient (from  $a$  to  $j$ ) represents a transformation or a transport flux (single  $D$  value or sum of  $D$  values) divided by the proper product of volume and fugacity capacity  $Z$  (Table 2). All  $D$  and  $Z$  values are listed in Table 1.

It must be remarked that, in the EcoDynA mass balance, the chemical uptake from food is not expressed by means of a  $D$  value. As shown in Table 2, this process is modelled as a chemical source and, therefore, can be found in the  $a$  coefficient. The term  $C_{Af}$ , which appears in  $a$ , is the chemical concentration in food ( $mol m^{-3}$ ) computed using the water fugacity calculated for the previous hour (food is assumed to be in equilibrium with water).

To allow mass conservation, the original DynA Model mass balance was also updated so that, for each compartment, the residue moles (instead of fugacities) represent the state variable: more specifically, at the end of each time step, fugacities are converted to residue moles and, at the beginning of the following time step, residue moles are converted to fugacities again by dividing residue moles by the actual compartment volumes and  $Z$  values, which are subject to hourly changes.

### 3.4. Organism Scenarios for Model Simulations

For the simulations presented here, the linear-growth assumption generally used in bioaccumulation models (van Beusekom et al., 2006) was replaced with the volume trends depicted in Fig. 2a for “lavarello” and Fig. S3a for “bondella”. In these charts, for simplicity, weight instead of volume was plotted (a fish density equal to  $1 kg L^{-1}$  was assumed).

**Table 1**  
 $Z$  ( $mol m^{-3} Pa^{-1}$ ) and  $D$  values ( $mol Pa^{-1} h^{-1}$ ) in EcoDynA.

Parameter	Description	Equation
$Z_A$	Z for pure air	$1/RT$
$Z_Q$	Z for aerosol particles	$6E + 06/P_L * Z_A$
$Z_{Abulk}$	Z for bulk air	$Z_A * (1 - v_Q) + Z_Q * v_Q$
$Z_W$	Z for pure water	$1/H$
$Z_{Wp}$	Z for water column particles	$0.41 * K_{OW} * f_p * \sigma_p * Z_W/1000$
$Z_{Wbulk}$	Z for bulk water	$Z_W * (1 - v_p) + Z_{Wp} * v_p$
$Z_S$	Z for sediment particles	$0.41 * K_{OW} * f_s * \sigma_s * Z_W/1000$
$Z_{Sbulk}$	Z for bulk sediment	$Z_W * (1 - v_s) + Z_S * v_s$
$Z_O$	Z for octanol	$Z_W * K_{OW}$
$Z_{Org}$	Z for aquatic organism	$Z_W * K_{OW} * lf$
$Z_{Food}$	Z for aquatic organism food	$Z_W * K_{OW} * lf_{Food}$
$D_I$	Water inflow	$G_I * Z_W$
$D_X$	Water particle inflow	$G_X * Z_{Wp}$
$D_J$	Water outflow	$G_J * Z_W$
$D_Y$	Water particle outflow	$G_Y * Z_{Wp}$
$D_V$	Absorption/Volatilization	$k_V * A_W * Z_W$
$D_M$	Rain dissolution	$G_M * Z_W$
$D_C$	Wet particle deposition	$G_C * Z_Q$
$D_Q$	Dry particle deposition	$G_Q * Z_Q$
$D_T$	Sediment-to-water/ water-to-sediment diffusion	$k_T * A_S * Z_W$
$D_D$	Sediment deposition	$G_D * Z_{Wp}$
$D_R$	Sediment resuspension	$G_R * Z_S$
$D_B$	Sediment burial	$G_B * Z_S$
$D_W$	Water transformation	$k_W * V_W * Z_W$
$D_S$	Sediment transformation	$k_S * V_S * Z_S$
$D_{VentIn}$	Input ventilation (exchange via gills)	$k_I * V_{Org} * Z_W$
$D_{VentOut}$	Output ventilation (exchange via gills)	$k_2 * V_{Org} * Z_{Org}$
$D_{Upt}$	Uptake from food	$E_A * G_A * Z_{Food}$
$D_{Met}$	Metabolism transformation	$k_M * V_{Org} * Z_{Org}$
$D_{Growth}$	Growth dilution	$k_C * V_{Org} * Z_{Org}$
$D_{Eges}$	Fecal egestion	$D_{Upt}/QF$

$R$  = gas constant ( $8.314 J mol^{-1} K^{-1}$ ).

$T$  = absolute temperature (K).

$H$  = Henry's Law constant ( $Pa m^3 mol^{-1}$ ).

$P_L$  = sub-cooled liquid vapor pressure (Pa).

$v_Q, v_p$  and  $v_s$  = volume fractions of aerosol in air, particles in water and solids in surface sediments, respectively.

$f_p$  and  $f_s$  = fractions of organic carbon in water particles and sediment solids, respectively.  $\sigma_p$  and  $\sigma_s$  = densities ( $kg m^{-3}$ ) of water particles and sediment particles, respectively.  $lf$  and  $lf_{Food}$  = aquatic organism and food lipid fractions.

$k_V$  = overall (water-side) air–water mass transfer coefficient ( $m h^{-1}$ ).

$k_T$  = sediment–water mass transfer coefficient ( $m h^{-1}$ ).

$k_W$  = water transformation rate constant ( $h^{-1}$ ).

$k_S$  = sediment transformation rate constant ( $h^{-1}$ ).

$k_I$  = uptake via gills rate constant ( $L kg^{-1} d^{-1}$ ).

$k_2$  = depuration rate constant ( $d^{-1}$ ).

$k_M$  = metabolism rate constant ( $d^{-1}$ ).

$k_C$  = growth rate (fraction of body volume or weight  $d^{-1}$ ).

$E_A$  = gut absorption chemical efficiency.

$QF$  = limiting biomagnification factor.

$A_W$  and  $A_S$  = water and sediment areas ( $m^2$ ).

$V_W, V_S$  and  $V_{Org}$  = water, sediment and aquatic organism volumes ( $m^3$ ).

$G$  represents flow of phase ( $I$  = water inflow,  $X$  = particle inflow,  $J$  = water outflow,  $Y$  = particle outflow,  $M$  = rain dissolution,  $C$  = wet particle deposition,  $Q$  = dry particle deposition,  $D$  = sediment deposition,  $R$  = sediment resuspension,  $B$  = sediment burial) ( $m^3 h^{-1}$ ).

$G_A$  = food ingestion rate ( $m^3 h^{-1}$ ).

For “lavarello”, two different volume profiles for females and males were created adapting the growth curves depicted in Berg and Grimaldi (1965) to the fish weights measured in this study. According to these trends, during the period between May and September, “lavarello” whitefish linearly increase in weight, whereas they slowly decrease during the pre-reproduction period (October–December). From December to March, reproduction causes a rapid reduction of body weight in females; the decrease in weight observed in males, although less pronounced, is due to the lower winter feeding rate. Then, in spring, they again increase in weight (Fig. 2a). Since no growth curve was available for “bondella”, the same trends used for “lavarello” were adapted to the weights measured by Volta et al. (2009) to create a single curve for females and males. The same remarks made for “lavarello” can be done,

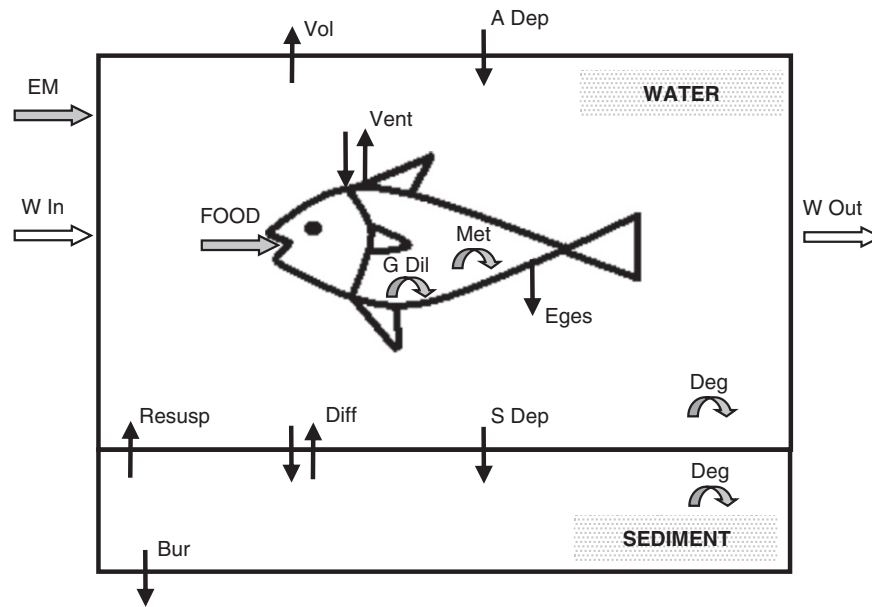


**Fig. 1.** Schematic representation of the EcoDyna model. Arrows represent processes, which include: emission to water compartment (EM), water inflow (W In) and outflow (W Out), volatilization to air (Vol), deposition from air (A Dep), sediment resuspension (Resusp), water–sediment diffusion (Diff), sediment deposition (Dep), sediment burial (Bur), degradation in water and sediment (Deg). Processes involving the aquatic organism include: uptake from food (FOOD), input and output ventilation (exchange via gills) (Vent), metabolic transformation (Met), growth dilution (G Dil) and elimination via fecal egestion (Eges).

even if shifted forward of one month: in fact, the sharpest growth is observed for “lavarello” in May–June, while for “bondella” in June–July (Berg and Grimaldi, 1965).

From volume trends, time-varying profiles of growth rate were also calculated using the following equation:

$$k_G(t) = \frac{V_{org2} - V_{org1}}{V_{org1} * \Delta t} \quad (11)$$

where  $V_{org1}$  and  $V_{org2}$  (L) are the fish volumes at times 1 and 2 and  $\Delta t$  (e.g., day) is the chosen time interval.

It is known that whitefish experience a seasonal oscillation of their lipid content related to gonad development and gamete spawning, as well as a general increase of lipids with age (Berg and Grimaldi, 1965). In order to account for this variability, lipid-fraction profiles for females and males of “lavarello” were compiled starting from the lipid data deriving from fish of the same species collected during a multi-year campaign in Lake Maggiore (CIPAI, 2002, 2003, 2004, 2005): the mean lipid values measured in specimens of different age four times a year (usually in March, July, September and December) were interpolated using pseudo-Gaussian regressions. Results are depicted in Fig. S4, where interpolations of the maximum and minimum values are also included. Since higher lipid contents were

observed in females, the trend obtained by maximum values (upper dashed line in Fig. S4) was used to simulate females, while the one obtained by minimum values (lower dashed line) for males. These trends were then adapted to simulate the lipid increase with age also confirmed by our measurements (see Text S2), as shown in Fig. 2b. For “bondella” whitefish, such a dataset from previous campaigns was not available; therefore, the lipid profiles created for “lavarello” were adjusted to fit the higher lipid contents typical of “bondella” whitefish (Volta et al., 2009) (Fig. S3b).

Finally, feeding rate profiles were created on the basis of the “maximum gastric replenishment coefficient” curves available in Berg and Grimaldi (1965), in order to obtain an average feeding rate (fraction of body weight per day) of 0.04 for “lavarello” (Campfens and Mackay, 1997) and of 0.03 for “bondella” (Volta et al., 2009) (Figs. 2c and S3c). Values for non-time varying parameters (digestion factor, metabolism half-life, lipid fraction in food and gut chemical absorption efficiency) and average values of physiological parameters used for static simulations are reported in Tables S4 and S5, respectively.

### 3.5. Model Application

The first application of EcoDyna was performed comparing the p,p'-DDT concentrations predicted in 2- to 4-year old “lavarello” whitefish to the concentrations measured in specimens of the same age classes (see 3.1). Two series of simulations were performed for each sex, one using the constant values for ecological parameters listed in Table S5, the other using the dynamic profiles described in 3.4 and depicted in Fig. 2. For each simulation, EcoDyna was run for 1600 days, following the aquatic organism life from the egg to the adult stage (4 years old).

The environmental scenario described in 2.6 was used. Water-dissolved p,p'-DDT concentrations during the whole simulation period, together with the adopted POC profile, are reported in Fig. 3.

The adopted POC profile presented three peaks (in April, August and November), which could be ascribed to different algal-bloom phases. Despite the overall POC variation was higher than a factor of 4, the water compartment responded with less significant oscillations (up to a factor of 1.2). These results suggested that, in such a system, the biological pump effect exerted by phytoplankton seems not to be

**Table 2**  
Groups of variables involved in the EcoDyna mass-balance equations.

a	$E_A * C_A * C_{Af}$
b	$D_{VentIn}/(V_W * Z_W)$
c	$(D_{Growth} + D_{Eges} + D_{VentOut} + D_{Met})/(V_{Org} * Z_{Org})$
d	$E_W + f_A * (D_V + D_M + D_C + D_Q)$
e	$(D_{VentOut} + D_{Eges})/(V_{Org} * Z_{Org})$
g	$(D_R + D_T)/(V_S * Z_{Sbulk})$
h	$(D_V + D_J + D_Y + D_D + D_T + D_{VentIn} + D_W)/(V_W * Z_{Wbulk})$
i	$E_S$
j	$(D_D + D_T)/(V_W * Z_{Wbulk})$
k	$(D_R + D_T + D_B + D_S)/(V_S * Z_{Sbulk})$

$E_W$  and  $E_S$  = emission to water and soil compartment (mol).  
 $f_A$  = bulk air fugacity (Pa).

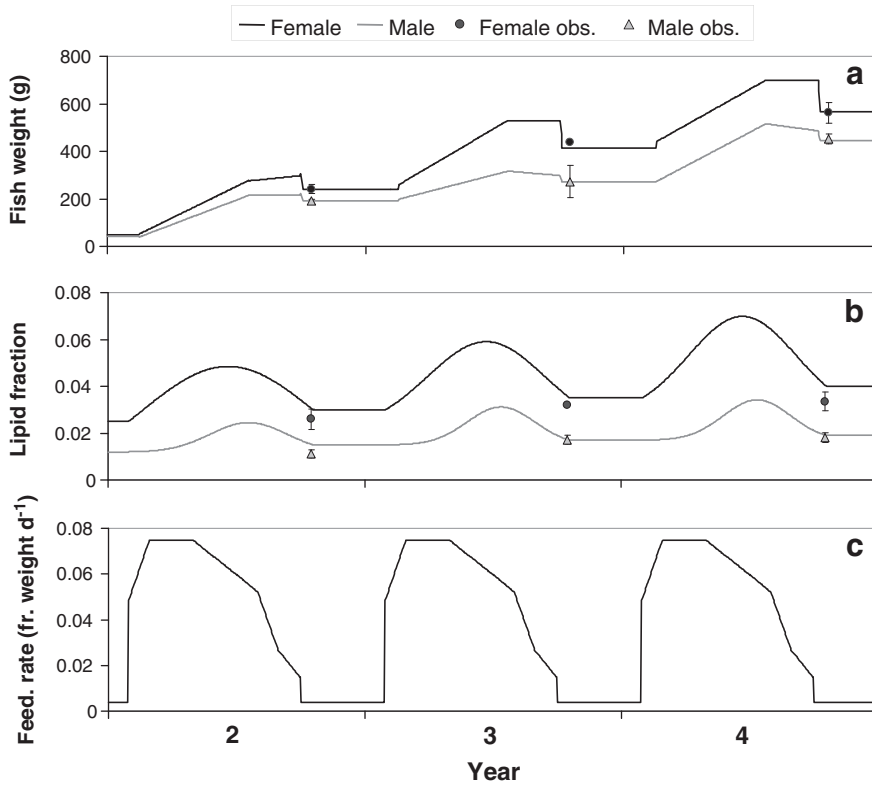


**Fig. 2.** Temporal trend of weight (g, chart a), lipid fraction (chart b) and feeding rate (fraction of body weight  $d^{-1}$ , chart c) adopted for 2- to 4-year old “lavarello” whitefish. In charts a and b, black lines refers to females, while grey ones to males. Markers correspond to the values measured in this study. Standard errors are also plotted. For feeding rate, a single temporal profile for both sexes was created.

not able to significantly affect water concentrations of p,p'-DDT; in contrast, the effectiveness of the biological pump in Lake Maggiore has been recently demonstrated for chemicals with higher  $\log K_{OW}$  (e.g., PCB 138, 153/132 and 180) (Nizzetto et al., 2012). However, the lack of measured data for concentrations in air during this period and the lack of precise information about the emissions do not allow to fully evaluate the issue.

Simulation results for “lavarello” whitefish are depicted in Fig. 4, in which a and b charts represent the comparisons for female and male whitefish performed using the static organism scenario, while c and d charts represent the results obtained considering dynamic ecological parameters, accounting for the contribution from food uptake (black line) or not (grey line). Concentrations are expressed on a fresh weight basis. For simplicity, the bioaccumulation curves of 4-year old female and male organisms were shown, and measured

concentrations of 2-, 3- and 4-year old whitefish were plotted on them in correspondence of sampling periods.

It is evident, from both measured values and modelled ones, that bioaccumulation leads to higher chemical levels in females than in males; this behavior can be ascribed to the higher female lipid content (Fig. 2b), which causes an increase in bioaccumulation. The results of the simulations performed with the dynamic organism scenario (black lines in Fig. 4c and d) generally showed a good agreement with measured values, for both female and male organisms. The use of dynamic ecological parameters clearly improved model predictions with respect to static ones (Fig. 4a and b). The oscillations in predicted concentrations observed in Fig. 4c and d were due to a combination of the dynamics of fish volume, lipid fraction and feeding rate: for example, the increase in concentrations (sudden for females, smooth for males) observed in the second half of the year is related to

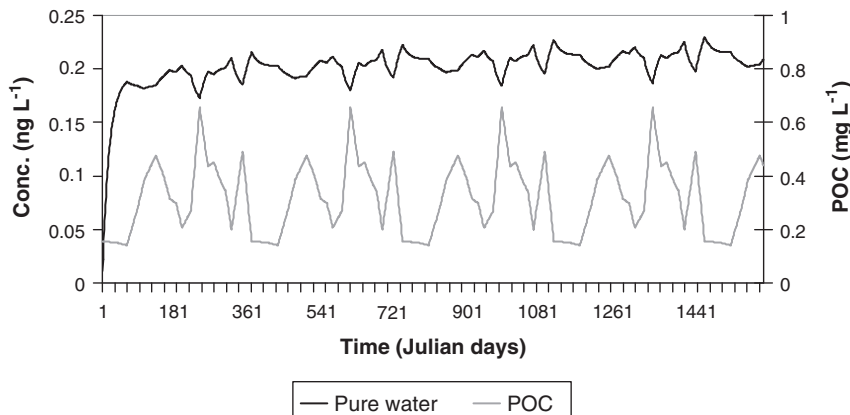


**Fig. 3.** p,p'-DDT ( $ng L^{-1}$ ) and POC ( $mg L^{-1}$ ) concentration profiles adopted for the simulations.

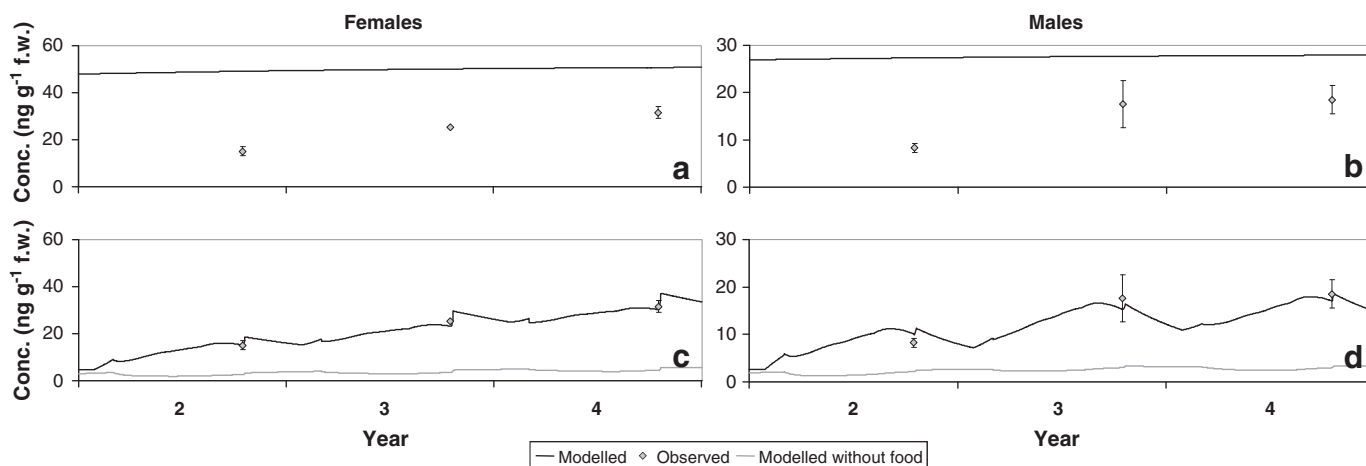


**Fig. 4.** Comparison between p,p'-DDT observed and predicted concentrations for females and males of "lavarello" whitefish (ages 2–4). Charts a and b report the comparison of observed values with static model predictions, while charts c and d with dynamic ones, accounting (black lines) or not (grey lines) for chemical uptake from food. Concentrations are on a fresh weight basis. Experimental values are indicated by grey markers.

the volume drop occurring in winter (related to egg spawning for females and winter fast for males) (Fig. 2a). For males, the seasonal profile is more marked and minimum values are observed when lipid fraction and feeding rate are smaller.

A comparison of the main fluxes influencing the mass balance of DDT in female "lavarello" whitefish can be found in Text S4 and Fig. S9. The role of the main driving forces (ventilation, food uptake, egestion, metabolic degradation, etc.) in the different seasons is briefly illustrated.

The second application of EcoDynA concerned the comparison with the p,p'-DDT concentrations measured in the "bondella" whitefish sampled by Volta and co-workers in 2003 (Volta et al., 2009). Similarly to the ones described for "lavarello", simulations were performed for female and male whitefish for 1600 days, but using the dynamic organism scenario only (see 3.4 and Fig. S3). Results, shown in Fig. S5, confirmed the generally good model performance, despite the greater uncertainties characterizing the "bondella" scenario with respect to the "lavarello" one.

In order to verify the predictive ability of EcoDynA, the model was tested against a number of PCBs of varying physical chemical properties for which data were available in the literature (Text S2 and Fig. S7). Results confirmed the general good predictive ability of the model.

### 3.6. Preliminary Sensitivity Analysis

A simple sensitivity analysis of EcoDynA was performed simulating p,p'-DDT fate in an organism–water–sediment system. The model was run for 1600 days and three target parameters were selected: average concentrations in 2-, 3- and 4-year old female organisms. EcoDynA was tested for substance physical-chemical properties, main environmental parameters (water and sediment compartment depth and concentration of suspended solids in water), emission to water and organism properties. As a reference, the environmental scenario described in 2.6 and the dynamic organism scenario developed for females of "lavarello" whitefish (see 3.4 and Fig. 2) were selected. Each parameter was reduced and increased by 50% and the sensitivity was recorded as a percentage variation with respect to the target value in the reference simulation. Results and more details can be found in Text S3. This preliminary sensitivity analysis revealed that chemical emission to water was the main influential parameter, followed by organism lipid fraction, gut absorption efficiency, feeding rate and lipid fraction in food, causing variations ranging from 17 to 39%. Among physical-chemical properties, the only influential parameter was  $K_{ow}$ .

## 4. Conclusions

A new model (EcoDynA) was developed to simulate the fate and bioaccumulation of organic chemicals in a single organism–water–sediment system. The model is dynamic not only in terms of emissions and environmental parameters such as water fluxes and depth, temperature or concentration of suspended solids in water, but also in terms of ecological parameters (e.g., organism volume, growth rate, lipid fraction, feeding rate). Preliminary applications of the model revealed its general adequacy for studying bioaccumulation in aquatic organisms such as zooplanktivorous fish and highlighted the importance of building accurate input scenarios. This was stressed by the simple sensitivity analysis performed. The inclusion of a trophic web and, therefore, of phytoplankton and zooplankton compartments, will be matter of future work.

### Conflict of interest

No conflict of interest exists.

### Acknowledgments

Gaetano Gentili (GRAIA, Varano Borghi, VA, Italy) and Manuela Frisone are acknowledged for the sampling and analytical parts. Matteo Semplice (University of Torino, TO, Italy) is acknowledged for the assistance in the implementation of the EcoDynA numerical solution.

### Appendix A. Supplementary data

Supplementary data to this article can be found online at <http://dx.doi.org/10.1016/j.scitotenv.2013.03.026>.

## References

- Ashauer R, Boxall A, Brown C. Predicting effects on aquatic organisms from fluctuating or pulsed exposure to pesticides. *Environ Toxicol Chem* 2006;25:1899–912.
- Berg A, Grimaldi E. La biologia delle due forme di coregone (*Coregonus* sp.) del Lago Maggiore. *Memorie dell'Istituto Italiano di Idrobiologia*, 18; 1965:25–196.
- Bettinetti R, Croce V, Galassi S, Volta P. pp'DDT and pp'DDE accumulation in a food chain of Lake Maggiore (Northern Italy): testing steady-state conditions. *Environ Sci Pollut Res* 2006;13:59–66.
- Bettinetti R, Galassi S, Guzzella L, Croce V, Volta P. The role of zooplankton in DDT biomagnification in a pelagic food web of Lake Maggiore (Northern Italy). *Environ Sci Pollut Res* 2010;17:1508–18.
- Bettinetti R, Quadroni S, Manca M, Piscia R, Volta P, Guzzella L, et al. Seasonal fluctuations of DDTs and PCBs in zooplankton and fish of Lake Maggiore (Northern Italy). *Chemosphere* 2012;88:344–51.

- Borgà K, Fisk AT, Hoekstra PF, Muir DCG. Biological and chemical factors of importance in the bioaccumulation and trophic transfer of persistent organochlorine contaminants in arctic marine food webs. *Environ Toxicol Chem* 2004;23:2367–85.
- Campens J, Mackay D. Fugacity-based model of PCB bioaccumulation in complex aquatic food webs. *Environ Sci Technol* 1997;31:577–83.
- Ceschi M, De Rossa M, Jaggi M. Contaminanti organici, inorganici e radionuclidi nell'ittiofauna dei laghi Ceresio e Verbano (bacini svizzeri). *Trav Chim Aliment Hyg* 1996;87:189–211.
- CIP AIS. Istituto Italiano di Idrobiologia – C.N.R., Ricerche sull'evoluzione del Lago Maggiore. Aspetti limnologici. Campagna 1997. In: Commissione Internazionale per la protezione delle acque italo-svizzere, editor. Relazione finale per il quinquennio; 1998. [83 pp. <http://www.cipais.org/html/lago-maggiore-pubblicazioni.asp>].
- CIP AIS. Istituto Italiano di Idrobiologia – C.N.R., Ricerche sull'evoluzione del Lago Maggiore. In: Commissione Internazionale per la protezione delle acque italo-svizzere, editor. Aspetti limnologici. Programma quinquennale 1998–2002. Campagna 1999; 2000. [71 pp. <http://www.cipais.org/html/lago-maggiore-pubblicazioni.asp>].
- CIP AIS. Istituto Italiano di Idrobiologia – C.N.R., Ricerche sull'evoluzione del Lago Maggiore. In: Commissione Internazionale per la protezione delle acque italo-svizzere, editor. Aspetti limnologici. Programma quinquennale 1998–2002. Campagna 2000; 2001. [77 pp. <http://www.cipais.org/html/lago-maggiore-pubblicazioni.asp>].
- CIP AIS. Istituto Italiano di Idrobiologia – C.N.R., Ricerche sulla Distribuzione e gli Effetti del DDT nell'Ecosistema del Lago Maggiore. In: Commissione Internazionale per la protezione delle acque italo-svizzere, editor. Rapporto Finale sui Risultati delle Indagini; 1999. p. 81. [<http://www.cipais.org/html/lago-maggiore-pubblicazioni.asp>].
- CIP AIS. Istituto Italiano di Idrobiologia – C.N.R., Monitoraggio della Presenza del DDT e di altri Contaminanti nell'Ecosistema Lago Maggiore. In: Commissione Internazionale per la protezione delle acque italo-svizzere, editor. Rapporto Annuale Aprile 2001 – Marzo 2002; 2002. p. 90. [<http://www.cipais.org/html/lago-maggiore-pubblicazioni.asp>].
- CIP AIS. Istituto Italiano di Idrobiologia – C.N.R., Monitoraggio della Presenza del DDT e di altri Contaminanti nell'Ecosistema Lago Maggiore. In: Commissione Internazionale per la protezione delle acque italo-svizzere, editor. Rapporto Annuale Aprile 2002 – Marzo 2003; 2003. p. 69. [<http://www.cipais.org/html/lago-maggiore-pubblicazioni.asp>].
- CIP AIS. Istituto Italiano di Idrobiologia – C.N.R., Monitoraggio della Presenza del DDT e di altri Contaminanti nell'Ecosistema Lago Maggiore. In: Commissione Internazionale per la protezione delle acque italo-svizzere, editor. Rapporto Annuale Aprile 2003 – Marzo 2004; 2004. p. 78. [<http://www.cipais.org/html/lago-maggiore-pubblicazioni.asp>].
- CIP AIS. Istituto Italiano di Idrobiologia – C.N.R., Monitoraggio della Presenza del DDT e di altri Contaminanti nell'Ecosistema Lago Maggiore. In: Commissione Internazionale per la protezione delle acque italo-svizzere, editor. Rapporto Annuale Aprile 2004 – Marzo 2005; 2005. p. 76. [<http://www.cipais.org/html/lago-maggiore-pubblicazioni.asp>].
- Clark KE, Gobas FAPC, Mackay D. Model of organic chemical uptake and clearance by fish from food and water. *Environ Sci Technol* 1990;24:1203–13.
- De Laender F, van Oevelen D, Middelburg JJ, Soetaert K. Incorporating ecological data and associated uncertainty in bioaccumulation modeling: methodology development and case study. *Environ Sci Technol* 2009;43:2620–6.
- De Laender F, van Oevelen D, Frantzen S, Middelburg JJ, Soetaert K. Seasonal PCB bioaccumulation in an Arctic marine ecosystem: a model analysis incorporating lipid dynamics, food-web productivity and migration. *Environ Sci Technol* 2010a;44:356–61.
- De Laender F, van Oevelen D, Middelburg JJ, Soetaert K. Uncertainties in ecological, chemical and physiological parameters of a bioaccumulation model: implications for internal concentrations and tissue based risk quotients. *Ecotoxicol Environ Saf* 2010b;73:240–6.
- Di Guardo A, Ferrari C, Infantino A. Development of a dynamic aquatic model (DynA Model): estimating temporal emissions of DDT to Lake Maggiore (N. Italy). *Environ Sci Pollut Res* 2006;13:50–8.
- Foreman WT, Gates PM. Matrix-enhanced degradation of p, p-DDT during gas chromatographic analysis: a consideration. *Environ Sci Technol* 1997;31:905–10.
- Gobas FAPC. A model for predicting the bioaccumulation of hydrophobic organic chemicals in aquatic food webs: application to Lake Ontario. *Ecol Model* 1993;69:1–17.
- Gobas FAPC, Arnot JA. Food web bioaccumulation model for polychlorinated biphenyls in San Francisco Bay, California, USA. *Environ Toxicol Chem* 2010;29(6):1385–95.
- Gobas FAPC, Muir DC, Mackay D. Dynamics of dietary bioaccumulation and faecal elimination of hydrophobic organic chemicals in fish. *Chemosphere* 1988;17:943–62.
- Infantino A, Pereira T, Ferrari C, Cerejeira MJ, Di Guardo A. Calibration and validation of a dynamic water model in agricultural scenarios. *Chemosphere* 2008;70:1298–308.
- Kwong RWM, Yu PKN, Lam PKS, Wang W-X. Uptake, elimination, and biotransformation of aqueous and dietary DDT in marine fish. *Environ Toxicol Chem* 2008;27:2053–63.
- Mackay D. Multimedia environmental models: the fugacity approach. 2nd ed. Boca Raton: Lewis Publishers; 2001.
- Mackay D, Fraser A. Bioaccumulation of persistent organic chemicals: mechanisms and models. *Environ Pollut* 2000;110:375–91.
- Nfon E, Armitage JM, Cousins IT. Development of a dynamic model for estimating the food web transfer of chemicals in small aquatic ecosystems. *Sci Total Environ* 2011;409:5416–22.
- Nizzetto L, Gioia R, Li J, Borgà K, Pomati F, Bettinetti R, et al. Biological pump control of the fate and distribution of hydrophobic organic pollutants in water and plankton. *Environ Sci Technol* 2012;46:3204–11.
- Patwa Z, Christensen R, Lasenby DC, Webster E, Mackay D. An exploration of the role of mysids in benthic-pelagic coupling and biomagnification using a dynamic bioaccumulation model. *Environ Toxicol Chem* 2007;26:1224–32.
- Reinert KH, Giddings JM, Judd L. Effects analysis of time-varying or repeated exposures in aquatic ecological risk assessment of agrochemicals. *Environ Toxicol Chem* 2002;21:1977–92.
- Semplice M, Ghirardello D, Morselli M, Di Guardo A. Guidance on the selection of efficient computational methods for multimedia fate models. *Environ Sci Technol* 2012;46:1616–23.
- US EPA. Guidance for assessing chemical contaminant data for use in fish advisories. Volume 1. Office of Science and Technology, Office of Water. Washington, DC: USEPA; 1995.
- van Beusekom OC, Eljarrat E, Barcelò D, Koelmans AA. Dynamic modeling of food-chain accumulation of brominated flame retardants in fish from the Ebro river basin, Spain. *Environ Toxicol Chem* 2006;25:2553–60.
- Volta P, Tremolada P, Neri MC, Giussani G, Galassi S. Age-dependent bioaccumulation of organochlorine compounds in fish and their selective biotransformation in top predators from Lake Maggiore (Italy). *Water Air Soil Pollut* 2009;197:193–209.
- von Bertalanffy L. A quantitative theory of organic growth. *Hum Biol* 1938;10:181–213.

## **Chapter 2. Paper I**

**Supporting information for**

# **Integration of a dynamic organism model into the DynA Model: Development and application to the case of DDT in Lake Maggiore, Italy**

Alfonso Infantino<sup>1</sup>, Melissa Morselli<sup>1</sup> and Antonio di Guardo<sup>1\*</sup>

<sup>1</sup>Department of Science and High Technology, University of Insubria, Via Valleggio, 11, 22100  
Como CO, Italy

\*Corresponding author

*Science of the Total Environment* **2013**, 454-455, 358–365

Contains 9 figures, 7 tables and 4 texts.



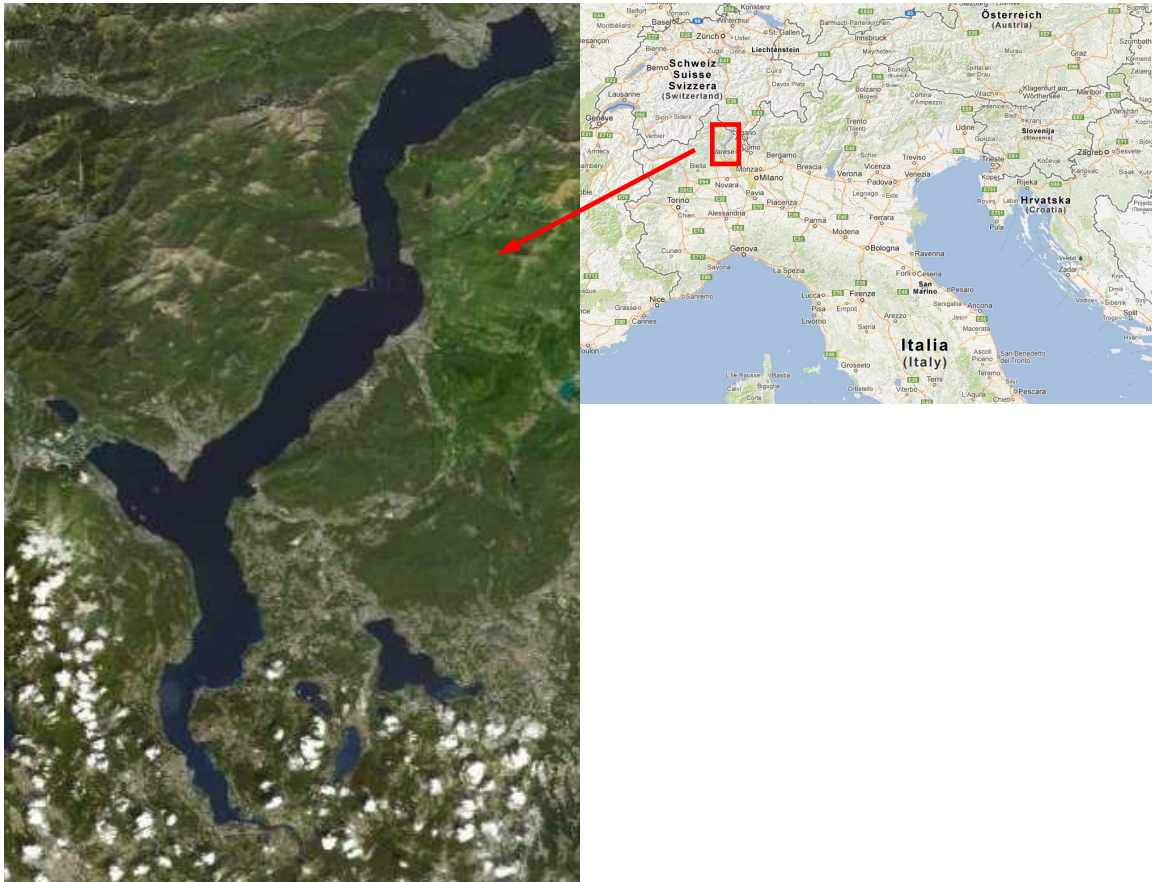


Figure S1. Satellite view and location of Lake Maggiore (Northern Italy) (Google Maps, 2013).

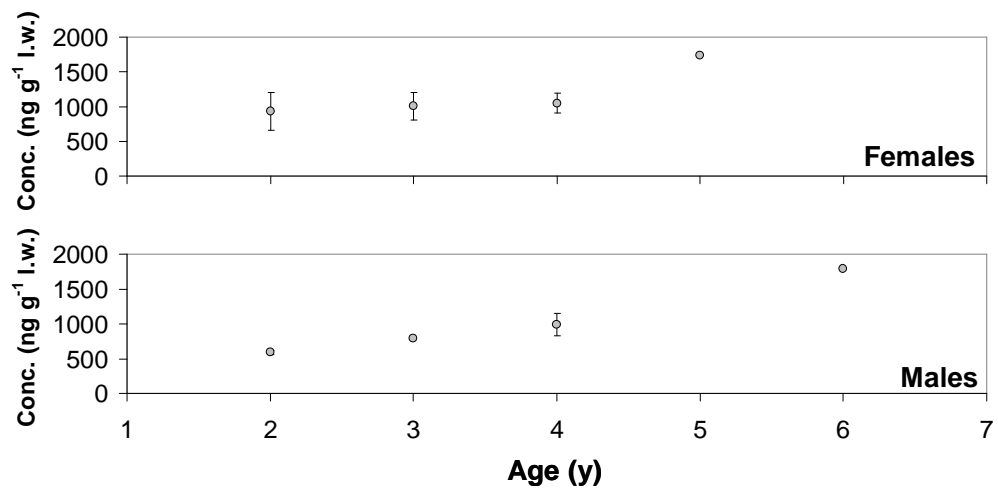


Figure S2. Lipid-normalized p,p'-DDT concentrations (average and standard error, when available) in females and males of "lavarello" whitefish.

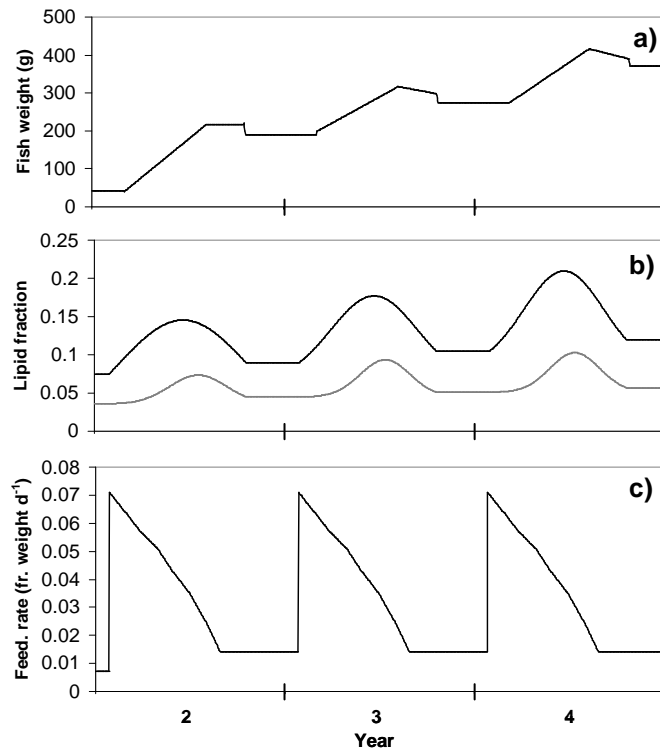


Figure S3. Temporal trend of weight (g, chart a), lipid fraction (chart b) and feeding rate (fraction of body weight  $d^{-1}$ , chart c) adopted for 2- to 4-year old “bondella” whitefish. In chart b, the black line refers to females, while the grey one to males. For weight and feeding rate, a single profile for both sexes was created.

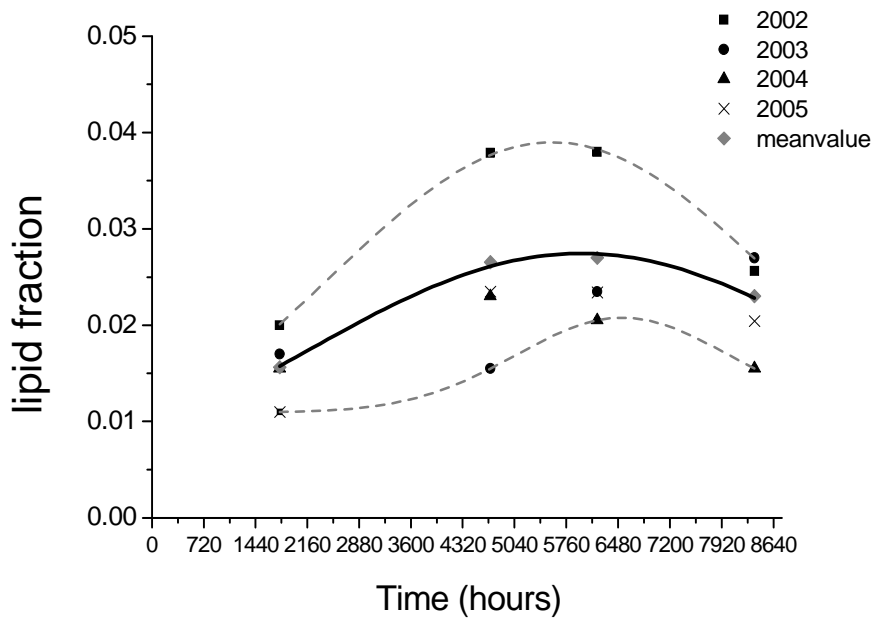


Figure S4. Lipid fraction seasonal variation in “lavarello” whitefish: the solid curve was extrapolated using pseudo-Gaussian regressions for mean values. Dashed lines represent maximum and minimum trends, calculated in the same way. All markers represent the lipid content values measured during CIPAIS campaigns from 2002 to 2005 (CIPAIS, 2002-2005).

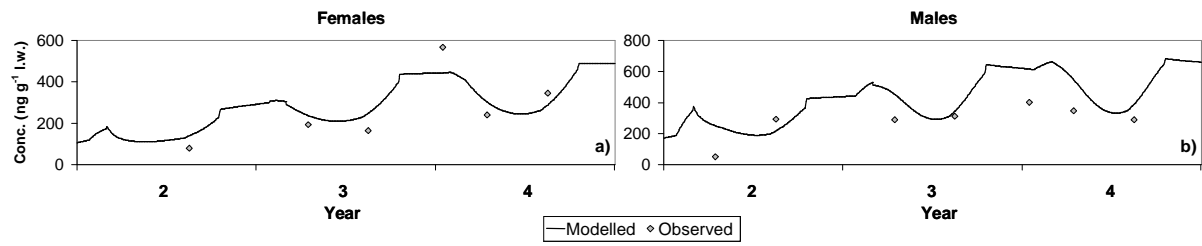


Figure S5. Comparison between p,p'-DDT observed and predicted concentrations for females (chart a) and males (chart b) of "bondella" whitefish (age 2-4). Concentrations are on a lipid weight basis. Black lines represent model predictions, while experimental values are indicated by grey markers.

Table S1. Environmental scenario used for the simulations.

Parameter	Units	Value	References
Water surface area	m <sup>2</sup>	2.12·10 <sup>8</sup>	Di Guardo et al. (2006)
Water depth	m	25	CIPAIS limnology (1998; 2000; 2001)
Sediment active layer depth	cm	1	Di Guardo et al. (2006)
River water inflow	m <sup>3</sup> y <sup>-1</sup>	9.51·10 <sup>9</sup>	Equal to water outflow rate
Water outflow rate	m <sup>3</sup> y <sup>-1</sup>	9.51·10 <sup>9</sup>	CIPAIS limnology (1998; 2000; 2001)
Conc. of particles in water column	mg L <sup>-1</sup>	1.146	Calculated from POC values obtained from CIPAIS limnology (1998)
Conc. of particles in inflow water	mg L <sup>-1</sup>	1.146	Equal to concentration of particles in water column
Conc. of aerosol particles	µg m <sup>-3</sup>	30	Di Guardo et al. (2006)
Vol. frac. of particles in surface sediments	/	0.305	Di Guardo et al. (2006)
Density of particles in water	kg m <sup>-3</sup>	2400	Di Guardo et al. (2006)
Density of sediment particles	kg m <sup>-3</sup>	2400	Di Guardo et al. (2006)
Density of aerosol particles	kg m <sup>-3</sup>	1500	Di Guardo et al. (2006)
Fraction of OC in water column particles	/	0.27	Di Guardo et al. (2006)
Fraction of OC in sediment solids	/	0.0171	Di Guardo et al. (2006)
Fraction of OC in resusp. sed. particles	/	0.0171	Di Guardo et al. (2006)
Fraction of OC in inflow susp. sed. solids	/	0.0171	Di Guardo et al. (2006)
Rain rate	m y <sup>-1</sup>	1.7	Di Guardo et al. (2006)
Aerosol dry deposition velocity	m h <sup>-1</sup>	7.2	Di Guardo et al. (2006)
Scavenging ratio	/	200000	Di Guardo et al. (2006)
Volatilization MTC (air side)	m h <sup>-1</sup>	1	Di Guardo et al. (2006)
Volatilization MTC (water side)	m h <sup>-1</sup>	0.01	Di Guardo et al. (2006)
Deposition rate of solids	g m <sup>-2</sup> d <sup>-1</sup>	8.27	Di Guardo et al. (2006)
Resuspension rate of solids	g m <sup>-2</sup> d <sup>-1</sup>	0.75	Di Guardo et al. (2006)
Burial rate of solids	g m <sup>-2</sup> d <sup>-1</sup>	7.52	Di Guardo et al. (2006)
Sediment-water diffusion MTC	m h <sup>-1</sup>	0.0004	Mackay (1989)

Table S2. p,p'-DDT physical-chemical properties at 25 °C (Mackay et al., 1997).

<b>Parameter</b>	<b>Value</b>
Molecular weight (g/mol)	354.5
Melting point (°C)	109
Water solubility (g/m <sup>3</sup> )	0.0055
Vapor pressure (Pa)	0.00002
Log K <sub>ow</sub>	6.19
Half-life in water (h)	5500
Half-life in sediment (h)	55000

Table S3. Lipid-normalized p,p'-DDT, p,p'-DDD and p,p'-DDE concentrations (ng g<sup>-1</sup> l.w., average and standard error, when available) in females and males of “lavarello” whitefish.

	<b>p,p'-DDT</b>	<b>p,p'-DDD</b>	<b>p,p'-DDE</b>
Females Age 2	590.19 (± 28.48)	1276.22 (± 154.16)	1874.00 (± 234.90)
Females Age 3	791.25	1176.25	1674.69
Females Age 4	986.18 (± 160.11)	1406.25 (± 144.92)	2834.55 (± 923.93)
Females Age 6	1788.71	1917.42	8955.48
Females Age 8	777.41	1953.15	14611.48
Males Age 2	926.30 (± 273.91)	1727.52 (± 429.88)	2583.21 (± 562.81)
Males Age 3	1002.79 (± 197.51)	1860.17 (± 239.02)	2834.39 (± 464.88)
Males Age 4	1046.95 (± 140.70)	1643.18 (± 154.04)	2762.13 (± 445.83)
Males Age 5	1742.00	2406.67	6650.67

Table S4. Values used for non-time varying organism parameters in the simulations.

Parameter	“Lavarello”	“Bondella”
Digestion factor	4 <sup>a), b)</sup>	3 <sup>c)</sup>
Metabolism half-life (d)	5000 <sup>d)</sup>	5000 <sup>d)</sup>
Lipid fraction in food	0.015 <sup>d)</sup>	0.015 <sup>d)</sup>
Gut chemical absorption efficiency	0.63 <sup>e)</sup>	0.63 <sup>e)</sup>

<sup>a)</sup>: Clark et al. (1990); <sup>b)</sup>: Mackay and Fraser (2000); <sup>c)</sup>: Volta et al. (2009); <sup>d)</sup>: Campfens and Mackay (1997); <sup>e)</sup>: Gobas et al. (1988).

Table S5. Constant values used for ecological parameters in static simulations. These values were obtained averaging the dynamic organism profiles used for dynamic simulations for “lavarello” whitefish of age 2 to 4 (Fig. 2, main text). For non-time varying organism parameters refer to Table S4.

<b>Parameter</b>	<b>Females</b>	<b>Males</b>
Weight (g)	385	270
Growth rate (fraction of body volume d <sup>-1</sup> )	0	0
Lipid fraction	0.04	0.02
Feeding rate (fraction of body volume d <sup>-1</sup> )	0.04	0.04

Text S1.

***Relationships between body weight/lipid content and fish age in sampled “lavarello” whitefish***

The length and weight of the sampled whitefish were linearly correlated for both sexes ( $p < 0.0001$ ). Female weight was generally 1.3 times higher than male one and ranged between 200 and 900 g in the collected samples. Other biometric parameters measured in whitefish of different age and sex were considered, in order to identify age-dependent relationships. No correlation was found between weight and lipid content (female  $p < 0.13$ , male  $p < 0.07$ ). Increase in weight with age was observed in both males and females, showing significant statistical correlation ( $p < 0.0001$ ) (Figure S6a and b). In spite of the difference in average weight between females and males ( $426 \pm 60$  and  $310 \pm 133$  g, respectively), correlation of weight and age could be described by a similar linear equation, as underlined by the slope value (128 for females and 132 for males). Average lipid content in females and males were  $3.9 \pm 1$  and  $1.5 \pm 0.5$ , respectively. Figure S6c and d show the significant correlation between lipid content and age in both sexes ( $p < 0.02$  for females and  $p < 0.05$  for males). Between females and males, significant differences were noticed for both size ( $p = 0.028$ ) and lipid content ( $p < 0.001$ ).

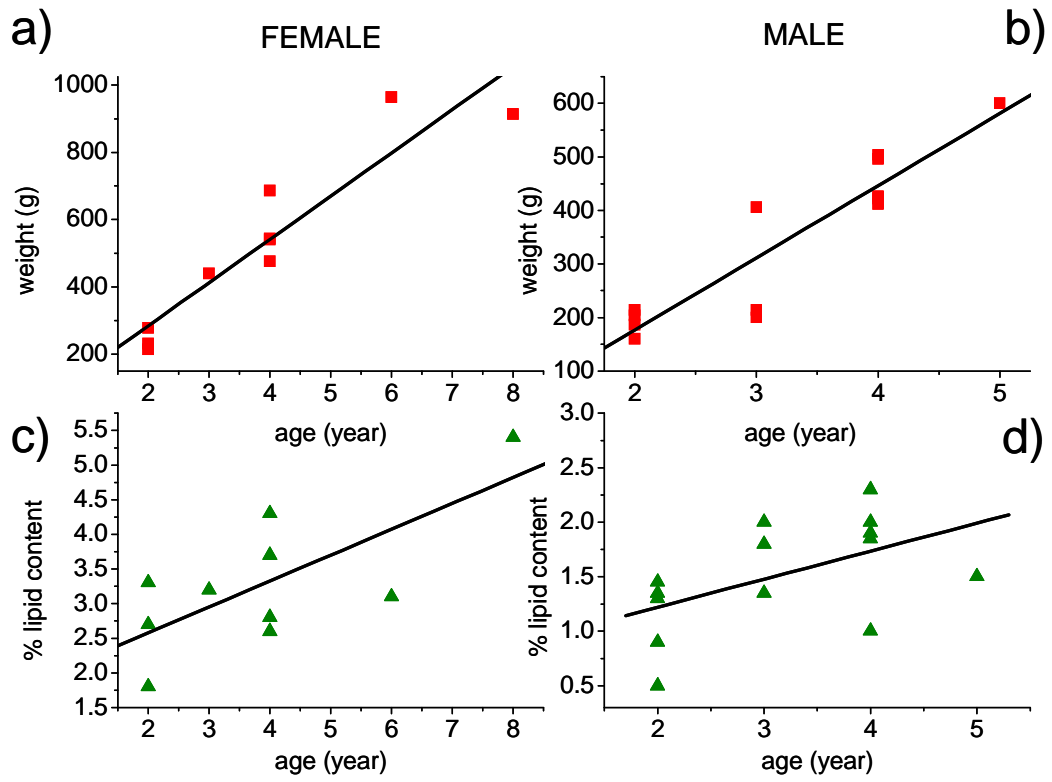


Figure S6. Dependence of fish physiological parameters (weight and lipid content) on age. All regressions were statistically significant (see main text for details).

Text S2.

***Model application to PCB 18, 52 and 149***

The EcoDyna model was applied, using the same environmental scenario for DDT, to three PCBs (PCB 18, PCB 52 and 149) for which concentrations in water (Nizzetto et al., 2012) and females of “lavarello” whitefish fish specimens sampled during CIPAIS campaigns from March 2008 to January 2011 (CIPAIS 2009-2011).

The physical chemical properties employed for the simulation can be found in Table S6.

Table S6. Physical-chemical properties at 25 °C (Mackay et al., 1997) for the three PCB congeners selected for the simulations.

<b>Parameter</b>	<b>PCB 18</b>	<b>PCB 52</b>	<b>PCB 149*</b>
Molecular weight (g/mol)	257.5	292	360.9
Melting point (°C)	44	87	103*
Water solubility (g/m <sup>3</sup> )	0.4	0.03	0.001*
Vapor pressure (Pa)	0.143	0.0049	0.000119*
Log K <sub>OW</sub>	5.6	6.1	6.9*
Half-life in water (h)	17000	55000	55000
Half-life in sediment (h)	55000	55000	55000

Note: \*Since no complete data set was available for PCB 149, physical chemical properties for PCB 153 were used.

Figure S7 shows the result of the comparison modeled/measured results for the three PCBs. The dashed lines represent the interval obtained varying feeding rate by plus or minus 50%.

While the scatter of the measured result is relatively high, it must be considered that the emission scenario of PCBs (which were not related to the spill episodes of DDT) is probably related to other sources (atmospheric/drainage basin etc.). The modelling results seem to span generally within a factor of two to 4, confirming the predicting adequacy of EcoDyna.

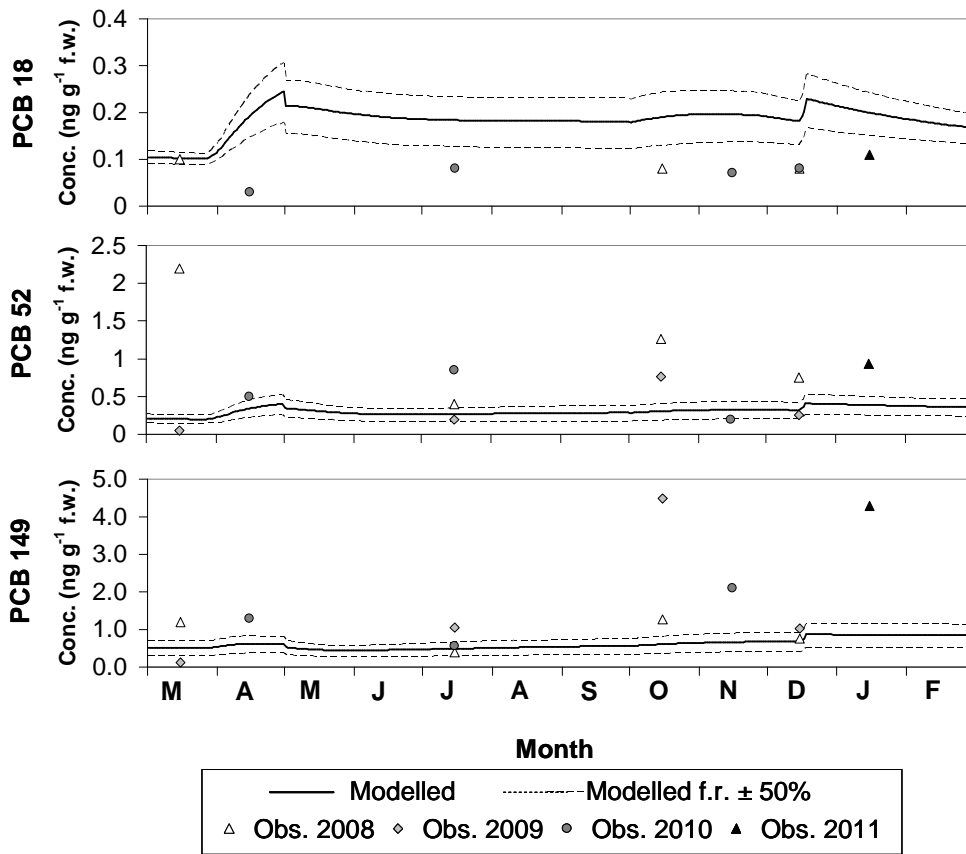


Figure S7. Results of the comparison between model predictions for females of “lavarello” whitefish and concentrations in fish specimens sampled during CIP AIS campaigns from March 2008 to January 2011 (CIP AIS 2009-2011).

Text S3.

### ***Preliminary sensitivity analysis***

A simple sensitivity analysis of EcoDynA was performed simulating p,p'-DDT fate in an organism-water-sediment system. The model was run for 1600 days, reducing and increasing by 50% the values of 20 parameters, including substance physical-chemical properties, main environmental parameters (water and sediment compartment depth and concentration of suspended solids in water), emission to water and organism properties. As a reference, the environmental scenario described in 2.6 (main text) and the dynamic organism scenario developed for females of “lavarello” whitefish (see 3.4 and Figure 2, main text) were adopted. The percent variations caused by modifications in tested parameters were evaluated for three targets: average concentrations in 2-, 3- and 4-year old female fishes. Percent variations for each tested parameter were calculated as follows:

$$\%Variation = (NewConc - RefConc) / RefConc * 100$$

where *NewConc* is the yearly average chemical concentration in fish when varying the tested parameter, while *RefConc* is the yearly average chemical concentration in fish in the reference simulation.

Results are shown in Table S6. For all targets, the most influential parameter was the emission to the water compartment, since a 50% modification caused an equivalent variation in organism concentrations. Organism lipid fraction (17-39%), gut absorption efficiency (25-37%), feeding rate (25-36%) and lipid fraction in food (25-36%) followed, revealing the importance of an accurate definition of organism physiological parameters when assessing bioaccumulation. Tested environmental parameters were less influential, causing variations which were always smaller than 4%. Among the physical-chemical parameters, the only one causing noticeable variations was  $K_{OW}$  (7-23%). The effect of the most influential parameters on the targets is shown in Figure S7.

Table S7. Percent variations of target parameters corresponding to  $\pm 50\%$  variations of the tested parameters.

	Ave 2nd	Ave 3rd	Ave 4th
MW+50%	-0.22	-0.22	-0.23
MW-50%	0.23	0.23	0.23
MeltingP+50%	0.00	0.00	0.00
MeltingP-50%	0.00	0.00	0.00
WS+50%	0.15	0.15	0.15
WS-50%	-5.10	-5.20	-5.27
Vp+50%	-0.22	-0.22	-0.23
Vp-50%	0.23	0.23	0.23
KOW+50%	6.83	10.23	11.19
KOW-50%	-16.44	-21.46	-22.98
HLwat+50%	1.96	2.00	2.03
HLwat-50%	-5.46	-5.56	-5.64
HLsed+50%	0.17	0.30	0.44
HLsed-50%	-0.46	-0.82	-1.16
Wdepth+50%	-2.96	-2.97	-2.97
Wdepth-50%	3.15	3.16	3.16
Seddepth+50%	-1.83	-2.10	-2.15
Seddepth-50%	3.84	3.73	3.32
SuspSol+50%	-1.25	-1.27	-1.28
SuspSol-50%	1.29	1.31	1.32
Emis+50%	50.00	50.00	50.00
Emis-50%	-50.00	-50.00	-50.00
FishVol+50%	1.34	2.79	3.25
FishVol-50%	-2.69	-5.24	-6.05
LipFrac+50%	16.97	22.89	26.41
LipFrac-50%	-31.28	-36.75	-39.30
Q+50%	6.31	9.65	12.00
Q-50%	-15.33	-21.24	-24.69
MetabHL+50%	0.38	0.64	0.88
MetabHL-50%	-1.12	-1.88	-2.55
GrowthRate+50%	0.00	0.00	0.00
GrowthRate-50%	0.00	0.00	0.00
LFfood+50%	29.62	26.91	24.53
LFfood-50%	-35.64	-35.36	-34.24
AbsEffic+50%	29.62	26.91	24.53
AbsEffic-50%	-36.41	-36.71	-36.16
FeedRate+50%	29.62	26.91	24.53
FeedRate-50%	-35.64	-35.36	-34.24
Temper+50%	8.92	6.22	5.24
Temper-50%	-6.10	-4.25	-3.58

Ave 2nd: average chemical concentration in the organism during the second year of life; Ave 3rd: average chemical concentration in the organism during the third year of life; Ave 4th: average chemical concentration in the organism during the fourth year of life; MW: molecular weight; MeltingP: melting point; WS: water solubility; Vp: vapor pressure; KOW:  $K_{OW}$ ; HLwat: half-life in water; HLsed: half-life in sediment; Wdepth: depth of the water compartment; Seddepth: depth of the sediment compartment; SuspSol: suspended solids in water; Emis: chemical emission to the water compartment; FishVol: fish volume; LipFrac: fish lipid fraction; Q: digestion factor; MetabHL: metabolism half-life; GrowthRate: fish growth rate; LFfood: lipid fraction in food; AbsEffic: gut chemical absorption efficiency; FeedRate: fish feeding rate; Temper: water temperature.

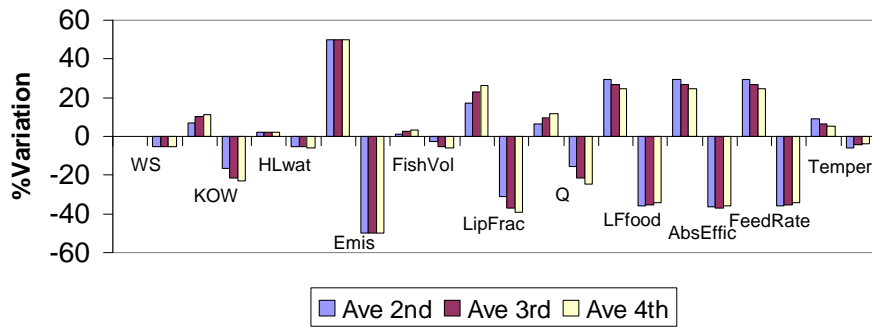


Figure S8. Percent variations caused by the most influential model parameters (%Variation > 5%).  
 WS: water solubility; KOW:  $K_{OW}$ ; HLwat: half-life in water; Emis: chemical emission to the water compartment; FishVol: fish volume; LipFrac: fish lipid fraction; Q: digestion factor; LFfood: lipid fraction in food; AbsEffic: gut chemical absorption efficiency; FeedRate: fish feeding rate; Temper: water temperature.

Text S4.

***Mass balance of p,p'-DDT in fish***

Figure S9 shows the seasonal fluxes of p,p'-DDT (mol) in females of “lavarello” whitefish (second year of organism life). As it can be seen, uptake from food prevales among the fluxes, with a considerable seasonal variation, while output ventilation (gill exchange with water) and growth dilution are the most important loss processes.

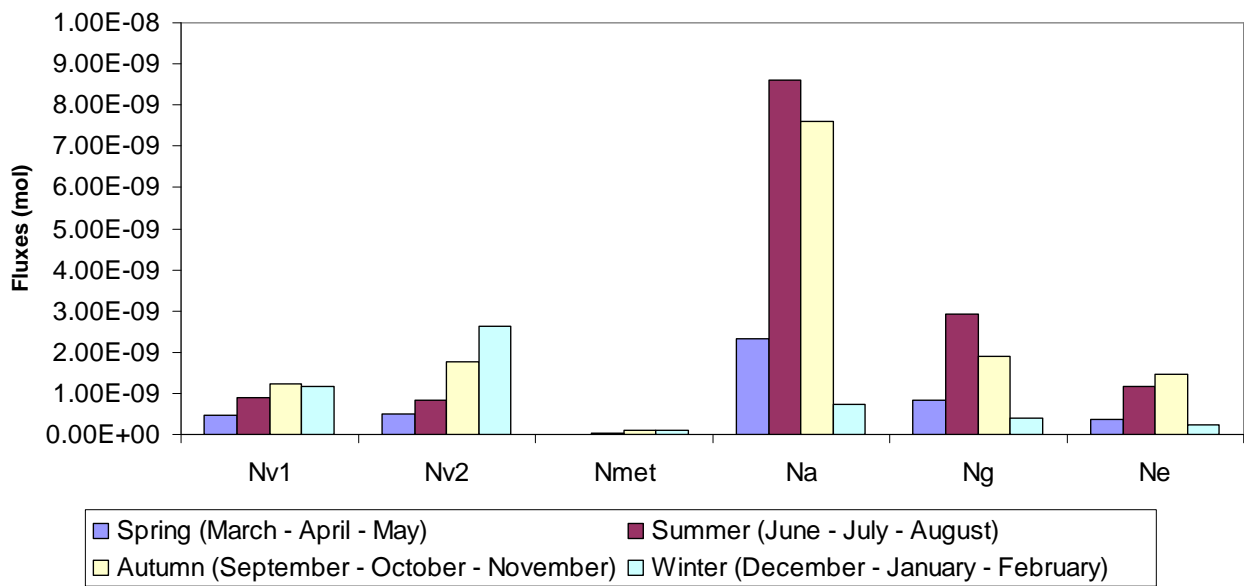


Figure S9. Comparison of seasonal p,p'-DDT fluxes in females of “lavarello” whitefish. Nv1 is input ventilation, Nv2 is output ventilation, Nmet is metabolic degradation, Na is uptake from food, Ng is growth dilution and Ne is egestion.

## References

Campfens J, Mackay D. Fugacity-based model of PCB bioaccumulation in complex aquatic food webs. *Env Sci Technol* 1997;31:577-583.

CIP AIS. Istituto Italiano di Idrobiologia - C.N.R. 2002. Monitoraggio della Presenza del DDT e di altri Contaminanti nell'Ecosistema Lago Maggiore. Rapporto Annuale Aprile 2001 - Marzo 2002.

Commissione Internazionale per la protezione delle acque italo-svizzere (Ed.): p. 90.

CIP AIS. Istituto Italiano di Idrobiologia - C.N.R. 2003. Monitoraggio della Presenza del DDT e di altri Contaminanti nell'Ecosistema Lago Maggiore. Rapporto Annuale Aprile 2002 - Marzo 2003.

Commissione Internazionale per la protezione delle acque italo-svizzere (Ed.): p. 69.

CIP AIS. Istituto Italiano di Idrobiologia - C.N.R. 2004. Monitoraggio della Presenza del DDT e di altri Contaminanti nell'Ecosistema Lago Maggiore. Rapporto Annuale Aprile 2003 - Marzo 2004.

Commissione Internazionale per la protezione delle acque italo-svizzere (Ed.): p. 78.

CIP AIS. Istituto Italiano di Idrobiologia - C.N.R. 2005. Monitoraggio della Presenza del DDT e di altri Contaminanti nell'Ecosistema Lago Maggiore. Rapporto Annuale Aprile 2004 - Marzo 2005.

Commissione Internazionale per la protezione delle acque italo-svizzere (Ed.): p. 76.

CIP AIS limnology. Istituto Italiano di Idrobiologia - C.N.R. 1998. Ricerche sull'evoluzione del Lago Maggiore. Aspetti limnologici. Campagna 1997. Relazione finale per il quinquennio.

Commissione Internazionale per la protezione delle acque italo-svizzere (Ed.): 83 pp.

CIPAIS limnology. Istituto Italiano di Idrobiologia - C.N.R. 2000. Ricerche sull'evoluzione del Lago Maggiore. Aspetti limnologici. Programma quinquennale 1998-2002. Campagna 1999. Commissione Internazionale per la protezione delle acque italo-svizzere (Ed.): 71 pp.

CIPAIS limnology. Istituto Italiano di Idrobiologia - C.N.R. 2001. Ricerche sull'evoluzione del Lago Maggiore. Aspetti limnologici. Programma quinquennale 1998-2002. Campagna 2000. Commissione Internazionale per la protezione delle acque italo-svizzere (Ed.): 77 pp.

CIPAIS limnology. Istituto Italiano di Idrobiologia - C.N.R. 2009. Indagini su DDT e sostanze pericolose nell'ecosistema del lago maggiore programma 2008-2012, rapporto annuale 2008. Commissione Internazionale per la protezione delle acque italo-svizzere (Ed.): 89 pp.

CIPAIS limnology. Istituto Italiano di Idrobiologia - C.N.R. 2010. Indagini su DDT e sostanze pericolose nell'ecosistema del lago maggiore programma 2008-2012, rapporto annuale 2009. Commissione Internazionale per la protezione delle acque italo-svizzere (Ed.): 112 pp.

CIPAIS limnology. Istituto Italiano di Idrobiologia - C.N.R. 2011. Indagini su DDT e sostanze pericolose nell'ecosistema del lago maggiore programma 2008-2012, rapporto annuale 2010. Commissione Internazionale per la protezione delle acque italo-svizzere (Ed.): 134 pp.

Clark KE, Gobas FAPC, Mackay D. Model of organic chemical uptake and clearance by fish from food and water. *Environ Sci Technol* 1990;24:1203-1213.

Di Guardo A, Ferrari C, Infantino A. Development of a dynamic aquatic model (DynA Model): Estimating temporal emissions of DDT to Lake Maggiore (N. Italy). *Environ Sci Pollut R* 2006;13:50-58.

Gobas FAPC, Muir DC, Mackay D. Dynamics of dietary bioaccumulation and faecal elimination of hydrophobic organic chemicals in fish. *Chemosphere* 1988;17:943-962.

Google Maps [Internet]. Google Maps - ©2013 Google; 2013 [cited 2013 Jan 17]. Available from: [www.google.com/maps](http://www.google.com/maps).

Mackay D. Modeling the long-term behavior of an organic contaminant in a large lake: Application to PCBs in Lake Ontario. *J Great Lake Res* 1989;15:283-297.

Mackay D, Shiu WY, Ma KC. Illustrated handbook of physical-chemical properties and environmental fate for organic chemicals. Vol V. Boca Raton: Lewis Publishers; 1997.

Mackay D, Fraser A. Bioaccumulation of persistent organic chemicals: mechanisms and models. *Environ Pollut* 2000;110:375-391.

Volta P, Tremolada P, Neri MC, Giussani G, Galassi S. Age-dependent bioaccumulation of organochlorine compounds in fish and their selective biotransformation in top predators from Lake Maggiore (Italy). *Water Air Soil Poll* 2009;197:193-209.



## Chapter 3. Paper II

# Evaluating the temporal variability of concentrations of POPs in a glacier-fed stream food chain using a combined modeling approach

Melissa Morselli<sup>1</sup>, Matteo Semplice<sup>2</sup>, Sara Villa<sup>3</sup> and Antonio di Guardo<sup>1\*</sup>

<sup>1</sup>Department of Science and High Technology, University of Insubria, Via Valleggio, 11, 22100 Como CO, Italy

<sup>2</sup>Dipartimento di Matematica, Università degli Studi di Torino, Via C. Alberto 10, 10123 Torino TO, Italy

<sup>3</sup>Department of Earth and Environmental Sciences, University of Milano-Bicocca, Piazza della Scienza 1, 20126 Milano MI, Italy

\*Corresponding author

*Science of the Total Environment* **2014**, 493, 571–579





## Evaluating the temporal variability of concentrations of POPs in a glacier-fed stream food chain using a combined modeling approach



Melissa Morselli <sup>a</sup>, Matteo Semplice <sup>b</sup>, Sara Villa <sup>c</sup>, Antonio Di Guardo <sup>a,\*</sup>

<sup>a</sup> Department of Science and High Technology, University of Insubria, Via Valleggio 11, 22100 Como CO, Italy

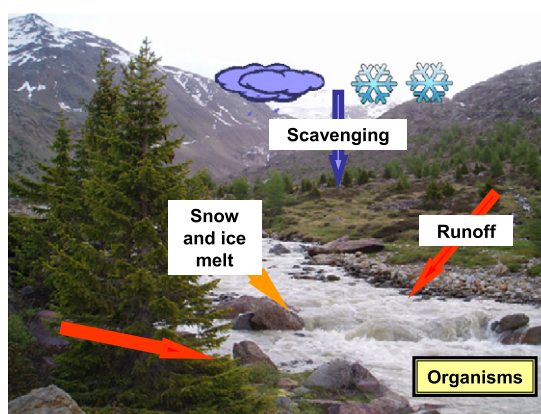
<sup>b</sup> Dipartimento di Matematica, Università degli Studi di Torino, Via C. Alberto 10, 10123 Torino TO, Italy

<sup>c</sup> Department of Earth and Environmental Sciences, University of Milano-Bicocca, Piazza della Scienza 1, 20126 Milano MI, Italy

### HIGHLIGHTS

- Glaciers and snow accumulate and release POPs at different times in streams.
- High mountain ecosystems are exposed to contaminant peaks of different ages and sources.
- Models developed reconstructed dynamics of water and chemicals for PCBs and DDE.
- Estimate of the exposure of 4 macroinvertebrate group during spring and summer is provided.

### GRAPHICAL ABSTRACT



### ARTICLE INFO

#### Article history:

Received 6 April 2014

Received in revised form 28 May 2014

Accepted 28 May 2014

Available online 27 June 2014

Editor: Damia Barcelo

#### Keywords:

EcoDyna model

Macroinvertebrates

PCBs

DDE

Snow

Exposure

### ABSTRACT

Falling snow acts as an efficient scavenger of contaminants from the atmosphere and, accumulating on the ground surface, behaves as a temporary storage reservoir; during snow aging and metamorphosis, contaminants may concentrate and be subject to pulsed release during intense snow melt events. In high-mountain areas, firn and ice play a similar role. The consequent concentration peaks in surface waters can pose a risk to high-altitude ecosystems, since snow and ice melt often coincide with periods of intense biological activity. In such situations, the role of dynamic models can be crucial when assessing environmental behavior of contaminants and their accumulation patterns in aquatic organisms. In the present work, a dynamic fate modeling approach was combined to a hydrological module capable of estimating water discharge and snow/ice melt contributions on an hourly basis, starting from hourly air temperatures. The model was applied to the case study of the Frodolfo glacier-fed stream (Italian Alps), for which concentrations of a number of persistent organic pollutants (POPs), such as polychlorinated biphenyl (PCBs) and p,p'-dichlorodiphenyldichloroethylene (p,p'-DDE) in stream water and four macroinvertebrate groups were available. Considering the uncertainties in input data, results showed a satisfying agreement for both water and organism concentrations. This study showed the model adequacy for the estimation of pollutant concentrations in surface waters and bioaccumulation in aquatic organisms, as well as its possible role in assessing the consequences of climate change on the cycle of POPs.

© 2014 Elsevier B.V. All rights reserved.

\* Corresponding author.

## 1. Introduction

Snow scavenging efficiently removes contaminants from the atmosphere (Franz and Eisenreich, 1998; Herbert et al., 2006); such process is of particular importance in the Northern hemisphere, where snow covers up to 50% of the land and most of the contaminants are emitted (Meyer and Wania, 2008). Snow, accumulating on the ground surface, acts as a temporary storage reservoir of contaminants (Daly and Wania, 2004). During snowpack aging and metamorphosis, contaminants may undergo several fate processes: for example, they may be degraded, released with melt water to aquatic and terrestrial ecosystems, or volatilize back to the atmosphere (Wania, 1997; Daly and Wania, 2004). Depending on their physical–chemical characteristics and snow properties, contaminants may also concentrate in the snowpack, and be rapidly released to surface waters during a short melt period. This can result in spring peak concentrations, which were measured in a number of studies (e.g., Qu  merais et al., 1994; Lafreni  re et al., 2006; Bizzotto et al., 2009a). Moreover, in high-mountain areas, where snow-fall rates are high and low temperatures allow snow accumulation, a fraction of the chemical burden contained in snow is incorporated into firn and ice. Similarly to the snowpack, glaciers can be important sources of pollutants to surface waters: for example, Blais et al. (2001) showed that melting glaciers supply 50 to 97% of the organochlorine pesticide input to the sub-alpine Bow Lake (Alberta, Canada).

The timing of contaminant release from snow and ice with respect to the seasonal cycle of ecosystems is crucial: in high-altitude areas, snow and ice melt often coincide with periods of intense biological activity, when organisms are at a vulnerable stage of development (Meyer and Wania, 2008). Moreover, such ecosystems experience extremely harsh conditions such as daily and seasonal extremes in temperature, wind speed and water discharge; for this reason, the growing season is limited and survival, development and reproduction of organisms is difficult (F  reder et al., 2005). However, only few comprehensive studies were conducted on the occurrence and fate of POPs in organisms living at high altitudes (e.g., Grimalt et al., 2001; Blais et al., 2003; Vives et al., 2004a, 2004b, 2004c; Bartrons et al., 2007).

In such context, in which pulsed pollutant loadings and fast biological cycles regulate water contamination and bioaccumulation, dynamic models could play a vital role in the understanding of the fate of POPs and their transfer to the ecosystems. This has been underlined in a recent opinion of the three scientific committees of the European Commission (EU, SCHER (Scientific Committee on Health) et al., 2013). Additionally, the lack of temporally and spatially resolved concentrations in water and sediment does not allow to evaluate realistic concentrations of exposure (Di Guardo and Hermens, 2013). The prediction of the potential for snowmelt to cause spring concentration peaks in water, air and soil has been the object of a number of publications: for example, Daly and Wania (2004) incorporated a snow compartment into a dynamic model to investigate the effect of snow on the temporal variability of the concentrations of some organic contaminants. Despite the inclusion of a snow or ice compartment that could substantially improve fate predictions, model parameterization (e.g., snow and ice melting rates) could be extremely difficult. Moreover, there is quite a large spatial variability in snow and ice accumulation as well as for melting patterns; such heterogeneity could be hard to assess given the low accessibility typical of high-altitude areas. In hydrological models, snow and ice melt contributions are generally computed using either energy balance approaches, which attempt to quantify melt as residual in the heat balance equation, or temperature-index approaches, which assume an empirical relationship between air temperatures and melt rates (Hock, 2003). While the former can provide a more accurate picture of runoff deriving from snow and ice melt, they require data which are generally not available in cold, remote regions (Mou et al., 2008); in contrast, temperature-index models rely on temperature, which correlates well with melt, and are the most widely used approaches for runoff computations from glacierized basins (Singh et al., 2008).

In this work, the concentrations of three POPs (PCB 70, PCB 101 and p,p'-DDE) measured in the Frodolfo stream (Italian Alps) (Bizzotto et al., 2009a) were selected and used as model compounds to reconstruct water concentration profiles deriving from ice and snow melt during the year 2006 and to investigate the subsequent accumulation patterns in four macroinvertebrate trophic groups for which concentrations of POPs were measured in the same year (Bizzotto et al., 2009b); this was done by means of a dynamic organism–water–sediment model, in which the organism compartment was parameterized to simulate individuals belonging to the macroinvertebrate groups sampled in the Frodolfo stream. The model incorporated a hydrological module which permitted the estimation of water discharge and snow/ice melt contributions on an hourly basis. This allowed to: (I) observe the influence of the high variability of environmental characteristics (e.g., water discharge) and organism properties (e.g., organism volume and lipid fraction) on pollutant concentrations in water and on the consequent accumulation in aquatic organisms and (II) preliminarily calculate chemical loadings to the Frodolfo stream determined by the melting of the glacier and of the snowpack.

## 2. Materials and methods

### 2.1. Case study description

During the year 2006, water, sediment and macroinvertebrate sampling campaigns were performed on the Frodolfo stream, a glacial stream fed by the Forni glacier (Ortles–Cevedale group, Italian Alps) in order to investigate the concentrations of a number of POPs and their relationship with glacier and snow melt (Bizzotto et al., 2009a,b). Investigated chemicals included DDTs (dichlorodiphenyltrichloroethane, all isomers and metabolites), HCB (hexachlorobenzene),  $\alpha$ -,  $\beta$ - and  $\gamma$ -HCH (hexachlorocyclohexane), and a selection of PCB congeners (from trichloro- to octachloro-biphenyls). The sampling campaigns were performed on May 31st, June 18–19th, July 18–19th, September 12th, and October 11th. Frodolfo stream water and sediment were collected at four sites located at different distances from the glacier lobe, while organisms were sampled at one of the four sites, located at a distance of about 2.5 km from the glacier lobe; in such site environmental characteristics that allow a benthic community to reach a relatively high level of biodiversity. Details concerning the sampling and analytical results can be found in Bizzotto et al. (2009a,b).

Fig. 1 shows the location of the study area in the Italian Alps, together with a map of the Frodolfo stream course from its source (the Forni glacier) and the site investigated in the present work (i.e., the site in which macroinvertebrates were collected).

### 2.2. Modeling approach

EcoDynA (Infantino et al., 2013), a fugacity-based model (Mackay, 2001) developed to investigate the fate of organic chemicals in a dynamic organism–water–sediment system, was used for the simulations. In EcoDynA, chemical fate in the three compartments (organism, water and sediment) is described by a system of 1st-order ordinary differential equations (ODEs), one for each compartment, which is solved using a 5th-order adaptive, diagonally implicit Runge–Kutta numerical method (Semplice et al., 2012).

Model dynamics concern not only chemical emission (which can be varied on an hourly basis) but also environmental and organism properties. More specifically, model input include hourly values of parameters such as water temperature, water inflow and outflow and suspended solid concentration in water. In the current version of EcoDynA, suspended solids are modeled as a water sub-compartment, and the presence of particulate organic carbon (POC) is simulated by specifying the organic fraction of suspended solids. Organism properties can also be input on an hourly basis and include organism volume and

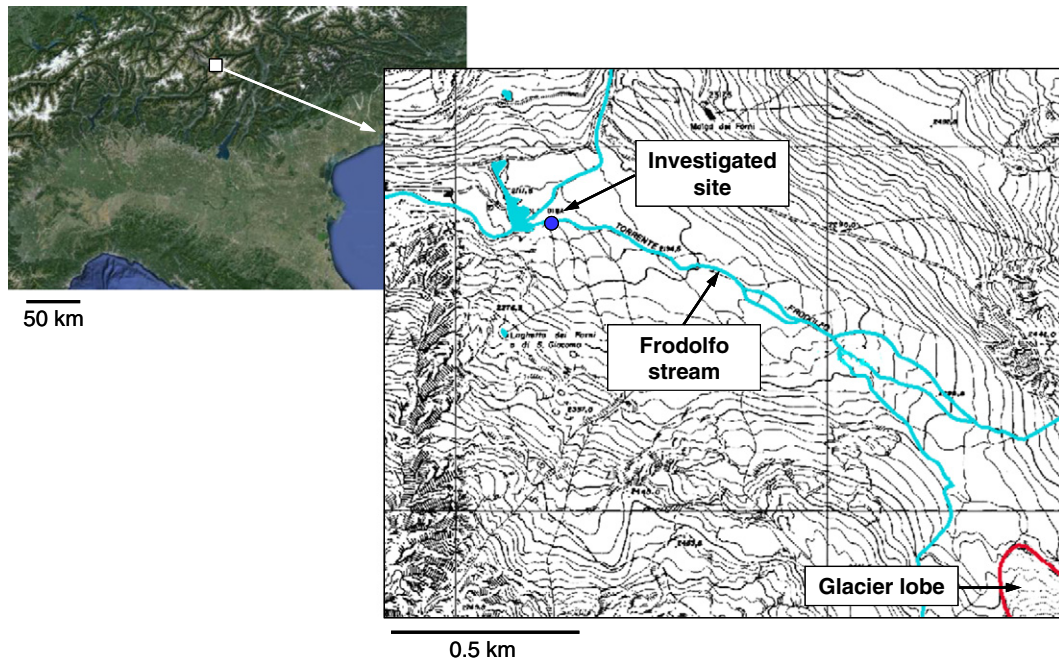


Fig. 1. Location of the study area in the Italian Alps, of the investigated site on the Frodolfo stream, with respect to the Forni glacier frontal lobe. Satellite image from Google Maps (2014).

lipid fraction, feeding rate, gut absorption efficiency, digestion factor, metabolism half-life and lipid fraction in food.

In the present work, the organism compartment was parameterized to simulate single macroinvertebrate representative individuals belonging to different trophic groups (see Section 2.4). Uptake from food was modeled considering food in equilibrium with water. More details on model formulation can be found in Infantino et al. (2013), which also illustrates an application of EcoDynA to a case of bioaccumulation of DDTs in fish.

### 2.3. Environmental scenario

The EcoDynA model was parameterized to simulate a 50-m segment of the Frodolfo stream (Fig. S1 1). Daily averages of water discharge measured at a dam located about a hundred meters downstream from the investigated site were obtained by A2A Company (Bondiolotti, personal communication). However, (i) measured discharge includes different contributions (snow and ice melt, precipitation) and provides no information on how such contributions could be distinguished and (ii) since glacier-fed rivers are characterized by high diel fluctuations in discharge (Cuffey and Paterson, 2010), the use of daily averages as model input can be misleading. For these reasons, in the present work, an effort was made to calculate hourly values of water discharge from estimates of snow and ice melt on an hourly basis.

For a period of  $n$  time intervals, temperature-index models can be described as follows (Hock, 2003):

$$\sum_{i=1}^n M_i = DDF \sum_{i=1}^n T_i^+ \Delta T \quad (1)$$

where  $M_i$  (mm) is the amount of ice or snow melt in the time interval  $i$ ,  $DDF$  ( $\text{mm d}^{-1} \text{ } ^\circ\text{C}^{-1}$ ) is a proportionality factor known as “degree-day factor”,  $T_i^+$  ( $^\circ\text{C}$ ) is the sum of positive air temperatures in  $i$ , and  $\Delta T$  (d) is the duration of  $i$ . Given the need for hourly values of discharge, Eq. (1) was modified as follows:

$$M_h = \frac{DDF}{dT_h} T \quad (2)$$

where  $M_h$  (mm) is the amount of ice or snow melt in the time interval of 1 h,  $dTh$  ( $= 24 \text{ h d}^{-1}$ ) is a unit conversion factor, and  $T$  ( $^\circ\text{C}$ ) is a positive air temperature. No melt was assumed for  $T \leq 0$   $^\circ\text{C}$ . Since DDF depends on a number of factors (e.g., solar radiation, albedo, snow/ice physical properties) which considerably vary in space and time (e.g., seasonally), DDF itself is also subject to such variability (Singh et al., 2008; Hock, 2005). However, for simplicity, in the present work fixed values of DDF for snow and ice were adopted. Hourly air temperatures for the year 2006 were acquired for the “Valfurva - Forni” meteorological station (2118 m a.m.s.l.) (ARPA Lombardia, 2014). Hourly observations of precipitations were also collected, in order to calculate runoff deriving from rain.

For computations, the total watershed area (29  $\text{km}^2$ ) was divided into 9 elevation zones (Fig. S1 2) (altitude interval = 200 m), in which the glacierized and non-glacierized areas were distinguished. In order to calculate snow cover, temporal profiles of the snow line for both ice-covered and ice-free areas throughout 2006 were defined (SGL, 2006). This allowed the estimation of the temporal variation of the snow covered areas for each elevation zone. Ice melt was assumed to occur in case of free ice-surface only. For each elevation zone, temperature records were corrected using a lapse rate of 0.6  $^\circ\text{C}$  every 100 m (Singh et al., 2008). In case of precipitation, rain contribution to runoff was calculated when  $T \geq 1$   $^\circ\text{C}$  only. Infiltration and sub-surface runoff were neglected, but for all contributions (from snow/ice melt and rain) a delay of 2 days was adopted to account for water transport from its source in the watershed to the investigated site. This 2-day time lag was a result of the calibration process to account for partial melting and accumulation processes along the watershed; furthermore, for rain contribution, a “retention factor” was applied (see Section 3.1).

The hourly values of  $M_h$  (mm) computed using Eq. (2) for snow and ice were converted into meters and multiplied by the corresponding snow or ice covered areas, in order to obtain runoff fluxes ( $\text{m}^3 \text{ h}^{-1}$ ). By adding the rain contribution, hourly discharge estimates were obtained. Such values were used as inflow and outflow rates from the 50-m stream segment; hourly values of water volume were then calculated assuming a rectangular section and establishing the relationships “discharge–stream width” and “discharge–water level” in order to derive hourly values of such parameters. Details are reported in Text S1 1.

Since suspended solids concentrations (SSC) can also vary during the day, and variations are often related to discharge (Lenzi et al., 2003; Singh et al., 2005; Haritashya et al., 2010; Iida et al., 2012; Wulf et al., 2012), a relationship was built in order to derive hourly values of SSC (see Section 3.1); such relationship was grounded on SSC values measured in Frodolfo stream water sampled during summer campaigns in 2011 and 2013, as described in Text SI 2.

For the simulations presented here, sediment depth was set to 5 mm, basing on field observations; this value was obtained from a weighted average, considering that 1/10 of the riverbed was occupied by 5-cm deep sediment, while the remainder by cobbles and boulders with no sediment on them. This simplification was required because of the non-spatial nature of the sediment compartment in the model. Since measurements conducted in the Frodolfo stream from May to October 2006 revealed an almost constant temperature of approximately 5 °C (Bizzotto et al., 2009b), such value was adopted for the simulations. In Table SI 3 the values selected for static environmental parameters and mass-transfer coefficients (MTCs) are reported.

#### 2.4. Organism compartment

Information concerning the typical macroinvertebrate community structure in glacier-fed Alpine streams can be found in Text SI 3. These organisms represent the most abundant/representative species for each trophic level. Such picture is confirmed by the organism sampling performed in 2006 in the Frodolfo stream (Bizzotto et al., 2009b). Starting from such knowledge, 4 keystone species, classified according to their trophic role (Vannote et al., 1980), were selected for the simulations: *Baetis alpinus* (Baetidae) and *Diamesa nivoriunda* (Chironomidae) for collectors, *Rhithrogena nivata* (Heptageniidae) for scrapers and a stonefly of the family Perlodidae (*Dictyogenus fontium*) for predators.

For the simulations presented here, temporal profiles of organism volume (Fig. SI 9) were built for all the macroinvertebrate species; such profiles were derived from growth rates and relationships between body length and mass available in the literature (Berg and Hellenthal, 1991; Ritter, 1990; Cereghino and Lavandier, 1998). Despite the fact that lipid fraction in macroinvertebrates is known to vary with time and is generally maximum in summer (Meier et al., 2000), fixed values of organism lipid fraction were adopted in the present work to match the ones measured in the macroinvertebrates sampled in the Frodolfo stream in 2006 (Bizzotto et al., 2009b). More details can be found in Text SI 3. Given the lack of data, the other organism properties were kept constant throughout the simulation period: values for digestion factor (4), gut absorption efficiency (63%), and feeding rate (4% body weight  $d^{-1}$ ) were taken from Campfens and Mackay (1997). A high chemical metabolic half-life (i.e., 10,000 d) was adopted as typical of non-metabolizing substances. Collectors and scrapers were assumed

to feed on periphyton, for which a lipid content of 0.3% was adopted (Walters et al., 2008). Predators were assumed to feed on Chironomidae (70%), Baetidae (10%), Heptageniidae (10%) and Perlodidae themselves (10%) (Silveri et al., 2008, 2009; Fenoglio et al., 2007), with their corresponding lipid fraction; predator feeding preferences were adapted according to prey availability (see Fig. SI 9).

#### 2.5. Chemicals

Two PCB congeners (PCB 70 and 101) and p,p'-DDE were selected for the simulations as model substances; this allowed to investigate the fate of chemicals which, during the 2006 campaign on the Frodolfo stream, had shown different behaviors (Bizzotto et al., 2009a). Among DDT isomers and metabolites, p,p'-DDE only was always found; its water bulk concentrations were similar in May and June ( $\sim 60 \text{ pg L}^{-1}$ ), peaked in July ( $1323 \text{ pg L}^{-1}$ ) and decreased to about  $80 \text{ pg L}^{-1}$  in September and October. In contrast, all the analyzed PCBs occurred at the highest levels in June. PCB 70 concentrations were of  $30 \text{ pg L}^{-1}$  in May,  $2526 \text{ pg L}^{-1}$  in June, again  $30 \text{ pg L}^{-1}$  in July, and not detectable in September and October; similarly, PCB 101, which was not detected in May, peaked in June ( $5091 \text{ pg L}^{-1}$ ), decreased to  $76 \text{ pg L}^{-1}$  in July and to lower levels (near the method detection limit) in the following months. In Table SI 4 the physical-chemical properties adopted for the three chemicals are listed.

### 3. Results and discussion

#### 3.1. Water discharge

The first effort was devoted to estimate the contributions of snow and ice melt to total discharge on an hourly basis. In order to do so, DDF values for snow and ice were calibrated to obtain the best fit between predicted and measured average daily discharges, which were the only experimental data available concerning stream flow. Fig. 2 reports the results of the comparison. The adopted DDF values ( $3.7 \text{ mm d}^{-1} \text{ } ^\circ\text{C}^{-1}$  for snow and  $7.1 \text{ mm d}^{-1} \text{ } ^\circ\text{C}^{-1}$  for ice) were in line with those found in the literature (e.g., Hock, 2005; Pellicciotti et al., 2005). In order to account for the loss of water due to infiltration and evaporation, precipitation contribution to runoff was scaled using a "retention factor", which was also calibrated in order to improve the fit; the optimal value was found to be 0.45.

Generally, a good agreement was obtained ( $R^2 = 0.66$ , Fig. SI 13). The best fit was observed for the central part of the year, from May to August; an exception was the underestimation in the first half of July. Poorer fit, mostly due to an overestimation of the snow contribution, was observed in spring, especially in April, and from September to November. On a yearly basis, a total discharge of  $6.46 \cdot 10^7$  was predicted, while from measured data a value of  $5.54 \cdot 10^7$  can be obtained. Such discrepancies can be ascribed to the assumptions made for runoff

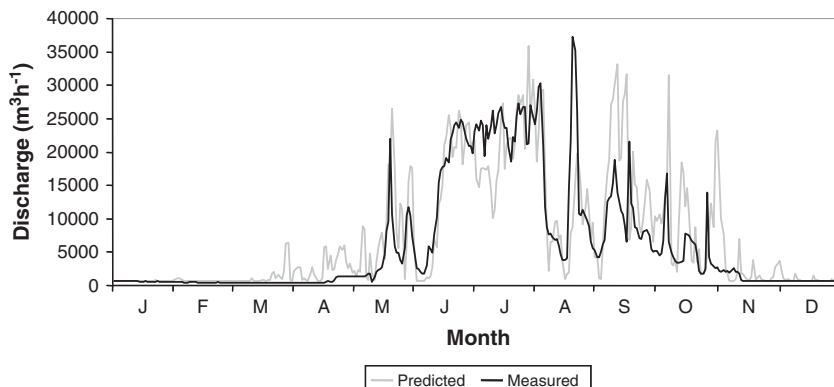


Fig. 2. Comparison between predicted and measured discharge ( $\text{m}^3 \text{ h}^{-1}$ ). For comparison purposes, hourly predictions were averaged on a daily basis.

calculations, in particular to the use of fixed values of DDF, of a “retention factor” for liquid precipitations instead of accounting for infiltration, and to the adoption of a 2-day lag instead of accounting for sub-surface runoff. Moreover, it must be remarked that predictions were compared to measured values computed assuming Frodolfo discharge was equal to 2/3 the discharge provided by A2A (Bondiolotti, personal communication), since in the original values the contribution of a relatively important stream (coming from the Cedèc Valley) was included; this factor was selected on the grounds of field observations, but it is unlikely to be constant during the year. A picture of the temporal variation of the different contributions to total discharge is provided in Fig. 3, where the different sources (minimum flow, snow melt, ice melt and rain) are distinguished. Ice melt mainly occurred in July, August and September; snow melt was always dominant, except on some occasions during the month of August, when ice melt prevailed. The first relevant episode of snow melt occurred in late June, when most of the winter snow pack over terrain in the Frodolfo watershed melted. Finally, the contribution of liquid precipitation was limited, in some cases comparable to minimum stream flow. Given the number of assumptions and the lack of data which would have been necessary in order to apply a more accurate melt model, the obtained agreement was considered satisfying; this allowed the computed hourly discharges and relative contributions from the different sources to be used for chemical loading calculations (see Section 3.3).

### 3.2. Suspended solids

A positive correlation between discharge and suspended solid concentration (SSC) generally exists (e.g., Lenzi et al., 2003; Iida et al., 2012; Wulf et al., 2012); such relationship is strong at the beginning and at the end of the ablation period and poorer in the peak melt season. In the latter case some events may occur so as to increase SSC to a much higher extent than discharge (Singh et al., 2005). Since no data concerning suspended solids were available from the 2006 campaigns on the Frodolfo stream, field investigations were conducted in 2011 and 2013, in order to obtain an estimate of SSC. Sampling and analysis are discussed in detail in Text SI 2. Results (Fig. SI 7) showed concentrations in the range of 1000 to 2000 mg L<sup>-1</sup> in all the three afternoon samples, while water sampled in the morning revealed SSCs which were lower by more than one order of magnitude with respect to the afternoon ones. All the measured values were in line with those found in the literature for glacial streams (e.g., Haritashya et al., 2010). Starting from the obtained data, a linear relationship between the hypothesized discharge at the sampling times and the measured SSCs was built, which allowed the calculation of hourly values, which were used as model input (Fig. SI 8). The solids obtained from the filtration of the water samples collected in 2013 were also analyzed for organic carbon content (see Text SI 2); results indicated a very low organic carbon content, of

0.74% (S.D. = 0.03) in the morning water and 0.38% (S.D. = 0.01) in the afternoon one. Given the lack of other information, the latter value was adopted as static organic carbon fraction of suspended solids.

### 3.3. Chemical concentrations in water

For the investigated chemicals, temporal profiles of bulk water concentrations were derived assigning time-varying concentrations to melting snow and ice; this allowed the calculation of hourly chemical loadings to the water compartment. Although some evidence of increased background air concentrations around contaminated sites close to two former production plants in northern Italy exists for DDT (Di Guardo et al., 2003, 2008) and PCBs (Colombo et al., 2013), their influence in terms of potential secondary sources of POPs to the Alps is still to be properly quantified. However, some data seem to confirm higher PCB level in the snow of the Alps (Carrera et al., 2001). Given the total lack of data concerning local soil and snow characteristics, no chemical loadings were assumed to derive from rainfall and subsequent runoff. A fit with the contaminant concentrations measured in the Frodolfo stream in 2006 (Bizzotto et al., 2009a) was pursued; this was performed with the only aim of investigating the potential exposure levels (and thus accumulation in organisms) when measures were not available. The obtained temporal profiles of bulk water concentrations (pg L<sup>-1</sup>) for the selected contaminants are reported in Fig. 4. PCB 70 and 101, as all the other measured PCB congeners, peaked in June (see Section 2.5 and Bizzotto et al., 2009a). From Fig. 3 it is evident that, starting from the second half of June, snow melt represented the main contribution, accounting from 65 to 95% of the total discharge. Since in July PCB concentrations decreased although snow melt contribution was still important (5–85%) and ice melt occurred at high rates (5–75%), it was hypothesized that the first snow melt water reaching the stream was highly concentrated. The observed PCB levels also suggested that the contribution from ice melt was relatively unimportant. According to these considerations, during all the simulation year, with the exception of the second half of June, snow concentrations of 15 pg L<sup>-1</sup> for PCB 70 and 20 pg L<sup>-1</sup> for PCB 101 were assigned. Such values are within the range of the ones measured in nearby locations (data presented for the first time in this work, reported in Text SI 4). Fixed concentrations were assigned to ice (60 pg L<sup>-1</sup> for PCB 70, 100 pg L<sup>-1</sup> for PCB 101); such values are similar to the ones measured in a 300-km far Alpine glacier (Villa et al., 2001). In order to match the PCB levels measured in June, concentration of 5 ng L<sup>-1</sup> for PCB 70 and 15 ng L<sup>-1</sup> for PCB 101 were necessary; these values are more than two orders of magnitude higher than the ones measured in the snow sampled in nearby locations (Text SI 4) and other Alpine sites (Herbert et al., 2004; Finizio et al., 2006) and would indicate the concentration occurred in the winter snowpack before late-spring sudden

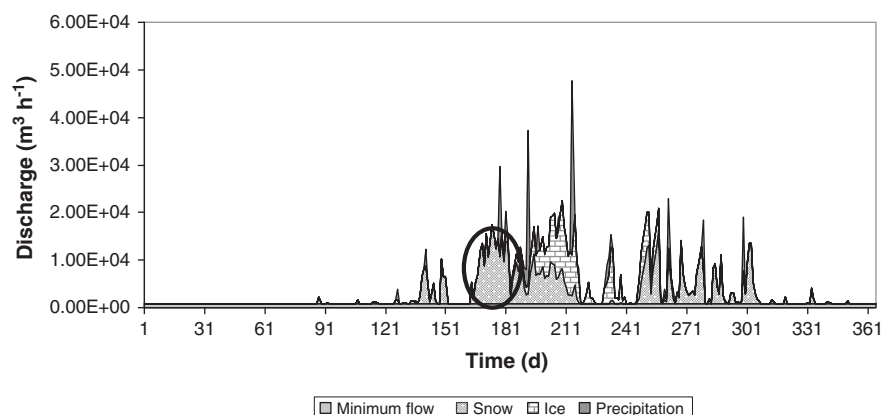
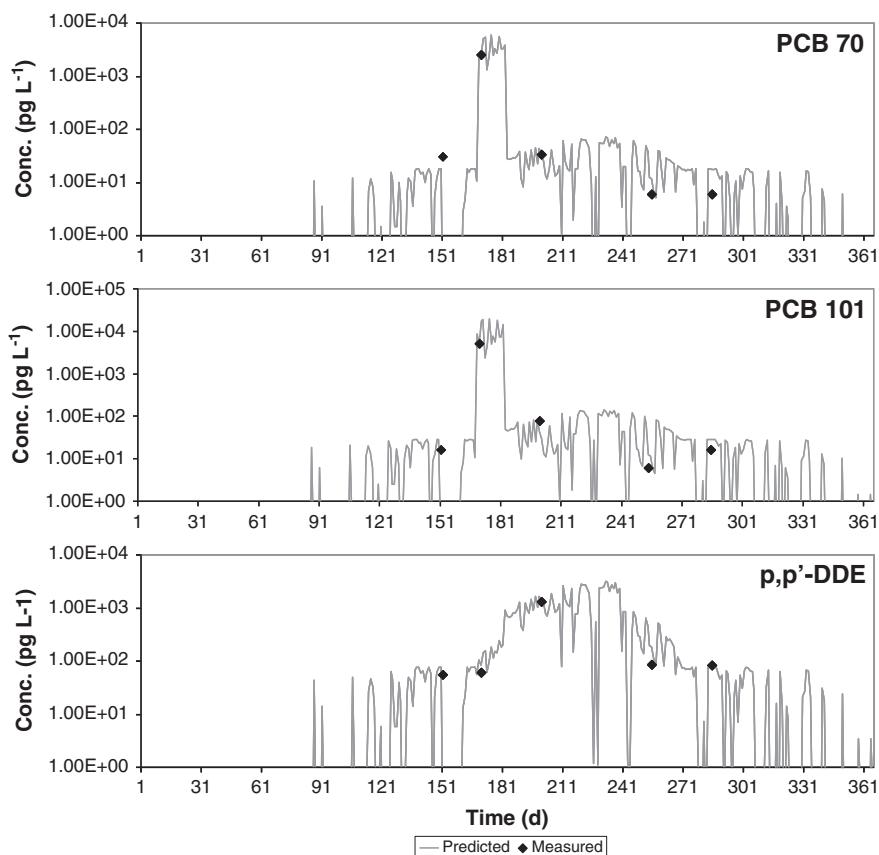


Fig. 3. Temporal profile of computed discharge (daily averages, m<sup>3</sup> h<sup>-1</sup>) divided according to the different contributions. The circle indicates the late-spring flush due to sudden snow melt.



**Fig. 4.** Temporal profiles of bulk water concentrations ( $\text{pg L}^{-1}$ ) obtained for the modeled chemicals. Gray lines depict model results, while markers represent measured concentrations. The y-axis is on a log-scale.

melt. It is known that, if the snowpack is relatively warm, the wet snow metamorphism preceding the melt period may concentrate chemicals (Meyer and Wania, 2008); in the subsequent melt phase, which can be extremely rapid (a few days or weeks), chemicals may be rapidly released to surface waters in two distinct flushes (water-dissolved and particle-bound). Given the high  $\log K_{OW}$  values of both PCB 70 and 101 (6 and 6.4, respectively), the two chemicals are expected to be eluted from the snowpack with a certain time delay with respect to the first melt water formation, due to their affinity to organic particles (Daly and Wania, 2004; Meyer and Wania, 2008). However, Lafrenière et al. (2006) measured very high concentrations even of the most hydrophobic compounds (e.g., DDTs, PCBs) in the first snowmelt samples taken from an alpine snowfield. This was ascribed to a low content of particulate organic matter in the snowmelt water, which would have kept even the more hydrophobic substances in the dissolved phase. A similar situation, confirmed by a low organic carbon content of the suspended solids in the Frodolfo stream (see Section 3.2), could be associated to this case study. It was observed that, even during high-SSC episodes (i.e., in case of elevated discharges), the low organic carbon content resulted in a negligible influence of suspended solids in determining reduced water-dissolved contaminant concentrations.

In contrast, p,p'-DDE peaked in July (see Section 2.5 and Bizzotto et al., 2009a), and the same behavior was described in a previous study on the Frodolfo stream (Villa et al., 2006a). A fixed snow concentration of  $70 \text{ pg L}^{-1}$  was adopted, equal to the minimum concentration measured in the snow sampled in 2008 (Text SI 4); since no late-spring peak was observed for this chemical, no p,p'-DDE enrichment in snow was assumed to occur. In ice, a fixed chemical concentration of  $1000 \text{ pg L}^{-1}$  was assumed, except for the month of July: it was observed that, in order to match the concentration value measured in the Frodolfo stream, a concentration in ice of  $3000 \text{ pg L}^{-1}$  was necessary. No data

concerning p,p'-DDE concentration in Alpine glaciers were available for a comparison, but the adopted values were one order of magnitude higher than the concentrations measured in firn at a 300-km far Alpine site (Villa et al., 2006b).

### 3.4. Bioaccumulation in organisms

In Figs. 5, 6 and 7 the results of the comparison between predicted and measured concentrations ( $\text{ng g}^{-1} \text{ d.w.}$ ) of the investigated chemicals in the four modeled macroinvertebrate species are reported.

A preliminary sensitivity analysis conducted on the EcoDynA model revealed that the parameters which mostly affect organism concentrations are organism lipid fraction, gut absorption efficiency, feeding rate and lipid fraction in food (Infantino et al., 2013). Given the high uncertainty associated to such parameters, it was chosen to perform additional simulations increasing and decreasing the most influential one (i.e., organism lipid fraction) of 50% (gray lines in the figures). A different fresh to dry weight ratio for each macroinvertebrate group was used to convert concentration to a dry weight basis; these values, measured in the organism sampled in the Frodolfo stream in 2006, were 4.2 for collectors, 3.5 for scrapers, 3.55 for predators.

Considering all uncertainties in model input, a satisfying agreement between predictions and observations was generally observed for PCB 70; the best model performance concerned scrapers (Heptageniidae) and predators (Perlodidae), while for Baetidae and Chironomidae the model underestimated July and September concentrations of a factor of 2 to 7. A similar good model performance was observed for PCB 101, for which the only underestimated concentration was the September one for collectors and scrapers (factor of 2 to 4). The comparison between predicted and measured p,p'-DDE concentrations was less satisfying, since the model generally underestimated chemical levels in

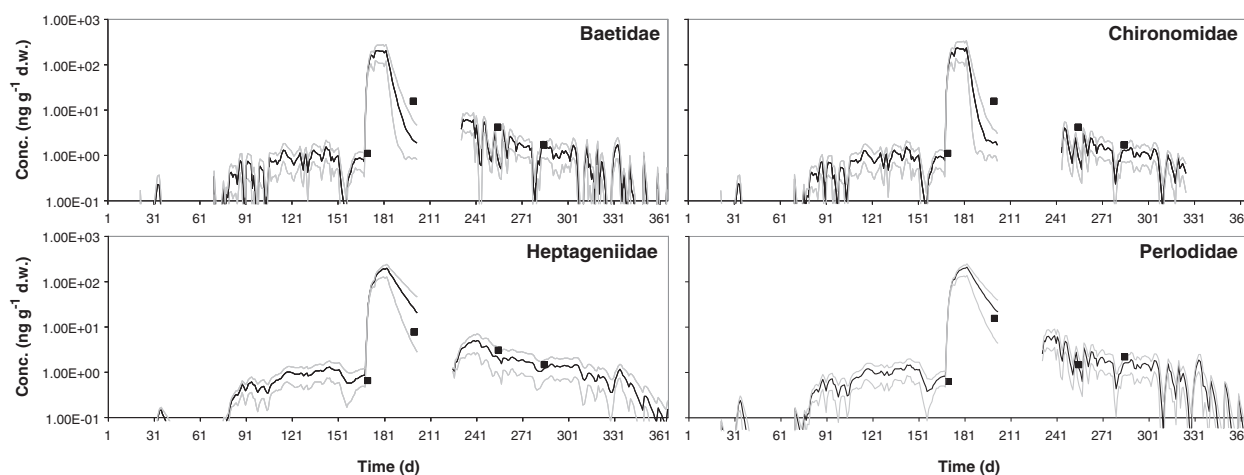


**Fig. 5.** Comparison between PCB 70 measured and predicted concentrations ( $\text{ng g}^{-1} \text{d.w.}$ ) in the modeled organisms. Black lines represent model predictions obtained using organism lipid fractions described in Text SI 3, while gray lines represent model predictions obtained increasing (upper line) or decreasing (lower line) organism lipid fraction of 50%. Markers indicate measured values. The y-axis is on a log-scale.

all macroinvertebrates, in some cases even of one order of magnitude. As for PCB 70, the best agreement was observed for scrapers and predators. Despite the fact that uptake from food is usually one of the most important bioaccumulation pathways for hydrophobic and persistent organic chemicals in aquatic organisms such as fish or macroinvertebrates, it was substantially negligible for collectors and scrapers; in contrast, it was relatively important for predators, responsible for 15% of the accumulation of PCB 70, 30% of PCB 101, and 12% of p,p'-DDE.

The observed discrepancies could be attributed, for example, to the use of static values of organism lipid fraction and other organism parameters (e.g., absorption efficiency and feeding rate) instead of temporal profiles. More accurate data on the modeled organisms could dramatically improve model performance. Moreover, considering food in equilibrium with water could also be misleading; this could be overcome by simulating a food web, although much more information would be required.

### 3.5. Considerations on chemical loadings to surface water

The modeling effort presented in this work allowed a very preliminary and rough estimation of the total amounts of the investigated pollutants which were released to Frodolfo stream water from ice and snow during 2006. According to our calculations, the total released amounts were  $2.86 \cdot 10^{-2} \text{ kg}$  for PCB 70,  $8.64 \cdot 10^{-2} \text{ kg}$  for PCB 101,

and  $4.09 \cdot 10^{-2} \text{ kg}$  for p,p'-DDE. While for PCB 70 and 101 the most important contribution was snow melt, accounting for about 98% of the total chemical burden, for p,p'-DDE ice was the main chemical source (92%). These results highlight the possible valuable role of dynamic modeling approaches such as the one presented here in the estimation of the consequences of changing climate regimes on exposure levels and environmental fate of POPs stored in cold archives such as glaciers. This modeling approach could help in the identification and quantification of chemical sources to surface waters in these circumstances. Starting from basic information concerning the environmental scenario (watershed morphology, air temperatures, ice cover, etc.) and from some measured chemical concentrations in surface water, snow or ice, temporal profiles of chemical concentrations could be obtained. Moreover, possible scenarios characterized by higher air temperatures or more intense precipitation events could be investigated.

## 4. Conclusions

A dynamic organism–water–sediment modeling approach was combined with a hydrological module capable of estimating water discharge and snow/ice melt contributions on an hourly basis, starting from hourly air temperatures. The application of the model to the Frodolfo case study showed its adequacy for the estimation of pollutant concentrations in surface waters and consequent bioaccumulation in

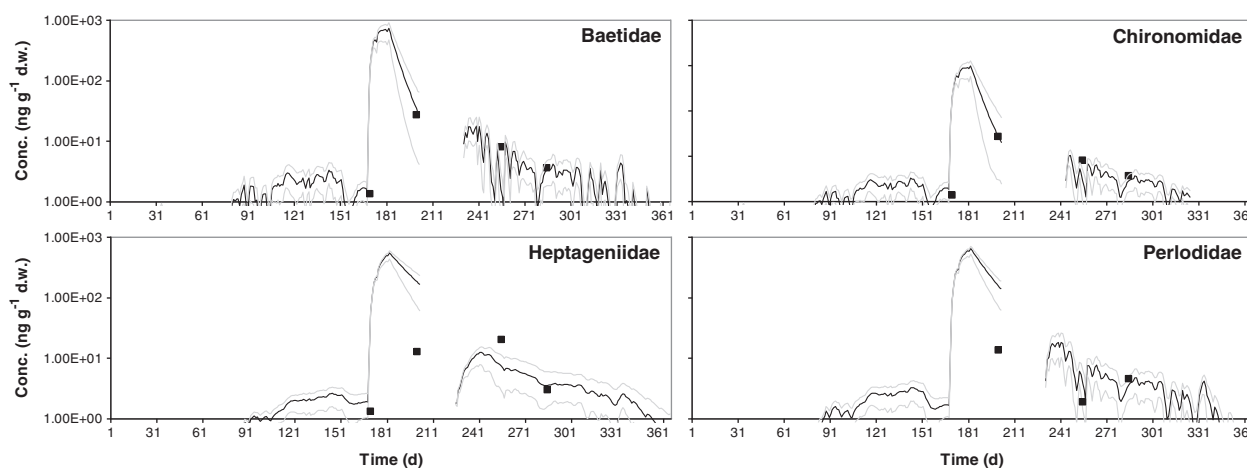


**Fig. 6.** Comparison between PCB 101 measured and predicted concentrations ( $\text{ng g}^{-1} \text{d.w.}$ ) in the modeled organisms. Black lines represent model predictions obtained using organism lipid fractions described in Text SI 3, while gray lines represent model predictions obtained increasing (upper line) or decreasing (lower line) organism lipid fraction of 50%. Markers indicate measured values. The y-axis is on a log-scale.

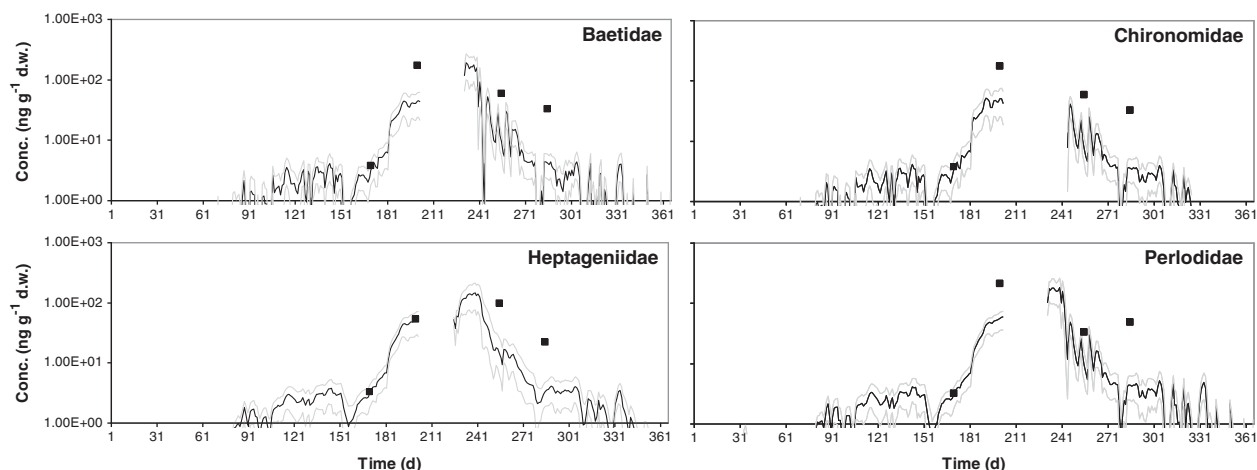


**Fig. 7.** Comparison between p,p'-DDE measured and predicted concentrations ( $\text{ng g}^{-1} \text{d.w.}$ ) in the modeled organisms. Black lines represent model predictions obtained using organism lipid fractions described in Text SI 3, while gray lines represent model predictions obtained increasing (upper line) or decreasing (lower line) organism lipid fraction of 50%. Markers indicate measured values. The y-axis is on a log-scale.

aquatic organisms. Given the sudden response to variation in concentrations of the organisms living in a very changing environment, the tool provided allows to obtain the magnitude of peak exposure. This is in turn important to evaluate potential toxic effects of such dynamic exposure pattern. Additionally, the possible role of the model in assessing the consequences of climate change on cycle of POPs was also highlighted.

For a more thorough calibration and validation of the modeling approach presented here, which will be the object of future work, more information will be needed: for example, higher-temporal resolution water and organism samplings, as well as more detailed information on organism parameters (especially the most influential ones). More complete sensitivity and uncertainty analyses need also to be performed. However, the results presented here show the potential benefits of a dynamic predictive tool in the calculation of exposure variation in time of macroinvertebrates and, potentially, further levels in the food web for an alpine stream.

## Acknowledgments

We wish to thank Dr. Bruno Maiolini (Edmund Mach Foundation, San Michele all'Adige, Trento, Italy) for his help in the identification and characterization of key stone species representative of the alpine glacial stream macroinvertebrate community. We would also like to thank Eng. Ferdinando Bondiolotti (A2A company, Brescia, Italy) for kindly providing water discharge data and Dr. Walter Maggi (DISAT, University of Milano-Bicocca) for his help on the glacier dynamics. We would also like to thank Dr. Elisa Bizzotto and Dr. Elisa Terzaghi for their help during the field work and Dr. Alfonso Infantino for the initial modeling activities.

## Appendix A. Supplementary data

Supplementary data to this article can be found online at <http://dx.doi.org/10.1016/j.scitotenv.2014.05.150>.

## References

ARPA Lombardia. ARPA meteo website homepage. <http://www2.arpalombardia.it/siti/arpalombardia/meteo/previsionimeteo/meteolombardia/Pagine/default.aspx>, 2014. [Last accessed: March 27, 2014].

Bartrons M, Grimalt JO, Catalan J. Concentration changes of organochlorine compounds and polybromodiphenyl ethers during metamorphosis of aquatic insects. *Environ Sci Technol* 2007;41:6137–41.

Berg MB, Hellenthal RA. Secondary production of Chironomidae (Diptera) in a north temperate stream. *Freshw Biol* 1991;25:497–505.

Bizzotto EC, Villa S, Vaj C, Vighi M. Comparison of glacial and non-glacial-fed streams to evaluate the loading of persistent organic pollutants through seasonal snow/ice melt. *Chemosphere* 2009a;74:924–30.

Bizzotto EC, Villa S, Vighi M. POP bioaccumulation in macroinvertebrates of alpine freshwater systems. *Environ Pollut* 2009b;157:3192–8.

Blais JM, Schindler DW, Sharp M, Braekvelt E, Lafrenière M, McDonald K, et al. Fluxes of semivolatile organochlorine compounds in Bow Lake, a high-altitude, glacier-fed subalpine lake in the Canadian Rocky Mountains. *Limnol Oceanogr* 2001;46(8):2019–31.

Blais JM, Wilhelm F, Kidd KA, Muir DCG, Donald DB, Schindler DW. Concentrations of organochlorine pesticides and polychlorinated biphenyls in amphipods (*Gammarus lacustris*) along an elevation gradient in mountain lakes of Western Canada. *Environ Toxicol Chem* 2003;22(11):2605–13.

Campfens J, Mackay D. Fugacity-based model of PCB bioaccumulation in complex aquatic food webs. *Environ Sci Technol* 1997;31:577–83.

Carrera G, Fernandez P, Vilanova RM, Grimalt JO. Persistent organic pollutants in snow from European high mountain areas. *Atmos Environ* 2001;35:245–54.

Cereghino R, Lavandier P. Influence of hydropeaking on the distribution and larval development of the Plecoptera from a mountain stream. *Regul Rivers Res Manag* 1998;14:297–309.

Colombo A, Benfenati E, Bugatti SG, Lodi M, Mariani A, Musmeci L, et al. PCDD/Fs and PCBs in ambient air in a highly industrialized city in northern Italy. *Chemosphere* 2013;90:2352–7.

Cuffey KM, Paterson WSB. The physics of the glaciers. 4th ed. Burlington: Butterworth-Heinemann; 2010.

Daly GL, Wania F. Simulating the influence of snow on the fate of organic compounds. *Environ Sci Technol* 2004;38:4176–86.

Di Guardo A, Hermens JLM. Challenges for exposure prediction in ecological risk assessment. *Integr Environ Assess Manag* 2013;9:4–14.

Di Guardo A, Zaccara S, Cerabolini B, Acciarri M, Terzaghi G, Calamari D. Conifer needles as passive biomonitors of the spatial and temporal distribution of DDT from a point source. *Chemosphere* 2003;52:789–97.

Di Guardo A, Nizzetto L, Infantino A, Colombo I, Saporiti E, Jones KC. Field derived accumulation and release kinetics of DDTs in plants. *Chemosphere* 2008;72:1497–503.

EU. SCHER (Scientific Committee on Health, Environmental Risks), SCENIHR (Scientific Committee on Emerging, Newly Identified Health Risks), SCCS (Scientific Committee on Consumer Safety). Addressing the new challenges for risk assessment. Opinion adopted in March 2013 [http://ec.europa.eu/health/scientific\\_committees/consumer\\_safety/docs/scscs\\_o\\_131.pdf](http://ec.europa.eu/health/scientific_committees/consumer_safety/docs/scscs_o_131.pdf), 2013.

Fenoglio S, Bo T, Malacarne G. Preimaginal feeding habits of *Dictyogenus fontium* (Plecoptera, Perlodidae) in an alpine brook in NW Italy. *Entomol Fenn* 2007;18:27–31.

Finizio A, Villa S, Raffaele F, Vighi M. Variation of POP concentrations in fresh-fallen snow and air on an Alpine glacier (Monte Rosa). *Ecotoxicol Environ Saf* 2006;63:25–32.

Franz TP, Eisenreich SJ. Snow scavenging of polychlorinated biphenyls and polycyclic aromatic hydrocarbons in Minnesota. *Environ Sci Technol* 1998;32:1771–8.

Füreder L, Wallinger M, Burger R. Longitudinal and seasonal pattern of insect emergence in alpine streams. *Aquat Ecol* 2005;39:67–78.

Google Maps. Google Maps homepage website [www.google.com/maps](http://www.google.com/maps), 2014. [Last accessed: March 12, 2014].

Grimalt JO, Fernandez P, Berdie L, Vilanova RM, Catalan J, Psenner R, et al. Selective trapping of organochlorine compounds in mountain lakes of temperate areas. *Environ Sci Technol* 2001;35:2690–7.

- Haritashya UK, Kumar A, Singh P. Particle size characteristics of suspended sediment transported in meltwater from the Gangotri Glacier, central Himalaya – an indicator of subglacial sediment evacuation. *Geomorphology* 2010;122:140–52.
- Herbert BMJ, Halsall CJ, Fitzpatrick L, Villa S, Jones KC, Thomas GO. Use and validation of novel snow samplers for hydrophobic, semi-volatile organic compounds (SVOCs). *Chemosphere* 2004;56:227–35.
- Herbert BMJ, Villa S, Halsall CJ. Chemical interactions with snow: understanding the behavior and fate of semi-volatile organic compounds in snow. *Ecotoxicol Environ Saf* 2006;63:3–16.
- Hock R. Temperature index modelling in mountain areas. *J Hydrol* 2003;282:104–15.
- Hock R. Glacier melt: a review of processes and their modelling. *Prog Phys Geogr* 2005;29(3):362–91.
- Iida T, Kajihara A, Okubo H, Okajima K. Effect of seasonal snow cover on suspended sediment runoff in a mountainous catchment. *J Hydrol* 2012;428–429:116–28.
- Infantino A, Morselli M, Di Guardo A. Integration of a dynamic organism model into the DynA Model: development and application to the case of DDT in Lake Maggiore, Italy. *Sci Total Environ* 2013;454–455:358–65.
- Lafrenière MJ, Blais JM, Sharp MJ, Schindler DW. Organochlorine pesticide and polychlorinated biphenyl concentrations in snow, snowmelt, and runoff at Bow Lake, Alberta. *Environ Sci Technol* 2006;40:4909–15.
- Lenzi MA, Mao L, Comiti F. Interannual variation of suspended sediment load and sediment yield in an alpine catchment. *Hydrol Sci J* 2003;48(6):899–915.
- Mackay D. Multimedia environmental models: the fugacity approach. 2nd ed. Boca Raton: Lewis Publishers; 2001.
- Meier GM, Meyer EI, Meyns S. Lipid content of stream macroinvertebrates. *Arch Hydrobiol* 2000;147(4):447–63.
- Meyer T, Wania F. Organic contaminant amplification during snowmelt. *Water Res* 2008;42:1847–65.
- Mou L, Tian F, Hu H, Sivapalan M. Extension of the representative elementary watershed approach for cold regions: constitutive relationships and an application. *Hydrol Earth Syst Sci* 2008;12:565–85.
- Pellicciotti F, Brock B, Strasser U, Burlando P, Funk M, Corripio J. An enhanced temperature-index glacier melt model including the shortwave radiation balance: development and testing for Haut Glacier d'Arolla Switzerland. *J Glaciol* 2005;51(175):573–87.
- Quémérais B, Lemieux C, Lum KR. Temporal variation of PCB concentrations in the St. Lawrence river (Canada) and four of its tributaries. *Chemosphere* 1994;28:947–59.
- Ritter H. Ephemeroptera emergence from a high mountain stream in Tyrol, Austria in mayflies and stoneflies. Life history and biology. In: Campbell IC, editor. Proceedings of the 5th International Ephemeroptera Conference and the 9th International Plecoptera Conference. 1990. Series Entomologica Netherlands: Springer; 1990. [53–59 pp.].
- Semplice M, Ghirardello D, Morselli M, Di Guardo A. Guidance on the selection of efficient computational methods for multimedia fate models. *Environ Sci Technol* 2012;46:1616–23.
- SGL (Servizio Glaciologico Lombardo). Commissione Scientifica. Campagna glaciologica 2006. Alpi Centrali Italiane; 2006. <http://www2.sgl.cluster.it/Joomla1.5/> [Last accessed: March 27, 2014.].
- Silveri L, Tierno de Figueroa JM, Maiolini B. Feeding habits of Perlodidae (Plecoptera) in the hyporheic habitats of Alpine streams (Trentino-NE Italy). *Entomol Fenn* 2008;19(3):176–83.
- Silveri L, De Figueroa JT, Maiolini B. Life cycle and nymphal feeding in the stonefly species *Chloroperla susemicheli* (Plecoptera: Chloroperlidae). *Entomologia Generalis* 2009;32(2):97–103.
- Singh P, Haritashya UK, Ramasastri KS, Kumar N. Diurnal variation in discharge and suspended sediment concentration, including runoff-delaying characteristics, of the Gangotri Glacier in the Garhwal Himalayas. *Hydrol Processes* 2005;19:1445–57.
- Singh P, Haritashya UK, Kumar N. Modelling and estimation of different components of streamflow for Gangotri Glacier basin Himalayas. *Hydrol Sci J* 2008;53(2):309–22.
- Vannote RL, Minshall GW, Cummins KW, Sedell JR, Cushing CE. The river continuum concept. *Can J Fish Aquat Sci* 1980;37:130–7.
- Villa S, Maggi V, Negrelli C, Finizio A, Bolzacchini E, Vighi M. Historical profile of polychlorinated biphenyls (PCBs) in an Alpine glacier. *Fresenius Environ Bull* 2001;10(9):701–5.
- Villa S, Negrelli C, Finizio A, Flora O, Vighi M. Organochlorine compounds in ice melt water from Italian Alpine rivers. *Ecotoxicol Environ Saf* 2006a;63:84–90.
- Villa S, Negrelli C, Maggi V, Finizio A, Vighi M. Analysis of a firn core for assessing POP seasonal accumulation on an Alpine glacier. *Ecotoxicol Environ Saf* 2006b;63:17–24.
- Vives I, Grimalt JO, Catalan J, Rosseland BO, Battarbee RW. Influence of altitude and age in the accumulation of organochlorine compounds in fish from high mountain lakes. *Environ Sci Technol* 2004a;38:690–8.
- Vives I, Grimalt JO, Fernández P, Rosseland B. Polycyclic aromatic hydrocarbons in fish from remote and high mountain lakes in Europe and Greenland. *Sci Total Environ* 2004b;324:67–77.
- Vives I, Grimalt JO, Lacorte S, Guillaumon M, Barceló D, Rosseland BO. Polybromodiphenyl ether flame retardants in fish from lakes in European high mountains and Greenland. *Environ Sci Technol* 2004c;38:2338–44.
- Walters DM, Fritz KM, Johnson BR, Lazorchak JM, McCormick FH. Influence of trophic position and spatial location on polychlorinated biphenyl (PCB) bioaccumulation in a stream food web. *Environ Sci Technol* 2008;42:2316–22.
- Wania F. Modelling the fate of non-polar organic chemicals in an ageing snow pack. *Chemosphere* 1997;35(10):2345–63.
- Wulf H, Bookhagen B, Scherler D. Climatic and geologic controls on suspended sediment flux in the Sutlej River Valley, western Himalaya. *Hydrol Earth Syst Sci* 2012;16:2193–217.



## Chapter 3. Paper II

Supporting information for

### **Evaluating the temporal variability of concentrations of POPs in a glacier-fed stream food chain using a combined modeling approach**

Melissa Morselli<sup>1</sup>, Matteo Semplice<sup>2</sup>, Sara Villa<sup>3</sup> and Antonio di Guardo<sup>1\*</sup>

<sup>1</sup>Department of Science and High Technology, University of Insubria, Via Valleggio, 11, 22100 Como CO, Italy

<sup>2</sup>Dipartimento di Matematica, Università degli Studi di Torino, Via C. Alberto 10, 10123 Torino TO, Italy

<sup>3</sup>Department of Earth and Environmental Sciences, University of Milano-Bicocca, Piazza della Scienza 1, 20126 Milano MI, Italy

\*Corresponding author

*Science of the Total Environment* **2014**, 493, 571–579

Contains 4 texts, 4 tables and 13 figures.



Text SI 1

### Discharge and water volume calculations

For discharge computations, the total watershed area (29 km<sup>2</sup>) was divided into 9 elevation zones (altitude interval = 200 m), in which the glacierized and non-glacierized areas were distinguished. The first step consisted in Frodolfo basin delineation and was performed starting from a 20-m resolution digital elevation model (DEM) obtained from the Lombardy Region (2014). A shapefile of ice-covered areas at the end of summer obtained from the same source was then overlapped, in order to differentiate ice-free from ice-covered areas, as shown in Figure SI 1.

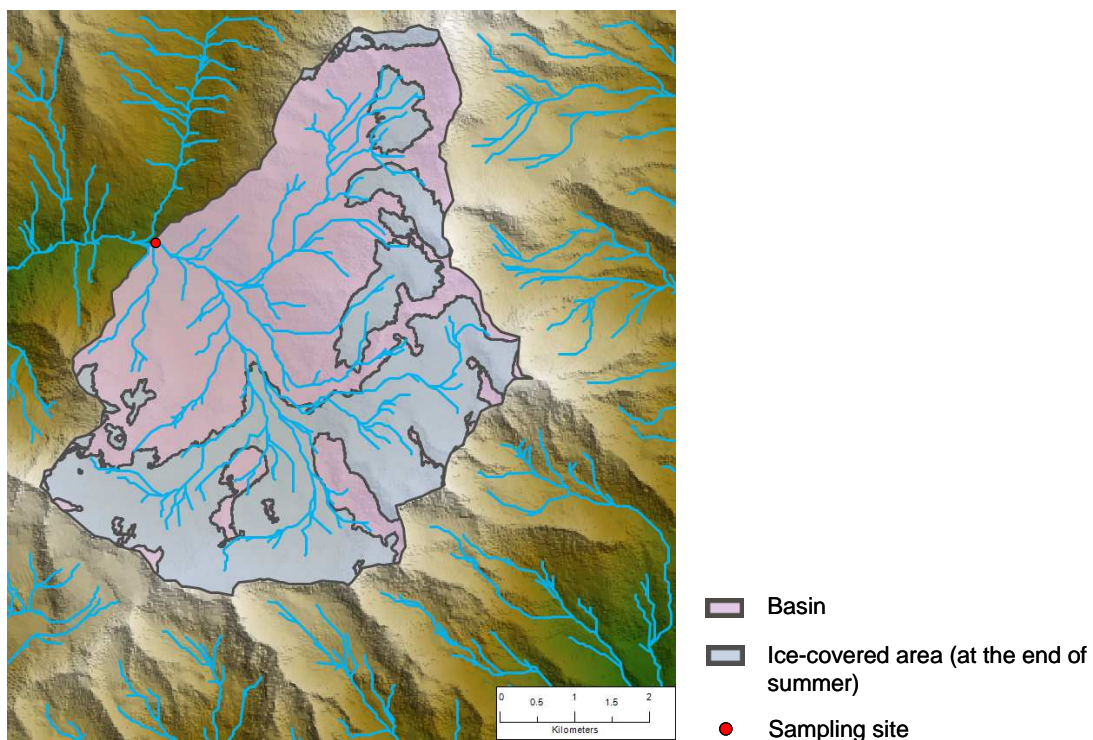


Figure SI 1. Frodolfo stream watershed and ice-covered area.

Afterwards, contour lines with an altitude interval of 200 m were delineated starting from the DEM; the resulting shapefile was used to divide the ice-free and ice-covered areas of the basin into elevation zones, as shown in Figure SI 2.

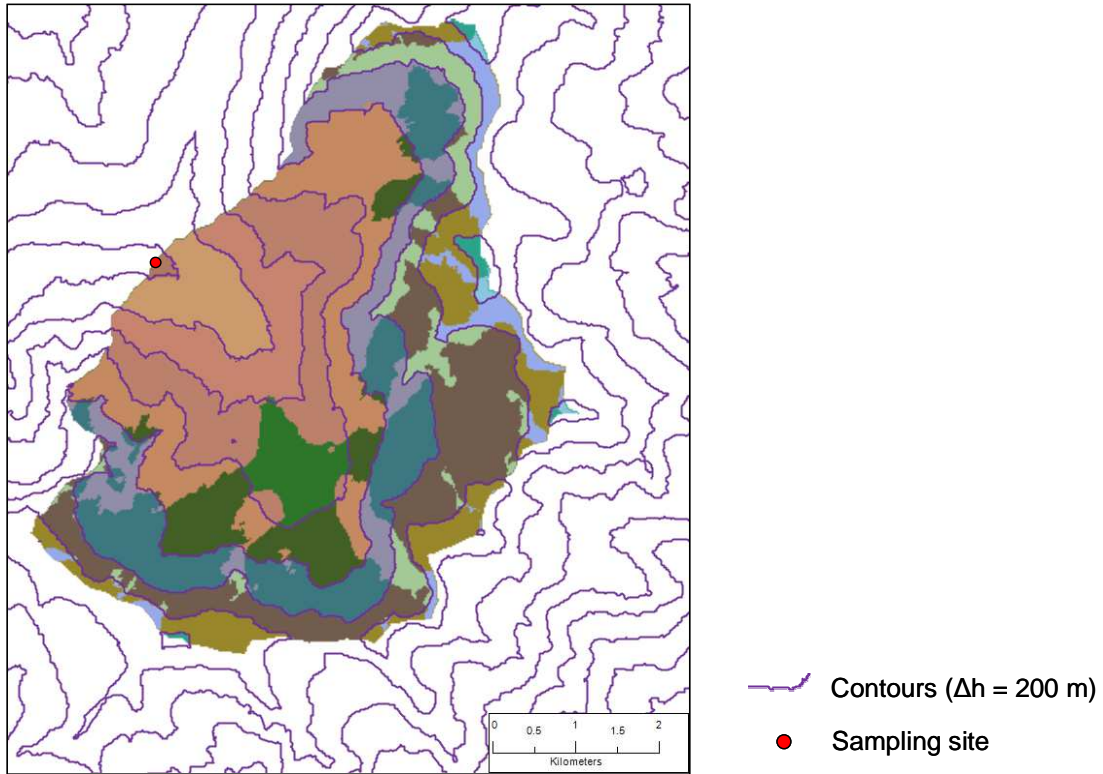


Figure SI 2. Watershed division in elevation zones and intersection with ice-covered areas.

The described procedures were performed using ESRI ArcView version 3.2 (ESRI, 1999) and ESRI ArcGIS version 9.3 (ESRI, 2008). Information concerning the elevation zones is reported in Table SI 1.

Table SI 1. Information concerning the 9 elevation zones into which the Frodolfo watershed was split.

Altitude range (m)	Total area (km <sup>2</sup> )	Ice-covered area (km <sup>2</sup> )	Ice-covered area (%)
< 2200	0.076	0	0
2200-2400	1.404	0	0
2400-2600	2.169	0.010	0.44
2600-2800	4.356	1.052	24.16
2800-3000	5.697	2.033	35.68
3000-3200	6.270	3.936	62.78
3200-3400	5.838	4.180	71.60
3400-3600	3.154	2.171	68.82
> 3600	0.248	0.153	61.87

In order to calculate the snow cover in each elevation zone, a profile of the snow line (i.e., the lower altitudinal boundary of a snow-covered area) throughout the year 2006 was defined for both the ice-free and the ice-covered areas (Figure SI 3), on the grounds of the observations collected during the 2006 glaciological campaign (SGL, 2006). The minimum value of the snow line for ice-covered areas was set to 2500 m, since no ice was found below such altitude.

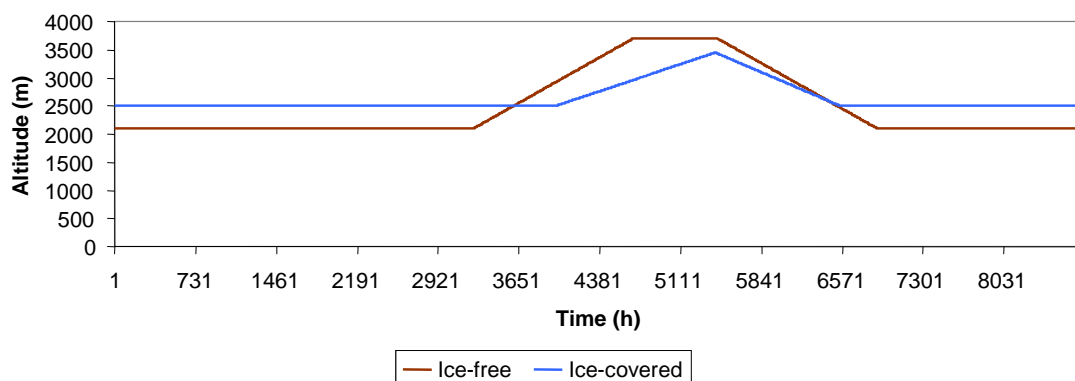


Figure SI 3. Assumed snow-line temporal profiles for ice-free and ice-covered areas in the Frodolfo watershed.

The collected data were used to estimate, for each elevation zone, the areas covered by snow and ice in the different periods of the year. In Figure SI 4, an example for the elevation zone 2600-2800 m is reported (zone total area = 4.356 km<sup>2</sup>).

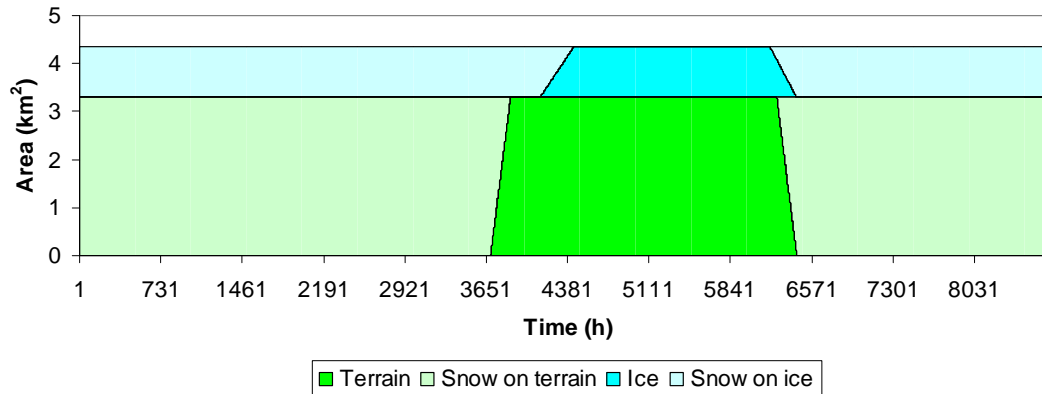


Figure SI 4. Temporal profiles of the different area types in the elevation zone 2600-2800 m in the Frodolfo watershed.

No ice melt was calculated in case of snow cover: in other words, ice melt was assumed to occur in case of free ice-surface only. In order to obtain representative temperature values for each elevation zone, the hourly values measured at the “Valfurva - Forni” meteorological station (ARPA Lombardia, 2014) were corrected using a lapse rate of 0.6 °C every 100 m (Singh et al., 2008). Afterwards, by applying Equation 2 (main text), the hourly contributions of snow and ice melt to flow were estimated, using DDF values for snow and ice (3.7 and 7.1 mm d<sup>-1</sup> °C<sup>-1</sup>, respectively) which were calibrated in order to obtain the best fit between predicted and measured discharge (see 3.1, main text). Estimated hourly values of  $M_h$  (mm) for snow and ice were then converted into meters and multiplied by the corresponding areas covered by snow or ice, in order to obtain

runoff fluxes ( $\text{m}^3 \text{h}^{-1}$ ). A first estimate of the contribution of rainfall to flow was obtained by multiplying hourly values of precipitation amount (in case of  $T \geq 1 \text{ }^\circ\text{C}$ ) by the elevation zone area. Such method obviously ignores processes such as infiltration, but given the lack of data concerning, for example, ice and snow density or soil type, it can provide a preliminary idea of rainfall contribution.

By summing all contributions (snow/ice melt and rain) and considering, in absence of melt and precipitation, a constant stream discharge of  $720 \text{ m}^3 \text{h}^{-1}$  (Bondiolotti, personal communication), hourly estimates of discharge were obtained in order to calculate compartment volume change with time and used in EcoDynA as inflow and outflow rates from the 50-m stream segment. Hourly values of water volume were computed assuming a rectangular section and using hourly values of stream width and water level. Since no measures were available for such parameters, two linear relationships were established, also on the grounds of field observations: discharge-stream width and discharge-water level. It was assumed that, in low-discharge conditions (i.e.,  $720 \text{ m}^3 \text{h}^{-1}$ ), stream width was 2 m and water level was 15 cm, while in high discharge conditions (i.e.,  $3.96 \cdot 10^4 \text{ m}^3 \text{h}^{-1}$ ), stream width was 6 m and water level was 1 m; maximum values of stream width and water level were set to 10 m and 2 m, respectively. In Figures SI 5 and 6 the computed temporal profiles of the two parameters are reported.

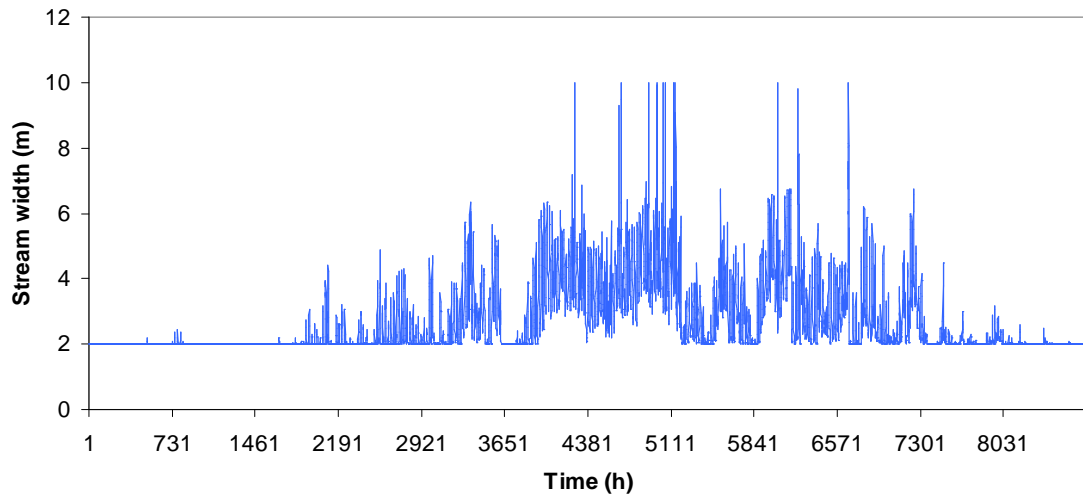


Figure SI 5. Temporal profile of the computed stream widths (m).

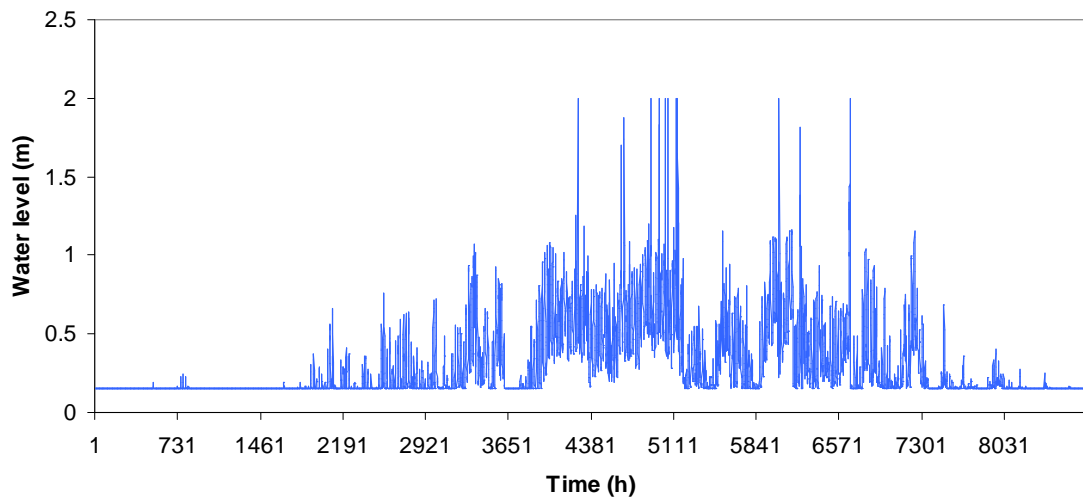


Figure SI 6. Temporal profile of the computed water levels (m).

Text SI 2

### **Suspended solids and organic carbon fraction: water sampling, analysis, results**

In 2011, Frodolfo stream water at the investigated site was collected twice, on July 31<sup>st</sup> and August 28<sup>th</sup>, at the same time of the day (3 PM), when discharge was estimated to be the highest; in 2013, water was sampled at different times of the same day (9.30 AM and 3 PM, September 1<sup>st</sup>), in order to take a picture of the SSC variability. Water was sampled using 5-L plastic tanks; for each sampling, 4 tanks were collected. Afterwards, water was stored at -30 °C until analysis.

The determination of total suspended solids was performed following a modified version of the Standard Method 2540 D (total suspended solids dried at 103-105 °C) (APHA, 1999). According to this procedure, a well-mixed sample is filtered through a weighed standard filter and the residue retained on the filter is dried to a constant weight at 103 to 105°C; the increase in weight of the filter represents the total suspended solids. In the present work, mixed cellulose esters membrane filters of nominal pore size of 0.45 µm (as indicated in APAT, 2003) instead of glass-fiber filters of nominal pore size of 0.2 µm were used. Filtration was carried out using a vacuum pump. Organic carbon fraction was measured using a Perkin Elmer 2400 CHN Elemental Analyzer.

SSCs for the different water samples are reported in Figure SI 7, while in Figure SI 8 the hourly SSC values computed by means of a linear relationship between the hypothesized discharge at the sampling times and the measured SSCs are depicted. The maximum value of SSC was set to 20 g L<sup>-1</sup>.

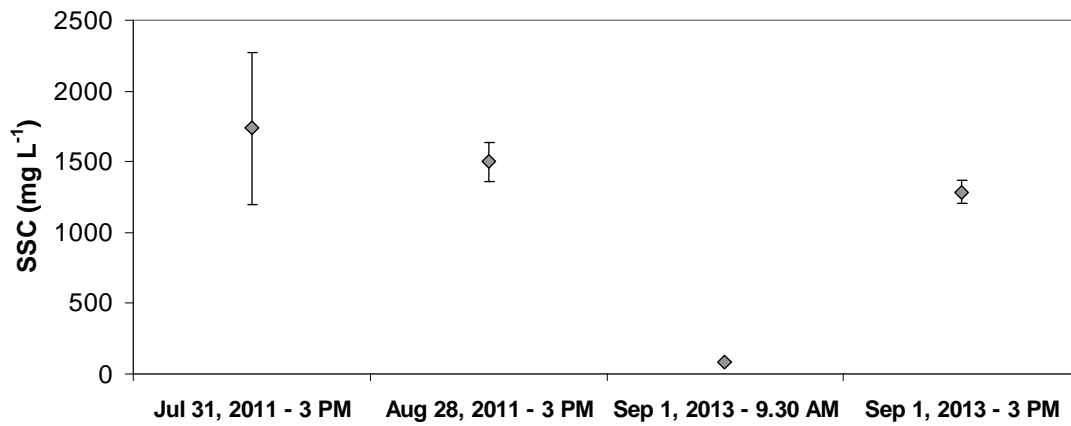


Figure SI 7. Suspended solids concentrations ( $\text{mg L}^{-1}$ ) measured in the water sampled on the Frodolfo stream in 2011 and 2013. Standard deviations are also reported.

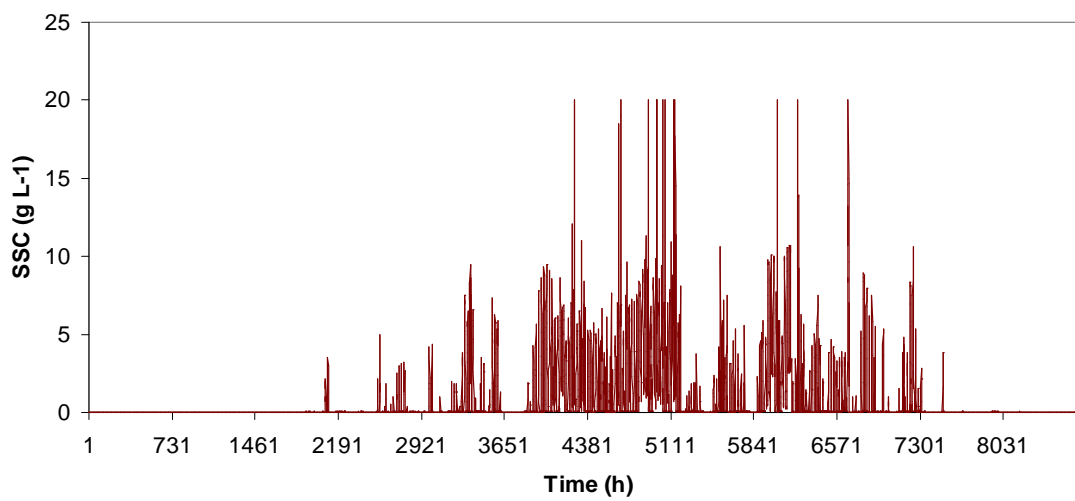


Figure SI 8. Temporal profile of the computed suspended solids concentrations ( $\text{g L}^{-1}$ ).

Text SI 3

### **Macroinvertebrates: community structure in a glacier-fed stream and model parameterization**

The macroinvertebrate community structure in a glacier-fed ecosystem, in terms of total abundance, is dominated by the mayfly *Baetis alpinus* (Baetidae) and the dipterans *Diamesa spp.* (Chironomidae). During the summer, *Diamesa spp.* can represent a large amount of the community, ranging from about 50 to 80% (Füreder et al., 2001; Robinson et al., 2001; Lencioni and Rossaro, 2005), while *Baetis spp.* represent more than 10% (Robinson et al., 2001). Other common *taxa* in glacier-fed ecosystems are: Ephemeroptera (*Rhithrogena spp.*), representing from 0.2 to 13% of the community (Robinson et al., 2001), Plecoptera (stoneflies), representing about 4% (Füreder et al., 2001), Tricoptera and other Diptera. In general, stoneflies communities are not highly diversified in Alpine streams in response to the harsh environmental conditions (Brittain et al., 2000; Ward, 1994). For Italian Alpine streams, for example, 11 species of Perlodidae stoneflies have been described (Silveri et al., 2008), 2 species belonging to the *Dictyogenus* genus, 2 to *Perlodes* and 7 to *Isoperla*.

A brief description of how macroinvertebrate volumes and lipid contents were derived follows.

#### **BAETIDAE (COLLECTORS)**

Hourly volumes for the simulated macroinvertebrate belonging to Baetidae were calculated starting from a relationship between dry mass and body length, computed as in Ritter (1990). The resulting profile is reported in Figure SI 9.

In the collectors sampled in 2006 in the Frodolfo stream, Bizzotto and co-workers (2009) measured an almost constant lipid content of about 15.3 % (dry weight); since, for collectors, a fresh/dry weight ratio of 4.2 was measured, such value was used to calculate the lipid content on a wet weight basis (i.e., 3.64%), which was adopted as constant model input.

#### **CHIRONOMIDAE (COLLECTORS)**

Hourly volumes for the simulated macroinvertebrate belonging to Chironomidae were calculated starting from a relationship between dry mass and growth rate; growth rate values were derived from the information reported in Berg and Hellenthal, (1991). The resulting profile is reported in Figure SI 9

As for Baetidae, a constant lipid content of 3.64% was used as model input.

#### **HEPTAGENIIDAE (SCRAPERS)**

Hourly volumes for the simulated macroinvertebrate belonging to Heptageniidae were calculated starting from a relationship between dry mass and growth rate; the seasonal values of growth rate reported in Cereghino and Lavandier (1998) were used. The resulting profile is reported in Figure SI 9.

From the 2006 campaign, a single value of lipid content was available for scrapers (i.e., 18.09% dry weight, measured in July) (Bizzotto et al., 2009). Such value was converted on a wet weight basis using the fresh/dry weight ratio measured for scrapers (3.5). The resulting lipid content (5.17% wet weight) was adopted as constant model input.

### PERLODIDAE (PREDATORS)

Hourly volumes for the simulated macroinvertebrate belonging to Perlodidae were calculated starting from a relationship between dry mass and body length, computed starting from the seasonal growth rate values found in Cereghino and Lavandier (1998). The resulting profile is reported in Figure SI 9.

Since in the 2006 campaign a temporal variability was observed in the lipid content of the sampled predators (similar, lower values in June, September, October and peak in July), the summer increase in such parameter was reproduced, as depicted in Figure SI 10. For the conversion from dry weight to fresh weight, a factor of 3.55 (the one measured for predators) was used.

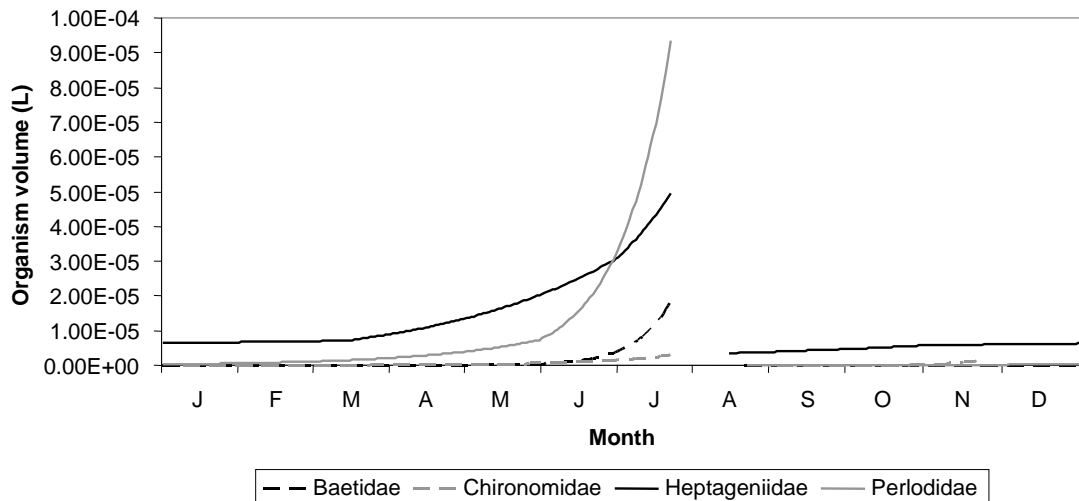


Figure SI 9. Temporal profiles of organism volume (L) created for the investigated macroinvertebrates.

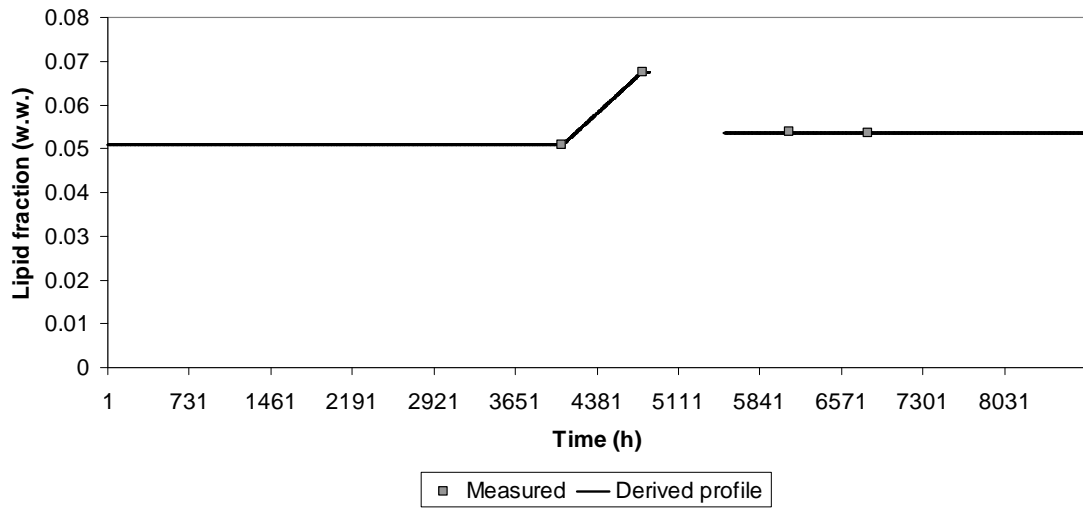


Figure SI 10. Temporal profile of organism lipid fraction (on a wet weight basis) for the macroinvertebrate belonging to Perlodidae. Markers represent the measured values (Bizzotto et al., 2009) from which the profile was derived.

Text SI 4

### **Snow sampling and analysis**

In winter 2008, two sampling campaigns were performed in order to investigate the concentrations of a number of chemicals (DDTs, HCB, HCHs, and a selection of PCB congeners, from trichloro- to octachloro-biphenyls) in snow. Two sampling sites were chosen: in the first one, located in Spiazzi di Gromo (municipality of Gromo, Bergamo), at an altitude of 1200 m a.m.s.l., snow was sampled once (on February 2<sup>nd</sup>); in the second one, in Gavia Valley (Sondrio), at 2000 m a.m.s.l., snow was sampled on January 16<sup>th</sup> and February 2<sup>nd</sup>. Sampling locations are shown in Figure SI 11.



Figure SI 11. Location of the snow sampling sites (“Gavia Valley” and “Spiazzi di Gromo”) with respect to the investigated site (“Frodolfo”). Satellite image from Google Maps (2014).

Snow samples were taken from the first 10 cm of snow. Snow was collected using a stainless-steel shovel and stored in pre-cleaned aluminium cans (average melted water volume of about 3 L). The recovery standard (a mix of PCB 128 and 140) was added in the field and the same procedure was repeated for blanks (Milli-Q water). Afterwards, samples and blanks were stored at -20 °C until analysis. Extractions were carried out with pesticide-grade methylene chloride (DCM) in a liquid-liquid extractor (3 x 200 mL); to minimize the re-equilibration of pesticides with the atmosphere, samples and blanks were

extracted as soon as the last bit of ice had melted. Dissolved and particulate fractions were not analyzed separately; therefore, measured concentrations should be interpreted as “bulk”. After concentration by rotary evaporation, extracts were purified in a silica gel (3 g) column, eluted first with 34 mL of hexane and then with 15 mL of hexane/DCM (1:1). All extracts were further concentrated under N<sub>2</sub> flux to facilitate solvent exchange to dodecane containing two internal standards (PCB 30 and 141). Analyses were performed with an Agilent Technologies 6890N Series gas chromatograph equipped with a 50-m 0.25-mm internal diameter CPSil8 capillary column (Chrompak) fitted with a retention gap (2-m long, 0.53-mm internal diameter FSOT column with a methyl stationary phase). Carrier gas was helium, and flux was set to 1 mL/min. The GC was coupled with a MS detector (5973N, Agilent Technologies), which was operated in single-ion monitoring mode.

Method detection limit was determined as the instrument detection limit of the lowest concentration standard of each analyte, and was 5.7 pg/L for the Gavia Valley snow sampled on January 16<sup>th</sup>, 5.9 pg/L for the Gavia Valley snow sampled on February 2<sup>nd</sup>, and 32 pg/L for the Spiazzi di Gromo snow. More details on extraction and analytical procedures can be found in Villa et al. (2006) and Finizio et al. (2006). The results are reported in Table SI 2.

Table SI 2. Chemical concentrations (pg L<sup>-1</sup>) in the snow sampled in 2008 at the two sampling sites.

Chemical	Stelvio, January 16 <sup>th</sup>	Stelvio, February 2 <sup>nd</sup>	S. di Gromo, February 2 <sup>nd</sup>
o,p'-DDE	< MDL	< MDL	43.0
p,p'-DDE	70.8	118.0	162

HCB	110.3	72.1	134.5
PCB 31	< MDL	51.3	< MDL
PCB 49	18.7	8.4	< MDL
PCB 52	37.2	9.8	32.0 *
PCB 64	12.7	< MDL	< MDL
PCB 66	5.7 *	< MDL	< MDL
PCB 70	18.1	< MDL	< MDL
PCB 74	< MDL	5.9 *	< MDL
PCB 87	9.2	< MDL	< MDL
PCB 95	19.9	7.2	< MDL
PCB 97	< MDL	< MDL	61.9
PCB 99	5.7 *	< MDL	< MDL
PCB 101	27.2	17.3	32.0 *
PCB 110	27.9	33.3	60.6
PCB 118	22.5	34.7	56.4
PCB 132	< MDL	20.9	54.7
PCB 138	< MDL	62.3	67.5
PCB 149	26.9	31.6	55.5
PCB 151	< MDL	< MDL	32.6
PCB 153	26.8	42.9	82.2
PCB 156	22.7	< MDL	< MDL
PCB 174	< MDL	< MDL	33.2
PCB 177	< MDL	< MDL	32.0 *
PCB 180	< MDL	< MDL	100.5
PCB 187	< MDL	< MDL	< MDL

---

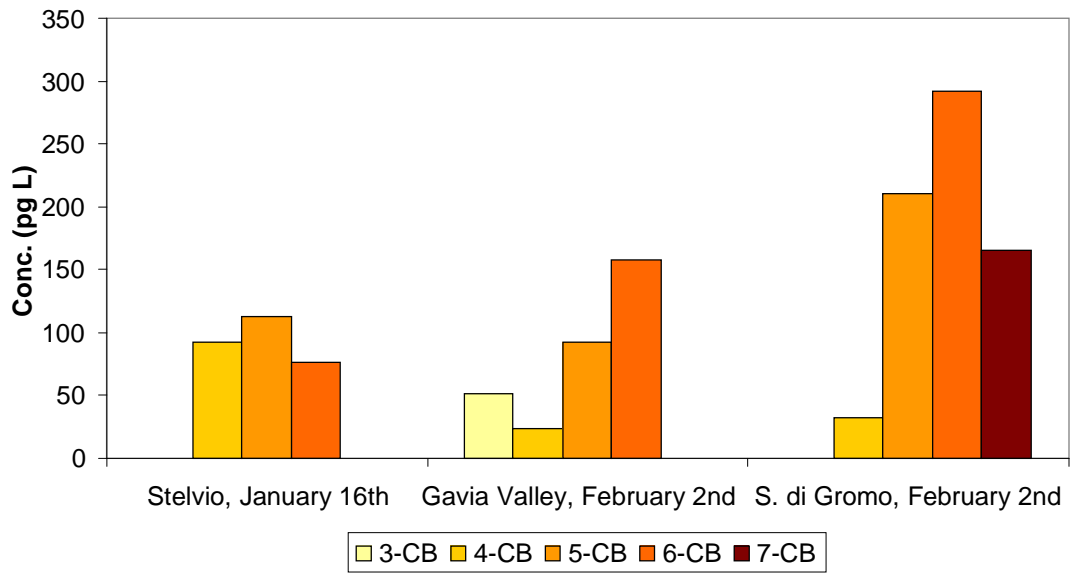


Figure SI 12. PCB fingerprints of the snow samples collected in 2008.

Table SI 3. Values for the non time-variable environmental parameters and mass-transfer coefficients (MTCs) adopted for the simulations.

Parameter	Unit	Value
Sediment active layer depth	m	0.005 <sup>a)</sup>
Aerosol particle concentration	$\mu\text{g m}^{-3}$	4 <sup>b)</sup>
Volume fraction of sediment particles	-	0.1 <sup>c)</sup>
Density of water particles	$\text{kg m}^{-3}$	1500 <sup>c)</sup>
Density of sediment particles	$\text{kg m}^{-3}$	1500 <sup>c)</sup>
Density of air particles	$\text{kg m}^{-3}$	1500 <sup>d)</sup>
OC fraction of suspended solids in water	-	$3.83 \cdot 10^{-3}$ <sup>e)</sup>
OC fraction of sediment particles	-	$3.83 \cdot 10^{-3}$ <sup>f)</sup>
Rain rate	$\text{m y}^{-1}$	0.7 <sup>g)</sup>
Aerosol dry deposition velocity	$\text{m h}^{-1}$	7.2 <sup>d)</sup>
Scavenging ratio	-	200000 <sup>d)</sup>
Volatilization MTC (air-side)	$\text{m h}^{-1}$	10 <sup>c)</sup>
Volatilization MTC (water-side)	$\text{m h}^{-1}$	1 <sup>c)</sup>
Sediment-water diffusion MTC	$\text{m h}^{-1}$	$1 \cdot 10^{-3}$ <sup>c)</sup>
Sediment deposition rate	$\text{g m}^{-2} \text{d}^{-1}$	400 <sup>h)</sup>
Sediment resuspension rate	$\text{g m}^{-2} \text{d}^{-1}$	200 <sup>h)</sup>
Sediment burial rate	$\text{g m}^{-2} \text{d}^{-1}$	200 <sup>h)</sup>

- a) Weighted average assuming that 1/10 of the riverbed is occupied by 5-cm deep sediment, while the remaining part by cobbles and boulders with no sediment on them
- b) Minimum  $\text{PM}_{10}$  value recorded in the nearby air quality station of Bormio (ARPA Lombardia, 2014b)
- c) Warren et al., 2005
- d) Mackay et al. (1989)
- e) Measured (see Text SI 3)
- f) Assumed as e)
- g) Calculated from meteorological observations at the “Valfurva - Forni” station for the year 2006 (ARPA Lombardia, 2014a)
- h) Calculated from the estimated average suspended solids concentration and using a deposition velocity of  $0.02 \text{ m h}^{-1}$ ; resuspension and burial rates are assumed to be half the deposition rate as in c)

Table SI 4. Physical-chemical properties of the three chemicals selected for the simulations (Mackay et al., 1992; 1997).

Parameter	PCB 70	PCB 101	p,p'-DDE
Molecular weight (g mol <sup>-1</sup> )	292	326.4	319
Melting point (°C)	104	76.5	89
Vapour pressure (Pa)	2.48·10 <sup>-3</sup> *	1.09·10 <sup>-3</sup>	8.66·10 <sup>-4</sup>
Water solubility (mg L <sup>-1</sup> )	6.55·10 <sup>-2</sup> *	1·10 <sup>-2</sup>	4·10 <sup>-2</sup>
log <i>K</i> <sub>ow</sub>	6 *	6.4	5.7
Half-life in water (h)	55000	55000	55000
Half-life in sediment (h)	55000	55000	55000

\* Derived from similar PCB congeners

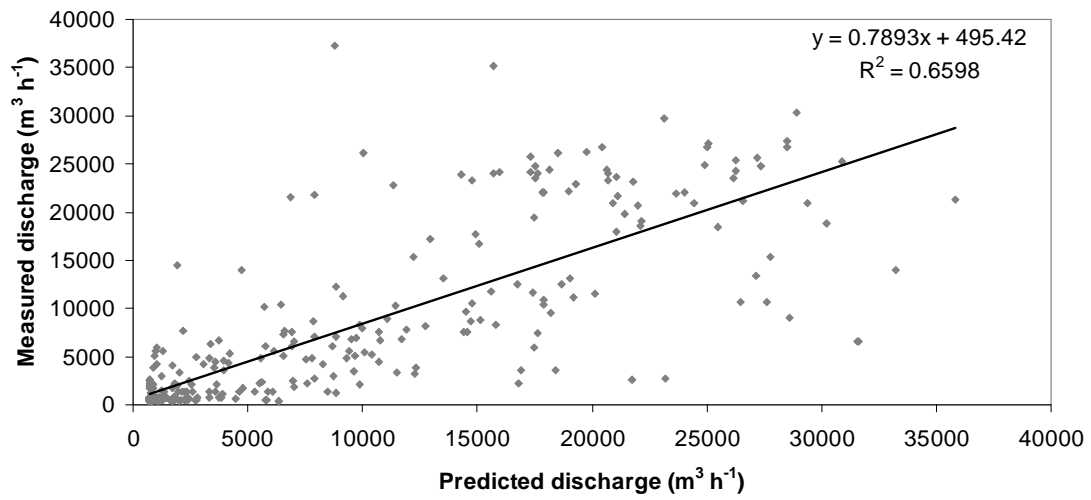


Figure SI 13. Comparison between measured and predicted water discharge. The correlation is significant ( $P < 0.001$  ).

## References

APAT (Agenzia per la protezione dell'ambiente e per i servizi tecnici). Metodi analitici per le acque. Manuali e Linee Guida 29/2003, Roma; 2003.

APHA (American Public Health Association). Solids, Method 2540 D. In: Clescerl LS, Greenberg AE, Eaton AD, editors. Standard Methods for the Examination of Water and Wastewater, 20<sup>th</sup> edition. New York: APHA; 1999.

ARPA Lombardia, 2014a. ARPA meteo website homepage: <http://www2.arpalombardia.it/siti/arpalombardia/meteo/previsionimeteo/meteolombardia/Pagine/default.aspx>. Last accessed: March 27, 2014.

ARPA Lombardia, 2014b. ARPA air quality website homepage: <http://ita.arpalombardia.it/ITA/qaria/Home.asp>. Last accessed: March 27, 2014.

Berg MB, RA Hellenthal. Secondary production of Chironomidae (Diptera) in a north temperate stream. *Freshwater Biol* 1991; 25: 497–505

Bizzotto EC, Villa S, Vighi M. POP bioaccumulation in macroinvertebrates of alpine freshwater systems. *Environ Pollut* 2009;157:3192-3198.

Brittain JE, Adalsteinsson H, Castella E, Gislason GM, Lencioni V, Lods-Crozet B, Maiolini B, Milner AM, Petts GE, Saltveit SJ. Towards a conceptual understanding of arctic and alpine streams. *Int Ver The* 2000;27:740-743.

Cereghino R, Lavandier P. Influence of hydropeaking on the distribution and larval development of the Plecoptera from a mountain stream. *Regul River* 1998;14:297-309.

ESRI, 1999. ESRI ArcView version 3.2 (software).

ESRI, 2008. ESRI ArcGIS version 9.3 (software).

Finizio A, Villa S, Raffaele F, Vighi M. Variation of POP concentrations in fresh-fallen snow and air on an Alpine glacier (Monte Rosa). *Ecotox Environ Safe* 2006;63:25-32.

Füreder L, Schütz C, Wallinger M, Burger R. Physico-chemistry and aquatic insects of a glacier-fed and spring-fed alpine stream. *Freshwater Biol* 2001;46:1673-1690.

Lencioni V, Rossaro B. Microdistribution of chironomids (Diptera: Chironomidae) in Alpine streams: an autoecological perspective. *Hydrobiologia* 2005;533:61-76.

Lombardy Region, 2014. Geo-portal of Lombardy website homepage:

<http://www.cartografia.regione.lombardia.it/geoportale> Last accessed: March 12, 2014.

Mackay D, Shiu WY, Ma KC. Illustrated handbook of physical-chemical properties and environmental fate for organic chemicals. Volume I: Monoaromatic Hydrocarbons, Chlorobenzenes, and PCBs. Chelsea: Lewis Publishers; 1992.

Mackay D, Shiu WY, Ma KC. Illustrated handbook of physical-chemical properties and environmental fate for organic chemicals. Volume V: Pesticide Chemicals. Boca Raton: Lewis Publishers; 1997.

Meier G.M., Meyer E.I., Meyns S. Lipid content of stream macroinvertebrates. Arch Hydrobiol 2000;147(4):447-463.

Ritter, H. Ephemeroptera Emergence from a High Mountain Stream in Tyrol, Austria in Mayflies and Stoneflies. Life history and biology. Proceedings of the 5th International Ephemeroptera Conference and the 9th International Plecoptera Conference. 1990 IC. Campbell (Ed). Series Entomologica. Springer Netherlands Volume 44 1990:53-59pp

Robinson CT, Uehlinger U, Hieber M. Spatio-temporal variation in macroinvertebrate assemblages of glacial streams in the Swiss Alps. Freshwater Biol 2001;46:1663-1672.

Silveri L, Tierno de Figueroa JM, Maiolini B. Feeding habits of Perlodidae (Plecoptera) in the hyporheic habitats of Alpine streams (Trentino-NE Italy). Entomol Fennica 2008;19(3):176-183.

Singh P, Haritashya UK, Kumar N. Modelling and estimation of different components of streamflow for Gangotri Glacier basin, Himalayas. *Hydrolog Sci J* 2008;53(2):309-322.

Villa S, Negrelli C, Maggi V, Finizio A, Vighi M. Analysis of a firn core for assessing POP seasonal accumulation on an Alpine glacier. *Ecotox Environ Safe* 2006b;63:17-24.

Ward JV. Ecology of alpine streams. *Freshwater Biol* 1994;32:277-294.

## Chapter 4. Paper III

# Theoretically exploring direct and indirect chemical effects across ecological and exposure scenarios using mechanistic fate and effects modelling

Frederik De Laender<sup>1\*</sup>, Melissa Morselli<sup>2</sup>, Hans Baveco<sup>3</sup>, Paul J. Van den Brink<sup>3,4</sup> and Antonio Di Guardo<sup>2</sup>

<sup>1</sup>Namur University, Research Unit in Environmental and Evolutionary Ecology, Rue de Bruxelles 61, 5000 Namur, Belgium

<sup>2</sup>Department of Science and High Technology, University of Insubria, Via Valleggio 11, 22100 Como, Italy

<sup>3</sup>Alterra, Wageningen University and Research Centre, P.O. Box 47, 6700 AA Wageningen, The Netherlands

<sup>4</sup>Department of Aquatic Ecology and Water Quality Management, Wageningen University, Wageningen University and Research Centre, P.O. Box 47, 6700 AA Wageningen, The Netherlands

\*Corresponding author

*Environment International* **2015**, *74*, 181–190





# Theoretically exploring direct and indirect chemical effects across ecological and exposure scenarios using mechanistic fate and effects modelling



F. De Laender<sup>a,\*</sup>, M. Morselli<sup>b</sup>, H. Baveco<sup>c</sup>, P.J. Van den Brink<sup>c,d,1</sup>, A. Di Guardo<sup>b</sup>

<sup>a</sup> Namur University, Research Unit in Environmental and Evolutionary Ecology, Rue de Bruxelles 61, 5000 Namur, Belgium

<sup>b</sup> Department of Science and High Technology, University of Insubria, Via Valleggio 11, 22100 Como, Italy

<sup>c</sup> Alterra, Wageningen University and Research Centre, P.O. Box 47, 6700 AA Wageningen, The Netherlands

<sup>d</sup> Department of Aquatic Ecology and Water Quality Management, Wageningen University, Wageningen University and Research Centre, P.O. Box 47, 6700 AA Wageningen, The Netherlands

## ARTICLE INFO

### Article history:

Received 18 June 2014

Accepted 14 October 2014

Available online xxxx

### Keywords:

Ecological risk assessment  
Ordinary differential equation models  
Ecosystem modelling  
Fugacity modelling  
Ecological scenario dynamics

## ABSTRACT

Predicting ecosystem response to chemicals is a complex problem in ecotoxicology and a challenge for risk assessors. The variables potentially influencing chemical fate and exposure define the exposure scenario while the variables determining effects at the ecosystem level define the ecological scenario. In absence of any empirical data, the objective of this paper is to present simulations by a fugacity-based fate model and a differential equation-based ecosystem model to theoretically explore how direct and indirect effects on invertebrate shallow pond communities vary with changing ecological and exposure scenarios. These simulations suggest that direct and indirect effects are larger in mesotrophic systems than in oligotrophic systems. In both trophic states, interaction strength (quantified using grazing rates) was suggested a more important driver for the size and recovery from direct and indirect effects than immigration rate. In general, weak interactions led to smaller direct and indirect effects. For chemicals targeting mesozooplankton only, indirect effects were common in (simple) food-chains but rare in (complex) food-webs. For chemicals directly affecting microzooplankton, the dominant zooplankton group in the modelled community, indirect effects occurred both in food-chains and food-webs. We conclude that the choice of the ecological and exposure scenarios in ecotoxicological modelling efforts needs to be justified because of its influence on the prevalence and magnitude of the predicted effects. Overall, more work needs to be done to empirically test the theoretical expectations formulated here.

© 2014 Elsevier Ltd. All rights reserved.

## 1. Introduction

Ecosystems are inherently complex and understanding how chemicals impact on their structure and functioning is at an incipient phase (Naito et al., 2003; De Laender et al., 2008b; Park et al., 2008; De Laender and Janssen, 2013). The number of variables potentially influencing how ecosystems respond to chemicals represents one dimension of this complexity. Although widely used, the concept of the ‘ecological scenario’ is, to the best of our knowledge, rarely defined. One approach to characterizing an ecological scenario consists of allocating one value to each variable potentially influencing population- and ecosystem-level responses to an environmental perturbation. Note that this approach does not constrain the number of variables needed to describe a given scenario, as this will depend on the ecosystem considered and the research questions asked.

Examples of variables making up an ecological scenario include trophic state, the degree of isolation of the exposed system, the interaction strength between species in a food-web and the complexity of this food-web. Trophic state may determine the response of individuals, populations, and ecosystems to chemicals through modifying resource availability (Noel et al., 2006; Pieters et al., 2006; Alexander et al., 2013; De Hoop et al., 2013; Gabsi et al., 2014). The degree of isolation will determine if immigration from areas with lower exposure levels can compensate for chemical effects and/or facilitate recovery and recolonization (Liess and Schulz, 1999; Caquet et al., 2007). Based on the ecological literature on disturbances in ecosystems, also interaction strength and food-web complexity can be hypothesised as key variables making up the ecological scenario. For example, the influence of these two variables on various stability measures has been a major topic in community and ecosystem ecology (May, 1972; Neutel et al., 2002; Allesina and Tang, 2012), although existing efforts have focused on random (non-specific) perturbations. To our knowledge, the influence of these two ecosystem descriptors on the response of ecosystems to chemicals has not been tested yet. We expect this response to be different for chemicals than for random perturbations because chemicals often affect specific taxa only. The

\* Corresponding author. Tel.: +32 81 724 405.

E-mail addresses: [frederik.delaender@unamur.be](mailto:frederik.delaender@unamur.be) (F. De Laender), [melissa.morselli@uninsubria.it](mailto:melissa.morselli@uninsubria.it) (M. Morselli), [paul.vandenbrink@wur.nl](mailto:paul.vandenbrink@wur.nl) (P.J. Van den Brink), [antonio.diguardo@uninsubria.it](mailto:antonio.diguardo@uninsubria.it) (A. Di Guardo).

<sup>1</sup> Tel.: +31 317 481615; fax: +31 419000.

way in which such direct impacts of chemicals travel through an ecological network such as a food-web will most likely depend on the identity of the impacted taxa.

Next to the ecological scenario, the exposure scenario is another dimension to the complexity surrounding ecological effect assessments at higher levels of biological organisation. Again, an approach to defining an exposure scenario consists of attributing values to variables determining chemical exposure. Such exposure is often related to chemical emissions in the environment (application and/or discharge). The timing of application is one potentially important variable making up the exposure scenario, although the influence of the application season is unclear at present (Willis et al., 2004; Van Wijngaarden et al., 2006). Other variables that characterize exposure include those determining chemical fate (e.g. partitioning coefficients) as well as chemical movement across compartments and degradation. In such view, the role of the ecological complexity in defining the exposure is often neglected or overlooked (Di Guardo and Hermens, 2013).

The influence of the exposure scenario on a chemical's effects on ecosystems needs to be examined in concert with that of the ecological scenario, as both scenarios may share common variables. More precisely, certain variables making up the ecological scenario will also define the exposure scenario, and vice versa. For example, trophic state, essentially a characteristic of the challenged ecosystem determining resource availability, will also influence chemical bioavailability in water, and therefore the actual exposure pelagic biota are facing. The timing of application, often considered as a part of the exposure scenario, will likewise determine the ecological scenario in case of strong seasonal fluctuations in community composition.

At present, no information is available on how ecosystem response to chemicals varies across different ecological and exposure scenarios. This may be partly due to the practical difficulty to experimentally test chemical effects on population- and ecosystem-level endpoints for a range of ecological and exposure scenarios and the resources that are required to do so. As opposed to experimental approaches, the use of mechanistic models does not suffer such constraints. Indeed, modelling can play a key role in theoretically exploring how ecological scenarios co-determine the ecological effects triggered by an array of exposure scenarios.

In the field of exposure and fate modelling, efforts are on-going to refine the incorporation of bioavailability into the exposure assessment of organic pollutants (Di Guardo et al., 2006; Infantino et al., 2013). Future efforts will include the evaluation and expression of the spatial and temporal variability of chemical fate in order to define more realistic exposure scenario (Di Guardo and Hermens, 2013). In recent years, advancements have been made in the field of mechanistic effect modelling as well, mostly at the population level (Grimm et al., 2009; Martin et al., 2013), and these efforts have led to strategies to enhance the realism of ecological effect assessments (Forbes et al., 2009). Currently, efforts are on-going to continue the upscaling of effects towards higher levels of biological organisation (De Laender et al., 2011; De Laender and Janssen, 2013).

The objective of the presented paper is to formulate theoretical expectations for ecological effects and recovery across a range of exposure and ecological scenarios, using a combined chemical fate and ecosystem model. The chemical fate model is based on the fugacity approach. The choice for a fugacity approach was based on the availability of a dynamic fugacity-based aquatic model (Di Guardo et al., 2006; Infantino et al., 2013), which could be easily modified to simulate exposure for this exercise. The ecosystem model is defined as a set of coupled ordinary differential equations, at present the only approach available to model ecosystem dynamics in ecotoxicology. We summarize effects on the biomasses of the included functional groups in two ways: (1) using the maximum difference in time between the exposed and control biomass, and (2) using the time-integrated biomass difference between the exposed and control dynamics. We consider both direct and indirect effects (Fleeger et al., 2003) across sixteen ecological scenarios, differing

in trophic state (oligo- vs. mesotrophic), the interaction strength between producers and consumers (high vs. low), the immigration rate (fast vs. slow), and the complexity of the ecological system (food-web vs. food-chain). The four chemicals considered represent all combinations of two sorption characteristics (hydrophobic vs. hydrophilic), and two toxicological profiles (targeting micro- vs. mesozooplankton). By also varying the season of emission between spring and late summer, a total of eight exposure scenarios were considered. The fate model was used to predict the dynamics of the water dissolved chemical concentrations, taking into account trophic state by using phytoplankton and detritus mass for bioavailability calculations. We stress that our exercise should be interpreted as a model-aided quantification of the theoretical expectations on how ecological effects of chemicals vary across ecological and exposure scenarios. In our discussion, we qualitatively confront our predictions with results from micro- and mesocosm studies but this comparison does not waive the need for a more formal confrontation with data in the future, when these become available.

## 2. Material and methods

### 2.1. Chemical fate model

Chemical fate was calculated using a modified version of the DynA (Di Guardo et al., 2006) and EcoDynA (Infantino et al., 2013) models. These models are fugacity-based (Mackay, 2001) and were developed to investigate the fate of organic chemicals in a dynamic aquatic system. Model dynamics depend on chemical emission (which can be varied on an hourly basis) and on environmental parameters. More specifically, model input includes hourly values of water temperature, water inflow and outflow rates and suspended solid concentration in water. Suspended solids are modelled as a water sub-compartment; equilibrium with water is therefore assumed. The presence of particulate organic carbon (POC) is simulated by defining the organic fraction of the suspended solids. In the implementation of the model used in the present work, also a dissolved organic matter (DOM) sub-compartment was included. More details concerning model formulation and the application in this paper can be found in Text S1.

For all simulations, the model was parameterized to represent a typical shallow pond, characterized by an area of 450 m<sup>2</sup> and a depth of 1 m. A water residence time of six months, sufficiently high to prevent the chemical outflow with POC and DOC to become the dominant fate process, was simulated, as the result of constant input and output water fluxes of 0.1 m<sup>3</sup> h<sup>-1</sup>. A seasonal profile of water temperature similar to those measured in a set of UK temperate ponds, with values ranging from 3 to 15 °C in winter and summer, respectively, was adopted (Martin, 1972; Young, 1975) (Fig. S1, Supporting information). The sediment compartment, in terms of the fraction of solids and fraction of organic carbon in solids, was parameterized elsewhere (Armitage et al., 2008).

### 2.2. Food-web model

A food-web model was implemented in R (R Development Core Team, 2010) as a set of ordinary differential equations. Each equation represented the dynamics of one functional group (mg C/m<sup>2</sup>), based on gain and loss processes quantified as surface-specific carbon exchange rates (mg C/m<sup>2</sup>/d), including functional group-specific immigration (Table 1 lists all parameters). The model included 6 functional groups: phytoplankton, omnivores, microzooplankton, mesozooplankton, detritivores, and invertebrate predators (consuming all heterotrophs) (Fig. 1). Phytoplankton growth was described as:

$$\frac{dPhy}{dt} = Phy \cdot \left[ \left[ 1 - a \cdot \cos\left(\frac{2 \cdot \pi \cdot t}{365}\right) \right] \cdot Gpp \cdot (1 - Resp - Excr) \cdot \left(1 - \frac{Phy}{K}\right) - Mort \right] - Predation + I$$

**Table 1**  
Parameters of the food-chain and food-web models.

Parameter	Explanation	Value	Unit	Source
<i>Abiotic</i>				
<i>a</i>	Amplitude of seasonal forcing	1		Scheffer et al. (1997)
<i>d</i>	Detritus dissolution rate	0.01	d <sup>-1</sup>	Donali et al. (1999)
<i>Biotic</i>				
All groups				
<i>I</i>	Immigration rate	10 <sup>-5</sup> (high); 10 <sup>-15</sup> (low)	mg C m <sup>-2</sup> d <sup>-1</sup>	Scenario-specific; similar to and smaller than (Scheffer et al., 1997), respectively
Phytoplankton				
<i>K</i>	Carrying capacity	50 (oligotrophic); 500 (mesotrophic)	mg C m <sup>-2</sup>	Scenario-specific (Carlson, 1977)
<i>Gpp</i>	Gross primary production rate	1.5	d <sup>-1</sup>	Moisan et al. (2002)
<i>Resp</i>	Fraction of Gpp spent to respiration	0.1		Bidwell (1977)
<i>Excr</i>	Fraction of Gpp spent to excretion	0.1		Baines and Pace (1991)
<i>Mort</i>	Mortality rate	0.2	d <sup>-1</sup>	Janse (2005)
Detritivores, omnivores, and predators				
<i>Ing, Het</i>	Ingestion rate	0.5	d <sup>-1</sup>	Hansen et al. (1997)
<i>AE, Het</i>	Assimilation efficiency	0.6		Hendriks (1999)
<i>Resp, Het</i>	Respiration rate	0.1	d <sup>-1</sup>	Park et al. (2008)
<i>Excr, Het</i>	Ratio of excretion to respiration	0.6		Vezina and Platt (1988)
<i>K, Het</i>	Half saturation constant for feeding	50; 500	mg C m <sup>-2</sup>	Scenario-specific; motivated in the text
<i>Mort, Het</i>	Mortality rate	0.01	d <sup>-1</sup>	De Laender et al. (2008c)
Microzooplankton				
<i>Ing, Miz</i>	Ingestion rate	2	d <sup>-1</sup>	Hansen et al. (1997)
<i>AE, Miz</i>	Assimilation efficiency	0.6		Hendriks (1999)
<i>Resp, Miz</i>	Respiration rate	0.1	d <sup>-1</sup>	Park et al. (2008)
<i>Excr, Miz</i>	Excretion	0.6		Vezina and Platt (1988)
<i>K, Miz</i>	Half saturation constant for feeding	50; 500	mg C m <sup>-2</sup>	Scenario-specific; motivated in the text
<i>Mort, Miz</i>	Mortality rate	0.05	d <sup>-1</sup>	De Laender et al. (2008c)
Mesozooplankton				
<i>Ing, Mez</i>	Ingestion rate	1	d <sup>-1</sup>	Hansen et al. (1997)
<i>AE, Mez</i>	Assimilation efficiency	0.6		Hendriks (1999)
<i>Resp, Mez</i>	Respiration rate	0.1	d <sup>-1</sup>	Park et al. (2008)
<i>Excr, Mez</i>	Excretion	0.6		Vezina and Platt (1988)
<i>K, Mez</i>	Half saturation constant for feeding	50; 500	mg C m <sup>-2</sup>	Scenario-specific; motivated in the text
<i>Mort, Mez</i>	Mortality rate	0.01	d <sup>-1</sup>	De Laender et al. (2008c)

where  $1 - a \cdot \cos\left(\frac{2 \cdot \pi \cdot t}{365}\right)$  and *Predation* represent seasonal forcing and predation by higher trophic levels, respectively. *Predation* was calculated by summing phytoplankton ingestion by omnivores, microzooplankton, and mesozooplankton. These variables are calculated dynamically during model simulation.

Growth of the heterotrophic groups (*Het* = omnivores, microzooplankton, mesozooplankton, detritivores, or invertebrate predators) was described as:

$$\frac{dHet}{dt} = Het \cdot \left[ Ing_{Het} \cdot AE_{Het} \cdot \frac{Food}{Food + K_{Het}} - Resp_{Het} \cdot (1 - Excr_{Het}) \cdot \max \left[ Mort_{Het}, \ln \left[ 1 + \left( \frac{C}{LC_{50Het}} \right)^{slope} \right] \right] \right] - Predation + I$$

where *Food*, *C*, and *Predation* represent the total food concentration, the chemical concentration, and loss by predation (equal to zero for predators), respectively. *Food* was calculated as the biomass summed across all diet items (e.g. for omnivores, *Food* = *Phy* + *Det*, where *Det* represents the state variable for detritus). The dynamics of *Det* were included explicitly to simulate detritivory by detritivores and omnivores:

$$\frac{dDet}{dt} = \sum_{i=1}^5 \left[ Ing_i \cdot (1 - AE_i) \cdot \frac{Food_i}{Food_i + K_i} + Mort_i \right] - d \cdot Det$$

where **Ing**, **AE**, **Food**, **K**, and **Mort** represent arrays (of size 5) containing specific ingestion rates, assimilation efficiencies, food concentrations, half-saturation constants, and mortality rates of all six functional groups. Note that the entries for phytoplankton in **Ing**, **AE**, and **Food** are set to

zero. This equation represents detritus accumulation when egestion and mortality exceed dissolution, and depletion when the opposite is true.

The food-web model was equipped with logistic concentration–response functions to describe the direct toxic effects of an aqueous chemical concentration, *C* (input variable), on the mortality rate of mesozooplankton or microzooplankton (depending on the exposure scenario), as done previously (Traas et al., 2004; De Laender et al., 2008a). Parameters of these functions were the median lethal concentration (*LC*<sub>50</sub>) and *slope* (Table 2). Actual mortality was defined as the maximum of the toxicant-induced mortality and background mortality.

### 2.3. Food-chain model

We constructed two food-chain models as a special parameterisation of the food-web model. A first food-chain model only consisted of phytoplankton and mesozooplankton; a second food-chain model only consisted of phytoplankton and microzooplankton. These food-chain models were constructed by simply setting the initial biomass densities and immigration rates of all functional groups not present in the food-chains to zero.

### 2.4. The scenarios

Sixteen ecological scenarios were obtained by varying trophic state (mesotrophic vs. oligotrophic), immigration rate (high vs. low), grazing rate as a proxy for interaction strength between producers and consumers (strong vs. weak), and the complexity of the system (food-chain vs. food-web). Trophic state was altered by changing the phytoplankton carrying capacity from 1 µg Chlorophyll a/L for

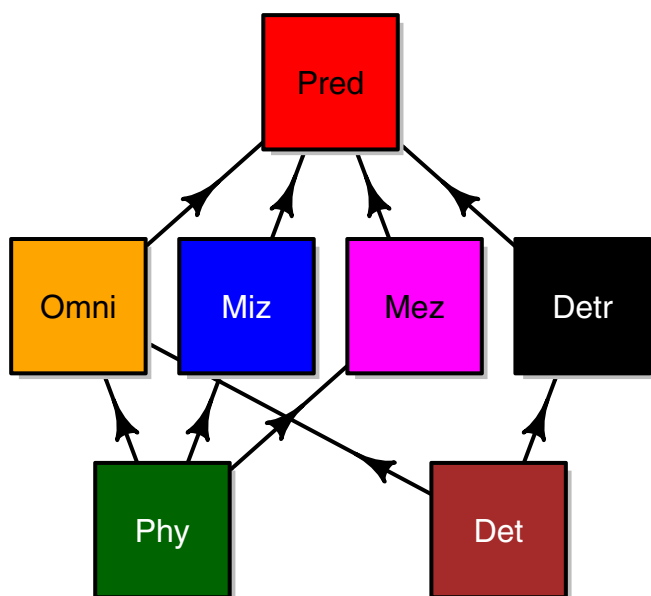


**Fig. 1.** Structure of a food-web including phytoplankton (Phy), detritus (Det), omnivores (Omni); microzooplankton (Miz), mesozooplankton (Mez), detritivores (Detr), and invertebrate predators (Pred). The structure of the food-chain can be obtained by removing all groups except for phytoplankton and mesozooplankton (exposure to chemical 1 or 2) or microzooplankton (exposure to chemical 3 or 4).

oligotrophic scenarios to 10  $\mu\text{g}$  Chlorophyll a/L for mesotrophic scenarios (Carlson, 1977). Average carbon to Chlorophyll a ratios of 50  $\mu\text{g}$  carbon/ $\mu\text{g}$  Chlorophyll a and the pond depth of 1 m were used to convert these numbers to  $\text{mg C m}^{-2}$ , the currency used by the food-web and food-chain models (Riemann et al., 1989). Immigration rates ( $I$ ) were set to values that were either comparable to (high immigration) or smaller than (low immigration) those used elsewhere (Table 1). Grazing rates were changed by setting the half saturation rate constant  $K$  from 50 (fast grazing) to 500 (slow grazing), i.e. corresponding to the carrying capacity of the phytoplankton in the oligotrophic and mesotrophic scenarios, respectively. This choice was made to prevent grazing limitation to be either too high or too low in all scenarios. Lastly, system complexity was altered by using the food-chain model (simple) or the food-web model (complex).

We considered four hypothetical model chemicals, characterized by different physical–chemical and toxicological properties. Chemicals 1 and 3 (hydrophilic), and 2 and 4 (hydrophobic) share environmental fate determinants with atrazine and pyrene, respectively (Table 2). The fate of these two types of chemicals (hydrophilic and hydrophobic) was calculated separately for the two trophic states considered in the ecological scenarios. We used the phytoplankton and detritus control densities predicted by the food-chain and food-web models to estimate

**Table 2**

Physical–chemical properties at 25 °C, and toxicity to zooplankton of the chemicals selected for the simulations. Note that other groups than micro- and mesozooplankton are always tolerant to both chemicals (i.e.  $\text{LC}_{50\text{s}} \gg$ ).

Parameter	Chemicals 1, 3	Chemicals 2, 4
Molecular weight (g/mol)	216	202
Melting point (°C)	176	156
Water solubility (g/m <sup>3</sup> )	33	0.13
Vapour pressure (Pa)	$3.85 \cdot 10^{-5}$	$6 \cdot 10^{-4}$
Log $K_{\text{OW}}$	2.5	5.2
Half-life in water (h)	1320	1700
Half-life in sediment (h)	4800	55,000
24 h- $\text{LC}_{50}$ for mesozooplankton (chemicals 1, 2) or for microzooplankton (chemicals 3, 4) (ng/L)	1000	1000
Slope of concentration response curve for micro- or mesozooplankton (-)	2	2

POC concentrations in the fate model. In addition, fate calculations for the oligotrophic state were performed using a sediment depth of 5 cm and a constant DOC concentration of 5 mg/L, while in the mesotrophic state sediment depth was set to 7 cm and a constant DOC concentration to 50 mg/L was assumed. No feedback from chemical-induced changes in phytoplankton and detritus stocks to chemical fate was considered in the current exercise. The four chemicals also differed in their toxicological profile. Chemicals 1 and 2 selectively targeted mesozooplankton, while chemicals 3 and 4 selectively targeted micro- or mesozooplankton. We assumed that these chemicals affected micro- or mesozooplankton by reducing survival in a concentration-dependent fashion. By combining these four chemical types with two seasons of emission (spring: April 4th–June 4th; late summer: August 5th–October 6th) we created eight different exposure scenarios.

All simulations were ran using a time-step of 1 h (0.04 days) and initial conditions were always set to 50 (the carrying capacity of the oligotrophic system), 1, and 0  $\text{mg C m}^{-2}$  for autotrophs, heterotrophs, and detritus, respectively.

We used the fate and effect models to inspect how direct and indirect effects varied across the ecological and exposure scenarios. We note that calculations for chemicals 1 and 2 (targeting mesozooplankton) were done with the phytoplankton–mesozooplankton food-chain model. Calculations for chemicals 3 and 4 (targeting microzooplankton) were done using the phytoplankton–microzooplankton food-chain model. Direct effects were assessed by comparing meso- (chemicals 1 and 2) or microzooplankton biomass (chemicals 3 and 4) between the exposed and the control dynamics. Recovery was concluded when exposed and control biomasses were identical during the last 31 days of the simulation time. When this was the case, recovery time was calculated as the time between the onset of effects and the start of the 31-day period of permanent recovery. Because both groups only feed on phytoplankton, we evaluated indirect effects by calculating effects and recovery time for phytoplankton. To aid visualization of the modelled direct and indirect effects, we summarized these effects in two ways: (1) using the maximum effect size (unitless quotient of exposed and control dynamics), and (2) using the time-integrated difference between the control and exposed biomass ( $\text{mg C m}^{-2} \text{d}$ ). The maximum effect size was defined as the largest absolute deviation of the quotient of the exposed and control dynamics from 1.

### 3. Results

#### 3.1. Chemical fate

Water-dissolved concentrations of chemicals 1 and 3 were about two times higher than those of chemicals 2 and 4, as expected from the relatively high octanol–water partitioning coefficient ( $K_{\text{OW}}$ ) of chemicals 2 and 4, which caused their fast removal from water through partitioning onto POC and DOC and the subsequent deposition of particles (Fig. 2). The influence of trophic state and season of emission on the fate of chemicals 1 and 3 was small, as expected from their relatively low log  $K_{\text{OW}}$ . For this reason, very similar exposure levels were predicted for all emission timings and trophic states. Chemical removal processes were quite slow, due to a combination of the high residence time of the water compartment (i.e., 6 months) with the relatively high half-life of chemicals 1 and 3 in water (about 55 days).

In contrast to what was observed for chemicals 1 and 3, the higher affinity of chemicals 2 and 4 for the organic sub-compartments in water and sediment caused very different exposure profiles for the four simulation scenarios (Fig. 2). Concentrations following summer emission were about 15–20% lower than concentrations following spring emission, regardless of the trophic state. This behaviour can be mainly ascribed to the higher POC levels in summer than in spring, which caused a more effective chemical removal from the water phase. In the mesotrophic systems, the concentrations of chemicals 2 and 4 were about 5 times lower than in oligotrophic systems. Removal of chemicals 2 and 4 from the

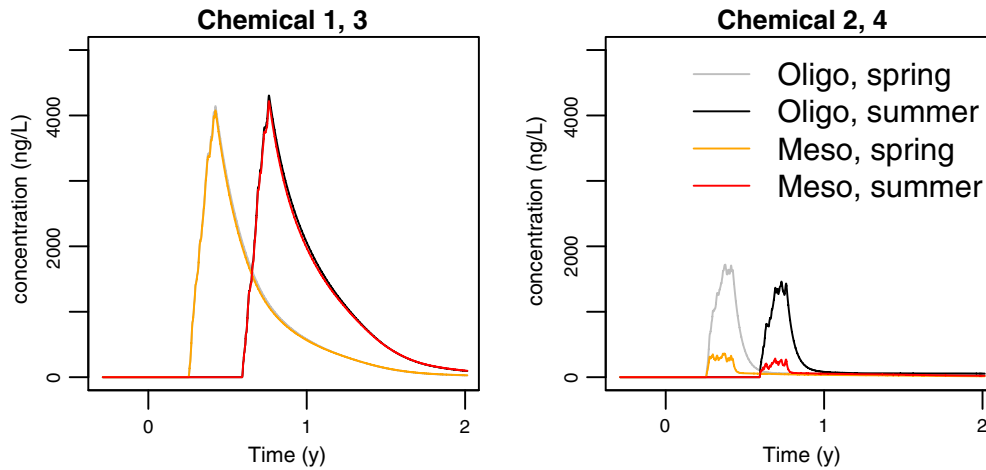


**Fig. 2.** Aqueous concentrations of chemicals 1, 2, 3, and 4 for the two trophic states (considered in the ecological scenarios) and two emission seasons (considered in the exposure scenarios).

water phase was faster than for chemicals 1 and 3, and the main process involved was suspended solid deposition. In mesotrophic systems, for example, the deposition flux was up to 90% of chemical emission.

3.2. Ecosystem dynamics: control

In general, oscillations through time were more pronounced in the mesotrophic systems than in the oligotrophic systems, both for the food-chain as for the food-web (Fig. 3 includes an example for the food-chain and food-web). In oligotrophic systems with low immigration rates and occupied by slow grazing heterotrophs, only phytoplankton maintained biomass densities  $> 10^{-8}$  mg C m<sup>-2</sup>, while the other groups virtually disappeared from the system (Fig. S2, Supporting information). Immigration promoted co-existence and limit cycle stability (an example is provided in Fig. S3, Supporting information). Mesozooplankton biomass density was lower in the food-web than in the food-chain (Fig. S4, Supporting information) and was mostly 10 to 100 times lower than that of microzooplankton when both groups were present in the food-web (Fig. 3A).

3.3. Ecosystem dynamics: exposure to chemicals 1 and 2

Because effects following spring and late summer emissions were similar, only the former are discussed, after which the differences between both exposure scenarios are briefly highlighted.

Exposure to chemicals 1 and 2 in spring always resulted in clear effects on mesozooplankton, the only functional group that was sensitive to these hypothetical chemicals. For mesozooplankton, the maximum effect size was comparable between chemicals 1 and 2 (Fig. 4A and Fig. S5A, Supplemental information). Also the time-integrated effects compared well between chemicals 1 and 2 emitted in spring (Figs. S6A and S7A, Supplemental information). The maximum effects of these chemicals on mesozooplankton were always negative (nearly 100% biomass reductions) in the food-web, but positive in the mesotrophic food-chain when grazing was fast. The maximum and time-integrated direct effects were mostly independent of immigration rate. The maximal direct effects of chemicals 1 and 2 were smaller at high immigration rates but only in mesotrophic food-chains with fast grazing heterotrophs. In contrast, the integrated effect of both chemicals emitted in spring in oligotrophic food-chains with fast grazing heterotrophs was larger at high immigration rates than at low immigration rates.

The maximum size of the indirect effects of chemicals 1 and 2 on phytoplankton was common and positive in the food-chain, and largest when grazing was fast (Fig. 4B, and Fig. S5B, Supplemental information). Also the time-integrated indirect effect on phytoplankton was apparent in food chains (Figs. S6B and S7B, Supplemental information). Regardless of the effect summary considered, indirect effects were mostly absent in the food-web. Both effect summaries suggested the indirect effect size to be nonresponsive to immigration rate.

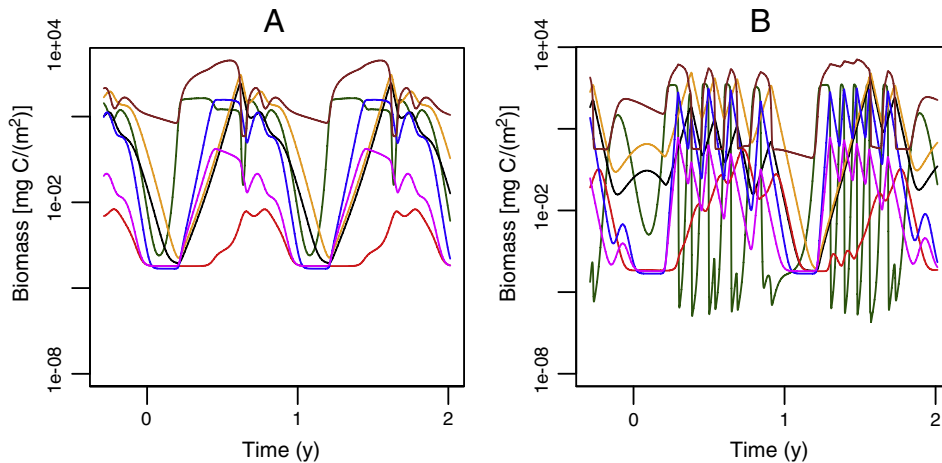


**Fig. 3.** Control simulations for a food-web with fast grazing heterotrophs, fast immigration and oligotrophic (A) or mesotrophic conditions (B). Colour codes are as in Fig. 1. (For interpretation of the references to colour in this figure legend, the reader is referred to the web version of this article.)

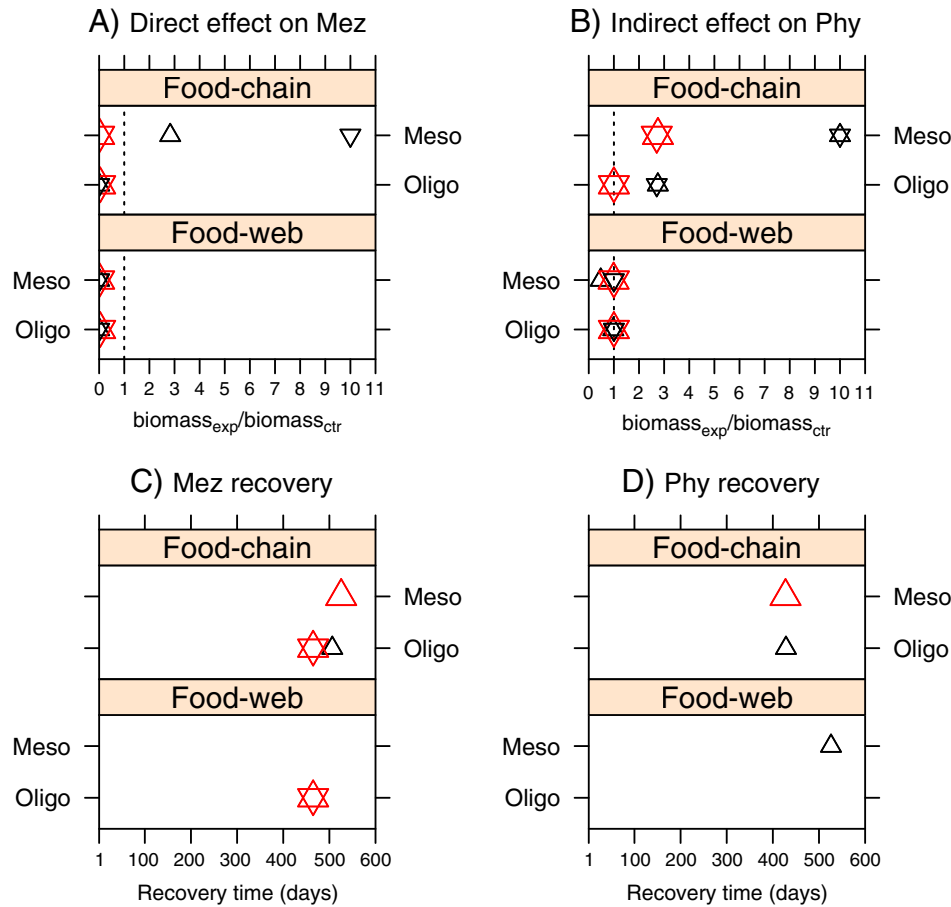


**Fig. 4.** Maximum effect sizes and recovery times for mesozooplankton and phytoplankton following exposure to chemical 1 in spring, in mesotrophic and oligotrophic food-webs and food-chains, characterized by fast (upward triangles) or slow immigration (downward triangles), and composed of fast (black symbols) or slow (red symbols) grazing heterotrophs. Maximum effects >10 are displayed as a maximum effect size of 10. Absence of a symbol for recovery time indicates no recovery. (For interpretation of the references to colour in this figure legend, the reader is referred to the web version of this article.)

Recovery of mesozooplankton and phytoplankton from chemical 2 was more frequently observed and occurred more rapidly than recovery from chemical 1 (Fig. 4C, D, and Fig. S5C, D, Supplemental information). Recovery from direct and indirect effects was also more frequently predicted (and was faster) when immigration was fast.

Maximal (Fig. S8, Supplemental information) and integrated effects (Fig. S9, Supplemental information) following summer emission of chemical 1 were comparable to those described for spring emission, both for mesozooplankton (direct) as for phytoplankton (indirect). The same was observed for the maximal effects caused by chemical 2 (Fig. S10, Supplemental information). However, time-integrated effects of chemical 2 were larger for spring than for summer emission (Fig. S11, Supplemental information). Recovery occurred more often and more rapidly following spring emission than summer emission of chemical 1. No consistent differences between recovery patterns of spring and summer emissions could be found for chemical 2 (compare Figs. S5 and S10, Supplemental information).

#### 3.4. Ecosystem dynamics: exposure to chemicals 3 and 4

Again, effects following spring and late summer emissions were similar, so that only the former are discussed in detail, after which the differences between both exposure scenarios are briefly highlighted.

According to the two effect summaries, chemicals 3 and 4 emitted in spring always affected microzooplankton, the only functional group that was sensitive to these two hypothetical chemicals. The maximum effect size for microzooplankton was comparable between chemicals 3 and 4 (Fig. 5A, Fig. S12A, Supplemental information) and mostly negative.

The maximum effect of these chemicals on microzooplankton was mostly negative but positive in mesotrophic food-chains and food-webs when grazing was fast. Also the time-integrated effect on microzooplankton compared well between chemicals 3 and 4 and differences between both chemicals were most pronounced in mesotrophic systems (Figs. S13A, S14A, Supplemental information). Maximum indirect effects of chemicals 3 and 4 on phytoplankton were common and always positive, both in the food-chain as in the food-web, regardless of the settings for grazing and immigration rate (Fig. 5B, Fig. S12B, Supplemental information). The maximum direct effect size was mostly independent of the immigration rate. The maximal direct effect of chemicals 3 and 4 was smaller at low immigration rates but only in mesotrophic food-chains with fast grazing heterotrophs. In mesotrophic food-webs, fast immigration lowered the maximum indirect effect size in case of slow grazing heterotrophs. The integrated direct and indirect effects were sensitive to the immigration rate but in an inconsistent manner (Figs. S13 and S14, Supplemental information).

Recovery of microzooplankton and phytoplankton from chemical 4 (Fig. S12C, D, Supplemental information) was more frequently observed and occurred more rapidly than recovery from chemical 3 (Fig. 5C, D). Recovery from these direct and indirect effects was also more frequently predicted and faster when immigration was fast, except in oligotrophic food-webs containing fast grazing heterotrophs and exposed to chemical 4.

The maximal direct and indirect effects of spring emission of chemical 3 (Fig. 5) were comparable to those following late summer emission (Fig. S15, Supplemental information). The same was found for the time-integrated effects (Fig. S16, Supplemental information). For chemical 4,

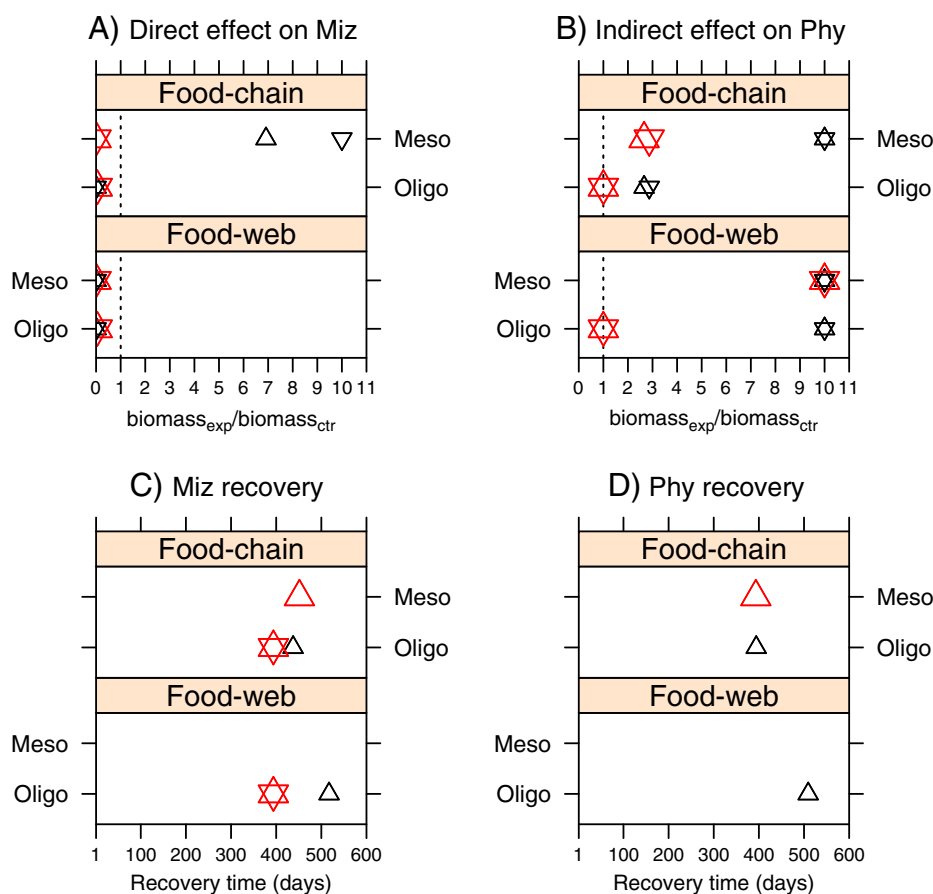


**Fig. 5.** Maximum effect sizes and recovery times for microzooplankton and phytoplankton following exposure to chemical 3 in spring, in mesotrophic and oligotrophic food-webs and food-chains, characterized by fast (upward triangles) or slow immigration (downward triangles), and composed of fast (black symbols) or slow (red symbols) grazing heterotrophs. Maximum effects > 10 are displayed as a maximum effect size of 10. Absence of a symbol for recovery time indicates no recovery. (For interpretation of the references to colour in this figure legend, the reader is referred to the web version of this article.)

maximal effects following spring emission (Fig. S12, Supplemental information) were larger than those following summer emission (Fig. S17, Supplemental information). The same was found for the time-integrated effects (Fig. S18, Supplemental information).

Recovery occurred more often and more rapidly following spring emission than following summer emission of chemical 3 (Fig. S15C, D, Supplemental information). No consistent differences between recovery patterns of spring and summer emissions could be found for chemical 4 (Fig. S17C, D, Supplemental information).

## 4. Discussion

### 4.1. Ecological and exposure scenarios

Our control simulations illustrated how immigration stabilized population dynamics and facilitated coexistence of trophically similar species, which is in line with findings from earlier theoretical exercises (McCallum, 1992). However, the expected positive effect of immigration on the recovery of the targeted functional group (Caquet et al., 2007) was only predicted for certain ecological scenarios. For other scenarios, the immigration rate did not affect recovery. In both oligo- and mesotrophic systems, interaction strength (using grazing rate as a proxy) was suggested as a more important driver for direct effects than immigration rate, and this result was robust to the effect summary considered (maximum effect vs. time-integrated). In general, weak consumer–producer interactions led to weaker direct (and indirect) effects, i.e. the biomasses of the targeted groups (micro- or mesozooplankton) and of phytoplankton in food-chains and food-webs were less affected

by the chemicals. This finding corroborates with several reports on the importance of strong interactions as determinants of population dynamics and extinction (May, 1972; McCann et al., 1998), although this view has been challenged (Allesina and Tang, 2012). It also suggests that the ‘weak interaction effect’, as defined in basic ecology, plays a role in the occurrence of ecological effects of chemicals as well (McCann, 2000). If half-saturation constants for grazing scale with the competition strength between grazers, our findings also correspond to those recently presented by Kattwinkel and Liess (Kattwinkel and Liess, 2014). It should be noted though that interaction strength can be modified by chemical-induced behavioural changes, e.g. as shown by Brooks et al. for the case of predator–prey interactions in Cd-exposed freshwater ecosystems (Brooks et al., 2009b). Such modifications in behaviour are typically not included in the type of models presented in the present paper. The findings presented by Brooks et al. (Brooks et al., 2009b), indicating that sublethal exposure of prey may modify its vulnerability to predators with specific hunting strategies, make it clear that such extensions are both scientifically challenging and relevant for risk assessment.

The mesotrophic systems we modelled were less dynamically stable, were less resistant to the chemical-induced perturbations, and recovered more slowly from such perturbations. Again, this finding is insensitive to the effect metric considered (maximum or time-integrated effects). Although the combined effects of nutrient enrichment and chemical exposure have been examined (Halstead et al., 2014), we do not know of experiments where the responses to chemicals of food-webs similar to those examined here were compared between different trophic states, so it is not possible at the moment to confirm or reject

this theoretical expectation. We only found reports of experiments where plankton communities were exposed to fish predation as a stressor, showing that effects of predation and recovery rates after fish removal were less severe and faster, respectively, in oligotrophic than in mesotrophic systems (Perez-Fuentetaja et al., 1996).

For some ecological scenarios, our models predicted direct effects that were positive. This result is at first counterintuitive but indicates that care should be taken when classifying a deviation of the most sensitive functional group from its control biomass as a direct effect. Indeed, such positive effects indicate feedbacks caused by large indirect effects on phytoplankton (mostly in mesotrophic systems with fast grazing heterotrophs, e.g. Fig. 5). Meso- (chemicals 1 and 2) or microzooplankton decimation (chemicals 3 and 4) causes phytoplankton blooms, which subsequently stimulate zooplankton density during the recovery phase, when chemical concentrations have dropped to zero. This result demonstrates that changes in the size of a functional group that is targeted by a given chemical cannot be always simply categorized as direct effects but may classify as indirect effects because they originate from a combination of chemical toxicity and a trophic cascade caused by interspecific interactions.

The toxicological profile of the chemical (i.e. what functional group was targeted by the chemical) was the most influential parameter of the exposure scenario. In contrast, the season of emission appeared far less important. However, it should be noted that the concentrations considered in this paper (500 to 4000 ng/L, depending on the chemical; Fig. 2) were relatively high because they approached or surpassed lethal values for 50% of the organisms tested in a single-species toxicity test (1000 ng/L; Table 2). As a result, effects were inherently large and recovery inherently slow so that differences in these descriptors of ecological effect between exposure scenarios may have been less detectable. Future efforts may perform similar exercises across a gradient of chemical exposure, but no such efforts were pursued in the present paper.

#### 4.2. Indirect effects

The modelling exercise we present in this paper suggests that indirect effects on phytoplankton following direct effects on mesozooplankton (chemicals 1 and 2) occur in simple food-chains but are highly exceptional in food-webs. In contrast, direct effects on microzooplankton (chemicals 3 and 4) more often resulted in indirect effects in food-webs. This difference in the occurrence of indirect effects between both chemical pairs makes both intuitive and mathematical sense. In food-webs, where both zooplankton groups were present, the biomass density of mesozooplankton was mostly 10 to 100 times lower than that of microzooplankton. Correcting for differences in maximum grazing rates between both groups (two times higher for micro- than for mesozooplankton), the maximum grazing pressure on phytoplankton exerted by mesozooplankton was 5 to 50 times lower than by microzooplankton. Thus, a given direct effect on mesozooplankton is likely to result in a smaller indirect effect on phytoplankton than a direct effect of the same size on microzooplankton. This result demonstrates the need to account for dominance patterns when predicting the potential for indirect effects. Our results suggest that, when dominance combines with sensitivity, indirect effects will be larger than when less abundant functional groups are most sensitive.

Are the indirect effects following direct effects of chemicals 1 and 2 on mesozooplankton indeed more likely in simple food-chains than in food-webs? Since we only considered one (simple) food-chain and one (more complex) food-web, it would be incautious to draw conclusions regarding the relationship between the probability of indirect effects and the number of functional groups in a food-web. Based on data from micro- and mesocosm studies, representing systems with varying food-web complexity but exposed to the same insecticide, some empirical support exists for such a relationship. Briefly, Daam and Van den Brink (2007) found positive indirect effects on phytoplankton following 0.1 µg/L chlorpyrifos exposure in indoor microcosms only

containing phyto- and zooplankton and snails. Brock et al. (Brock et al., 1992), using microcosms stocked with plankton and several macroinvertebrates, reported such indirect effects from 5 µg/L chlorpyrifos onwards. Studies with the same chemical in large outdoor experimental ditches by Van den Brink et al. (1996) and Kersting and Van den Brink (1997) only reported these indirect effects at concentrations from 44 µg/L chlorpyrifos onwards. Note that, in these experimental systems, mesozooplankton is more sensitive to the tested insecticides than microzooplankton, i.e. reasonably representative for our hypothetical chemicals 1 and 2. In these experimental studies, indirect effects would have been less likely to occur in complex systems than in simple systems when both would have been exposed to the same concentration. Taking together the predictions made by our models, which only reflect two samples from the full spectrum of system complexity, and these empirical cosm data, covering a broader range of system complexity, we argue that the relationship between food-web complexity and indirect chemical effects at least deserves further empirical testing and theoretical exploration. In addition to the number of functional groups or species, such empirical studies may also want to consider link density as a measure of food-web complexity, because food-web topology and the distribution of the number of links connecting a node in a food-web have been shown to affect the resistance of ecosystems to species removal (Dunne et al., 2002; Jonsson et al., 2006; Dunne and Williams, 2009; Montoya et al., 2009).

As stated in the **Material and methods** section, no feedback from chemical-induced changes in phytoplankton and detritus stocks to chemical fate was considered in the current exercise, because fate calculations were performed using the control biomass dynamics. Because of the indirect effects on phytoplankton observed here, i.e. algal blooms, we hypothesise that taking into account such feedbacks would probably moderate the effects on zooplankton by reducing chemical availability.

#### 4.3. The influence of chemical type

The direct and indirect effects of chemicals 1 and 3 were more pronounced than those of chemicals 2 and 4. This difference is purely driven by chemical fate, as the partitioning of chemicals 1 and 3 to the water phase (i.e. the bioavailability) was higher than for chemicals 2 and 4. Our simulations focused on pelagic systems and we acknowledge that including sediment consuming benthic species or top carnivores may yield contrasting results. Indeed, the models we present here ignore potential dietary uptake and biomagnification, which would increase (internal) exposure. However, our focus on planktonic systems, with organisms smaller than 5 mm, probably limits the contribution of the dietary uptake route to accumulation and toxicity (De Laender et al., 2010a). Experimental evidence indicates that for species with a larger body size, the hunting and feeding strategy, as well as the type of prey consumed, can influence the accumulation and toxicity of chemicals (Brooks et al., 2009a).

#### 4.4. Conclusions and recommendations

The inclusion of sensitivity and uncertainty analyses in ecotoxicological food-web and ecosystem models is common (Park et al., 2008; De Laender et al., 2010b) but the influence of the ecological and exposure scenario on the prevalence of direct and indirect chemical effects in multi-species systems has remained understudied. We show that combining a dynamic fate model and a food-web/food-chain model allows evaluating chemical availability together with the resulting population-level effects in an ecosystem context. The most notable conclusions include that (1) indirect effects are most likely when dominance patterns correlate with sensitivity patterns; (2) direct and indirect effects are most pronounced in eutrophic systems; and (3) interaction strength is a stronger determinant for effect size than the immigration rate. As an overarching conclusion drawn from our simulations, which represent theoretical expectations for a vast

array of ecological and exposure scenarios, we postulate that ecotoxicological research at the ecosystem level and risk assessments based on such research need to sufficiently justify the ecological scenario considered if direct and indirect effects of chemicals are to be assessed in a robust and transparent way.

## Acknowledgements

The Chimera project is financed by the Long Range Initiative of CEFIC ([www.cefic-lri.org](http://www.cefic-lri.org); project code: LRI-ECO19). Three anonymous reviewers are thanked for their constructive comments.

## Appendix A. Supplementary data

Supplementary data to this article can be found online at <http://dx.doi.org/10.1016/j.envint.2014.10.012>.

## References

- Alexander, A.C., Luis, A.T., Culp, J.M., Baird, D.J., Cessna, A.J., 2013. Can nutrients mask community responses to insecticide mixtures? *Ecotoxicology* 22 (7), 1085–1100.
- Allesina, S., Tang, S., 2012. Stability criteria for complex ecosystems. *Nature* 483 (7388), 205–208.
- Armitage, J.M., Franco, A., Gomez, S., Cousins, I.T., 2008. Modeling the potential influence of particle deposition on the accumulation of organic contaminants by submerged aquatic vegetation. *Environ. Sci. Technol.* 42 (11), 4052–4059.
- Baines, S.B., Pace, M.L., 1991. The production of dissolved organic matter by phytoplankton and its importance to bacteria – patterns across marine and fresh water systems. *Limnol. Oceanogr.* 36 (6), 1078–1090.
- Bidwell, R.G.S., 1977. Photosynthesis and light and dark respiration in freshwater algae. *Can. J. Bot.* 55 (7), 809–818.
- Brock, T.C., van den Bogaert, M., Bos, R., van Breukelen, S.W., Reiche, R., Terwoert, J., Suykerbuyk, R.E., Roijackers, R.M., 1992. Fate and effects of the insecticide Dursban 4E in indoor *Elodea*-dominated and macrophyte-free freshwater model ecosystems: II. Secondary effects on community structure. *Arch. Environ. Contam. Toxicol.* 23 (4), 391–409.
- Brooks, A.C., Gaskell, P.N., Maltby, L.L., 2009a. Importance of prey and predator feeding behaviors for trophic transfer and secondary poisoning. *Environ. Sci. Technol.* 43 (20), 7916–7923.
- Brooks, A.C., Gaskell, P.N., Maltby, L.L., 2009b. Sublethal effects and predator–prey interactions: implications for ecological risk assessment. *Environ. Toxicol. Chem.* 28 (11), 2449–2457.
- Caquet, T., Hanson, M.L., Roucaute, M., Graham, D.W., Lagadic, L., 2007. Influence of isolation on the recovery of pond mesocosms from the application of an insecticide. II. Benthic macroinvertebrate responses. *Environ. Toxicol. Chem.* 26 (6), 1280–1290.
- Carlson, R., 1977. A trophic state index for lakes. *Limnol. Oceanogr.* 22 (2).
- Daam, M.A., Van den Brink, P.J., 2007. Effects of chlorpyrifos, carbendazim, and linuron on the ecology of a small indoor aquatic microcosm. *Arch. Environ. Contam. Toxicol.* 53 (1), 22–35.
- De Hoop, L., De Troch, M., Hendriks, A.J., De Laender, F., 2013. Modeling toxic stress by atrazine in a marine consumer–resource system. *Environ. Toxicol. Chem.* 32 (5), 1088–1095.
- De Laender, F., Janssen, C.R., 2013. Brief communication: the ecosystem perspective in ecotoxicology as a way forward for the ecological risk assessment of chemicals. *Integr. Environ. Assess. Manag.* 9 (3), e34–e38.
- De Laender, F., De Schampelaere, K.A.C., Vanrolleghem, P.A., Janssen, C.R., 2008a. Comparison of different toxic effect sub-models in ecosystem modelling used for ecological effect assessments and water quality standard setting. *Ecotoxicol. Environ. Saf.* 69 (1), 13–23.
- De Laender, F., De Schampelaere, K.A.C., Vanrolleghem, P.A., Janssen, C.R., 2008b. Is ecosystem structure the target of concern in ecological effect assessments? *Water Res.* 42 (10–11), 2395–2402.
- De Laender, F., De Schampelaere, K.A.C., Vanrolleghem, P.A., Janssen, C.R., 2008c. Validation of an ecosystem modelling approach as a tool for ecological effect assessments. *Chemosphere* 71 (3), 529–545.
- De Laender, F., Van Oevelen, D., Middelburg, J.J., Soetaert, K., 2010a. Uncertainties in ecological, chemical and physiological parameters of a bioaccumulation model: implications for internal concentrations and tissue based risk quotients. *Ecotoxicol. Environ. Saf.* 73 (3), 240–246.
- De Laender, F., Soetaert, K., De Schampelaere, K.A.C., Middelburg, J.J., Janssen, C.R., 2010b. Ecological significance of hazardous concentrations in a planktonic food web. *Ecotoxicol. Environ. Saf.* 73 (3), 247–253.
- De Laender, F., Olsen, G.H., Frost, T., Grøsvik, B.E., Grung, M., Hansen, B.H., et al., 2011. Ecotoxicological mechanisms and models in an impact analysis tool for oil spills. *J. Toxicol. Environ. Health Part A* 74, 605–619.
- Di Guardo, A., Hermens, J.L.M., 2013. Challenges for exposure prediction in ecological risk assessment, integrated environmental assessment and management. *Integr. Environ. Assess. Manag.* 9, 4–14.
- Di Guardo, A., Ferrari, C., Infantino, A., 2006. Development of a dynamic aquatic model (Dyna Model): estimating temporal emissions of DDT to Lake Maggiore (N. Italy). *Environ. Sci. Pollut. Res. Int.* 13 (1), 50–58.
- Donali, E., Olli, K., Heiskanen, A.S., Andersen, T., 1999. Carbon flow patterns in the planktonic food web of the Gulf of Riga, the Baltic Sea: a reconstruction by the inverse method. *J. Mar. Syst.* 23 (1–3), 251–268.
- Dunne, J.A., Williams, R.J., 2009. Cascading extinctions and community collapse in model food webs. *Philos. Trans. R. Soc. Lond. B Biol. Sci.* 364 (1524), 1711–1723.
- Dunne, J.A., Williams, R.J., Martinez, N.D., 2002. Network topology and species loss in food webs: robustness increases with connectance. *Ecol. Lett.* 5 (4), 558–567.
- Fleeger, J.W., Carman, K.R., Nisbet, R.M., 2003. Indirect effects of contaminants in aquatic ecosystems. *Sci. Total Environ.* 317 (1–3), 207–233.
- Forbes, V.E., Hommen, U., Thorbek, P., Heimbach, F., Van den Brink, P.J., Wogram, J., Thulke, H., Grimm, V., 2009. Ecological models in support of regulatory risk assessments of pesticides: developing a strategy for the future. *Integr. Environ. Assess. Manag.* 5 (1), 167–172.
- Gabsi, F., Schäffer, A., Preuss, T.G., 2014. Predicting the sensitivity of populations from individual exposure to chemicals: the role of ecological interactions. *Environ. Toxicol. Chem.* 33 (7), 1449–1457.
- Grimm, V., Ashauer, R., Forbes, V., Hommen, U., Preuss, T.G., Schmidt, A., van den Brink, P.J., Wogram, J., Thorbek, P., 2009. CREAM: a European project on mechanistic effect models for ecological risk assessment of chemicals. *Environ. Sci. Pollut. Res. Int.* 16 (6), 614–617.
- Halstead, N.T., McMahon, T.A., Johnson, S.A., Raffel, T.R., Romansic, J.M., Crumrine, P.W., Rohr, J.R., 2014. Community ecology theory predicts the effects of agrochemical mixtures on aquatic biodiversity and ecosystem properties. *Ecol. Lett.* 17 (8), 932–941.
- Hansen, P.J., Bjørnsen, P.K., Hansen, B.W., 1997. Zooplankton grazing and growth: scaling within the 2–2,000- $\mu$ m body size range. *Limnol. Oceanogr.* 42 (4), 687–704.
- Hendriks, A.J., 1999. Allometric scaling of rate, age and density parameters in ecological models. *Oikos* 86 (2), 293–310.
- Infantino, A., Morselli, M., Di Guardo, A., 2013. Integration of a dynamic organism model into the DynA Model: development and application to the case of DDT in Lake Maggiore, Italy. *Sci. Total Environ.* 454–455, 358–365.
- Janse, J.H., 2005. Model Studies on the Eutrophication of Shallow Lakes and Ditches. PhD Dissertation Wageningen University.
- Jonsson, T., Karlsson, P., Jonsson, A., 2006. Food web structure affects the extinction risk of species in ecological communities. *Ecol. Modell.* 199 (1), 93–106.
- Kattwinkel, M., Liess, M., 2014. Competition matters: species interactions prolong the long-term effects of pulsed toxicant stress on populations. *Environ. Toxicol. Chem.* 33 (7), 1458–1465.
- Kersting, K., Van den Brink, P., 1997. Effects of the insecticide Dursban®4e (active ingredient chlorpyrifos) in outdoor experimental ditches: responses of ecosystem metabolism. *Environ. Toxicol. Chem.* 16 (2), 251–259.
- Liess, M., Schulz, R., 1999. Linking insecticide contamination and population response in an agricultural stream. *Environ. Toxicol. Chem.* 18 (9), 1948–1955.
- Mackay, D., 2001. Multimedia Environmental Models, The Fugacity Approach, 2nd ed. Lewis Publishers, Chelsea MI, USA.
- Martin, N.A., 1972. Temperature fluctuations within English lowland ponds. *Hydrobiologia* 40, 455–469.
- Martin, B.T., Jager, T., Nisbet, R.M., Preuss, T.G., Hammers-Wirtz, M., Grimm, V., 2013. Extrapolating ecotoxicological effects from individuals to populations: a generic approach based on Dynamic Energy Budget theory and individual-based modeling. *Ecotoxicology* 22 (3), 574–583.
- May, R.M., 1972. Will a large complex system be stable? *Nature* 238, 413–414.
- McCallum, H.I., 1992. Effects of immigration on chaotic population dynamics. *J. Theor. Biol.* 154, 277–284.
- McCann, K.S., 2000. The diversity–stability debate. *Nature* 405 (6783), 228–233.
- McCann, K.S., Hastings, A., Huxel, G.R., 1998. Weak trophic interactions and the balance of nature. *Nature* 395, 794–798.
- Moisan, J.R., Moisan, T.A., Abbott, M.R., 2002. Modelling the effect of temperature on the maximum growth rates of phytoplankton populations. *Ecol. Modell.* 153 (3), 197–215.
- Montoya, J.M., Woodward, G., Emmerson, M.C., Solé, R.V., 2009. Press perturbations and indirect effects in real food webs. *Ecology* 90 (9), 2426–2433.
- Naito, W., Miyamoto, K., Nakanishi, J., Masunaga, S., Bartell, S.M., 2003. Evaluation of an ecosystem model in ecological risk assessment of chemicals. *Chemosphere* 53 (4), 363–375.
- Neutel, A.-M., Heesterbeek, J. a P., De Ruiter, P.C., 2002. Stability in real food webs: weak links in long loops. *Science* 296 (5570), 1120–1123.
- Noel, H.L., Hopkin, S.P., Hutchinson, T.H., Williams, T.D., Sibby, R.M., 2006. Population growth rate and carrying capacity for springtails *Folsomia candida* exposed to ivermectin. *Ecol. Appl.* 16 (2), 656–665.
- Park, R.A., Clough, J.S., Wellman, M.C., 2008. AQUATOX: modeling environmental fate and ecological effects in aquatic ecosystems. *Ecol. Modell.* 213 (1), 1–15.
- Perez-Fuentetaja, A., McQueen, D., Demers, E., 1996. Stability of oligotrophic and eutrophic planktonic communities after disturbance by fish. *Oikos* 1 (1991), 98–110.
- Pieters, B.J., Jager, T., Kraak, M.H.S., Admiraal, W., 2006. Modeling responses of *Daphnia magna* to pesticide pulse exposure under varying food conditions: intrinsic versus apparent sensitivity. *Ecotoxicology* 15 (7), 601–608.
- R Development Core Team, 2010. R: A Language and Environment for Statistical Computing. R Foundation for Statistical Computing, Vienna, Austria.
- Riemann, B., Simonsen, P., Stensgaard, L., 1989. The carbon and chlorophyll content of phytoplankton from various nutrient regimes. *J. Plankton Res.* 11 (5), 1037–1045.
- Scheffer, M., Rinaldi, S., Kuznetsov, Y.A., vanNes, E.H., 1997. Seasonal dynamics of *Daphnia* and algae explained as a periodically forced predator–prey system. *Oikos* 80 (3), 519–532.
- Traas, T.P., Janse, J.H., Van den Brink, P.J., Brock, T.C.M., Aldenberg, T., 2004. A freshwater food web model for the combined effects of nutrients and insecticide stress and subsequent recovery. *Environ. Toxicol. Chem.* 23 (2), 521–529.

- Van den Brink, P., Van Wijngaarden, R., Lucassen, W., 1996. Effects of the insecticide Dursban® 4E (active ingredient chlorpyrifos) in outdoor experimental ditches: II. Invertebrate community responses and recovery. *Environ. Toxicol. Chem.* 15 (7), 1143–1153.
- Van Wijngaarden, R.P.A., Brock, T.C.M., van den Brink, P.J., Gylstra, R., Maund, S.J., 2006. Ecological effects of spring and late summer applications of lambda-cyhalothrin on freshwater microcosms. *Arch. Environ. Contam. Toxicol.* 50 (2), 220–239.
- Vezina, A.F., Platt, T., 1988. Food web dynamics in the ocean. 1. Best-estimates of flow networks using inverse methods. *Mar. Ecol. Ser.* 42 (3), 269–287.
- Willis, K.J., Van den Brink, P.J., Green, J.D., 2004. Seasonal variation in plankton community responses of mesocosms dosed with pentachlorophenol. *Ecotoxicology* 13 (7), 707–720.
- Young, J.O., 1975. Seasonal and diurnal changes in the water temperature of a temperate pond (England) and a tropical pond (Kenya). *Hydrobiologia* 47, 513–526.

## Chapter 4. Paper III

Supporting information for

### **Theoretically exploring direct and indirect chemical effects across ecological and exposure scenarios using mechanistic fate and effects modelling**

Frederik De Laender<sup>1\*</sup>, Melissa Morselli<sup>2</sup>, Hans Baveco<sup>3</sup>, Paul J. Van den Brink<sup>3,4</sup> and Antonio Di Guardo<sup>2</sup>

<sup>1</sup>Namur University, Research Unit in Environmental and Evolutionary Ecology, Rue de Bruxelles 61, 5000 Namur, Belgium

<sup>2</sup>Department of Science and High Technology, University of Insubria, Via Valleggio 11, 22100 Como, Italy

<sup>3</sup>Alterra, Wageningen University and Research Centre, P.O. Box 47, 6700 AA Wageningen, The Netherlands

<sup>4</sup>Department of Aquatic Ecology and Water Quality Management, Wageningen University, Wageningen University and Research Centre, P.O. Box 47, 6700 AA Wageningen, The Netherlands

\*Corresponding author

*Environment International* **2015**, *74*, 181–190



Supporting information for

**Theoretically exploring direct and indirect chemical effects across ecological and exposure scenarios using mechanistic fate and effects modelling**

**F. De Laender, M. Morselli, Hans Baveco, P.J. Van den Brink, A. Di Guardo**

**Text S1: Fate model**

Chemical mass balance: model equations

In the present work, chemical fate was simulated using a modified version of EcoDynA (Infantino et al. 2013), a fugacity-based (Mackay 2001) three-compartment model developed to investigate the fate of organic chemicals in dynamic organism-water-sediment systems.

In the original EcoDynA model, the dynamic chemical behavior in the three compartments (organism, water and sediment) is described by a system of three 1<sup>st</sup>-order ordinary differential equations (ODEs), one for each compartment. The ODEs, representing the variation of residue moles with time are:

$$dmolORG/dt = a + b * molWAT - c * molORG \quad (1)$$

$$dmolWAT/dt = d + e * molORG + g * molSED - h * molWAT \quad (2)$$

$$dmolSED/dt = i + j * molWAT - k * molSED \quad (3)$$

where *molORG*, *molWAT* and *molSED* represent the moles in the three compartments at a certain time, while each coefficient (from *a* to *k*) represents a transformation or a transport flux (single *D* value or sum of *D*-values) divided by the proper product of volume and fugacity capacity *Z*. All *D* and *Z*-values are listed in Table S1, while explanations for coefficients are reported in Table S2.

For the simulations presented here, the organism compartment was neglected by considering as null all the  $D$ -values describing transport from water to organism and *vice versa* (i.e.,  $D_{VentIn}$ ,  $D_{VentOut}$ ,  $D_{Upt}$ , and  $D_{Eges}$ , regulating input and output ventilation via gills, uptake from food, and fecal egestion, respectively).

### Solution and time step

The ODE system composed of Equations 1, 2 and 3 is solved using a modified 5<sup>th</sup>-order adaptive, diagonally implicit Runge-Kutta numerical method (ESDIRK5(4)) (Semplice et al. 2012). Calculations are performed with sub-hourly time steps, but results (fugacities, from which concentrations in the different compartments and phases are derived) are saved on an hourly basis.

The model was coded using Microsoft Visual Basic 6. At the end of the simulations, hourly outputs (i.e., compartment fugacities, concentrations in all phases and fluxes among compartments) are saved on an hourly basis into comma-separated values (CSV) files and can be input to other models. In this work, for example, bioavailable water concentrations of the modelled chemicals were used as input for the ecosystem model.

### Inclusion of the DOM sub-compartment

In order to account for the presence of dissolved organic matter (DOM), EcoDynA was provided with a new water sub-compartment, and dissolved organic carbon (DOC) was modelled as a fraction of DOM. The fugacity capacity of DOM ( $Z_{DOM}$ , mol m<sup>-3</sup> Pa<sup>-1</sup>) was described as:

$$Z_{DOM} = f_{OC\_DOM} Z_{DOC} \quad (4)$$

where  $f_{OC\_DOM}$  (unitless) is the organic carbon fraction of the DOM compartment and  $Z_{DOC}$  ( $\text{mol m}^{-3} \text{Pa}^{-1}$ ) is the fugacity capacity of DOC. The description of  $Z_{DOC}$  was taken from Armitage et al. (2008):

$$Z_{DOC} = Z_W K_{DOC} \rho_{DOC} \quad (5)$$

where  $Z_W$  ( $\text{mol m}^{-3} \text{Pa}^{-1}$ ) is the water fugacity capacity,  $K_{DOC}$  ( $\text{L kg}^{-1}$ ) is the DOC partition coefficient, calculated as  $0.08 * K_{OW}$ , and  $\rho_{DOC}$  ( $\text{kg L}^{-1}$ ) is the DOC density (for simplicity,  $1 \text{ kg L}^{-1}$ ).

Table S1.  $Z$  ( $\text{mol m}^{-3} \text{Pa}^{-1}$ ) and  $D$ -values ( $\text{mol Pa}^{-1} \text{h}^{-1}$ ) in EcoDynA.

Parameter	Description	Equation
$Z_A$	$Z$ for pure air	$1 / RT$
$Z_Q$	$Z$ for aerosol particles	$6\text{E}+06 / P_L * Z_A$
$Z_{Abulk}$	$Z$ for bulk air	$Z_A * (1 - v_Q) + Z_Q * v_Q$
$Z_W$	$Z$ for pure water	$1 / H$
$Z_{WP}$	$Z$ for water column particles	$0.41 * K_{OW} * f_P * \sigma_P * Z_W / 1000$
$Z_{Wbulk}$	$Z$ for bulk water	$Z_W * (1 - v_P) + Z_{WP} * v_P$
$Z_S$	$Z$ for sediment particles	$0.41 * K_{OW} * f_S * \sigma_S * Z_W / 1000$
$Z_{Sbulk}$	$Z$ for bulk sediment	$Z_W * (1 - v_S) + Z_S * v_S$
$Z_O$	$Z$ for octanol	$Z_W * K_{OW}$
$Z_{Org}$	$Z$ for aquatic organism	$Z_W * K_{OW} * lf$
$Z_{Food}$	$Z$ for aquatic organism food	$Z_W * K_{OW} * lf_{Food}$
$D_I$	Water inflow	$G_I * Z_W$
$D_X$	Water particle inflow	$G_X * Z_{WP}$
$D_J$	Water outflow	$G_J * Z_W$
$D_Y$	Water particle outflow	$G_Y * Z_{WP}$
$D_V$	Absorption / Volatilization	$k_V * A_W * Z_W$
$D_M$	Rain dissolution	$G_M * Z_W$
$D_C$	Wet particle deposition	$G_C * Z_Q$
$D_Q$	Dry particle deposition	$G_Q * Z_Q$
$D_T$	Sediment-to-water/water-to-sediment diffusion	$k_T * A_S * Z_W$
$D_D$	Sediment deposition	$G_D * Z_{WP}$

$D_R$	Sediment resuspension	$G_R * Z_S$
$D_B$	Sediment burial	$G_B * Z_S$
$D_W$	Water transformation	$k_W * V_W * Z_W$
$D_S$	Sediment transformation	$k_S * V_S * Z_S$
$D_{VentIn}$	Input ventilation (exchange via gills)	$k_1 * V_{Org} * Z_W$
$D_{VentOut}$	Output ventilation (exchange via gills)	$k_2 * V_{Org} * Z_{Org}$
$D_{Upt}$	Uptake from food	$E_A * G_A * Z_{Food}$
$D_{Met}$	Metabolism transformation	$k_M * V_{Org} * Z_{Org}$
$D_{Growth}$	Growth dilution	$k_G * V_{Org} * Z_{Org}$
$D_{Eges}$	Fecal egestion	$D_{Upt} / QF$

$R$  = gas constant ( $8.314 \text{ J mol}^{-1} \text{ K}^{-1}$ )

$T$  = absolute temperature (K)

$H$  = Henry's Law constant ( $\text{Pa m}^3 \text{ mol}^{-1}$ )

$P_L$  = sub-cooled liquid vapour pressure (Pa)

$v_Q$ ,  $v_P$  and  $v_S$  = volume fractions of aerosol in air, particles in water and solids in surface sediments, respectively

$f_P$  and  $f_S$  = fraction of organic carbon in water particles and sediment, respectively.

$lf$  and  $lf_{Food}$  = lipid fraction in organism and food, respectively. For additional details see Infantino et al. 2013.

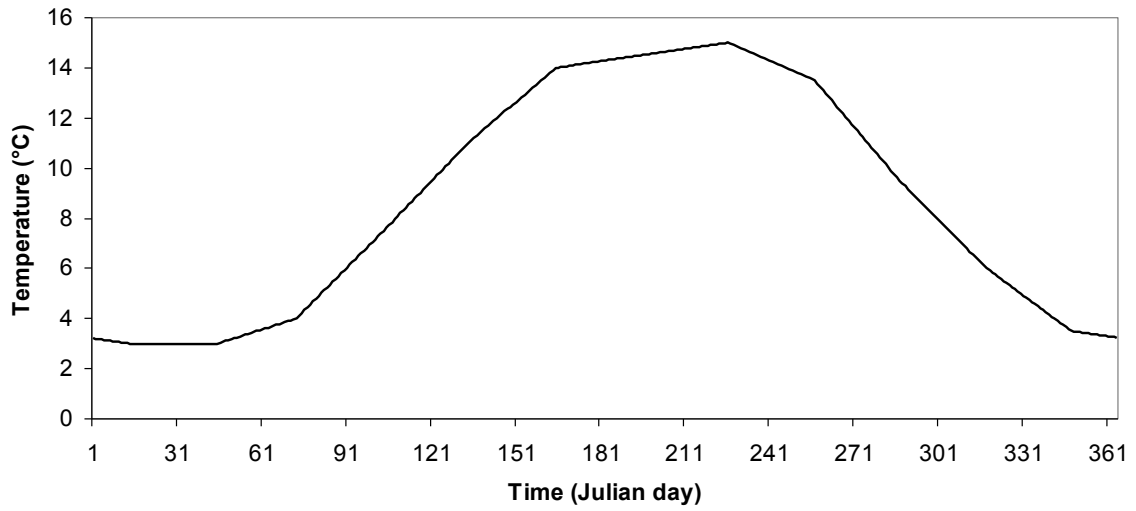


Figure S1. Seasonal profile of water temperature (°C) adopted for the simulations.

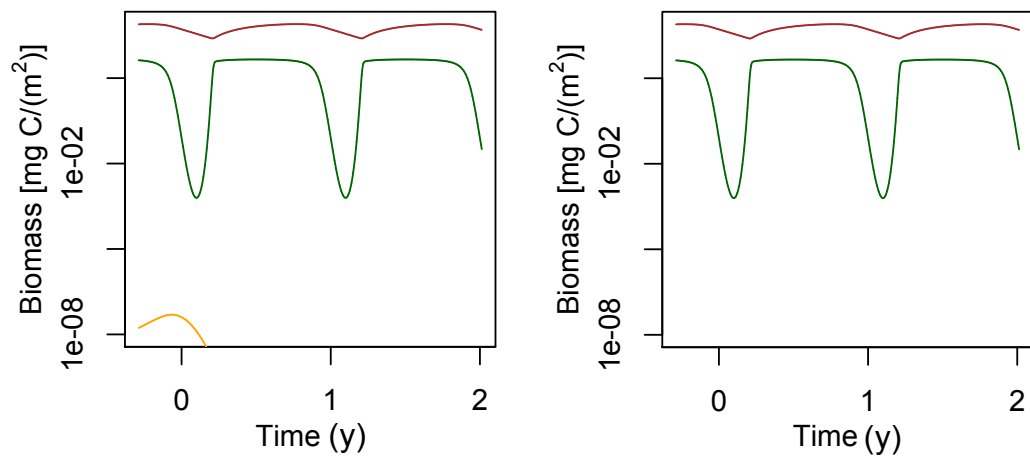


Figure S2: Food web (left) and food chain dynamics (right) when immigration rates are low in oligotrophic systems occupied by slow grazing heterotrophs: only phytoplankton (green) persists. Brown lines represent detritus.

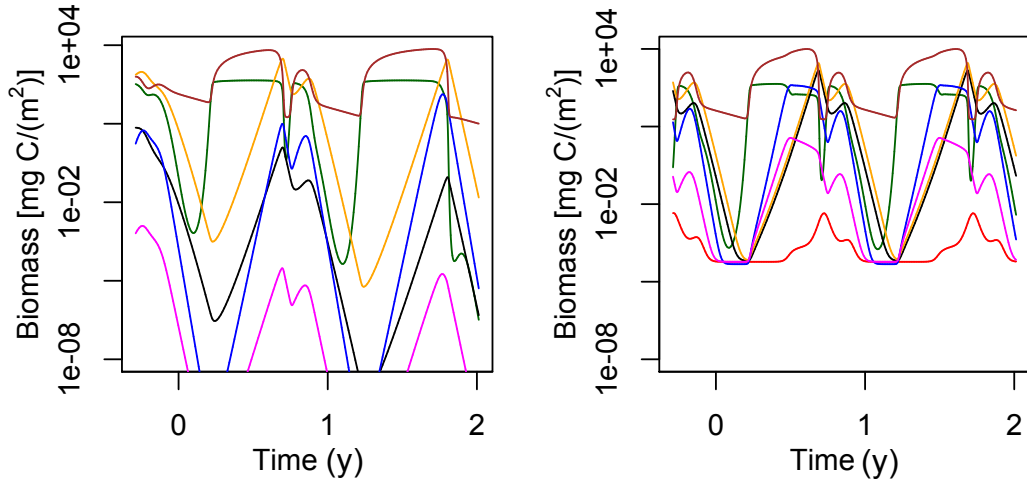


Figure S3: Dynamics of a food-web with slow grazing heterotrophs in a mesotrophic system with low (left) and high immigration rates (right). Color codes are as in Figure 1.

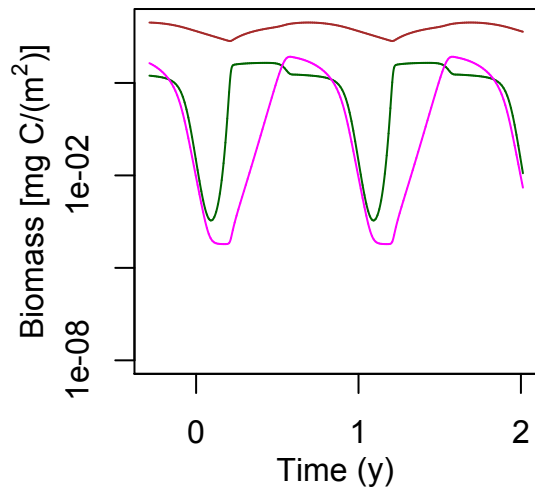
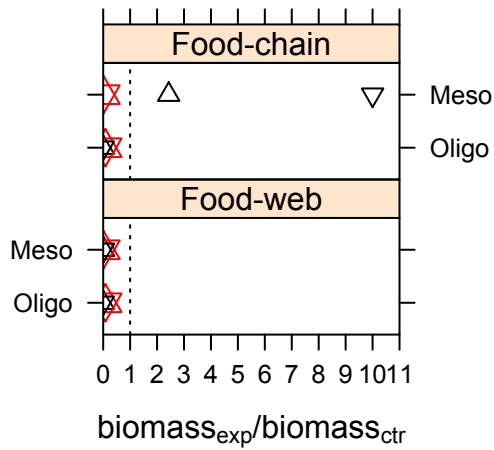
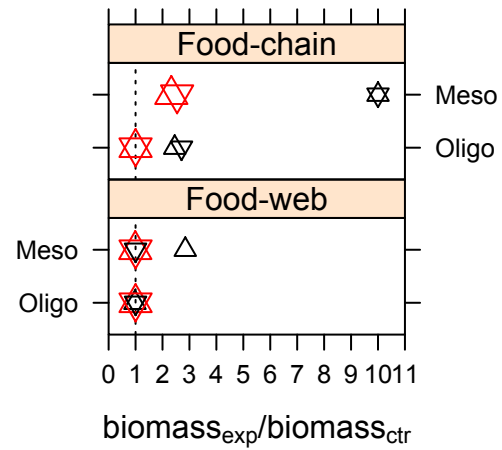


Figure S4: Dynamics of a food chain (phytoplankton and mesozooplankton) with fast grazing mesozooplankton, fast immigration in an oligotrophic system. Mesozooplankton biomass is higher than in a food web in the same ecological scenario (Figure 3A).

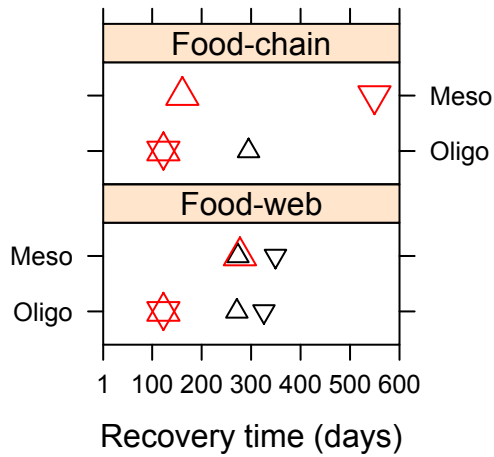
### A: Direct effect on Mez



### B: Indirect effect on Phy



### C: Mez recovery



### D: Phy recovery

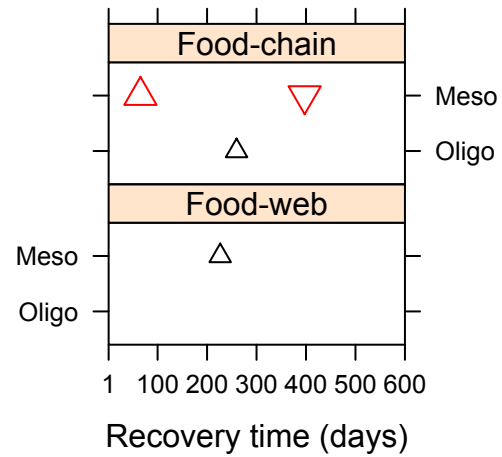
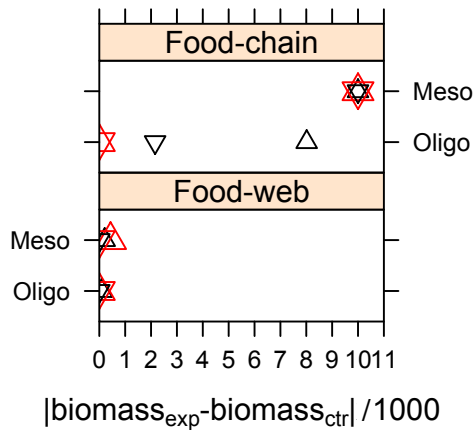


Figure S5: Maximum effect sizes and recovery times for mesozooplankton and phytoplankton following exposure to chemical 2 in spring, in mesotrophic and oligotrophic food-webs and food-chains, characterized by fast (upward triangles) or slow immigration (downward triangles), and composed of fast (black symbols) or slow (red symbols) grazing heterotrophs. Maximum effects > 10 are displayed as a maximum effect size of 10. Absence of a symbol for recovery time indicates no recovery.

### A: Direct effect on Mez



### B: Indirect effect on Phy

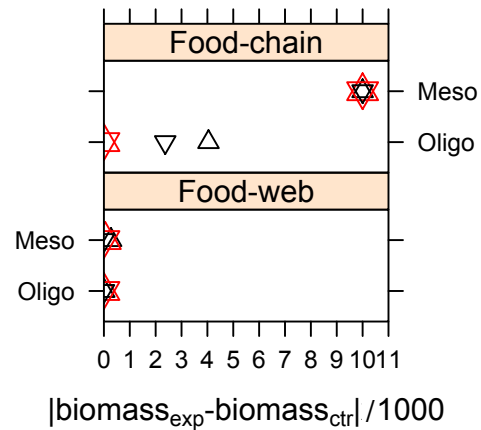
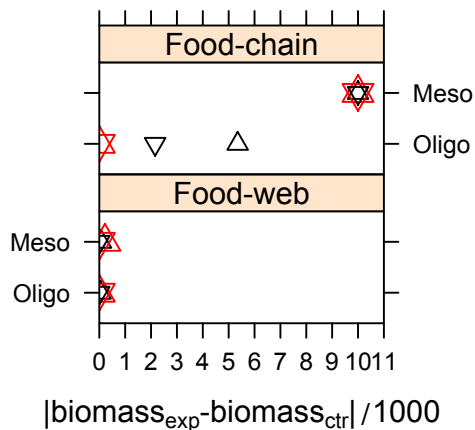


Figure S6: Time-integrated effects for mesozooplankton and phytoplankton following exposure to chemical 1 in spring, in mesotrophic and oligotrophic food-webs and food-chains, characterized by fast (upward triangles) or slow immigration (downward triangles), and composed of fast (black symbols) or slow (red symbols) grazing heterotrophs. Integrated effects > 10 are displayed as an integrated effect size of 10. Absence of a symbol for recovery time indicates no recovery.

### A: Direct effect on Mez



### B: Indirect effect on Phy

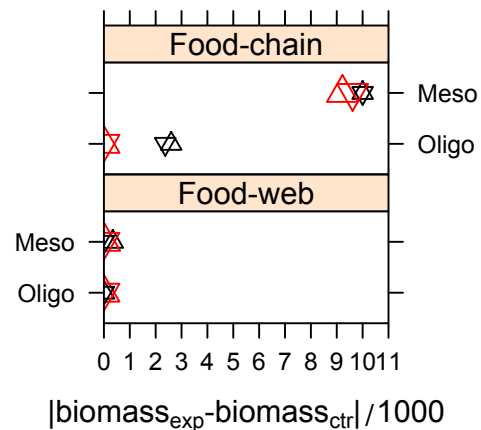


Figure S7: Time-integrated effects for mesozooplankton and phytoplankton following exposure to chemical 2 in spring, in mesotrophic and oligotrophic food-webs and food-chains, characterized by fast (upward triangles) or slow immigration (downward triangles), and composed of fast (black symbols) or slow (red symbols) grazing heterotrophs. Integrated effects > 10 are displayed as an integrated effect size of 10. Absence of a symbol for recovery time indicates no recovery.

heterotrophs. Integrated effects > 10 are displayed as an integrated effect size of 10.

Absence of a symbol for recovery time indicates no recovery.

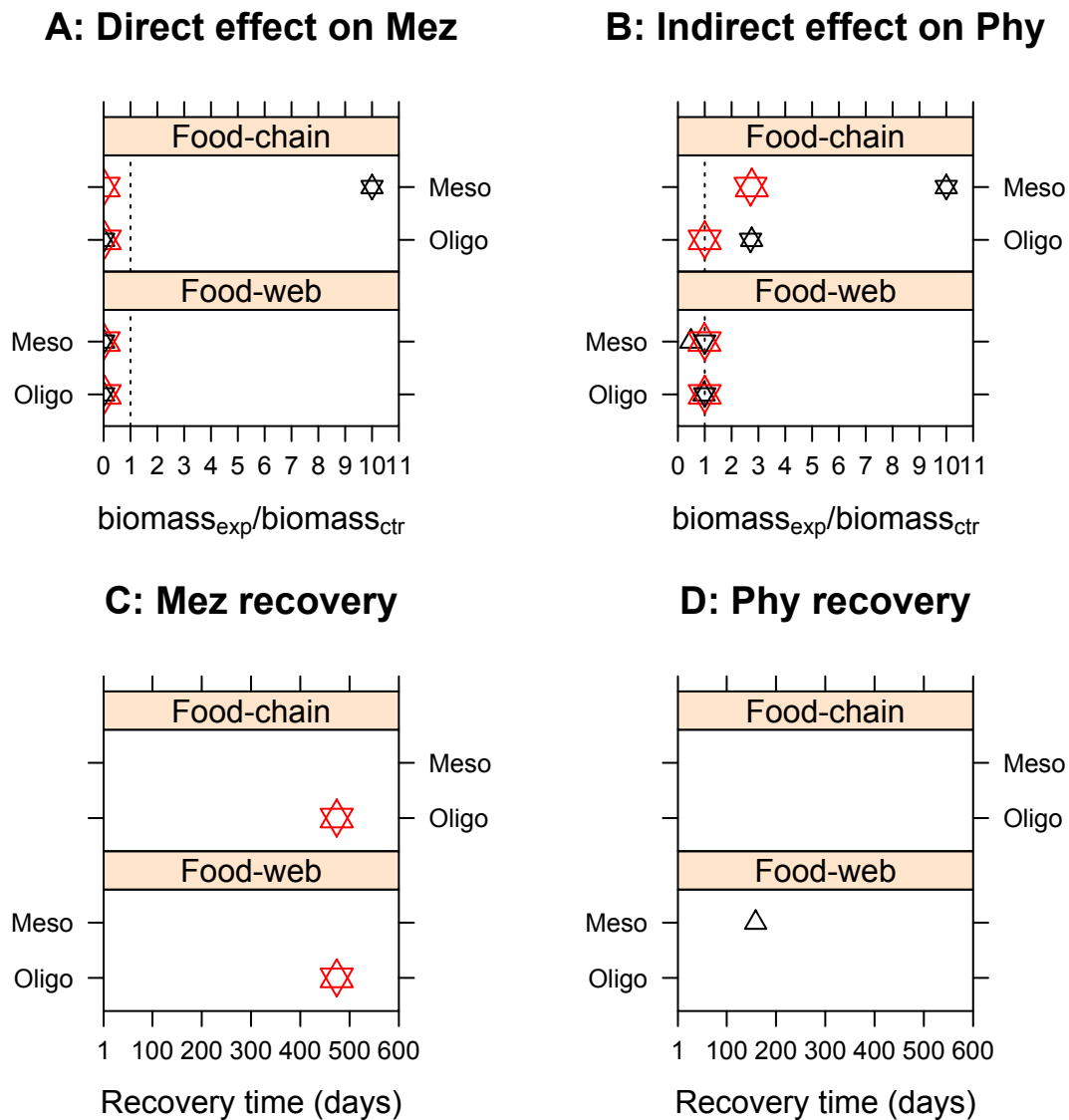
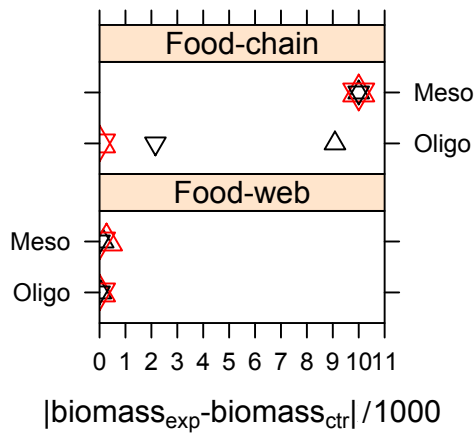


Figure S8: Maximum effect sizes and recovery times for mesozooplankton and phytoplankton following exposure to chemical 1 in summer, in mesotrophic and oligotrophic food-webs and food-chains, characterized by fast (upward triangles) or slow immigration (downward triangles), and composed of fast (black symbols) or slow (red symbols) grazing heterotrophs. Maximum effects > 10 are displayed as a maximum effect size of 10. Absence of a symbol for recovery time indicates no recovery.

### A: Direct effect on Mez



### B: Indirect effect on Phy

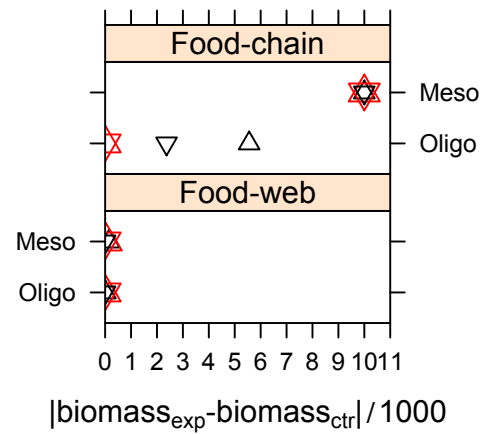
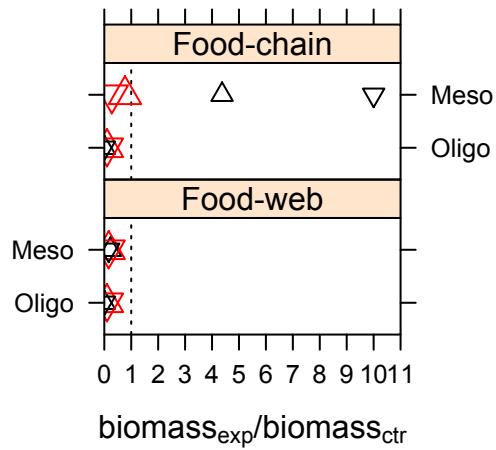
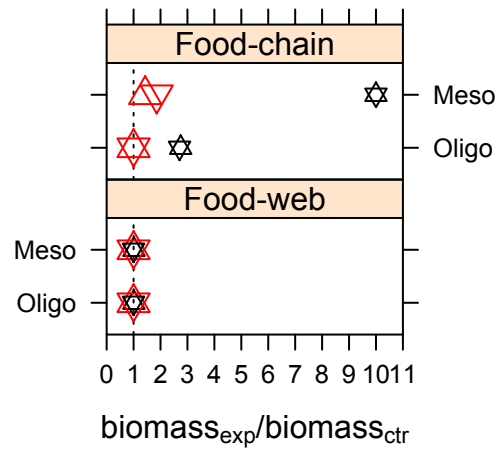


Figure S9: Time-integrated effects for mesozooplankton and phytoplankton following exposure to chemical 1 in summer, in mesotrophic and oligotrophic food-webs and food-chains, characterized by fast (upward triangles) or slow immigration (downward triangles), and composed of fast (black symbols) or slow (red symbols) grazing heterotrophs. Integrated effects  $> 10$  are displayed as an integrated effect size of 10. Absence of a symbol for recovery time indicates no recovery.

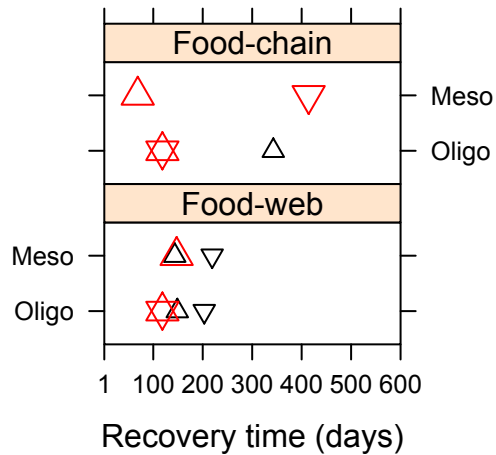
### A: Direct effect on Mez



### B: Indirect effect on Phy



### C: Mez recovery



### D: Phy recovery

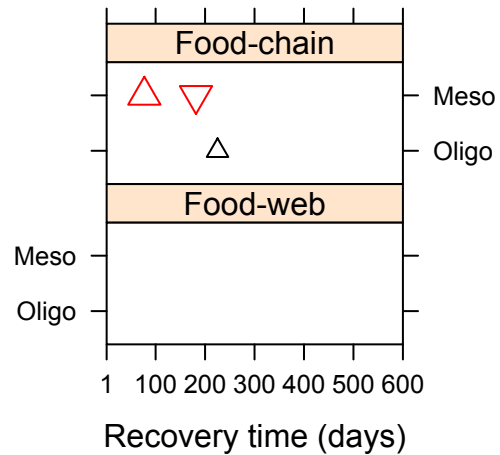
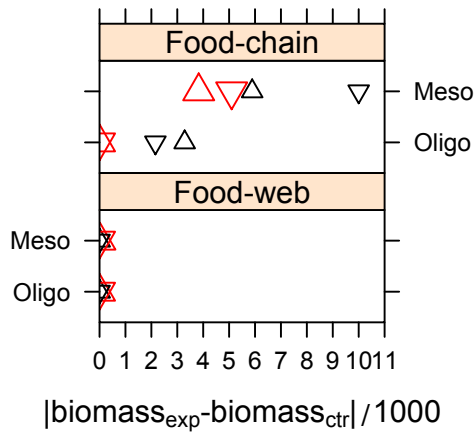


Figure S10: Maximum effect sizes and recovery times for mesozooplankton and phytoplankton following exposure to chemical 2 in summer, in mesotrophic and oligotrophic food-webs and food-chains, characterized by fast (upward triangles) or slow immigration (downward triangles), and composed of fast (black symbols) or slow (red symbols) grazing heterotrophs. Maximum effects  $> 10$  are displayed as a maximum effect size of 10. Absence of a symbol for recovery time indicates no recovery.

### A: Direct effect on Mez



### B: Indirect effect on Phy

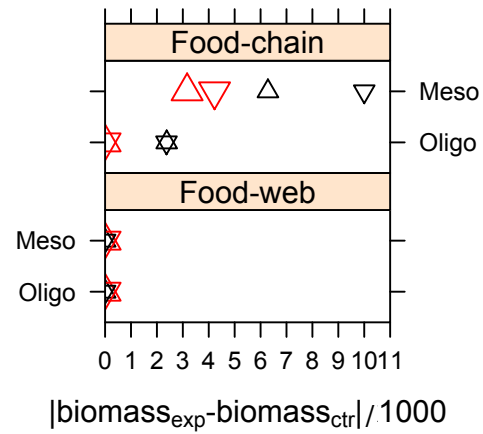
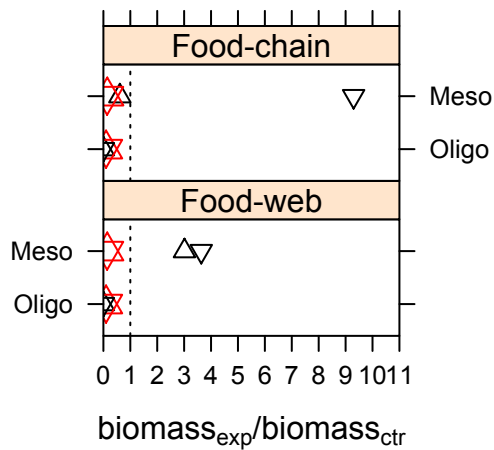
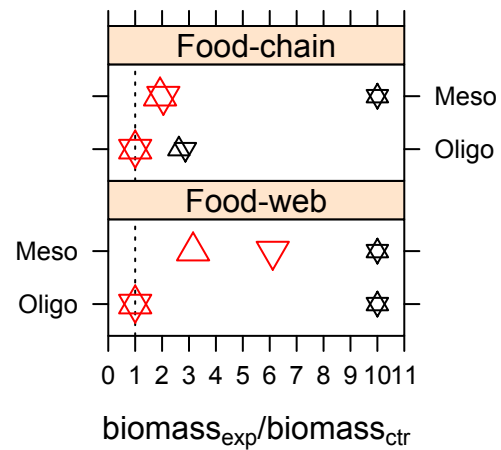


Figure S11: Time-integrated effects for mesozooplankton and phytoplankton following exposure to chemical 2 in summer, in mesotrophic and oligotrophic food-webs and food-chains, characterized by fast (upward triangles) or slow immigration (downward triangles), and composed of fast (black symbols) or slow (red symbols) grazing heterotrophs. Integrated effects > 10 are displayed as an integrated effect size of 10. Absence of a symbol for recovery time indicates no recovery.

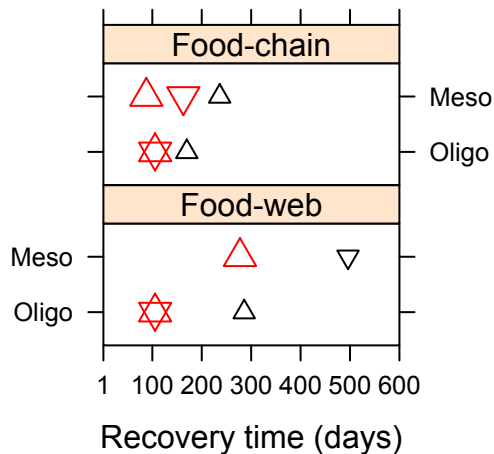
### A: Direct effect on Miz



### B: Indirect effect on Phy



### C: Miz recovery



### D: Phy recovery

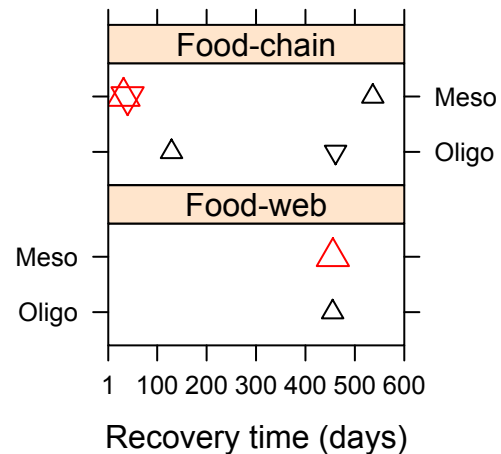


Figure S12: Maximum effect sizes and recovery times for microzooplankton and phytoplankton following exposure to chemical 4 in spring, in mesotrophic and oligotrophic food-webs and food-chains, characterized by fast (upward triangles) or slow immigration (downward triangles), and composed of fast (black symbols) or slow (red symbols) grazing heterotrophs. Maximum effects > 10 are displayed as a maximum effect size of 10. Absence of a symbol for recovery time indicates no recovery.

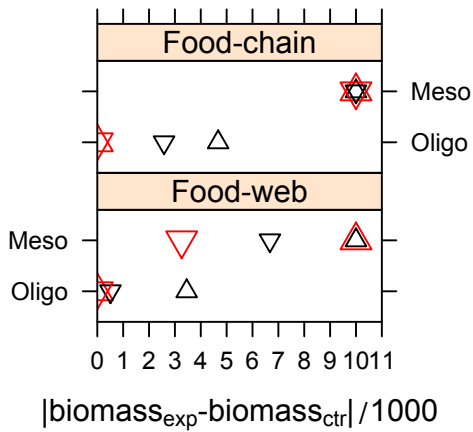
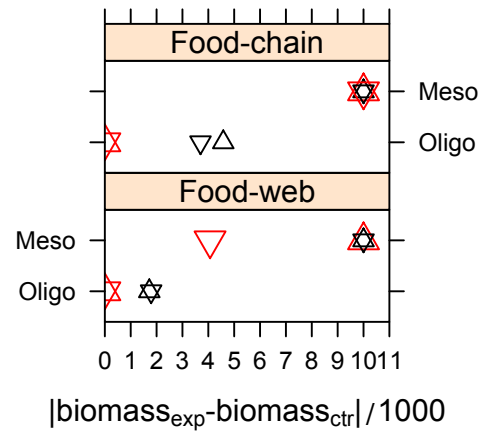
**A: Direct effect on Miz****B: Indirect effect on Phy**

Figure S13: Time-integrated effects for microzooplankton and phytoplankton following exposure to chemical 3 in spring, in mesotrophic and oligotrophic food-webs and food-chains, characterized by fast (upward triangles) or slow immigration (downward triangles), and composed of fast (black symbols) or slow (red symbols) grazing heterotrophs. Integrated effects  $> 10$  are displayed as an integrated effect size of 10. Absence of a symbol for recovery time indicates no recovery.

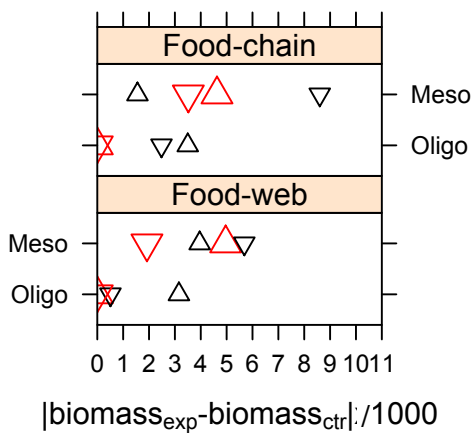
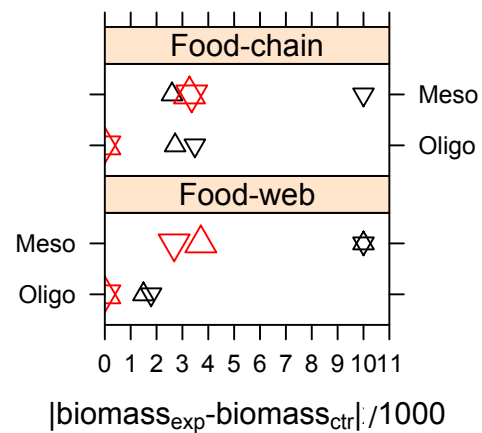
**A: Direct effect on Miz****B: Indirect effect on Phy**

Figure S14: Time-integrated effects for microzooplankton and phytoplankton following exposure to chemical 4 in spring, in mesotrophic and oligotrophic food-webs and food-chains, characterized by fast (upward triangles) or slow immigration (downward triangles), and composed of fast (black symbols) or slow (red symbols) grazing heterotrophs.

grazing heterotrophs. Integrated effects > 10 are displayed as an integrated effect size of 10. Absence of a symbol for recovery time indicates no recovery.

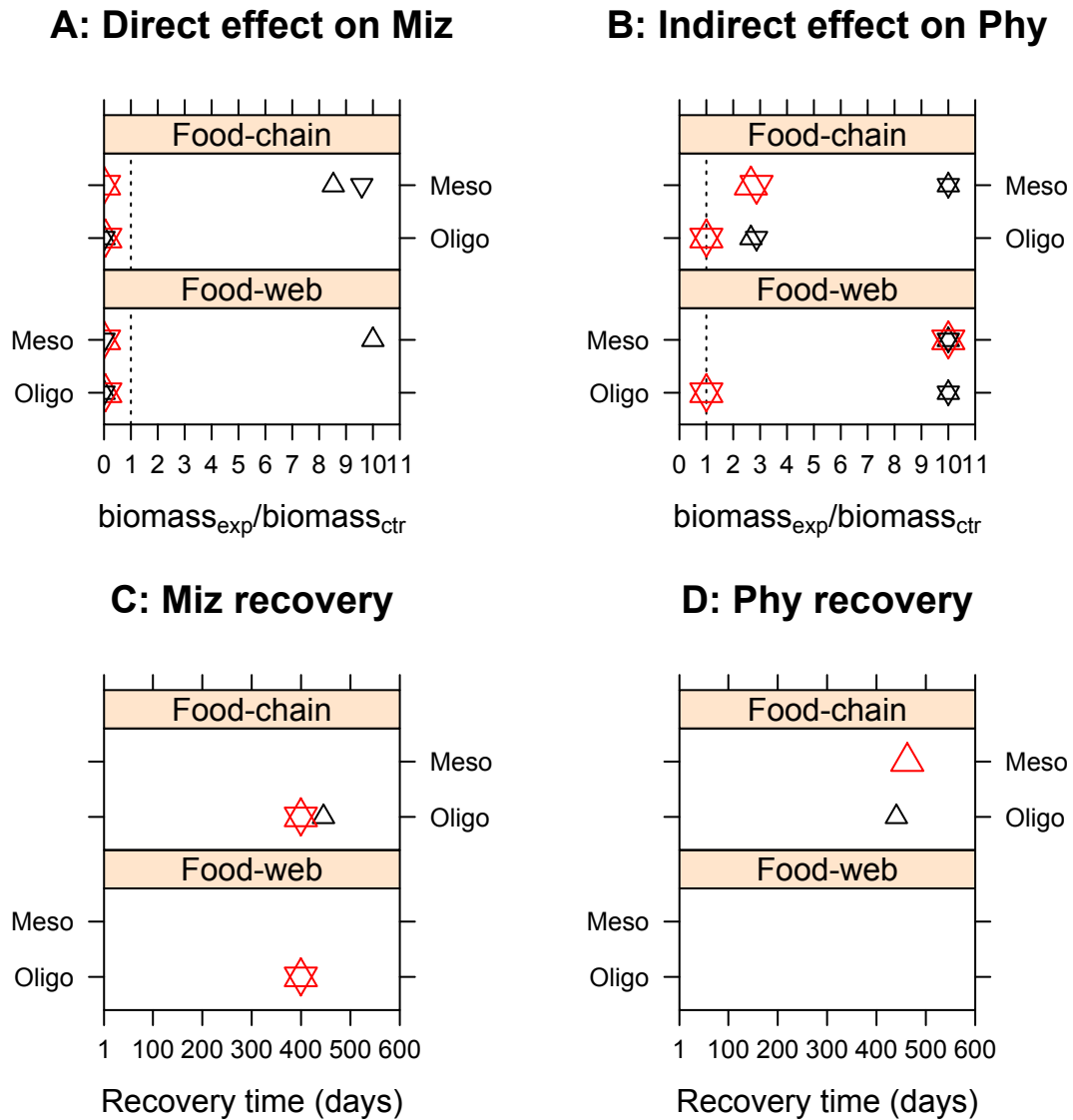
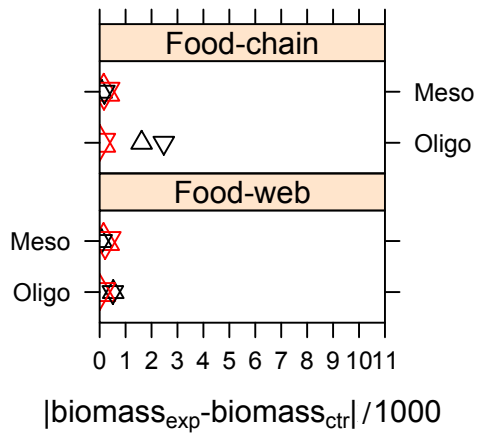


Figure S15: Maximum effect sizes and recovery times for microzooplankton and phytoplankton following exposure to chemical 3 in summer, in mesotrophic and oligotrophic food-webs and food-chains, characterized by fast (upward triangles) or slow immigration (downward triangles), and composed of fast (black symbols) or slow (red symbols) grazing heterotrophs. Maximum effects > 10 are displayed as a maximum effect size of 10. Absence of a symbol for recovery time indicates no recovery.

### A: Direct effect on Miz



### B: Indirect effect on Phy

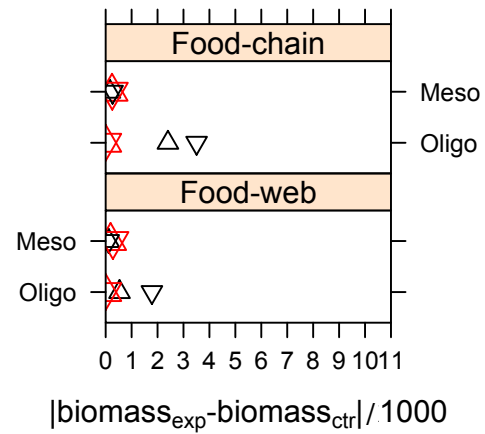
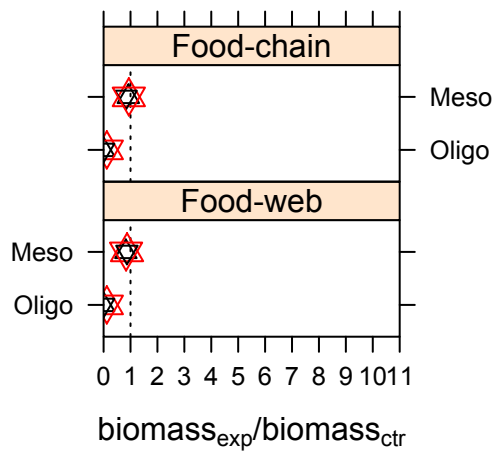
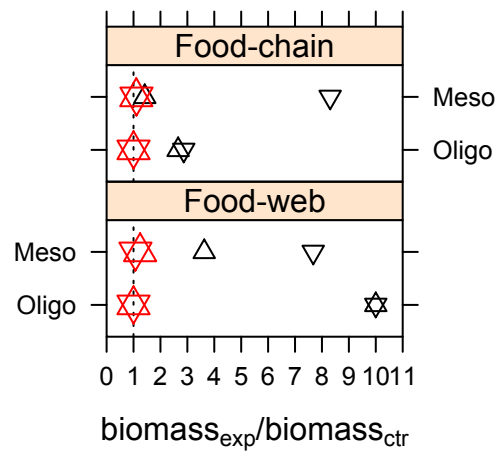


Figure S16: Time-integrated effects for microzooplankton and phytoplankton following exposure to chemical 3 in summer, in mesotrophic and oligotrophic food-webs and food-chains, characterized by fast (upward triangles) or slow immigration (downward triangles), and composed of fast (black symbols) or slow (red symbols) grazing heterotrophs. Integrated effects  $> 10$  are displayed as an integrated effect size of 10. Absence of a symbol for recovery time indicates no recovery.

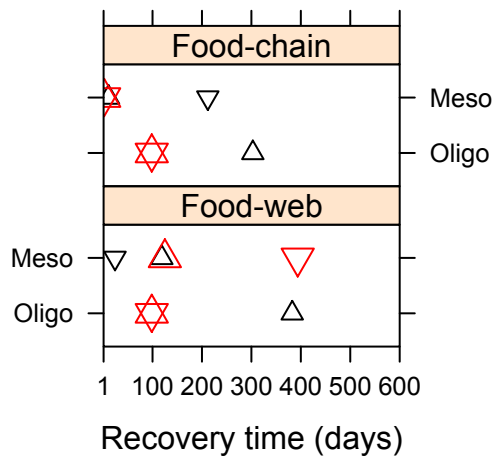
### A: Direct effect on Miz



### B: Indirect effect on Phy



### C: Miz recovery



### D: Phy recovery

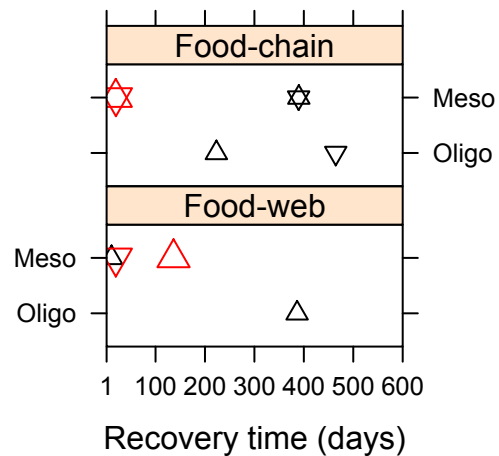
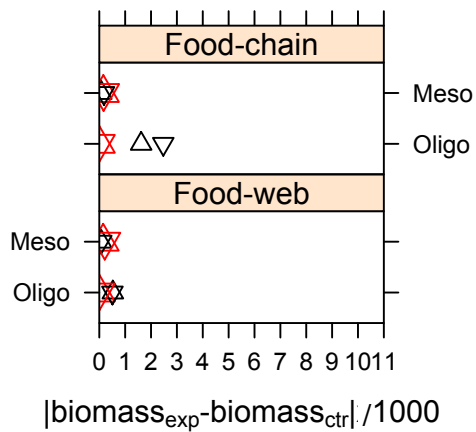


Figure S17: Maximum effect sizes and recovery times for microzooplankton and phytoplankton following exposure to chemical 4 in summer, in mesotrophic and oligotrophic food-webs and food-chains, characterized by fast (upward triangles) or slow immigration (downward triangles), and composed of fast (black symbols) or slow (red symbols) grazing heterotrophs. Maximum effects  $> 10$  are displayed as a maximum effect size of 10. Absence of a symbol for recovery time indicates no recovery.

### A: Direct effect on Miz



### B: Indirect effect on Phy

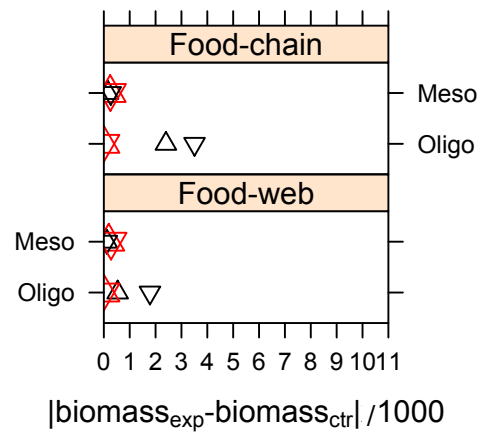


Figure S18: Time-integrated effects for microzooplankton and phytoplankton following exposure to chemical 4 in summer, in mesotrophic and oligotrophic food-webs and food-chains, characterized by fast (upward triangles) or slow immigration (downward triangles), and composed of fast (black symbols) or slow (red symbols) grazing heterotrophs. Integrated effects  $> 10$  are displayed as an integrated effect size of 10. Absence of a symbol for recovery time indicates no recovery.



## Chapter 5. Paper IV

# Importance of ecological dynamics in predicting chemical exposure in ecological risk assessment

Melissa Morselli<sup>1</sup>, Matteo Semplice<sup>2</sup>, Frederik De Laender<sup>3</sup>, Paul J. Van den Brink<sup>4,5</sup> and Antonio Di Guardo<sup>1\*</sup>

<sup>1</sup>Department of Science and High Technology - University of Insubria, Via Valleggio 11, 22100 Como CO, Italy

<sup>2</sup>Dipartimento di Matematica - Università degli Studi di Torino, Via C. Alberto 10, 10123 Torino TO, Italy

<sup>3</sup>University of Namur, Research Unit in Environmental and Evolutionary Ecology, Rue de Bruxelles 61, 5000 Namur, Belgium

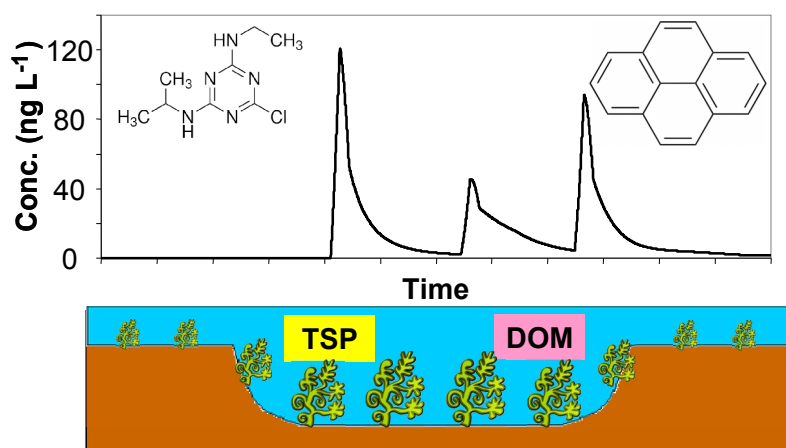
<sup>4</sup>Alterra, Wageningen University and Research Centre, P.O. box 47, 6700 AA Wageningen, The Netherlands

<sup>5</sup>Department of Aquatic Ecology and Water Quality Management, Wageningen University, 6700 AA Wageningen, The Netherlands

\*Corresponding author

*Submitted to Environmental Science & Technology*





TOC/Abstract Art

## Abstract

In currently used approaches for ecological risk assessment (ERA), exposure is generally modelled assuming steady-state in emissions and environmental properties and neglecting the potential role of ecological dynamics in affecting bioavailable concentrations. In order to investigate the potential influence of ecological scenario and emission dynamics on predicted exposure levels, the spatially-resolved dynamic model "ChimERA fate" was developed, incorporating macrophyte biomass and particulate/dissolved organic carbon dynamics into a water-sediment system. A comparison between model output and experimental observations for four case studies allowed verifying the implementation of the macrophyte compartment and assessing model performance, which was generally satisfying. Illustrative runs showed the potential spatio-temporal variability of bioavailable concentrations of two chemicals after a pulsed emission in a system composed of a pond and its inflow/outflow streams: biomass dynamics caused variations in concentrations of a factor of 2-3 during the simulation period, and of orders of magnitude in space (along the stream-pond system). Given the increased level of ecological realism, ChimERA fate could represent a vital tool for the identification of those environmental and ecological conditions where risk is expected to be highest (e.g., emissions associated with low biomass/POC/DOC levels).

## Introduction

Ecological risk assessment of chemicals (ERA) is a procedure which is commonly used to evaluate the impact of chemicals on ecosystems. This is generally done comparing the environmental exposure and the potential (ecological) effect threshold levels. The need of regulating a large number of chemicals and the complexity of the ecosystems to protect led to the development of simple and standardized tools<sup>1,2</sup>. However, most of these approaches do not properly address environmental realism in terms of, for example, the spatial and temporal variability of the ecological scenarios (affecting both exposure and effects)<sup>3</sup>, the interactions among individuals and populations and the co-occurrence with other stress factors (such as chemical or physical ones). A recent joint scientific opinion document from the three scientific committees of the European Commission<sup>4,5</sup> tried to address the new challenges for risk assessment for human health and the environment. Among the challenges devised, a number were related to the improvement of the exposure part in ERA. It was underlined that environmental exposure assessment (EEA) deserves particular attention when the desire of the evaluation of the concentrations in the environment should cover a large variety of habitats at different spatial scales and as well for terrestrial as aquatic environments<sup>6</sup>. In particular, a recent publication<sup>7</sup> listed a number of challenges for EEA. Some are related to the need of accounting for the bioavailability of chemicals, here defined as the freely dissolved concentration of a chemical (e.g. in water). This concentration, which is regarded as bioavailable for organismal uptake, can substantially vary seasonally in a surface water body because of changes in primary production (algae or macrophytes)<sup>8,9,10</sup>, or detritus concentration (influencing the concentration of particulate organic carbon, POC and/or dissolved organic carbon, DOC in water)<sup>11</sup>, or the presence of high concentrations of sorbing materials (organic matter or soot) in sediment<sup>12</sup>. Therefore, predictive fate models should be able to account for such temporal variability and capture the complexity of exposure in spatially variable environments. Most of the current exposure models, especially those used in regulative approaches (such as EUSES in European Union<sup>13</sup>) use fixed parameters representing “average” characteristics (such as

temperature, organic carbon fractions, volumes of compartments and phases, etc.) in a steady-state fashion (i.e., assuming continuous chemical discharge). Other models use an unsteady-state discharge formulation and are based on environmental scenarios with a variable environmental complexity, such as the TOXSWA model<sup>14,15,16</sup> or the more comprehensive but extremely complex model AQUATOX<sup>17,18</sup>. The above mentioned scientific opinion<sup>4</sup> also called for the integration of exposure and effect models (especially population and community models<sup>19,20,21</sup>) in order to be able to perform more realistic ERAs.

The recently funded project "ChimERA"<sup>22</sup> is one of the first attempts to couple exposure and effects models with the objective of achieving an integrated modelling framework. The aim of the study reported on here is to present the development of the fate model ("ChimERA fate") to be adopted as the exposure sub-model within the integrated modelling framework. This sub-model will represent, in the final integrated model, two adjacent small lentic water bodies connected via a stream as the simplest form of a spatial network of water bodies, in which emissions of multiple chemicals can take place, allowing unidirectional chemical movement (along the flow direction). In both water bodies, the same compartment types (water, sediment, phytoplankton and macrophytes) together with suspended matter and DOC will be considered for fate calculations. The objective is to show how the dynamic behaviour of primary producers, POC and DOC can influence the dynamics of the bioavailable concentrations of hydrophobic chemicals in aquatic ecosystems. Also the consequences for chemical exposure to organisms will be highlighted.

## **Materials and methods**

The ChimERA fate model, based on the fugacity concept<sup>23</sup>, was developed starting from an existing dynamic water-sediment model<sup>24</sup>, adding the new compartments and sub-compartments and connecting different model units to obtain a spatial discretization. In this first version of ChimERA fate, the model incorporates the macrophyte compartment, while the addition of the phytoplankton compartment will be described in a further paper. In Figure 1a, a schematic representation of the

model unit is provided. Details concerning model development and parameterization are presented in the following sections and in SI. A complete list of  $Z$ - and  $D$ -values can be found in Table S1 and S2.

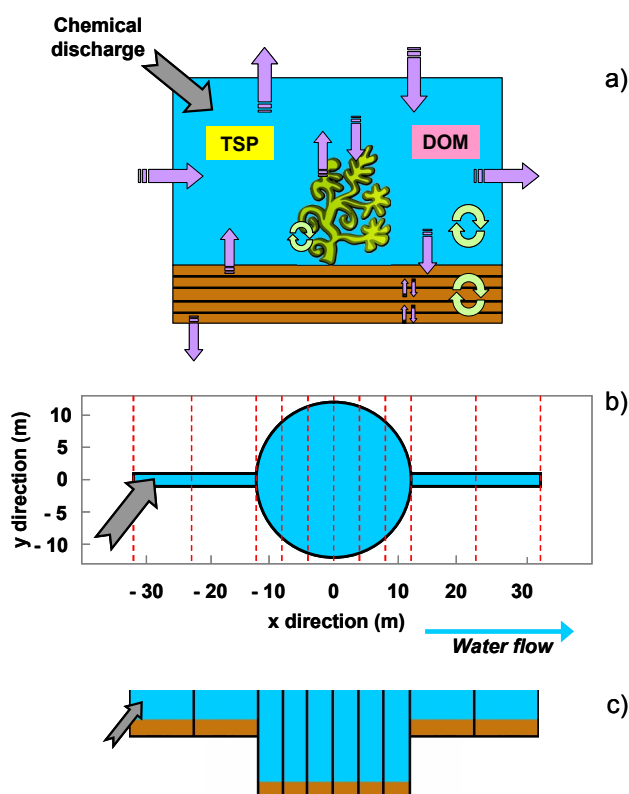


**Figure 1.** Schematic representation of (a) the ChimERA fate model unit, with purple arrows indicating chemical fluxes between compartments or accessing/leaving the system and circular green arrows indicating degradation processes; (b) top-view and (c) side-view (b) of the environmental system simulated in the model illustration.

### ***Model background***

ChimERA fate was grounded on the DynA Model<sup>24</sup>, developed to investigate the fate of organic chemicals in dynamic water-sediment systems. In DynA, dynamics concern input data, since time-varying chemical emissions and environmental parameters (e.g., water temperature and fluxes) can be specified, as well as model output, which is provided on an hourly basis. Suspended solids are modelled as a water sub-compartment (in equilibrium with water), and POC is simulated by specifying the organic fraction of suspended solids. The presence of DOC is neglected. The DynA

Model was calibrated and validated for herbicides in rice paddy scenarios<sup>25</sup>; more recently, an organism compartment was included and the model was applied to simulate uptake of DDTs by fish in an Italian sub-alpine lake<sup>26</sup> and of a number of POPs by macroinvertebrates in a glacier-fed stream<sup>27</sup>.

### ***Model formulation***

#### *Macrophyte compartment*

Macrophytes play a vital role in aquatic ecosystems, not only as primary producers, but also because of their ability to sequester pollutants, trap suspended solids containing them, and enhance degradation and thus their irreversible removal from water bodies<sup>28-30</sup>. For this reasons, the macrophyte compartment has been incorporated into a number of fate modelling approaches (e.g., refs. 31, 32). In ChimERA fate, such implementation was performed according to the work by Armitage and co-workers<sup>31</sup>. Modelled processes include diffusive exchanges with water, degradation in macrophytes, and particle-mediated deposition onto macrophyte leaves. For simplicity, in the present version of the model, only the above-sediment portion of vegetation biomass was modelled, thus neglecting diffusive exchange between roots and the sediment compartment. It was also assumed that macrophyte losses through mortality and excretion processes could occur, implying a chemical flux to total suspended particles (TSP) and dissolved organic matter (DOM), respectively<sup>18,33</sup>. Finally, a preliminary computation of the chemical loss through litterfall was included. Details concerning the calculation of the *D*-values for macrophyte-related processes are reported in Text S1.

#### *TSP and DOM sub-compartments*

As in the original DynA Model<sup>24</sup>, suspended particles were modelled as a water sub-compartment, characterized by a given fraction of organic carbon representing POC. Moreover, in order to account for the presence of DOM, a new water sub-compartment was added; its fugacity capacity

( $Z_{DOM}$ , mol m<sup>-3</sup> Pa<sup>-1</sup>) was calculated as in Armitage et al.<sup>31</sup> (Table S1). Processes involving water sub-compartments are TSP deposition to aquatic vegetation and sediment and resuspension from sediment and, for both TSP and DOM, inflow and outflow with water and chemical transfer from macrophytes through mortality and excretion (see above). A complete list of  $D$ -values can be found in Table S2.

#### *Sediment vertical discretization*

In ChimERA fate, the sediment compartment can be divided into a number of layers, in order to obtain a more accurate reconstruction of chemical vertical movement. The total number of layers can be user-selected and for each layer the different properties (e.g., depth, density, solids and organic carbon fractions) can be specified, in order to simulate specific sub-environments. Each sediment layer was modelled as a well-mixed box composed of two phases (i.e., solids and pore water), between which equilibrium was assumed. Chemical exchanges between adjacent layers included upward and downward diffusive fluxes; for simplicity, the top sediment layer (at the water-sediment interface) was assumed to be the only one to exchange with water, and therefore to be affected by diffusion from and to water, and particle deposition and resuspension. Similarly, the bottom sediment layer was assumed to be the one to lose chemical through burial. All  $D$ -values are listed in Table S2.

#### *Chemical mass balance, numerical solution and model code*

Chemical mass balance in ChimERA fate is described by a system of 1<sup>st</sup>-order ordinary differential equations (ODEs), one for each compartment, which is solved using a 5<sup>th</sup>-order accurate, diagonally implicit Runge-Kutta method with adaptive time stepping<sup>34</sup>. For a system consisting of water, macrophytes and one sediment layer, equations are:

$$\frac{dmol_{Mf}}{dt} = a \cdot mol_W - b \cdot mol_{Mf} \quad (1)$$

$$\frac{dmol_W}{dt} = c + d \cdot mol_{Mf} + e \cdot mol_S - g \cdot mol_W \quad (2)$$

$$\frac{dmol_S}{dt} = h + i \cdot mol_W - j \cdot mol_S \quad (3)$$

where  $mol_{Mf}$ ,  $mol_W$  and  $mol_S$  represent the moles in the three compartments at a certain time, while each coefficient (from  $a$  to  $j$ ) represents a transformation or a transport flux (single  $D$ -value or sum of  $D$ -values) divided by the proper product of volume and fugacity capacity  $Z$  (Table 1).

The ChimERA fate model, except for the hydrological module described in the following section and more in detail in Text S2, was coded using Microsoft Visual Basic 6.0 and was provided with a graphical user interface through which input data can be selected and uploaded and results can be visualized and processed.

**Table 1.** Coefficients appearing in the 1<sup>st</sup>-order differential equations describing the chemical mass balance in a water-macrophyte-sediment system (see main text). For  $Z$ -,  $D$ -values and other parameters see Tables S1 and S2.

<b>Coeff.</b>	<b>Explanation</b>	<b>Equation</b>
<b>a</b>	Water > Macro	$(D_{W\_Mf} + D_{TSP\_Mf}) / (V_W * Z_{Wbulk})$
<b>b</b>	Losses for Macro	$(D_{Deg\_Mf} + D_{Mf\_W} + D_{Mf\_TSP} + D_{Mf\_DOM} + D_{Lfall}) / (V_{Mf} * Z_{Mf})$
<b>c</b>	Sources for Water	$Discharge + G_I * C_I + FugAir * (D_V + D_M + D_C + D_Q)$
<b>d</b>	Macro > Water	$D_{Mf\_W} / (V_{Mf} * Z_{Mf})$
<b>e</b>	Sed > Water	$(D_T + D_{S\_TSP}) / (V_S * Z_{Sbulk})$
<b>g</b>	Losses for Water	$(D_V + D_W + D_J + D_T + D_{W\_Mf} + D_{TSP\_Mf} + D_{W\_Phyto1} + D_{W\_Phyto2} + D_{Out\_TSP} + D_{Out\_DOM} + D_{TSP\_S}) / (V_W * Z_{Wbulk})$
<b>h</b>	Sources for Sed	<i>Starting contamination</i>
<b>i</b>	Water > Sed	$(D_T + D_{TSP\_S}) / (V_W * Z_{Wbulk})$
<b>j</b>	Losses for Sed	$(D_S + D_{S\_TSP} + D_B + D_T) / (V_S * Z_{Sbulk})$

### *Spatial discretization*

The spatial discretization was obtained by connecting multiple model units by means of water flow. For this purpose, the ChimERA fate model was provided with a hydrological module capable of computing water volumes ( $\text{m}^3$ ) and fluxes ( $\text{m}^3 \text{h}^{-1}$ ) on an hourly basis in a user-specified number of adjacent boxes. Water flow was described using the Saint-Venant equations for a rectangular-section channel with variable width and depth<sup>35</sup>, with Manning's friction term. The numerical approximation of the equations was performed with a finite-volume conservative method, so that the total mass of water can change only through the inflow and outflow at the beginning and end, respectively, of the simulated portion of the water body and no artificial sources or losses can occur at the internal interfaces. For more details on the hydrological module see Text S2. Similarly, a conservative approach was adopted for the chemical flow: first, the flow across any given interface is computed and then that amount is subtracted from one compartment and added to the neighbouring one. Such discretization allows the simulation of complex environments such as systems of ponds and ditches (see Model illustration) and the description of peculiar sub-environments in water bodies (e.g., presence/absence of macrophytes, content of TSP or DOM, etc.). In the present version of ChimERA fate, no vertical discretization of the water compartment was included, since the model was designed to deal with shallow-water systems (1 m or less), where stratification phenomena due to temperature or density can be neglected and water can be assumed as “well mixed” in the vertical direction.

### *Sensitivity analysis*

A preliminary sensitivity analysis was conducted simulating the fate of two chemicals characterized by different hydrophobicity and persistence (Chemical A, atrazine-like, and Chemical B, pyrene-like, Table S5) in a macrophyte-water-sediment system. 1-year simulations were performed, for a simplified environmental scenario consisting of a  $450\text{-m}^2$ , 50-cm deep water body overlaying a 1-cm deep sediment compartment. A water residence time of 20 days, corresponding to a constant

water flux of  $0.47 \text{ m}^3 \text{ h}^{-1}$ , was selected. Constant values for macrophyte biomass density ( $134 \text{ g d.w. m}^{-2}$ ), POC and DOC concentrations ( $1.1$  and  $8.3 \text{ mg L}^{-1}$ , respectively), and water temperature ( $18.5 \text{ }^\circ\text{C}$ ) were assumed; such values were calculated as the average of the yearly profiles described for the illustration scenario (see also Fig. S1a,b,c). A single discharge to the water compartment was simulated, corresponding to the first of the three emission peaks simulated in Model illustration (Fig. S1d).

Tested parameters included chemical emission, physical-chemical properties, environmental half-lives, mass-transfer coefficients and rate constants, water temperature and fluxes, compartment volumes and organic carbon fractions. A local sensitivity analysis<sup>36</sup> was performed by varying each parameter by 0.1% and calculating the influence of such variations on two target parameters, namely peak dissolved-water and sediment pore-water concentrations, by assessing the index  $S$ <sup>37</sup>:

$$|S| = \left| \frac{\Delta O / O}{\Delta I / I} \right| \quad (4)$$

where  $I$  is the input variable,  $O$  is the output of interest, and  $\Delta I$  and  $\Delta O$  are the variations in input and output parameters, respectively.

### ***Model parameterization***

#### *Output verification and corroboration*

Following the terminology suggested by Augusiak and co-workers<sup>36</sup>, who introduced the term “evaludation” to indicate the entire process of assessing model quality and establishing model credibility throughout all stages of the “modelling cycle”, an output verification and an output corroboration step were performed for ChimERA fate in order to (1) verify the correctness of the implementation of the macrophyte compartment with respect to the reference approach<sup>31</sup> and (2) assess how well model output matched experimental observations (refs. 10, 38, 15). For this

purpose, ChimERA fate was parameterized by selecting values for the environmental parameters (e.g., water volumes, sediment depth, vegetation biomass and characteristics, TSP and DOM concentrations, etc.) equal to the ones characterizing the experimental systems (refs. 10, 38, 15). More details on model parameterization are reported in Text S3. Model performance was assessed by means of modelling efficiency (EF)<sup>39</sup>, a dimensionless statistics which directly relates model predictions to observations:

$$EF = 1 - \frac{\sum (y_i - \hat{y}_i)^2}{\sum (y_i - \bar{y})^2} \quad (5)$$

where  $y_i$  are observations,  $\hat{y}_i$  are predictions and  $\bar{y}$  is the average of observations. For such statistic, the "perfect fit" results in 1, and the degree of fit declines as it falls away from 1. EF between 0 and 1 still indicates good model performance, while negative values could indicate model bias or need for model re-calibration<sup>39</sup>.

#### *Model illustration*

In order to illustrate the potential of the ChimERA fate model in predicting concentration variability in response to spatio-temporal environmental heterogeneity, one-year simulations were performed for the two model chemicals investigated in the sensitivity analysis (Chemical A, atrazine-like, and Chemical B, pyrene-like, Table S5, Table S5) in a macrophyte-dominated spatially-resolved system consisting of a pond and its inflow and outflow streams. As depicted in Figure 1b,c, the system, with the same characteristics of the one adopted for the sensitivity analysis, was split into 10 adjacent boxes along the water flow direction. A constant water flow was selected to obtain an average residence time in the pond boxes of about 20 days. Realistic information concerning macrophyte biomass (Fig. S1a), DOC and POC concentrations (Fig. S1b) and water temperature (Fig. S1c) was derived from the literature<sup>40-42</sup>. It should be remarked that no effort was made to

simulate a specific situation and that the present scenario was adopted for illustration purposes only, since time-resolved data concerning macrophyte biomass densities, POC/DOC concentrations and other environmental parameters are often lacking. More details on model parameterization are reported in Text S3.

Since in the present version of ChimERA fate no litter compartment was included, an investigation of the potential role of dead aquatic vegetation in influencing chemical fate was performed by simulating a non-decreasing biomass after the peak was reached (dashed line in Fig. S1a) and assuming, for this portion of vegetation, (1) the same properties (e.g., organic carbon fraction, density) and uptake/depuration rate constants with respect to the living part and (2) no biomass transport with water to occur. These assumptions were obviously strong, since aquatic vegetation is subject to fragmentation and decomposition, and is often responsible for much of the organic matter production in shallow aquatic environments<sup>43,44</sup>; however, it can take months to years for litter to break completely<sup>44</sup>; for this reason, we assumed a static macrophyte biomass of 350 g d.w. m<sup>-2</sup> persisting until the end of the simulation period.

## **Results and discussion**

### ***Sensitivity analysis***

Figure S2 depicts the results of the sensitivity analysis performed for the more soluble Chemical A (chart a) and the higher-log  $K_{OW}$  Chemical (B) (for physical-chemical properties see Table S5). For both chemicals and targets, emission was the most influential parameter ( $S = 1$ ). For Chemical A (Fig. S2a), changes in water volume and flux significantly influenced both water-dissolved ( $S = 0.80$  and  $0.19$ , respectively) and sediment pore-water ( $S = 0.68$  and  $0.32$ , respectively) concentrations. Water-dissolved concentration was also slightly influenced by water temperature ( $0.04$ ) and half-life in water ( $0.03$ ), while sediment pore-water concentration was mainly affected by changes in sediment-water diffusion mass transfer coefficient  $K_T$  ( $0.33$ ), organic carbon fraction of sediment solids  $f_{OC_S}$  ( $0.24$ ), and  $K_{OW}$  ( $0.18$ ). A different picture appeared for Chemical B (Fig.

S2b): water dissolved concentration was mostly sensitive to  $K_{OW}$  (0.84), macrophyte biomass density  $Bio_{Mf}$  (0.61), TSP volume and organic carbon fraction (0.50 for both), particle settling velocity  $\gamma_p$  (0.49), and macrophyte uptake and depuration rate constants  $k_{W\_Mf}$  and  $k_{Mf\_W}$  (0.24 and 0.28, respectively); sediment pore-water concentrations showed a similar behaviour, but with the most influential parameter being the organic carbon fraction of sediment solids (0.99). In contrast with Chemical A, both targets for Chemical B were only moderately affected by changes in water volume and fluxes (Fig. S2). Being a local sensitivity analysis (i.e., one parameter varied a little at a time), the effort presented here did not allow capturing, for example, the effect of the interactions between parameters<sup>36</sup>; however, it helped in the identification of the crucial input parameters (chemical properties and environmental system descriptors), to which particular attention should be paid in order to obtain accurate results. Moreover, results were comparable, for instance, to those obtained from the global sensitivity analysis performed on the TOXSWA model (Adriaanse, 1997), which identified as the most sensitive parameters chemical properties such as half-life in water, the sorption coefficient to macrophytes and environmental characteristics such as water flux and depth<sup>45</sup>.

### ***Model output verification and corroboration***

A detailed discussion of the results of the model output verification is reported in Text S4, while results for output corroboration follow.

In Figure 2 the results of the comparison between predicted and measured prosulfocarb inventories, expressed as percentage of the applied dose in all compartments, are reported. Since in the reference manuscript<sup>15</sup> the authors also applied a modelling approach (i.e., TOXSWA<sup>14</sup>) to investigate measured patterns, the ChimERA fate input scenario was built using the same input data reported in the manuscript, whenever possible (prosulfocarb physical-chemical properties, water volume, sediment characteristics, etc.) (Table S3). However, being model formulations similar but not identical (at least in the description of water-sediment exchange and sorption onto macrophytes), a

full comparison between model predictions was not pursued and the effort was restricted to a comparison between ChimERA fate model output and field data.

Adriaanse and co-workers<sup>15</sup> identified half-life in water as the dominant factor regulating prosulfocarb concentrations in the system and selected 2.9 d as a suitable half-life for mesocosm studies (significantly shorter than the value of 204 d, deriving from small-scale laboratory tests, they used as a starting point for their model optimization procedure; Milles and Kaur, unpublished). For the ChimERA fate model application, a similar optimization of prosulfocarb half-life in water (from 204 to 5.8 d) was necessary to reproduce the observed concentration pattern. Moreover, it was observed that model output best fitted observations with a half-life in sediment set to double the one in water (11.6 d) and a half-life in macrophytes of 5.8 d.

Results (Fig. 2) indicated only a slight underestimation of water inventories (up to a factor of 1.4,  $EF_W = 0.98$ ; Fig. 2). However, comparisons for macrophytes and sediment revealed an overestimation of prosulfocarb inventories from a factor of 2 to 6.5 in macrophytes ( $EF_{MF} \ll 0$ ) and, in contrast, and underestimation of inventories up to a factor of 2.4 in sediment ( $EF_S = -0.50$ , Fig. 2). Despite predictions were always within an order of magnitude or less with respect to experimental observations, discrepancies for macrophyte and sediment compartments indicated that model parameterization was probably not sufficiently accurate (probably in terms of mass transfer coefficients and compartment properties) to allow a proper description of the system. For example, according to ChimERA fate simulations, macrophyte uptake was the dominant process of chemical removal from water, followed by particle deposition onto macrophyte leaves and particle deposition onto sediment; diffusion towards the sediment compartment was unimportant (Fig. S6). In contrast, experimental observations revealed that migration to sediment was the dominant pathway for prosulfocarb, while macrophytes were almost no influent (max inventory = 3%)<sup>15</sup>. In order to improve model predictions, more information on the environmental system (e.g., sediment density and organic matter content with depth) and probably a number of measurements (such as particle

sedimentation rates and patterns) would have been necessary. However, given the uncertainty associated with the environmental scenario description, the results can be considered satisfying.

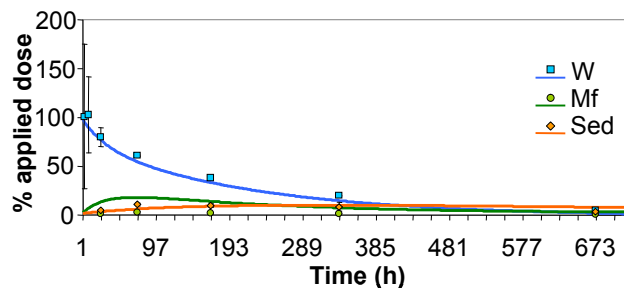


**Figure 2.** Results of the model output corroboration (lines) performed against the data reported in the reference manuscript<sup>15</sup> (markers) for water (W), macrophytes (Mf), and sediment (Sed). The comparison was performed on prosulfocarb inventories in the different compartments, expressed as percentage of the initially applied chemical amount.

### ***Model illustration***

#### ***Chemical A vs. Chemical B***

The concentration profiles obtained for the two model chemicals (A and B) in water (dissolved-phase,  $\mu\text{g L}^{-1}$ ) and sediment solids ( $\text{ng g}^{-1}$  d.w.) in the first, stream box (Box 1), where chemical discharge occurred, are depicted in Figure 3. The difference between the behaviours predicted for Chemical A and B is evident and mostly due to the higher  $\log K_{OW}$  of Chemical B with respect to A (5.18 vs. 2.5), which caused a rapid chemical migration towards the macrophyte and sediment compartments, also mediated by suspended solids deposition. This resulted in water-dissolved concentrations of Chemical A which were 5 times higher than those of Chemical B. It should also be noted that, for Chemical B, the second emission pulse, of the same entity of the other two pulses, caused lower water-dissolved concentrations ( $0.04 \mu\text{g L}^{-1}$  vs.  $0.1 \mu\text{g L}^{-1}$ ); this was a direct consequence of the higher macrophyte biomass density ( $\sim 300 \text{ g d.w. m}^{-2}$ ) and, to a lesser extent, of the higher DOC and POC concentrations ( $16$  and  $4 \text{ mg L}^{-1}$ , respectively) characterizing the month of July, when such emission pulse occurred (Fig. S1). Chemical B hourly losses from the water

compartment in Box 1 are depicted in Figure S7; it can be noticed that, in correspondence with the second emission pulse, chemical removal from water was actually significant, and this can be mainly ascribed to the higher suspended solids deposition flux on submerged aquatic vegetation caused by the higher biomass characterizing the system in July. The observed behaviour confirmed the importance of such process, especially for chemicals with  $\log K_{OW} > 5.5$ , as already shown by Armitage and co-workers<sup>31</sup> and before in this work (see Text S4). The crucial role of aquatic vegetation in influencing the fate and distribution of hydrophobic organic chemicals is also evident from numerous laboratory and field studies (e.g., refs. 28-30, 46-48). Chemical A, in contrast, was almost not influenced by the high levels of macrophyte biomass due to its low  $\log K_{OW}$ . In sediment (Fig. 3b), an opposite picture with respect to water appeared, with lower Chemical A concentrations reflecting the pulsed emission profile in water and higher Chemical B levels slowly oscillating in response to emission pulses but generally increasing; this last pattern was due to a combination of the high chemical flux towards the sediment compartment with the higher persistence of Chemical B (half-life: 2290 d) with respect to Chemical A (200 d). Chemical fluxes also indicated that Chemical B transport to the sediment was mainly particle-mediated (particle deposition flux was 2 orders of magnitude higher than water-sediment diffusion one; Fig. S7).

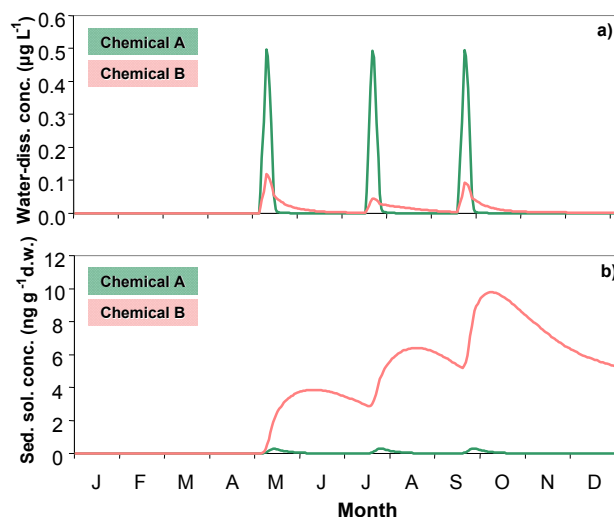


**Figure 3.** Concentrations in water (dissolved phase,  $\text{ng L}^{-1}$ ) (a) and sediment solids ( $\text{ng g}^{-1}$  d.w.) (b) of Chemical A and Chemical B during the simulation period (Box 1, stream, where emission occurred).

#### *Spatio-temporal variations in bioavailable concentrations*

In Figure 4, the spatio-temporal dynamics of Chemical B water-dissolved concentrations are depicted. A simplified side-view of the stream-pond system is reported, together with two charts comparing the temporal concentration profile in Box 1, where the application occurred (Fig. 4a), and the concentration profiles in the first three boxes of the pond (Box 3, 4 and 5, Fig. 4b). Solid lines represent the concentrations computed with the time-varying macrophyte biomass (solid line in Fig. S1a and Fig. 4c), while results indicated by dashed lines are discussed later on. A depletion of concentrations of about 2 orders of magnitude from Box 1 to Box 3 was observed: this was partially due to an obvious chemical dilution occurring when the stream water entered the pond; however, this phenomenon was not sufficient to explain such concentration decrease, since Box 3 volume was only 1 order of magnitude higher than Box 1 and 2 ones ( $10 \text{ m}^3$  vs.  $0.8 \text{ m}^3$ , respectively). During water transport from Box 1 to 3, chemical transfer to macrophytes and sediment regulated chemical fate, resulting in a further depletion of concentrations; this was confirmed by the fluxes representing losses from the water compartment for Box 3, which are depicted in Figure S8. From Box 3 to 4 and 5 the effect of dilution was negligible, but again

macrophytes and sediment contributed in sequestering chemical from water. Box 4 and 5 appeared less affected than the previous ones by direct emission pulses, since most of the chemical was sequestered in Box 1 to 3; however, the chemical release exerted by macrophytes in such boxes and the following transport with water were sufficient to cause an increase of chemical concentrations in Box 4 and 5 from October to November (Fig. 4b).

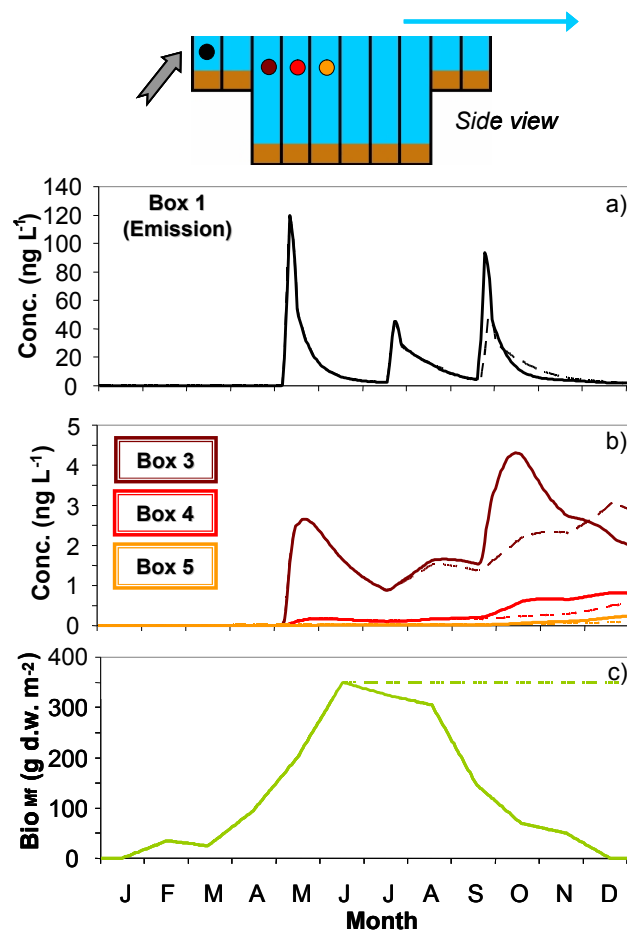


**Figure 4.** Temporal evolution of water-dissolved concentrations ( $\text{ng L}^{-1}$ ) of Chemical B (a) in Box 1 (stream, where the emission occurred) and (b) in the first three boxes constituting the pond environment (Box 3, 4 and 5). Solid lines refer to simulations performed with time-varying macrophyte biomass, while dashed lines refer to simulations performed with static macrophyte biomass after the June peak (c).

### *Potential role of dead macrophyte biomass*

A second set of simulations was performed to estimate the potential role of dead macrophyte biomass, and were run assuming no macrophyte biomass decrease after the peak in June (dashed line in Fig. S1a and Fig. 4c). Water dissolved concentrations in Box 1 (dashed line in Fig. 4a) responded to such modification in macrophyte biomass with a decrease of the third peak with respect to the reference simulation (solid line) of a factor of 2; concentrations in the following boxes (Fig. 4b) also decreased starting from July, in response to the fictitiously increased vegetation biomass, and showed the same gradual increase in the last part of the year related to release by macrophytes located in the previous boxes. This simulation allowed preliminarily exploring the potential role of dead aquatic vegetation in shallow aquatic environments and suggested the need of incorporating a litter compartment in models dealing with lentic systems as ponds or wetlands, where most of this material remains in-place and enters the detrital pool<sup>44,49</sup>.

### ***Implications for ecological risk assessment***

The illustrative simulations showed the potential temporal and spatial variability of chemical bioavailable concentrations derived from a pulsed emission in a natural system composed of a pond and its inflow and outflow streams. Concentration variability was observed to be related to physical-chemical characteristics, but also to environmental heterogeneity. For example, the variability in the presence and abundance of biota and organic phases (especially macrophytes) was able to strongly influence bioavailable concentrations and, consequently, the exposure of aquatic organisms. The experiments conducted by Roessink and co-workers<sup>48</sup> demonstrated the strong influence of aquatic vegetation on chemical fate also for sediment-bound organic compounds. The inclusion of the macrophyte compartment, the vertically-resolved sediment and the possibility to simulate different sub-environments through the connection of properly parameterized model sub-units allow an increase of ecological realism in exposure predictions. The results of the model output verification and corroboration processes suggested that a thorough model calibration is

mandatory in order to obtain accurate predictions, as is usual for fate models. For example, a more detailed description of the changes in sediment properties (e.g., density, solids and organic carbon content) with depth could dramatically improve the description of water-sediment exchange. Similarly, a higher spatial and temporal resolution in the POC and DOC concentrations and macrophyte biomass could help in the modelling of the complex spatio-temporal mosaic of exposure which may occur in such shallow-water systems. In the present version of ChimERA fate, macrophyte biomass temporal profiles are required as input; however, efforts will be devoted to the implementation of scenarios containing realistic values for such parameters and for DOC/POC concentrations. This, together with the implementation of a phytoplankton compartment, will be crucial in order to investigate the variability of chemical exposure in different environments at different latitudes or characterized by different properties (e.g., trophic status, climate zone, etc.) and will be the object of a further paper.

### **Associated content**

### **Supporting information**

Additional information concerning materials and methods (Table S1 and S2, Text S1-S3) and results (Text S4, Figure S8 and S9). This material is available free of charge via the Internet at <http://pubs.acs.org>.

### **Acknowledgments**

The Chimera project is financed by the Long Range Initiative of CEFIC ([www.cefic-lri.org](http://www.cefic-lri.org)) (project code: LRI-ECO19). Andreas Focks, from Alterra, Wageningen University and Research Centre (Wageningen, The Netherlands), is kindly acknowledged for the suggestions given at the first version of the manuscript.

## References

- (1) EPA (U.S. Environmental Protection Agency), 1998. *Guidelines for Ecological Risk Assessment*. EPA/630/R-95/002F. Risk Assessment Forum: Washington, DC, 1998;  
<http://www.epa.gov/raf/publications/pdfs/ECOTXTBX.PDF>.
- (2) EC (European Commission), 2003. *Technical guidance document on risk assessment*; 2nd ed; EUR 20418 EN/2; European Chemical Bureau, Joint Research Centre: Ispra, Italy, 2003;  
[http://echa.europa.eu/documents/10162/16960216/tgdpart2\\_2ed\\_en.pdf](http://echa.europa.eu/documents/10162/16960216/tgdpart2_2ed_en.pdf).
- (3) De Laender, F., van den Brink P. J., Janssen C.R., Di Guardo, A. The ChimERA project: coupling mechanistic exposure and effect models into an integrated platform for ecological risk assessment. *Environ. Sci. Pollut. Res.* **2014**, *21*, 6263–6267; DOI: 10.1007/s11356-014-2605-5.
- (4) EC (European Commission), 2013. *Addressing the new challenges for risk assessment*. Opinion adopted in March 2013. SCHER (Scientific Committee on Health and Environmental Risks), SCENIHR (Scientific Committee on Emerging and Newly Identified Health Risks), SCCS (Scientific Committee on Consumer Safety);  
[http://ec.europa.eu/health/scientific\\_committees/consumer\\_safety/docs/sccs\\_o\\_131.pdf](http://ec.europa.eu/health/scientific_committees/consumer_safety/docs/sccs_o_131.pdf).
- (5) Vighi, M. New challenges for ecological risk assessment. *Integr. Environ. Assess. Manag.* **2013**, *9* (3), e1–e3; DOI: 10.1002/ieam.1422.
- (6) Di Guardo, A. Environmental Exposure Assessment. In *Encyclopaedia of Toxicology*; Wexler, P., Ed.; 3rd ed., vol. 2; Elsevier Inc., Academic Press 2014, pp 366–371.

- (7) Di Guardo, A.; Hermens, J. L. M. Challenges for exposure prediction in ecological risk assessment. *Integr. Environ. Assess. Manag.* **2013**, *9* (3), e4–e14; DOI: 10.1002/ieam.1442.
- (8) Taylor, W. B.; Carey, J.H.; Lean, D. R. S.; McQueen, D. I. Organochlorine concentrations in the plankton of lakes in southern Ontario and their relationship to plankton biomass. *Can. J. Fish. Aquat. Sci.* **1991**, *48*, 1960–1966; DOI: 10.1139/f91-233.
- (9) Berglund, O.; Larsson, P.; Ewald, G.; Okla, L. Influence of trophic status on PCB distribution in lake sediment and biota. *Environ. Pollut.* **2001**, *82* (4), 199–210; DOI: 10.1016/S0269-7491(00)00166-4.
- (10) Leistra, M.; Zweers, A. J.; Warinton, J. S.; Crum, S. J. H.; Hand, L. H.; Beltman, W. H. J.; Maund, S. J. Fate of the insecticide lambda-cyhalothrin in ditch enclosures differing in vegetation density. *Pest. Manag. Sci.* **2003**, *60*, 75–84; DOI: 10.1002/ps.780.
- (11) Schwarzenbach, R. P.; Gschwend, P. M.; Imboden, D. M. *Environmental Organic Chemistry*; Wiley: New York, 1993.
- (12) Gustafsson, O.; Haghseta, F.; Chan, C.; MacFarlane, J.; Gschwend, P.M. Quantification of the dilute sedimentary soot phase: Implications for PAH speciation and bioavailability. *Environ. Sci. Technol.* **1997**, *31*, 203–209; DOI: 10.1021/es960317s.
- (13) EC (European Commission), 2004. *European Union System for the Evaluation of Substances 2.0 (EUSES 2.0)*. Background report 601900005/2004. National Institute of Public Health and the Environment (RIVM): Bilthoven, the Netherlands, 2004;  
<http://www.pbl.nl/sites/default/files/cms/publicaties/601900005.pdf>.

- (14) Adriaanse, P.I. Exposure assessment of pesticides in field ditches: the TOXSWA model. *Pestic. Sci.* **1997**, *49*, 210–212.
- (15) Adriaanse, P. I.; Boesten, J. J. T. I.; Crum, S. J. H. Estimating degradation rates in outdoor stagnant water by inverse modelling with TOXSWA: a case study with prosulfocarb. *Pest. Manag. Sci.* **2013**, *69*, 755–767; DOI 10.1002/ps.3435.
- (16) FOCUS, 2001. *FOCUS surface water scenarios in the EU evaluation process under 91/414*; rev. 2; EC Document Reference SANCO/4802/2001; FOCUS Working Group on Surface Water Scenarios.
- (17) EPA (U.S. Environmental Protection Agency), 2014. *AQUATOX (Release 3.1 plus) Modeling environmental fate and ecological effects in aquatic ecosystems, Volume 1: User's manual*; EPA-820-R-14-005; U.S. EPA Office of Water and Office of Science and Technology: Washington, DC, 2014;  
<http://www2.epa.gov/sites/production/files/2014-03/documents/user-s-manual-3-1.pdf>.
- (18) Park, R. A.; Clough, J. S.; Wellman, M.C. AQUATOX: Modeling Environmental Fate and Ecological Effects in Aquatic Ecosystems. *Ecol. Model.* **2008**, *213*, 1–15; DOI: 10.1016/j.ecolmodel.2008.01.015.
- (19) Forbes, V. E.; Hommen, U.; Thorbek, P.; Heimbach, F.; Van den Brink, P. J.; Wogram, J.; Thulke, H.; Grimm, V. Ecological models in support of regulatory risk assessments of pesticides: developing a strategy for the future. *Integr. Environ. Assess. Manag.* **2009**, *5*, 167–172; DOI: 10.1897/IEAM\_2008-029.1.

- (20) Grimm, V., Ashauer, R., Forbes, V.; et al. CREAM: a European project on mechanistic effect models for ecological risk assessment of chemicals. *Environ. Sci. Pollut. Res.* **2009**, *16* (6), 614–617; DOI: 10.1007/s11356-009-0228-z.
- (21) Van den Brink, P. J.; Baird, D. J.; Baveco, J. M. H.; Focks, A. The use of traits-based approaches and eco(toxico)logical models to advance the ecological risk assessment framework for chemicals. *Integr. Environ. Assess. Manag.* **2013**, *9*, 47–57; DOI: 10.1002/ieam.1443.
- (22) De Laender, F.; Morselli, M.; Baveco, H.; Van den Brink, P. J., Di Guardo, A. Theoretically exploring direct and indirect chemical effects across ecological and exposure scenarios using mechanistic fate and effects modelling. *Environ. Int.* **2015**, *74*, 181–190; DOI: 10.1016/j.envint.2014.10.012.
- (23) Mackay, D. *Multimedia environmental models: the fugacity approach*. 2nd ed. Lewis Publishers: Boca Raton, 2001.
- (24) Di Guardo, A.; Ferrari, C.; Infantino, A. Development of a Dynamic Aquatic Model (DynA Model): Estimating temporal emissions of DDT to Lake Maggiore (N. Italy). *Environ. Sci. Pollut. R.* **2006**, *13* (1), 50–58; DOI: 10.1065/espr2006.01.009.
- (25) Infantino, A.; Pereira, T.; Ferrari, C.; Cerejeira, M. J.; Di Guardo, A. Calibration and validation of a dynamic water model in agricultural scenarios. *Chemosphere* **2008**, *70*, 1298–1308; DOI: 10.1016/j.chemosphere.2007.07.047.

- (26) Infantino, A.; Morselli, M.; Di Guardo, A. Integration of a dynamic organism model into the DynA Model: Development and application to the case of DDT in Lake Maggiore, Italy. *Sci. Total Environ.* **2013**, *454-455*, 358–365; DOI: 10.1016/j.scitotenv.2013.03.026.
- (27) Morselli, M.; Semplice, M.; Villa, S.; Di Guardo, A. Evaluating the temporal variability of concentrations of POPs in a glacier-fed stream food chain using a combined modeling approach. *Sci. Total Environ.* **2014**, *493*, 571–579; DOI: 10.1016/j.scitotenv.2014.05.150.
- (28) Hinman, M.L.; Klaine, S.J. Uptake and translocation of selected organic pesticides by the rooted aquatic plant *Hydrilla verticillata* Royle. *Environ. Sci. Technol.* **1992**, *26*, 609–613; DOI: 10.1021/es00011a001.
- (29) Karen, D. J.; Joab, B. M.; Wallin, J. M.; Johnson, K. A. Partitioning of chlorpyrifos between water and an aquatic macrophyte (*Elodea densa*). *Chemosphere* **1998**, *37* (8), 1579–1586; DOI: 10.1016/S0045-6535(98)00141-6.
- (30) Hand, L.H.; Kuet, S.F.; Lane, M.C.G.; Maund, S.J.; Warinton, J.S.; Hill, I.R. Influences of aquatic plants on the fate of the pyrethroid insecticide *lambda*-cyhalothrin in aquatic environments. *Environ. Toxicol. Chem.* **2001**, *20* (8), 1740–1745; DOI: 10.1897/1551-5028(2001)020<1740:IOAPOT>2.0.CO;2.
- (31) Armitage, J. M.; Franco, A.; Gomez, S.; Cousins, I. T. Modeling the potential influence of particle deposition on the accumulation of organic contaminants by submerged aquatic vegetation. *Environ. Sci. Technol.* **2008**, *42*, 4052–4059; DOI 10.1021/es702439u.

- (32) Nfon, E.; Armitage, J. M.; Cousins, I. T. Development of a dynamic model for estimating the food web transfer of chemicals in small aquatic ecosystems. *Sci. Total Environ.* **2011**, *409*, 5416–5422; DOI: 10.1016/j.scitotenv.2011.08.070.
- (33) De Laender, F.; De Schamphelaere, K. A. C.; Vanrollenghem, P. A.; Janssen, C. R. Validation of an ecosystem modelling approach as a tool for ecological effect assessment. *Chemosphere* **2008**, *71*, 529–545; DOI: 10.1016/j.chemosphere.2007.09.052.
- (34) Semplice, M.; Ghirardello, D.; Morselli, M.; Di Guardo, A. Guidance on the selection of efficient computational methods for multimedia fate models. *Environ. Sci. Technol.* **2012**, *46*, 1616–1623; DOI: 10.1021/es201928d.
- (35) Balbas, J.; Karni, S. A central scheme for shallow water flows along channels with irregular geometry. *ESAIM: M2AN* **2009**, *43*, 333–351; DOI: 10.1051/m2an:2008050.
- (36) Augusiak, J.; Van den Brink, P. J.; Grimm, V. Merging validation and evaluation of ecological models to 'evaluation': A review of terminology and a practical approach. *Ecol. Model.* **2014**, *280*, 117–128; DOI: 10.1016/j.ecolmodel.2013.11.009.
- (37) MacLeod, M.; Fraser, A.J.; Mackay, D. Evaluating and expressing the propagation of uncertainty in chemical fate and bioaccumulation models. *Environ. Toxicol. Chem.* **2002**, *21* (4), 700–709; DOI: 10.1897/1551-5028(2002)021<0700:EAETPO>2.0.CO;2.
- (38) Knuth, M. L.; Heinis, L. J.; Anderson, L. E. Persistence and distribution of azinphos-methyl following application to littoral enclosure mesocosms. *Ecotox. Environ. Safe.* **2000**, *47*, 167–177; DOI: 10.1006/eesa.2000.1945.

- (39) Mayer, D. G.; Butler, D. G. Statistical validation. *Ecol. Modell.* **1993**, *68*, 21–32; DOI: 10.1016/0304-3800(93)90105-2.
- (40) Desmet, N. J. S.; Van Belleghem, S.; Seuntjens, P.; Bouma, T. J.; Buis, K.; Meire, P. Quantification of the impact of macrophytes on oxygen dynamics and nitrogen retention in a vegetated lowland river. *Phys. Chem. Earth* **2011**, *36*, 479–489; DOI: 10.1016/j.pce.2008.06.002.
- (41) de Figueiredo, D. R.; Reboleira, A. S. S. P.; Antunes, S. C.; Abrantes, N.; Azeiteiro, U.; Gonçalves, F.; Pereira, M. J. The effect of environmental parameters and cyanobacterial blooms on phytoplankton dynamics of a Portuguese temperate lake. *Hydrobiologia* **2006**, *568*, 145–157. DOI: 10.1007/s10750-006-0196-y.
- (42) Parszuto, K.; Kaliszewska, E.A. The evaluation of the trophy of selected Olsztyn lakes by means of indices of particulate organic carbon (POC) and dissolved organic carbon (DOC). *Limnological Review* **2007**, *7* (2), 87–93.
- (43) Wetzel, R. G.; Manny, B. A. Decomposition of dissolved organic carbon and nitrogen compounds from leaves in an experimental hard-water stream. *Limnol. Oceanogr.* **1972**, *17*, 927–931.
- (44) Chimney, M. J.; Pietro, K. C. Decomposition of macrophyte litter in a subtropical constructed wetland in south Florida (USA). *Ecol. Eng.* **2006**, *27*, 301–321; DOI: 10.1016/j.ecoleng.2006.05.016.

(45) Westein, E.; Jansen, M. J. W.; Adriaanse, P. I.; Beltman, W. H. J. Sensitivity analysis of the TOXSWA model simulating fate of pesticides in surface waters; Report 154 DLO Winand Staring Centre: Wageningen, The Netherlands 1998.

(46) Moore, M. T.; Schulz, R.; Cooper, C. M.; Smith Jr., S.; Rodgers Jr, J. H. Mitigation of chlorpyrifos runoff using constructed wetlands. *Chemosphere* **2002**, *46* (6), 827–835; DOI: 10.1016/S0045-6535(01)00189-8.

(47) Rose, M. T.; Crossan, A. N.; Kennedy, I. R. The effect of vegetation on pesticide dissipation from ponded treatment wetlands: Quantification using a simple model. *Chemosphere* **2008**, *72*, 999–1005; DOI: 10.1016/j.chemosphere.2008.04.059.

(48) Roessink, I.; Moermond, C. T. A.; Gillissen, F.; Koelmans, A. A. Impacts of manipulated regime shifts in shallow lake model ecosystems on the fate of hydrophobic organic compounds. *Water Res.* **2010**, *44*, 6153–6163; DOI: 10.1016/j.watres.2010.07.013.

(49) Kuehn, K. A.; Lemke, M. J.; Suberkropp, K.; Wetzel, R. G. Microbial mass and production associated with decaying leaf litter of the emergent macrophyte *Juncus effusus*. *Limnol. Oceanogr.* **2000**, *45*, 862–870; DOI: 10.4319/lo.2000.45.4.0862.



## Chapter 5. Paper IV

# Importance of ecological dynamics in predicting chemical exposure in ecological risk assessment

Melissa Morselli<sup>1</sup>, Matteo Semplice<sup>2</sup>, Frederik De Laender<sup>3</sup>, Paul J. Van den Brink<sup>4,5</sup> and Antonio Di Guardo<sup>1\*</sup>

<sup>1</sup>Department of Science and High Technology - University of Insubria, Via Valleggio 11, 22100 Como CO, Italy

<sup>2</sup>Dipartimento di Matematica - Università degli Studi di Torino, Via C. Alberto 10, 10123 Torino TO, Italy

<sup>3</sup>University of Namur, Research Unit in Environmental and Evolutionary Ecology, Rue de Bruxelles 61, 5000 Namur, Belgium

<sup>4</sup>Alterra, Wageningen University and Research Centre, P.O. box 47, 6700 AA Wageningen, The Netherlands

<sup>5</sup>Department of Aquatic Ecology and Water Quality Management, Wageningen University, 6700 AA Wageningen, The Netherlands

\*Corresponding author

*Submitted to Environmental Science & Technology*

Contains 4 texts, 5 tables and 8 figures.



**Table S1.** Z-values ( $\text{mol m}^{-3} \text{Pa}^{-1}$ ) in ChimERA fate.

Z-value	Phase/compartment	Equation
$Z_A$	Air	$1 / RT$
$Z_Q$	Aerosol	$6\text{E}+06 / P_L * Z_A$
$Z_{Abulk}$	Bulk air	$Z_A * (1 - v_Q) + Z_Q * v_Q$
$Z_W$	Water	$1 / H$
$Z_{TSP}$	TSP	$0.41 * K_{OW} * f_{OC\_TSP} * \rho_{TSP} * Z_W / 1000$
$Z_{DOM}$	DOM	$0.08 * K_{OW} * f_{OC\_DOM} * \rho_{DOM} * Z_W / 1000$
$Z_{Wbulk}$	Bulk water	$Z_W * (1 - v_{TSP} - v_{DOM}) + Z_{TSP} * v_{TSP} + Z_{DOM} * v_{DOM}$
$Z_{Mf}$	Macrophytes	$0.41 * K_{OW} * f_{OC\_Mf} * \rho_{Mf} * Z_W / 1000$
$Z_S$	Sediment solids	$0.41 * K_{OW} * f_{OC\_S} * \rho_S * Z_W / 1000$
$Z_{Sbulk}$	Bulk sediment	$Z_W * (1 - v_S) + Z_S * v_S$

$f_{OC\_TSP}, f_{OC\_DOM}, f_{OC\_Mf}$  and  $f_{OC\_S}$  = organic carbon fraction in TSP, DOM, macrophytes and sediment solids, respectively

$H$  = Henry's Law constant ( $\text{Pa m}^3 \text{mol}^{-1}$ )

$K_{OW}$  = octanol-water partition coefficient (-)

$P_L$  = sub-cooled liquid vapor pressure (Pa)

$R$  = gas constant ( $8.314 \text{ J mol}^{-1} \text{ K}^{-1}$ )

$T$  = absolute temperature (K)

$v_Q, v_{TSP}, v_{DOM}, v_S$  = volume fractions (-) of aerosol in air, TSP and DOM in water, and solids in sediments, respectively

$\rho_{TSP}, \rho_{DOM}, \rho_{Mf}$  and  $\rho_S$  = densities ( $\text{kg m}^{-3}$ ) of water particles and sediment particles, respectively, macrophytes (w.w.) and sediment solids

**Table S2.** *D*-values (mol Pa<sup>-1</sup> h<sup>-1</sup>) in ChimERA fate. Subscripts *i* are: *W* = water, *S* = sediment, *TSP* = total suspended particles, *DOM* = dissolved organic matter, and *Mf* = macrophyte. *SLy* = sediment layer.

<i>D</i> -value	Process	Equation
$D_V$	Absorption / volatilization	$VolMTC * A_W * Z_W$
$D_M$	Rain dissolution	$G_M * Z_W$
$D_C$	Wet particle deposition	$G_C * Z_Q$
$D_Q$	Dry particle deposition	$G_Q * Z_Q$
$D_I$	Water inflow	$G_I * Z_W$
$D_J$	Water outflow	$G_J * Z_W$
$D_W$	Degradation in water	$k_W * V_W * Z_W$
$D_{In\_TSP}$	TSP inflow	$G_{In\_TSP} * Z_{In\_TSP}$
$D_{Out\_TSP}$	TSP outflow	$G_{Out\_TSP} * Z_{TSP}$
$D_{In\_DOM}$	DOM inflow	$G_{In\_DOM} * Z_{In\_DOM}$
$D_{Out\_DOM}$	DOM outflow	$G_{Out\_DOM} * Z_{DOM}$
$D_{W\_Mf}$	Water > Macro (uptake)	$k_{W\_Mf} * V_{Mf} * Z_W$
$D_{Mf\_W}$	Macro > Water (elimination)	$k_{Mf\_W} * V_{Mf} * Z_{Mf}$
$D_{TSP\_Mf}$	TSP > Macro (deposition)	$U_{Dep} * A_{Mf} * Z_{TSP}$
$D_{Mf\_TSP}$	Macro > TSP (mortality)	$G_{Mort\_Mf} * Z_{Mf}$
$D_{Mf\_DOM}$	Macro > DOM (excretion)	$G_{Excr\_Mf} * Z_{Mf}$
$D_{Deg\_Mf}$	Degradation in macro	$k_{Mf} * V_{Mf} * Z_{Mf}$
$D_{Lfall}$	Litterfall	$G_{Lfall} * Z_{Mf}$
$D_T$	Sed > Water / Water > Sed	$DiffMTC * A_S * Z_W$
$D_{TSP\_S}$	TSP > Sed	$U_{Dep} * A_S * Z_{TSP}$
$D_{S\_TSP}$	Sediment resuspension	$U_{Dep} * A_S * f_{Resusp} * Z_S$
$D_B$	Sediment burial	$U_{Dep} * A_S * f_{Burial} * Z_S$
$D_{Sly\_Down}$	SedLy > SedLy + 1 (downward diffusion)	$1 / (1 / Dw(SLy) + 1 + Dw(SLy + 1))$
$D_{Sly\_Up}$	SedLy > SedLy - 1 (upward diffusion)	$1 / (1 / Dw(SLy) + 1 + Dw(SLy - 1))$

$D_w$	Diffusion in the water phase	$B_{ew} * A_s * Z_w / Y$
$D_s$	Degradation in Sed	$k_s * V_s * Z_{Sbulk}$

$A_{Mf}$  = surface area of submerged aquatic vegetation ( $m^2$ )

$A_w$  and  $A_s$  = water and sediment areas ( $m^2$ )

$B_{ew}$  = effective diffusivity in water ( $m^2 h^{-1}$ , calculated according to the Millington-Quirk eq.)

$C_i$  = water concentrations of  $i$  ( $kg m^{-3}$ )

$DiffMTC$  = sediment-water mass transfer coefficient ( $m h^{-1}$ )

$D_w$  = D value for the diffusion in the water phase ( $mol Pa^{-1} h^{-1}$ )

$f_{Burial}$  = fraction of deposited particles which is subject to burial

$f_{Resusp}$  = fraction of deposited particles which is subject to resuspension

$G$  represents flow of phase ( $m^3 h^{-1}$ ):

$G_I$  = water inflow

$G_J$  = water outflow

$G_M$  = rain dissolution

$G_C$  = wet particle deposition

$G_Q$  = dry particle deposition

$G_{In\_TSP}$  = TSP inflow

$G_{Out\_TSP}$  = TSP outflow

$G_{In\_DOM}$  = DOM inflow

$G_{Out\_DOM}$  = DOM outflow

$G_{Mort\_Mf}$  = macrophyte mortality (to form TSP)

$G_{Excr\_Mf}$  = macrophyte excretion (to form DOM)

$G_{Lfall}$  = macrophyte biomass loss (litterfall)

$k$  is a rate constant:

$k_i$  = degradation in compartment  $i$  ( $h^{-1}$ )

$k_{W\_TSP}$  = TSP adsorption from water ( $m^3 kg^{-1} h^{-1}$ )

$k_{TSP\_W}$  = TSP desorption to water ( $h^{-1}$ )

$k_{W\_DOM}$  = DOM adsorption from water ( $m^3 kg^{-1} h^{-1}$ )

$k_{DOM\_W}$  = DOM desorption to water ( $h^{-1}$ )

$k_{W\_Mf}$  = macrophyte uptake from water ( $h^{-1}$ )

$k_{Mf\_W}$  = macrophyte elimination to water ( $h^{-1}$ )

$U_{Dep}$  = mass transfer coefficient for particle deposition ( $m h^{-1}$ )

$V_i$  = compartment volumes ( $m^3$ )

$VolMTC$  = overall (water-side) air-water mass transfer coefficient ( $m h^{-1}$ )

$Y$  = diffusion path length (m)

$Z_i$  = phase or compartment fugacity capacities ( $mol m^{-3} Pa^{-1}$ ) (see Table S1)

$Z_{In\_i}$  = fugacity capacities of inflow phases ( $mol m^{-3} Pa^{-1}$ )

## Materials and methods

### Text S1. Calculation of $D$ -values for macrophytes

Diffusive exchanges between submerged vegetation and water were described by means of uptake ( $k_1$ , d<sup>-1</sup>) and elimination ( $k_2$ , d<sup>-1</sup>) rate constants<sup>1,2</sup>, calculated as a function of the octanol-water partition coefficient ( $K_{OW}$ ):

$$\frac{1}{k_1} = 0.002 + \frac{500}{K_{OW}} \quad (1)$$

$$\frac{1}{k_2} = 1.58 + 0.000015K_{OW} \quad (2)$$

From  $k_1$  and  $k_2$ , the hourly rate constants were derived ( $k_{W\_Mf} = k_1 / 24$ ,  $k_{Mf\_W} = k_2 / 24$ , h<sup>-1</sup>). The corresponding  $D$ -values (mol Pa<sup>-1</sup> h<sup>-1</sup>) for uptake from water ( $D_{W\_Mf}$ ) and elimination ( $D_{Mf\_W}$ ) were calculated as follows:

$$D_{W\_Mf} = k_{W\_Mf} V_{Mf} Z_W \quad (3)$$

$$D_{Mf\_W} = k_{Mf\_W} V_{Mf} Z_{Mf} \quad (4)$$

where  $V_{Mf}$  (m<sup>3</sup>) is the volume of the submerged vegetation excluding roots, and  $Z_W$  and  $Z_{Mf}$  (mol m<sup>-3</sup> Pa<sup>-1</sup>) are the fugacity capacities for water and macrophytes, respectively (Table S1). The description of degradation in macrophytes was similar to that in water and sediment (see  $D_W$  and  $D_S$  in Table S2), and was obtained from:

$$D_{Deg\_Mf} = k_{Mf} V_{Mf} Z_{Mf} \quad (5)$$

where  $k_{Deg\_Mf}$  ( $h^{-1}$ ) is the degradation rate constant in macrophytes, computed from the degradation half-life ( $HL_{Mf}$ , h) as  $\ln 2 / HL_{Mf}$ .

As in the work by Armitage and co-workers<sup>2</sup>, particle deposition onto macrophyte leaves ( $D_{TSP\_Mf}$ ) was described as dry particle deposition onto terrestrial plant surfaces:

$$D_{TSP\_Mf} = U_{Dep} A_{Mf} Z_{TSP} \quad (6)$$

where  $U_{Dep}$  ( $m\ h^{-1}$ ) is the mass transfer coefficient for particle deposition,  $A_{Mf}$  ( $m^2$ ) is the effective surface area of the submerged vegetation compartment, and  $Z_{TSP}$  ( $mol\ m^{-3}\ Pa^{-1}$ ) is the Z-value for total suspended particles (Table S1).

$U_{Dep}$  was estimated as:

$$U_{dep} = \gamma_{TSP} \frac{C_{TSP}}{\rho_{TSP}} \quad (7)$$

where  $\gamma_{TSP}$  ( $m\ h^{-1}$ ) is the mean particle settling velocity,  $C_{TSP}$  ( $g\ TSP\ m^{-3}\ water$ ) is the TSP concentration in water and  $\rho_{TSP}$  ( $g\ m^{-3}$ ) is the particle density. Different values for  $\gamma_{TSP}$  have been proposed in the literature; however, given the lack of specific measures, in this work a value of  $1\ m\ d^{-1}$  (i.e.,  $0.0417\ m\ h^{-1}$ ) was adopted<sup>2</sup>.

The macrophyte effective surface area  $A_{Mf}$  ( $m^2$ ) was estimated from the leaf area index ( $LAI$ ,  $m^2\ leaf\ m^{-2}\ water/sediment$ ) and water-sediment interface area ( $A_{WSed}$ ,  $m^2$ ):

$$A_{Mf} = LAI \cdot A_{WSed} \quad (8)$$

and  $LAI$  was derived by the mass of the leaves ( $M_L$ ,  $g\ d.w.$ ) and specific leaf area (SLA,  $m^2\ g^{-1}\ leaf\ d.w.$ ) as follows:

$$LAI = M_L SLA \quad (9)$$

Chemical losses with biomass through mortality and excretion and consequent transfer to TSP ( $D_{Mf\_TSP}$ ) and DOM ( $D_{Mf\_DOM}$ ) were calculated as advective processes:

$$D_{Mf\_TSP} = G_{Mort\_Mf} Z_{Mf} \quad (10)$$

$$D_{Mf\_DOM} = G_{Excr\_Mf} Z_{Mf} \quad (11)$$

where  $G_{Mort\_Mf}$  and  $G_{Excr\_Mf}$  ( $m^3 h^{-1}$ ) are the macrophyte mortality and excretion rates, respectively.

In ChimERA fate, macrophyte volume, computed from user-input biomass density, can vary with time. In case of decreasing volume, a fictitious increase of chemical concentrations in macrophytes would be computed as the result of the compartment volume reduction. In order to avoid such phenomenon, a  $D$ -value ( $D_{Lfall}$ ) was computed to preliminarily represent the "litterfall" process:

$$D_{Lfall} = G_{Lfall} Z_{Mf} \quad (12)$$

where  $G_{Lfall}$  ( $m^3 h^{-1}$ ) is the macrophyte volume loss on an hourly basis, calculated as  $(V_{Mf}(t) - V_{Mf}(t-1)) / 1$  h. Since in the present version of ChimERA fate no litter compartment was included, in the chemical mass balance such  $D$ -value was only considered as a loss for macrophytes, i.e., the chemical amount lost with macrophyte biomass is immediately lost from the whole system. The effect of this assumption is discussed in the Model illustration section (main text).

## Text S2. Hydrological module description

The flow of water in the spatially explicit version of ChimERA fate is described by the Saint-Venant equations for a one dimensional channel with varying bottom topography and varying width. Letting  $x$  denote the coordinate along the channel, the system consists of the two following partial differential equations:

$$\frac{\partial A}{\partial t} + \frac{\partial Q}{\partial x} = 0$$
$$\frac{\partial Q}{\partial t} + \frac{\partial}{\partial x} \left( \frac{Q^2}{A} + \frac{1}{2} g w h^2 \right) = \frac{1}{2} g h^2 w' - g w h z'$$

where  $w(x)$  is the width of the channel,  $z(x)$  the topography of the bottom,  $A(t,x) = w(x) * h(t,x)$  the wet cross section,  $h(t,x)$  the water height,  $u(t,x)$  the cross sectional average of the water velocity,  $Q(t,x) = A(t,x) * u(t,x)$  the discharge and  $g = 9.8 \text{ m s}^{-2}$  the acceleration of gravity.

Mathematically, this is an hyperbolic balance equation with two geometric source terms representing, respectively, the effects of the varying width and bottom topography on the water flow. The properties of the equation, the subtleties arising from the nature of the source terms and a numerical method to approximate its solutions are described in Balbas and Karni<sup>3</sup>. We also added a third source term in the second equation, namely a friction term of the Manning's type.

In the simulations for this paper, following Cowan's parameterization<sup>4</sup>, the Manning coefficient  $M$  was assumed as  $(0.02 + 0.005 + 0 + 0 + 0.005) * 1.0$ , where the numerical values, in order of appearance, have the meaning of "earth bottom", "moderate bottom irregularity", "no cross-section variations" (this is already accounted for in the partial differential equation), "no obstructions", "no meandering".

The channel geometry used in the simulations for model illustration (see Text S4) is a pond of radius 12 m with two streams of with 1 m and length 20 m as inflow and outflow, corresponding to:

$$R_{pond} = 12, L_{canal} = 20, \sigma = 0.001$$

$$w(x) = 2 * \max\left(0.5, \sqrt{\max(0, R_{pond}^2 - x^2)}\right)$$

$$z(x) = \begin{cases} -\sigma(x + R_{pond}), & x < -R_{pond} \\ -0.4(x/R_{pond} + 1)(1 - x/R_{pond}), & |x| < R_{pond} \\ -\sigma(x - R_{pond}), & x > R_{pond} \end{cases}$$

The computational domain is the interval  $[-R_{pond} - L_{canal}, R_{pond} + L_{canal}]$ .

The numerical scheme is based on a discretization of the computational domain in  $N = 64$  cells of length  $\Delta x = 1$  m. For a channel of length  $N$  meters, the cell index  $i$  takes values from 1 to  $N$ , but also the values 0 and  $N+1$  will be used in order to denote fictitious computational cells placed at the beginning and the end of the computational domain and that are needed to impose correctly the boundary conditions.  $z_i, A_i, Q_i, W_i$  denote the values of the variables at the center of each computational cell. From these values, the water height  $h_i = A_i / W_i$ , the water level  $H_i = h_i + z_i$ , and the “total area”  $AT_i = H_i * W_i$  may be computed.

At the beginning of the simulation, all the variables are set to their initial values in cells from 1 to  $N$  and then a sequence of time steps is computed in order to update the values of the time-dependent variables until the final time of the simulation is reached. In each time step, the “flux” of water and of momentum is computed for each interface between cells and then the cell values are updated, thus obtaining a “conservative scheme” (i.e. all changes in the total mass of water and total momentum come from the boundaries and no losses may occur at internal interfaces). First, the “interface values” of the bottom topography are computed as  $Z_{i+1/2} = (Z_i + Z_{i+1}) / 2$ .

The first step is to impose the boundary conditions, computing the fictitious values for cells number 0 and  $N+1$ . The discharge  $Q_{in}$  (taken as  $0.05 \text{ m}^3 \text{ s}^{-1}$  for the present paper) is imposed at the inlet by setting:

$$Q_0 = Q_{in}, \tilde{h} = AT_1 / W_1 - Z_1, AT_0 = W_0 * (\tilde{h} + Z_0)$$

and free-flow type boundary conditions are imposed at the outlet as follows:

$$Q_{N+1} = Q_N, \tilde{h} = AT_N / W_N - Z_N, AT_{N+1} = W_{N+1} * (\tilde{h} + Z_{N+1})$$

Next, for each computational cell, the first order accurate “hydrostatic reconstruction” is computed:

$$\begin{aligned} H_i &= AT_i / W_i \\ H_{i+1/2}^+ &= H_{i+1}, H_{i+1/2}^- = H_i \\ h_{i+1/2}^\pm &= H_{i+1/2}^\pm - Z_{i+1/2} \\ H_{i+1/2}^+ &= H_{i+1}, H_{i+1/2}^- = H_i \\ Q_{i+1/2}^+ &= Q_{i+1}, Q_{i+1/2}^- = Q_i \\ W_{i+1/2}^+ &= AT_{i+1} / H_{i+1/2}^+, W_{i+1/2}^- = AT_i / H_{i+1/2}^- \\ W_{i+1/2} &= \max(W_{i+1/2}^+, W_{i+1/2}^-) \\ u_{i+1/2}^\pm &= Q_{i+1/2}^\pm / (h_{i+1/2}^\pm * W_{i+1/2}) \end{aligned}$$

In order to obtain a numerically stable scheme, the amount of artificial diffusion is controlled by the (local) Lax-Friedrichs parameter

$$\alpha_{i+1/2} = \max(u_{i+1/2}^\pm + \sqrt{gh_{i+1/2}^\pm})$$

and the maximum time step length is computed as

$$\begin{aligned} a &= \max_i (W_{i+1/2} * \alpha_{i+1/2}) \\ \Delta t &= 0.5 * \Delta x * \min_i (W_{i+1/2}) / a \end{aligned}$$

When needed for output purposes, the time step length is shortened in order to meet the end of each simulation hour. The fluxes at each interface are computed by the local Lax-Friedrichs formula

$$F_{i+1/2}^{(1)} = \frac{1}{2} \left[ Q_{i+1/2}^+ + Q_{i+1/2}^- - \alpha_{i+1/2} (H_{i+1/2}^+ - H_{i+1/2}^-) \right]$$

$$F_{i+1/2}^{(2)} = \frac{1}{2} \left[ \begin{aligned} & W_{i+1/2}^+ * h_{i+1/2}^+ * (u_{i+1/2}^+)^2 + \frac{g}{2} W_{i+1/2}^+ * (h_{i+1/2}^+)^2 + W_{i+1/2}^- * h_{i+1/2}^- * (u_{i+1/2}^-)^2 + \frac{g}{2} W_{i+1/2}^- * (h_{i+1/2}^-)^2 \\ & - \alpha_{i+1/2} (Q_{i+1/2}^+ - Q_{i+1/2}^-) \end{aligned} \right]$$

and the source terms are given by

$$S_i^{(W)} = \frac{g}{2} \left( \frac{W_{i+1/2} + W_{i-1/2}}{\Delta x} \right) \left( \frac{h_{i+1/2}^- + h_{i-1/2}^+}{2} \right)$$

$$S_i^{(Z)} = g \left( \frac{W_{i+1/2} + W_{i-1/2}}{2} \right) \left( \frac{h_{i+1/2}^- + h_{i-1/2}^+}{2} \right) \left( \frac{Z_{i+1/2} + Z_{i-1/2}}{\Delta x} \right)$$

$$h_i^{(M)} = \left( \frac{h_{i+1/2}^- + h_{i-1/2}^+}{2} \right)$$

$$Ri = \frac{W_i * h_i^{(M)}}{W_i + 2h_i^{(M)}}$$

$$S_i^{(M)} = \frac{gM^2 Q_i |Q_i|}{W_i h_i^{(M)} (Ri)^{4/3}}$$

Finally the time update of the variables is performed

$$AT_i = AT_i - \frac{\Delta t}{\Delta x} (F_{i+1/2}^{(1)} - F_{i-1/2}^{(1)})$$

$$Q_i = Q_i - \frac{\Delta t}{\Delta x} (F_{i+1/2}^{(2)} - F_{i-1/2}^{(2)}) - \Delta t * S_i^{(W)} - \Delta t * S_i^{(Z)} - \Delta t * S_i^{(M)}$$

Before proceeding to the next time step, the values of  $\Delta t * F_{i+1/2}^{(1)}$  are accumulated, since they represent the amount of water that flowed from cell  $i$  to cell  $i+1$  in the time step. The sum of these quantities in each simulation hour, together with the volume of water at the end of each simulation

hour, is passed to the ChimERA computational model. For simulations in which the spatial discretization in the ChimERA model is coarser than the one employed here, of course the water volumes are gathered accordingly and only the fluxes across boundaries of ChimERA computational cells are retained.

### **Text S3. Model parameterization**

#### *Output verification*

Output verification was performed by comparing the chemical inventories or concentrations in water, macrophytes and sediment predicted by the model with the ones measured in three different environmental scenarios, as also done by Armitage and co-workers<sup>2</sup>. This allowed (1) assessing how well model output matched experimental observations and (2) verifying the correctness of the implementation of the macrophyte compartment with respect to the reference approach<sup>2</sup>. The first two scenarios<sup>5</sup> concerned the application of lambda-cyhalothrin to ditch enclosures in Renkum, the Netherlands, characterized by different vegetation densities (Case 1 and 2), while in the third scenario<sup>6</sup> azinphos-methyl was applied to a ditch enclosure in Duluth, Minnesota, characterized by low vegetation density (Case 3). In all cases, simulations with ChimERA fate were performed considering one sediment layer only (no vertical discretization). As in Armitage and co-workers<sup>2</sup>, the model was parameterized by setting water volumes, sediment depth, volume fraction of solids and organic carbon content, vegetation biomass and characteristics, TSP and DOM concentrations and properties, and water temperature equal to the ones characterizing the experimental systems<sup>5,6</sup>. All details concerning model parameterization can be found in Table S3, while physical-chemical properties and environmental half-lives of the modelled chemicals are reported in Table S4.

Model performance was considered satisfying when predictions were within an order of magnitude with respect to observations; moreover, modelling efficiency (EF) (Eq. 5, main text) was computed following the approach of Mayer and Butler<sup>7</sup>, and model performance was considered good for EF ranging from 0 to 1.

### *Output corroboration*

Output corroboration was performed by comparing model predictions to experimental data collected in a 40-m long stagnant ditch in Renkum, the Netherlands, in which prosulfocarb was applied and subsequently measured at different times in water, sediment and macrophytes<sup>8</sup>. As did for the output verification, ChimERA fate was parameterized by setting environmental parameters equal to the ones characterizing the experimental system. In Adriaanse and co-workers<sup>8</sup>, the authors used the TOXSWA model<sup>9</sup> to estimate a degradation rate in water for prosulfocarb that was suitable for mesocosm studies; since their simulations showed that prosulfocarb penetrated no deeper than the upper centimetre of sediment, a single 1-cm deep sediment layer was simulated with ChimERA fate. All details concerning model parameterization can be found in Table S3, while prosulfocarb physical-chemical properties and environmental half-lives of are reported in Table S4. Again, model performance was assessed by means of modelling efficiency EF<sup>7</sup>.

**Table S3.** Values for the key parameters adopted for ChimERA fate output verification and corroboration.

Parameter	Unit	Output verification			Output corroboration
		Case 1	Case 2	Case 3	
Simulation time	d	8	8	16	30 <sup>c</sup>
Water surface area	m <sup>2</sup>	0.865	0.865	50.5	132 <sup>c</sup>
Water depth	m	0.5	0.5	0.6	0.57 <sup>c</sup>
Water temperature	°C	21 <sup>a</sup>	21 <sup>a</sup>	27.6 <sup>b</sup>	14 <sup>c</sup>
Sediment depth	m	0.05	0.05	0.05	0.01 <sup>c</sup>
Vol. frac. sediment solids	-	0.15	0.15	0.15	0.46 <sup>c</sup>
OC frac. sediment solids	-	0.1	0.1	0.15	0.17 <sup>c</sup>
TSP concentration	mg L <sup>-1</sup>	16	16	2.65	10 <sup>c</sup>
OC frac. TSP	-	0.35	0.35	0.2	0.05 <sup>c</sup>
Vegetation biomass	kg d.w. m <sup>-2</sup>	0.145	0.043	0.01	0.0949 <sup>c</sup>
OC frac. vegetation (w.w.)	-	0.045	0.045	0.0339	0.04
Veg. dry/wet mass ratio	-	0.113	0.113	0.113	0.113
Specific Leaf Area (SLA)	m <sup>2</sup> g <sup>-1</sup> d.w.	0.1	0.1	0.1	0.1
DOC concentration	mg L <sup>-1</sup>	8	8	11	-
Sediment particle density	kg m <sup>-3</sup>	1500	1500	1500	1210 <sup>c</sup>
TSP density	kg m <sup>-3</sup>	1500	1500	1500	1210 <sup>c</sup>
OC density	kg m <sup>-3</sup>	1000	1000	1000	1000
Vegetation (wet) density	kg m <sup>-3</sup>	1000	1000	1000	1000
Particle settling velocity	m d <sup>-1</sup>	1	1	1	1
Fraction resuspension	-	0.7	0.7	0.7	0.7
Fraction burial	-	0.3	0.3	0.3	0.3
$G_{Mort\_Mf}$	m <sup>3</sup> h <sup>-1</sup>	0	0	0	0
$G_{Excr\_Mf}$	m <sup>3</sup> h <sup>-1</sup>	0	0	0	0

All values were taken from Armitage et al.<sup>2</sup>, except for <sup>a</sup> (Leistra et al.<sup>5</sup>), <sup>b</sup> (Knuth et al.<sup>6</sup>) and <sup>c</sup> (Adriaanse et al.<sup>8</sup>).

**Table S4.** Physical-chemical properties and environmental half-lives of the chemicals modelled in the output verification and corroboration cases.

Property	Unit	Lambda-cyhalothrin	Azinphos-methyl	Prosulfocarb
Molecular weight	g mol <sup>-1</sup>	449.9 <sup>a</sup>	317.32 <sup>a</sup>	251.4 <sup>b</sup>
Reference temperature	°C	25	25	20 <sup>b</sup>
Melting point	°C	49.2 <sup>b</sup>	73 <sup>b</sup>	-20 <sup>c</sup>
Vapour pressure	Pa	2.04E-07 <sup>a</sup>	2.8E-05 <sup>a</sup>	7.9E-04 <sup>b</sup>
Water solubility	g m <sup>-3</sup>	5E-03 <sup>a</sup>	30 <sup>a</sup>	13 <sup>b</sup>
log <i>K<sub>OW</sub></i>	-	7 <sup>a</sup>	2.75 <sup>a</sup>	4.48 <sup>b</sup>
Half-life in water	d	7 <sup>a</sup>	3 <sup>a</sup>	5.8
Half-life in sediment	d	10 <sup>a</sup>	10 <sup>a</sup>	11.6
Half-life in macrophyte	d	2 <sup>a</sup>	2 <sup>a</sup>	5.8

<sup>a</sup> Armitage et al.<sup>2</sup>; <sup>b</sup> Tomlin<sup>10</sup>; <sup>c</sup> FOOTPRINT<sup>11</sup>; <sup>d</sup> Adriaanse et al.<sup>8</sup>

### *Model illustration*

One-year illustrative simulations were performed for two model chemicals characterized by different hydrophobicity and persistence (Table S5) in a macrophyte-dominated system consisting of a pond and its inflow and outflow streams. As depicted in Figure 1b,c (main text), the system was split into 10 adjacent boxes along the water flow direction: the first two and the last two boxes, 10-m long, represented the inflow and outflow streams, respectively, while the 6 central boxes, 4-m long, represented the 450-m<sup>2</sup>, 0.5-m deep pond. A constant water flow was selected to obtain an average residence time in the pond boxes of about 20 days.

**Table S5.** Physical-chemical properties and environmental half-lives of the two model chemicals selected for the illustration: Chemical A (atrazine-like)<sup>10</sup> and Chemical B (pyrene-like)<sup>12</sup>.

Property	Unit	Chemical A	Chemical B
Molecular weight	g mol <sup>-1</sup>	215.7	202.3
Reference temperature	°C	25	25
Melting point	°C	175.8	156
Vapour pressure	Pa	3.85E-05	6E-04
Water solubility	g m <sup>-3</sup>	33	0.132
log <i>K<sub>OW</sub></i>	-	2.5	5.18
Half-life in water	d	55	70
Half-life in sediment	d	200	2290
Half-life in macrophyte	d	55	70

Realistic information concerning macrophyte biomass (Fig. S1a), DOC and POC concentrations (Fig. S1b) and water temperature (Fig. S1c) was derived from the literature: more specifically, POC values were obtained from the monthly averages of TSP concentrations for a Portuguese eutrophied pond<sup>13</sup> and considering an OC fraction of 0.05, while DOC was derived assuming a POC/DOC constant ratio of 0.21 (average of the ones reported by Parszuto and Kaliszewska<sup>14</sup>); water temperature was also taken from de Figueiredo and co-workers (Portuguese eutrophied pond)<sup>13</sup>, while values for macrophyte biomass density were taken from Desmet and co-workers<sup>15</sup> and assumed as uniform for the whole stream-pond system. Since monthly averages were generally available for environmental parameters, hourly ones were obtained by linear interpolation. It should be remarked that no effort was made to simulate a specific situation and that the present scenario was adopted for illustration purposes only; moreover, time-resolved data concerning macrophyte biomass densities, POC/DOC concentrations and other environmental parameters are often lacking. A sediment depth of 1 cm was selected, while all other model parameters (e.g., densities, settling velocities) were identical to the ones adopted for model output verification (Table S3). A pulsed

chemical emission to the first box (stream) was simulated (Figure S1c) in order to investigate the influence of different combinations of POC/DOC concentrations and macrophyte biomass densities on bioavailable concentrations.

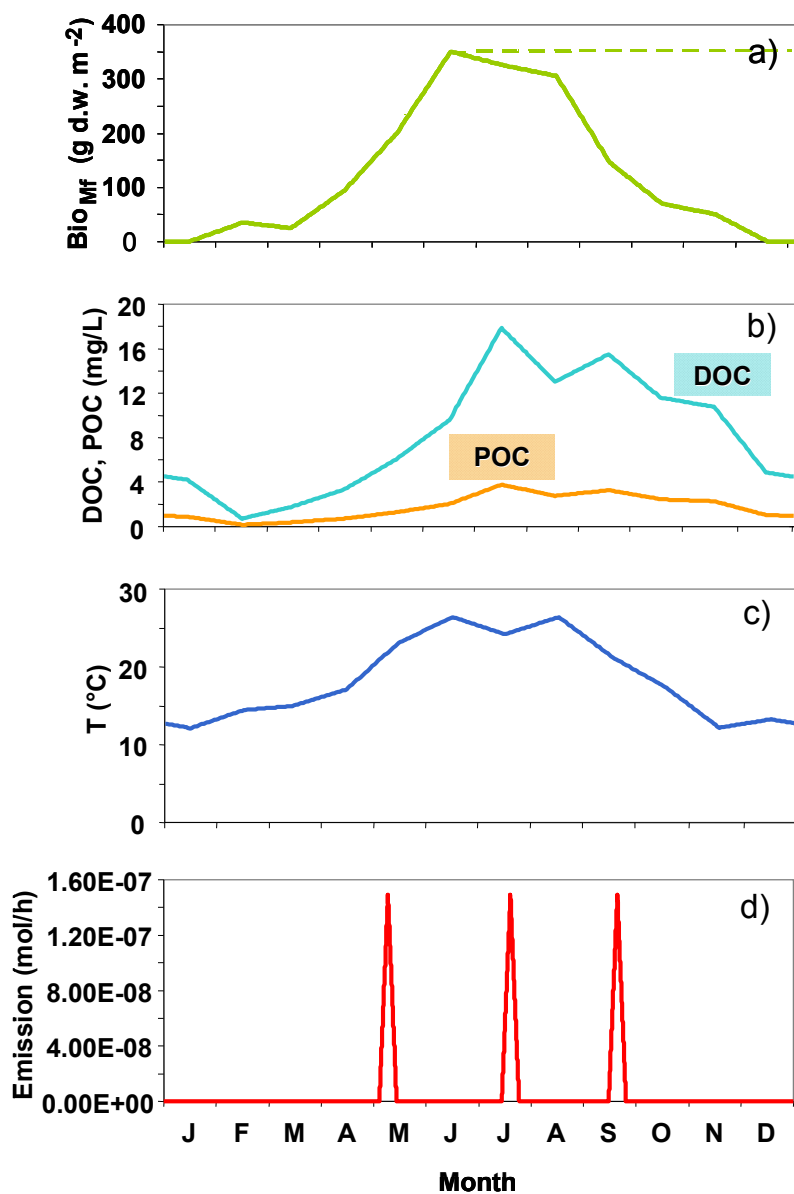


**Figure S1.** (a) Macrophyte biomass ( $\text{g d.w. m}^{-2}$ )<sup>15</sup>, (b) DOC and POC concentrations ( $\text{mg L}^{-1}$ )<sup>13,14</sup>, (c) water temperature profile<sup>13</sup> and (d) emission profile to Box 1 (stream) for the two model chemicals adopted for model illustration.

## Results and discussion

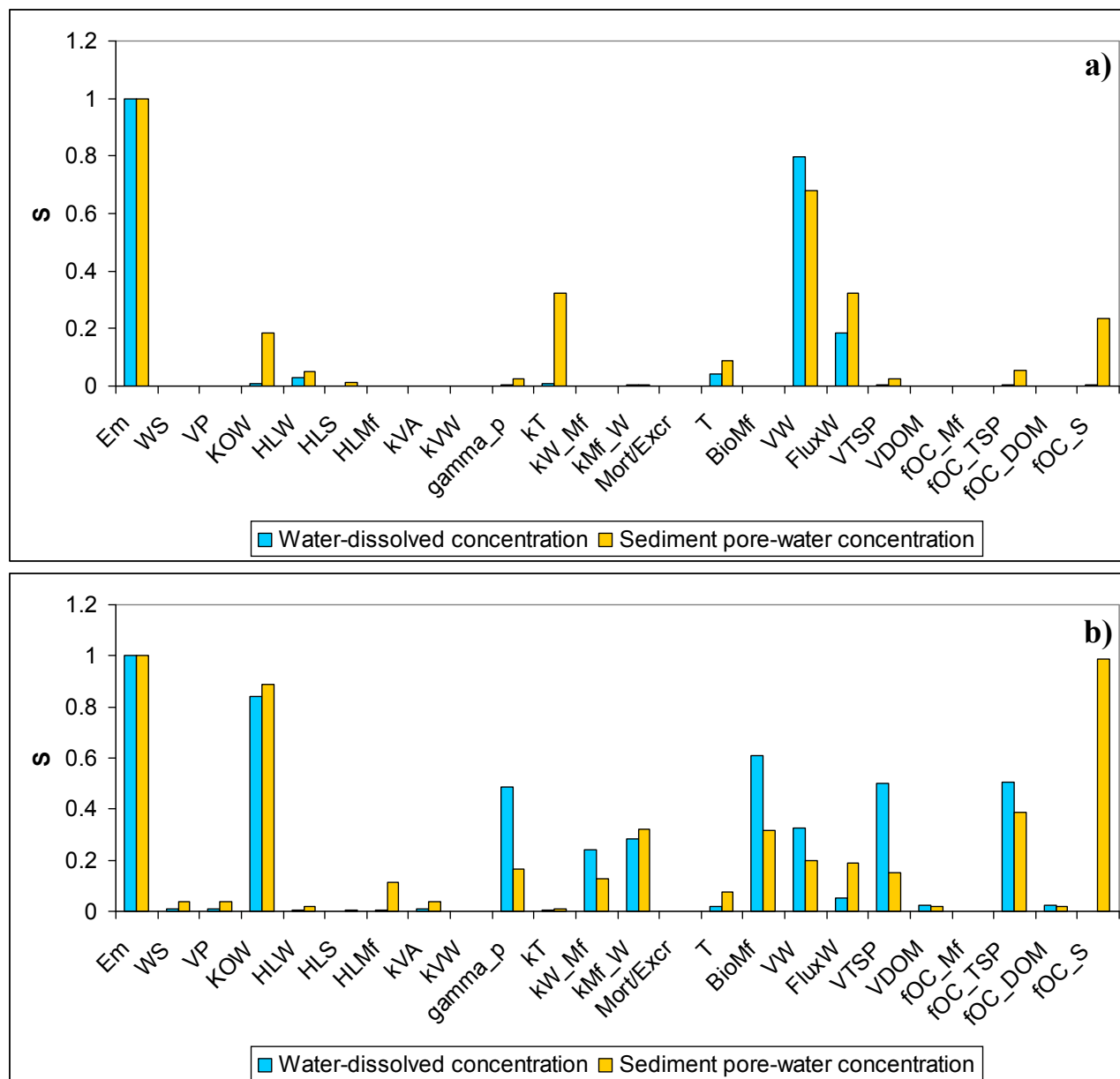


**Figure S2.** Sensitivity analysis results for Chemical A (a) and Chemical B (b).

Tested parameters were: emission ( $\text{mol h}^{-1}$ ,  $Em$ ), water solubility ( $\text{mg L}^{-1}$ ,  $WS$ ), vapour pressure (Pa,  $VP$ ), octanol-water partition coefficient (dimensionless,  $K_{OW}$ ), chemical half-life in water (h,  $HL_W$ ), chemical half-life in sediment (h,  $HL_S$ ), chemical half-life in macrophyte (h,  $HL_{Mf}$ ), volatilization MTC - air side ( $\text{m h}^{-1}$ ,  $k_{VA}$ ), volatilization MTC - water side ( $\text{m h}^{-1}$ ,  $k_{VW}$ ), particle settling velocity ( $\text{m h}^{-1}$ ,  $gamma_p$ ), sediment-water diffusion MTC ( $\text{m h}^{-1}$ ,  $k_T$ ), macrophyte uptake rate constant ( $\text{h}^{-1}$ ,  $k_{W_{Mf}}$ ), macrophyte depuration rate constant ( $\text{h}^{-1}$ ,  $k_{Mf_W}$ ), mortality/excretion rate ( $\text{h}^{-1}$ ,  $Mort/Excr$ ), temperature ( $^{\circ}\text{C}$ ,  $T$ ), macrophyte biomass density ( $\text{g d.w. m}^{-2}$ ,  $Bio_{Mf}$ ), water volume ( $\text{m}^3$ ,  $V_W$ ), water flux ( $\text{m}^3 \text{h}^{-1}$ ,  $Flux_W$ ), TSP volume ( $\text{m}^3$ ,  $V_{TSP}$ ), DOM volume ( $\text{m}^3$ ,  $V_{DOM}$ ), organic carbon fractions of macrophytes (dimensionless,  $f_{OC_{Mf}}$ ), TSP (dimensionless,  $f_{OC_{TSP}}$ ), DOM (dimensionless,  $f_{OC_{DOM}}$ ), sediment solids (dimensionless,  $f_{OC_S}$ ).

#### **Text S4. Results for output verification**

The results of the comparison between ChimERA fate predictions and experimental observations for Case 1, 2 and 3 are presented in Figures S3, S4 and S5, respectively. While for Case 1 and 2 inventories in the different compartments were compared, expressed as percentage of the applied dose, for Case 3 the comparison was based on concentrations. For Case 1 and 2, simulations were first performed using the scenario described in Table S3, which was built using the same input data selected by Armitage and co-workers for testing their modelling approach<sup>2</sup>. These first model runs (“Predicted” in Figs. S3 and S4) indicated in both cases an excessively rapid chemical transport from water to macrophytes and sediment, which led to a general overestimation of concentrations in these two compartments (charts b and c), at least in the first 25-50 hours ( $EF < 0$  for macrophyte and sediment in both Case 1 and 2); such overestimation was particularly evident in Case 2 (lambda-cyhalothrin, low vegetation biomass) (Fig. S4). Since dominant fluxes were particle deposition onto macrophyte and sediment (at least two orders of magnitude higher than the other losses for the water compartment; results not shown), a second model run was performed for both cases halving the deposition velocity from 1 to 0.5 m d<sup>-1</sup>, as also done by Armitage and co-workers<sup>2</sup>. Such values were in the range of those suggested in the literature (e.g., refs. 16, 17). Results (“Pred. dep/2” in Figs. S3 and S4) showed a general, slight improvement of the fit between predicted and observed concentrations, especially for the water compartment during the first simulation hours, but such modification was not able to significantly improve the fit for sediment ( $EF < 0$ ). Armitage and co-workers obtained the same results from their model application for both cases and all compartments, and ascribed the poor representation of the uptake of lambda-cyhalothrin by sediment in the first 1-2 days to two factors: (1) the assumption that the contaminant immediately became well-mixed in the water column and (2) the assumption of equifugacity between suspended solids and water<sup>2</sup>. Our simulations confirmed such hypotheses, since an investigation of chemical fluxes showed a fast particle-mediated deposition onto sediment (and macrophyte leaves) immediately after dosing, also due to the high log  $K_{OW}$  of lambda-cyhalothrin. A third set of

simulations was performed, as also done by Armitage and co-workers, halving the lambda-cyhalothrin half-life in macrophytes: almost no changes were observed for predictions in water and sediment, and no substantial improvement was observed for macrophytes (“Pred. HLMf/2” in Figure S3b and S4b).

From the simulations for azinphos-methyl (Case 3) (Fig. S5) a different picture appeared. Results obtained from the first model run (“Predicted”), performed using the scenario described in Table S3, revealed a good model performance, at least for water and macrophytes (within a factor of 1.5 or less, with  $EF_W = 0.92$  and  $EF_{MF} = 0.95$ ), but again the chemical behaviour in sediment was not accurately captured ( $EF = -0.55$ ). Armitage and co-workers obtained the same results from their model application for water and macrophytes, but their predictions revealed a better fit for the sediment compartment<sup>2</sup>. Since model formulations were very similar, this was probably due to a different parameterization in terms of mass-transfer coefficients. In a second model run (“Pred 5\*KT” in Fig. S5), the influence of the water-sediment diffusion mass transfer coefficient  $k_T$  was investigated, by adopting a value of  $0.0005 \text{ m h}^{-1}$  instead of the default one (i.e.,  $0.0001 \text{ m h}^{-1}$ <sup>18</sup>): for water and macrophytes almost no changes were observed, while the fit for sediment concentrations considerably improved ( $EF = 0.35$ ). In the case of azinphos-methyl, characterized by definitely lower  $\log K_{OW}$  with respect to lambda-cyhalothrin (2.75 vs. 7), particle-mediated deposition processes were evidently less important than in Case 1 and 2, and degradation in water and water outflow were the dominant fluxes in determining chemical depletion from water (results not shown); however, the predicted concentration profile in sediment suggested that a more complex description of the physical environment (e.g., sediment properties with depth) and of water-sediment exchange may be needed to improve model performance. In all cases, the high similarity of ChimERA fate predictions with respect to Armitage's ones suggested a correct implementation of the macrophyte compartment.

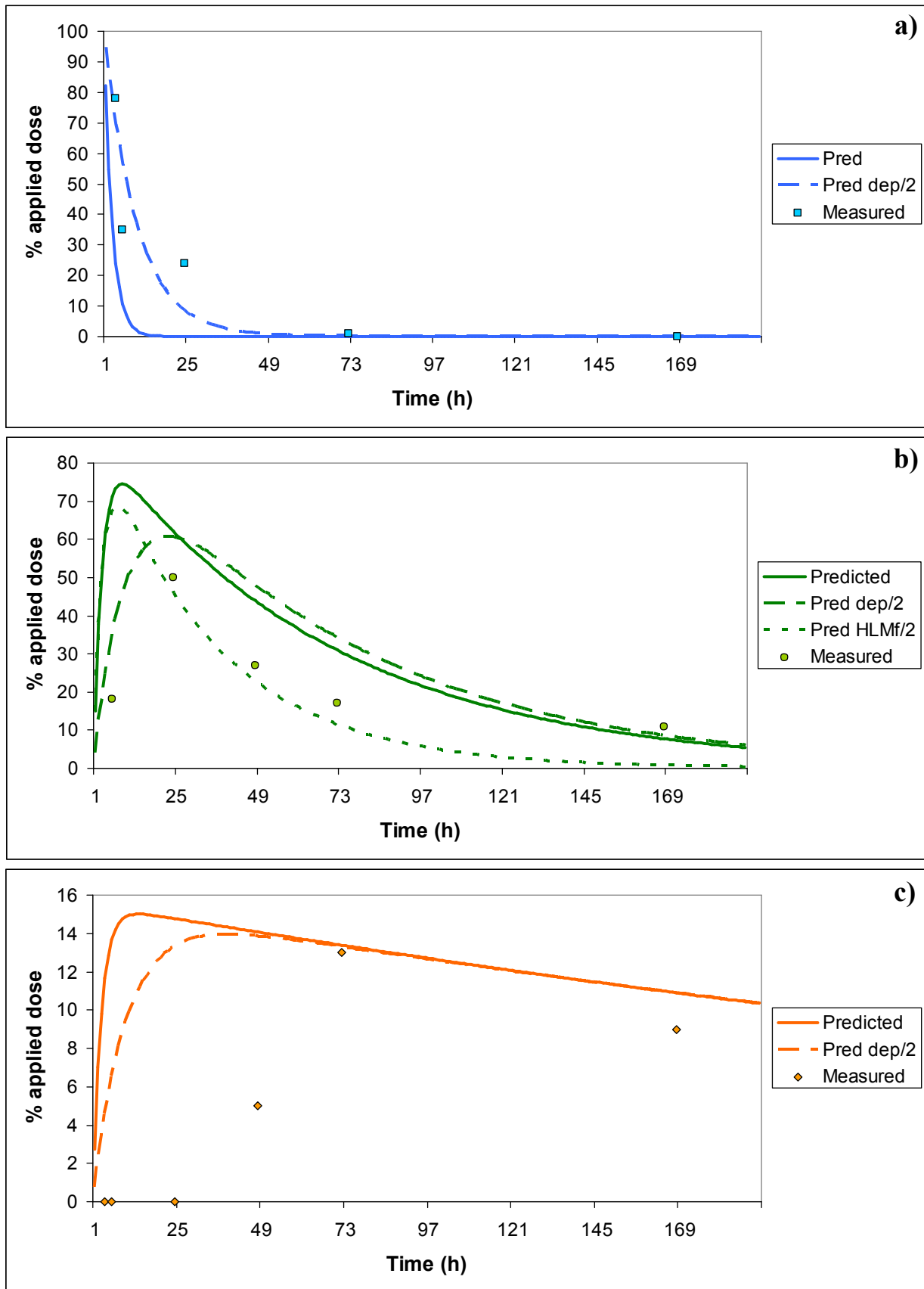


**Figure S3.** Results of the model output verification for water (a), macrophytes (b), and sediment (c): Case 1 (lambda-cyhalothrin, high veg)<sup>2</sup>.

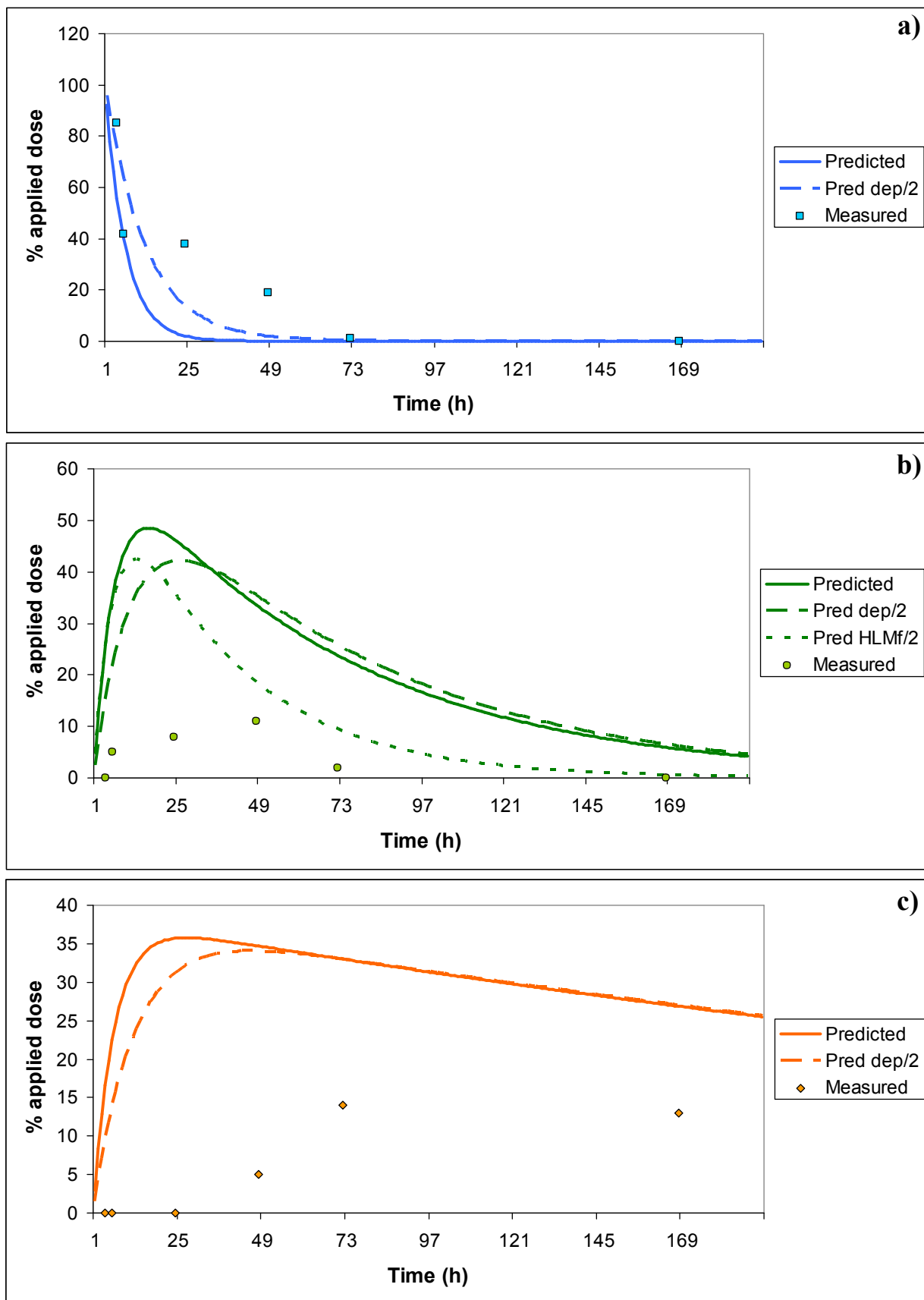


**Figure S4.** Results of the model output verification for water (a), macrophytes (b), and sediment (c): Case 2 (lambda-cyhalothrin, low veg.)<sup>2</sup>.

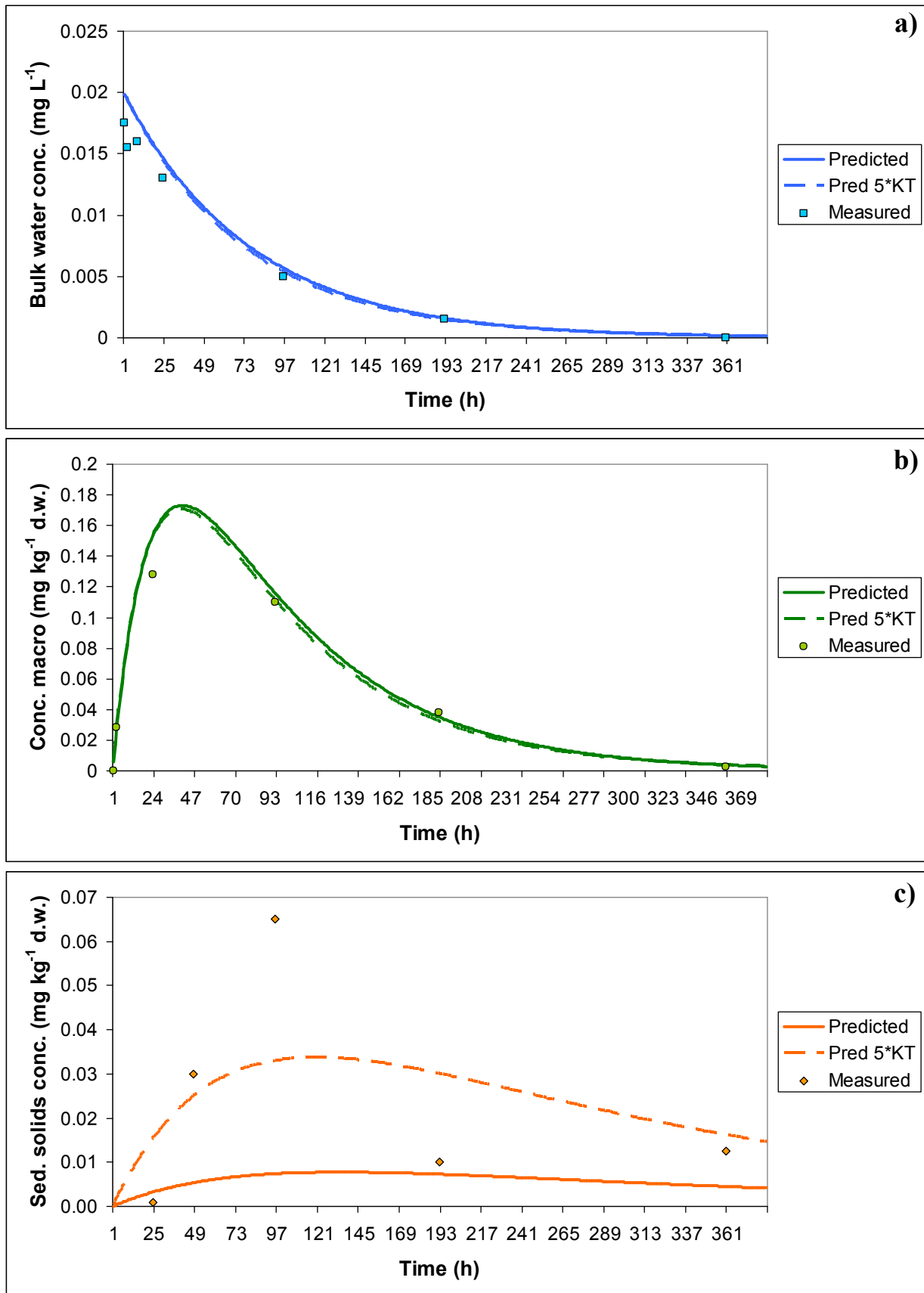


**Figure S5.** Results of the model output verification for water (a), macrophytes (b), and sediment (c): Case 3 (azinphos-methyl)<sup>2</sup>.

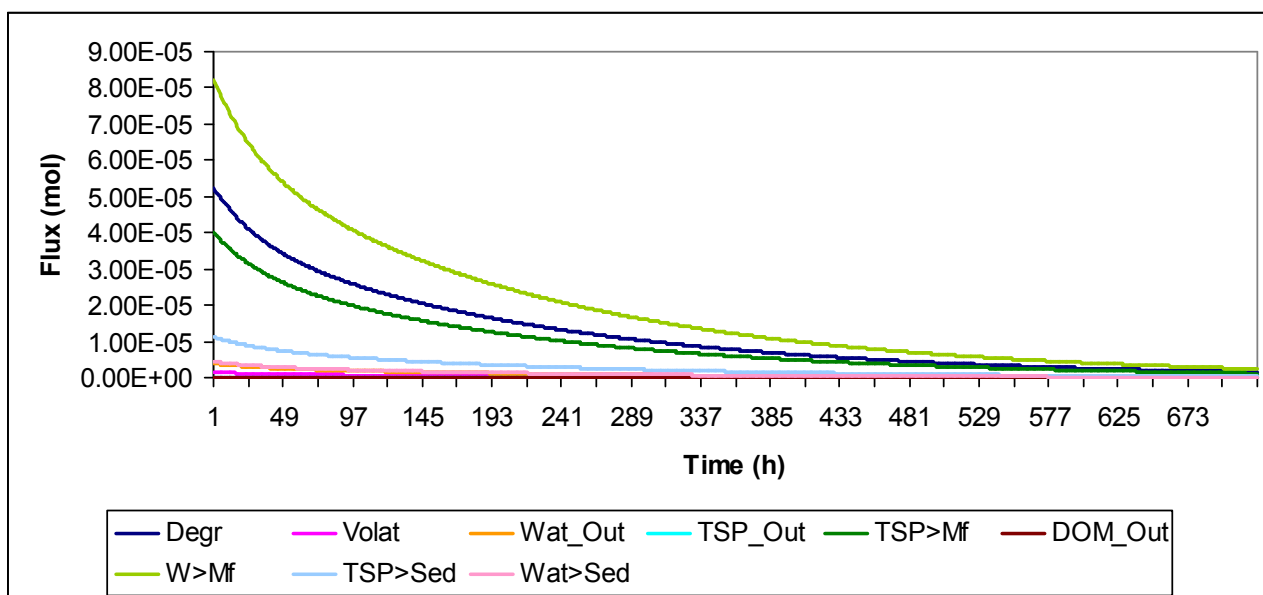


**Figure S6.** Hourly prosulfocarb fluxes describing losses from the water compartment: degradation (“Degr”), volatilization (“Vol”), water outflow (“Wat\_Out”), TSP outflow (“TSP\_Out”), TSP deposition onto macrophyte leaves (“TSP>Mf”), DOM outflow (“DOM\_Out”), uptake by macrophyte (“W>Mf”), TSP deposition onto sediment (“TSP>Sed”), water-sediment diffusion (“Wat>Sed”).

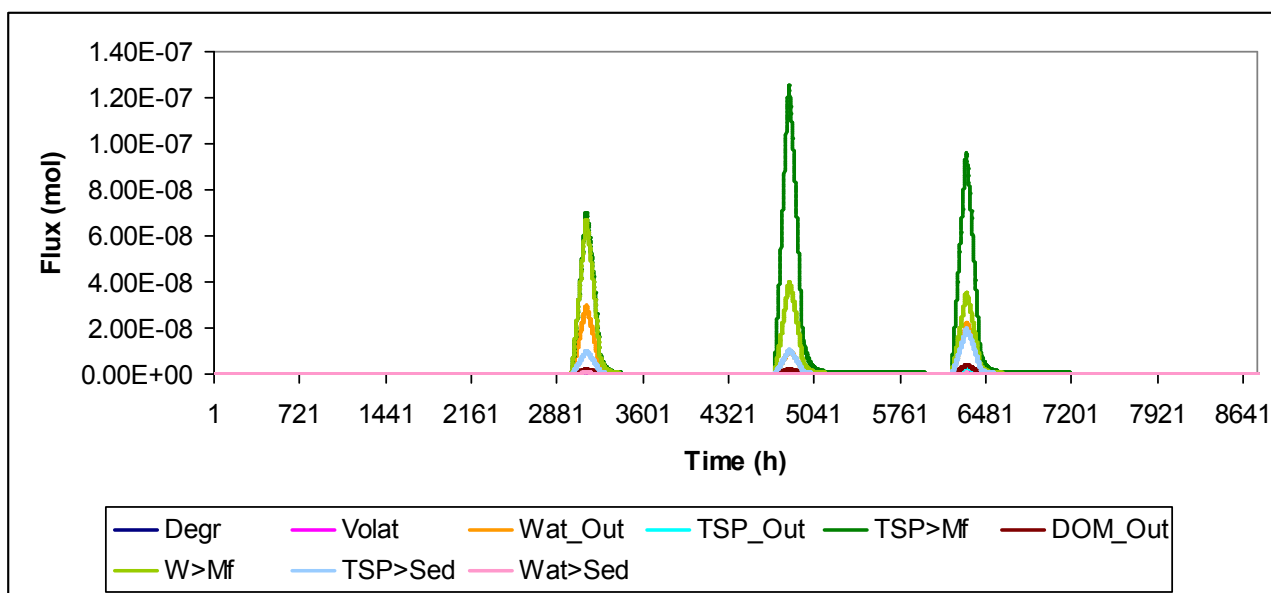


**Figure S7.** Hourly Chemical B fluxes describing losses from the water compartment for Box 1 (stream, where emission occurred): degradation (“Degr”), volatilization (“Vol”), water outflow (“Wat\_Out”), TSP outflow (“TSP\_Out”), TSP deposition onto macrophyte leaves (“TSP>Mf”), DOM outflow (“DOM\_Out”), uptake by macrophyte (“W>Mf”), TSP deposition onto sediment (“TSP>Sed”), water-sediment diffusion (“Wat>Sed”).

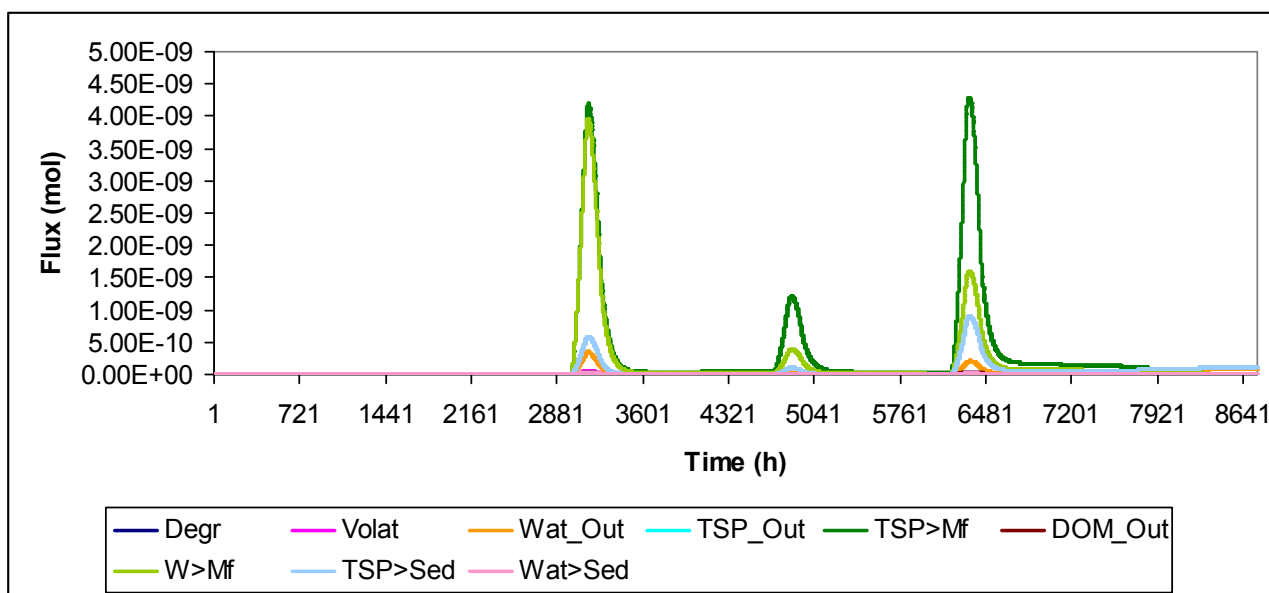


**Figure S8.** Hourly Chemical B fluxes describing losses from the water compartment for Box 3 (first box of the pond): degradation (“Degr”), volatilization (“Vol”), water outflow (“Wat\_Out”), TSP outflow (“TSP\_Out”), TSP deposition onto macrophyte leaves (“TSP>Mf”), DOM outflow (“DOM\_Out”), uptake by macrophyte (“W>Mf”), TSP deposition onto sediment (“TSP>Sed”), water-sediment diffusion (“Wat>Sed”).

## References

- (1) Gobas, F. A. P. C.; McNeil, E. J.; Lovett-Doust, L.; Haffner, G. D. Bioconcentration of chlorinated aromatic hydrocarbons in aquatic macrophytes. *Environ. Sci. Technol.* **1991**, *25* (5), 924–929; DOI: 10.1021/es00017a015.
- (2) Armitage, J. M.; Franco, A.; Gomez, S.; Cousins, I. T. Modeling the potential influence of particle deposition on the accumulation of organic contaminants by submerged aquatic vegetation. *Environ. Sci. Technol.* **2008**, *42*, 4052–4059; DOI 10.1021/es702439u.
- (3) Balbas, J.; Karni, S. A central scheme for shallow water flows along channels with irregular geometry. *ESAIM: M2AN* **2009**, *43*, 333–351; DOI: 10.1051/m2an:2008050.
- (4) Gordon, N.D.; McMahon, T.A.; Finlayson, B.L.; Gippel, C.J.; Nathan, R.J. *Stream Hydrology. An Introduction for Ecologists*. 2nd ed. Wiley: West Sussex, 2004.
- (5) Leistra, M.; Zweers, A. J.; Warinton, J. S.; Crum, S. J. H.; Hand, L. H.; Beltman, W. H. J.; Maund, S. J. Fate of the insecticide lambda-cyhalothrin in ditch enclosures differing in vegetation density. *Pest. Manag. Sci.* **2003**, *60*, 75–84; DOI: 10.1002/ps.780.
- (6) Knuth, M. L.; Heinis, L. J.; Anderson, L. E. Persistence and distribution of azinphos-methyl following application to littoral enclosure mesocosms. *Ecotox. Environ. Safe.* **2000**, *47*, 167–177; DOI: 10.1006/eesa.2000.1945.
- (7) Mayer, D. G.; Butler, D. G. Statistical validation. *Ecol. Modell.* **1993**, *68*, 21–32; DOI: 10.1016/0304-3800(93)90105-2.

- (8) Adriaanse, P. I.; Boesten, J. J. T. I.; Crum, S. J. H. Estimating degradation rates in outdoor stagnant water by inverse modelling with TOXSWA: a case study with prosulfocarb. *Pest. Manag. Sci.* **2013**, *69*, 755–767; DOI 10.1002/ps.3435.
- (9) Adriaanse, P.I. Exposure assessment of pesticides in field ditches: the TOXSWA model. *Pestic. Sci.* **1997**, *49*, 210–212.
- (10) Tomlin, C. D. S., Ed. *The Pesticide Manual*, 11th, ed; British Crop Protection Council: Farnham, Surrey, 1997.
- (11) FOOTPRINT *Pesticide Properties Database* Website; <http://www.eu-footprint.org/it/ppdb.html>
- (12) Mackay, D.; Shiu, W. Y.; Ma, K. C. *Illustrated handbook of physical-chemical properties and environmental fate for organic chemicals. Volume II: Polynuclear Aromatic Hydrocarbons, Polychlorinated Dioxins, and Dibenzofurans*. Lewis Publishers: Chelsea, USA, 1992.
- (13) de Figueiredo, D. R.; Reboleira, A. S. S. P.; Antunes, S. C.; Abrantes, N.; Azeiteiro, U.; Gonçalves, F.; Pereira, M. J. The effect of environmental parameters and cyanobacterial blooms on phytoplankton dynamics of a Portuguese temperate lake. *Hydrobiologia* **2006**, *568*, 145–157. DOI: 10.1007/s10750-006-0196-y.
- (14) Parszuto, K.; Kaliszewska, E.A. The evaluation of the trophy of selected Olsztyn lakes by means of indices of particulate organic carbon (POC) and dissolved organic carbon (DOC). *Limnological Review* **2007**, *7* (2), 87–93.

- (15) Desmet, N. J. S.; Van Belleghem, S.; Seuntjens, P.; Bouma, T. J.; Buis, K.; Meire, P. Quantification of the impact of macrophytes on oxygen dynamics and nitrogen retention in a vegetated lowland river. *Phys. Chem. Earth* **2011**, *36*, 479–489; DOI: 10.1016/j.pce.2008.06.002.
- (16) Schwarzenbach, R. P.; Gschwend, P. M.; Imboden, D. M. *Environmental Organic Chemistry*; Wiley: New York, 1993.
- (17) Mackay, D. *Multimedia environmental models: the fugacity approach*. 2nd ed. Lewis Publishers: Boca Raton, 2001.
- (18) Morselli, M.; Semplice, M.; Villa, S.; Di Guardo, A. Evaluating the temporal variability of concentrations of POPs in a glacier-fed stream food chain using a combined modeling approach. *Sci. Total Environ.* **2014**, *493*, 571–579; DOI: 10.1016/j.scitotenv.2014.05.150.



## Chapter 6. Paper V

### Combined effects of intra- and interspecific interactions and pyrene on *Daphnia magna* populations

K. P. J. Viaene<sup>a,\*</sup>, F. De Laender<sup>b</sup>, A. Rico<sup>c,d</sup>, P.J. Van den Brink<sup>c,d</sup>, Antonio Di Guardo<sup>e</sup>, Melissa Morselli<sup>e</sup>, C. R. Janssen<sup>a</sup>

<sup>a</sup>Ghent University (UGent), Laboratory of Environmental Toxicology and Aquatic Ecology, Environmental Toxicology Unit (GhEnToxLab), Plateaustraat 22, 9000 Ghent, Belgium. Tel: +32 (0) 9 264 3779; Fax: +32 (0) 9 264 4199. karel.viaene@ugent.be; colin.janssen@ugent.be.

<sup>b</sup>Namur University, Research Unit in Environmental and Evolutionary Ecology, Rue de Bruxelles 61, 5000 Namur, Belgium. frederik.delaender@unamur.be;

<sup>c</sup>Department of Aquatic Ecology and Water Quality Management, Wageningen University, Wageningen University and Research centre, P.O. Box 47, 6700 AA Wageningen, The Netherlands. Tel: +31-317-481615, Fax: 419000. andreu.rico@wur.nl; paul.vandenbrink@wur.nl.

<sup>d</sup>Alterra, Wageningen University and Research centre, P.O. Box 47, 6700 AA Wageningen, The Netherlands. paul.vandenbrink@wur.nl.

<sup>e</sup>Department of Science and High Technology, University of Insubria, via Valleggio 11, 22100 Como, Italy. antonio.diguardo@uninsubria.it; melissa.morselli@uninsubria.it.

\*Corresponding author

*Submitted to Environmental Toxicology and Chemistry*



## **Abstract**

Species interactions are often suggested as an important factor when assessing the effects of chemicals on higher levels of biological organisation. Nevertheless, the contribution of intraspecific (competition) and interspecific interactions (competition and predation) to chemical effects on populations is often overlooked. In the current study, *Daphnia magna* populations were initiated with different levels of intra- and interspecific competition and predation and exposed to two pyrene pulses. Generalized linear models were used to test which of these factors significantly explained population size and structure at different time points. Pyrene had a negative effect on total population densities, with effects being more pronounced on smaller *D. magna* individuals. Among all species interactions tested, predation had the largest negative effect on population densities. Predation and high initial intraspecific competition were shown to interact antagonistically with pyrene exposure. This was attributed to differences in population structure prior to pyrene exposure and pyrene-induced reduced feeding by *Chaoborus* sp. larvae. The current study provides empirical evidence that species interactions within and between populations can alter the response of aquatic populations to chemical exposure, suggesting complex interactions between the underlying mechanisms.

## **Keywords:**

Pyrene; species interactions; competition; predation; *Daphnia magna*

## 1. Introduction

Current procedures for the ecological risk assessment (ERA) of chemicals are generally based on the extrapolation of individual-level responses to the whole ecosystem and often fail to integrate a sufficient level of ecological realism (Chapman 2002; De Laender et al. 2008a; Schmitt-Jansen et al. 2008; SCHER 2013). In ecosystems, individuals exposed to a chemical are rarely isolated but interact with other individuals of the same and/or of other species. Despite being one of the key characteristics of ecosystems, interactions within and between species are rarely included in current prospective ERAs, especially for non-pesticidal chemicals (De Laender et al. 2008b; Schmitt-Jansen et al. 2008). Species interactions can alter the direct effects of a chemical on sensitive species (Hanazato 2001). Alternatively, by interacting with sensitive species, tolerant species can also be affected (positively or negatively) by a chemical, leading to indirect effects on more sensitive species (Hanazato 1998; Rohr and Crumrine 2005; De Hoop et al. 2013). It has been suggested that, at least for pesticides, indirect effects are more common and more complex than direct effects (Fleeger et al. 2003; Rohr et al. 2006). Interactions with other species can either increase or decrease the susceptibility of populations and communities to a chemical (Preston 2002; Fleeger et al. 2003). For example, the no observed effect concentration (NOEC) of prometryn for ciliates was more than two orders of magnitude lower in microcosms compared with a single-species toxicity test because of the sensitivity of their food source to prometryn (Liebig et al. 2008). Also, elimination of grazers by the fungicide carbendazim allowed certain phytoplankton species to increase in abundance (Van den Brink et al. 2000) and exposure to insecticides resulted in the development of anti-predator structures in daphnids, potentially reducing the effect of predation (Hanazato 2001). Accurately assessing species interactions is thus essential to perform ecologically realistic chemical risk assessments (De Laender et al. 2014).

Competition and predation are regarded as the most important species interactions when considering indirect effects of chemicals (Preston 2002). Interactions can occur between individuals of different

species (interspecific competition) but also within one population of the same species (intraspecific competition). Although some studies exist on the combined effects of interspecific competition and chemicals (Liess 2002; Foit et al. 2012), studies on how intraspecific competition affects the response of populations to chemical exposure are rather underrepresented in the ecotoxicological literature.

The objective of the current study was to investigate how initial differences in species interactions influence the response of aquatic invertebrate populations to chemical stress. To this end, *Daphnia magna* populations were initiated with different levels of intraspecific and interspecific competition and predation. After seven and fifteen days, pyrene was added as a chemical stressor. The combined effects of species interactions and chemical stress were assessed by analysing population size and structure at different time intervals using generalized linear models.

## **2. Materials and Methods**

### **Experimental design**

*D. magna* populations were exposed to six levels of species interactions (i.e. species interaction control, low and high intraspecific competition, low and high interspecific competition, and predation) and to five different pyrene exposure profiles (i.e. control, solvent control, and low, medium and high exposure; see Table 1). The experiment was performed in triplicate ( $n = 3$ ). Two additional replicates were added for the species interaction control treatment exposed to no pyrene or only solvent ( $n = 5$ ). The experiment was carried out in 94 glass vessels (1.5 L) filled with 0.5 L of fresh water RT medium (Tollrian 1993). The test vessels were randomly distributed within a water bath placed in a temperature-controlled room ( $20.8 \pm 1$  °C) and exposed to low artificial light conditions (1000-1500 lux). The experiment lasted for 29 days with an adaptation period of 7 days (day -7 until day 0). Pyrene was added twice, on day 0 and day 8. After the second pyrene addition, population densities were monitored for another 14 days until day 22. The *D. magna* organisms used

in the experiment were obtained from the laboratory culture of the department of Aquatic Ecology and Water Quality Management from Wageningen University (The Netherlands). *Scenedesmus obliquus* was used as a food source for the *D. magna* cultures prior to the experiment and throughout the course of the experiment. Test vessels were fed six times a week with *S. obliquus* ( $1 \text{ mg carbon} \cdot \text{L}^{-1} \cdot \text{day}^{-1}$ ). The rotifer *Brachionus calyciflorus*, which also feeds on *S. obliquus*, is expected to compete with *D. magna* for food and was used to simulate interspecific competition. *B. calyciflorus* cysts were obtained from MicroBioTest Inc.<sup>©</sup> (Gent, Belgium) and a stock culture was set up in RT medium at 20°C. *Chaoborus* sp. larvae, which were added to simulate predation, were collected from unpolluted mesocosms at ‘de Sinderhoeve’ research station ([www.sinderhoeve.org](http://www.sinderhoeve.org), Renkum, The Netherlands).

Identical *D. magna* population structures were introduced in all test vessels. They were composed of 20% adults, 40% subadults and 40% juveniles. The classification of *D. magna* organisms within these three groups was based on size, and was performed by filtering the culture medium through sieves with different mesh sizes (i.e., adults > 800  $\mu\text{m}$ ; subadults between 800 and 500  $\mu\text{m}$ ; and juveniles < 500  $\mu\text{m}$ ). By using populations composed of different life stages, we wanted to simulate realistic population structures and also to study the sensitivity of different life stages and its implications for the *D. magna* population dynamics. To study the effect of intraspecific competition on *D. magna* populations, initial densities of 10 (species interaction control), 20 (low intraspecific competition) and 40 (high intraspecific competition) *D. magna* individuals per test vessel were used. To study how interspecific competition affects the *D. magna* population, *B. calyciflorus* was added to the test vessels at the start of the experiment in densities of approximately 333 rotifers  $\cdot \text{vessel}^{-1}$  (low interspecific competition) and 999 rotifers  $\cdot \text{vessel}^{-1}$  (high interspecific competition). Predation was imposed by the addition of one *Chaoborus* sp. larva per test vessel 3 days after the addition of daphnids to the test vessels. When a *Chaoborus* sp. larva died during the experiment, it was replaced to assure continuous predation pressure.

Pyrene was chosen as model compound for this experiment because of its non-specific, narcotic mode of action. Acetonitrile was used as solvent for pyrene and, therefore, a solvent control was included in the experimental design (38 and 75 µg/L added for the first and second addition, respectively). A stock solution of 0.75 g/L pyrene was prepared in acetonitrile and stirred intensively before addition to the test vessels. Pyrene was applied twice to the test vessels. The first dosing was applied 7 days after the start of the experiment (day 0) at a nominal concentration of 7.5, 20 and 55 µg/L for the low, medium and high pyrene exposure profile, respectively. The second application was performed 15 days after the start of the experiment (day 8) with a nominal pyrene concentration of 15, 40 and 110 µg/L, corresponding to the low, medium and high pyrene exposure profile, respectively. Pyrene concentrations were chosen between the EC<sub>10</sub> and EC<sub>50</sub> values for immobilization. An EC<sub>50,immobilization</sub> value of 68 [44-106] µg/L values was estimated based on a 48 hours toxicity test with *D. magna* (OECD 2004; See SI Figure 1 for the concentration response curve). Using a similar protocol, no mortality effects were observed for *B. calyciflorus* and the *Chaoborus* sp. larvae at pyrene concentrations up to 150 µg/L.

### **Biological monitoring**

*D. magna* and *B. calyciflorus* abundances in the test vessels were monitored on day -4, 0, 2, 4, 7, 10, 15 and 22 after the start of the experiment. *D. magna* were counted and divided into the size classes adult, subadult and juvenile by filtering the test medium over sieves with mesh sizes of 800 µm, 500 µm and 200 µm, respectively. *B. calyciflorus* abundances in the test medium of the interspecific treatments were monitored by taking two 6 mL sub-samples per test vessel and counting swimming rotifers using an inverted microscope (magnification 10x).

### **Chemical analyses**

Samples for pyrene analysis were taken after the first pyrene application, before the second pyrene application and two, four and twelve days after the second pyrene application. Pyrene samples were

stored in the dark at -20 °C in glass tubes. The chemical analysis was performed with gas chromatography–mass spectrometry (Trace GC 2000 series, Thermoquest, DSQ, Finnigan/Thermoquest). An apolar Zebron ZB 5-ms column (Phenomenex) was used for the analysis, and extraction and elution were performed by solid-phase extraction according to the manufacturer's instructions (Waters and Phenomenex). An internal standard (fluoranthene-d<sub>10</sub>) at a concentration of 10-50 µg/L (depending on expected pyrene concentration) was used to control and correct for extraction losses. The method's recovery was always >75%. Immediately before injection of the sample, a recovery standard was also applied to control for the injection itself.

### **Fate model analysis**

A recently developed dynamic water-sediment organism model (EcoDyna; Morselli et al. 2014) was used to predict the temporal fate of pyrene during the experiments. The model was calibrated using the nominal water volume (500 mL) of the experiment and water-sediment interaction was minimized to simulate negligible exchange, given the lack of a sediment phase in the vessels used. In order to calculate potential algal uptake, a daily contribution of 1 mg carbon /L was assumed, while organism biomass was calculated taking into account worst case conditions (10 *Daphnia* individuals plus 1 *Chaoborus* larva at all times) respectively using Dumont et al., (1975) and Dumont and Balvay, (1979), respectively. Physical-chemical properties for pyrene were obtained from Mackay et al., (1992).

### **Statistical analyses**

All analyses were performed using the statistical software package R (R Core Team 2012). For each sampling time, generalized linear models (GLMs) were constructed. Total, adult, subadult and juvenile *D. magna* abundances were considered as response variables, allowing for the examination of population structure. The effect of intraspecific competition (control, low, high), interspecific competition (control, low, high) and predation (non-predation, and predation) was assessed by

constructing a GLM with the respective species interaction, pyrene exposure (control, low, medium, high) and their interaction as predictor variables.

GLMs were initially constructed assuming a Poisson distribution (Zuur et al. 2009) but this led to unsatisfactory model validation. We therefore opted to perform GLM analyses with a normal distribution on the  $\log_{10}$ -transformed *D. magna* abundance data. The solvent control treatment was not included in the GLM analysis as preliminary tests showed no significant differences between the control and the solvent control treatments. Backwards model selection was used, dropping predictor variables based on the Akaike's Information Criterion (AIC), hypothesis testing and model validation analysis (Zuur et al. 2009). As model validation analysis, we (1) inspected if patterns in the data were present using predicted versus observed plots, (2) inspected if patterns in the residuals were present using predictor versus residuals plots, and (3) we tested the normality of the residuals using QQ-plots (Zuur et al. 2009).

### **3. Results**

#### **Pyrene concentrations**

Measured pyrene concentrations in water were lower than expected from the nominal values (Figure 1). Nevertheless, there was a clear difference between the three pyrene exposure profiles at any given point in time. The EcoDyna model was used to simulate pyrene concentration variations in water. The model was run to fit actual water concentrations, and the importance of the main fluxes dominating the change in concentration with time after the spikes. The most important parameter contributing to pyrene disappearance from water was half-life (no distinction could be made between biotic and abiotic processes), which was estimated being 30 h, and the second was volatilization, which accounted for about 20 % of losses. Simulations confirmed that pyrene uptake in algae and animal biomass was negligible.

## Statistical analyses

The effects of the different explanatory variables and their interactions are discussed below. We only included the results for the total *D. magna* abundance, results for the size classes are included in the supporting information. Model validation plots are also included as Supporting Information. Independent of the explanatory variables, a clear trend in the model intercept value could be observed. There was an increase in the intercept until day 7, afterwards the intercept slowly decreased (Table 2-4). This trend reflects the population dynamics of *D. magna* as they are approaching carrying capacity (Figure 2).

## Effects of pyrene

The estimated direct effects of pyrene were almost identical between the different treatments of species interactions (Table 2-4). We will therefore only refer to Table 2 here. The first pyrene addition did not significantly affect *D. magna* population densities (Figure 2 and Table 2). However, the highest pyrene exposure did reduce total population densities seven days after the second pyrene addition (day 15). The description and discussion of the experiment results will therefore focus on the observed effects after the second pyrene addition. Effects of the medium and low pyrene exposure profiles on total *D. magna* abundance were absent or negligible (Table 2). The variance of the total population densities explained by pyrene exposure at day 15 was >45% (SI Table 1-3). Fourteen days after the second pyrene addition, *D. magna* populations were recovering (day 22): no differences in total population densities were observed between pyrene exposure profiles. However, at that time, the abundances of juveniles were higher in the high pyrene exposure profile compared to the control treatment (SI Table 6 and Figure 3). Also, the negative effect of high pyrene exposure on the abundances of adults persisted on day 22, although this effect was smaller compared to day 15 (SI Table 4). Although the total population densities had recovered, differences in population structure were thus still observed between pyrene treatments (Figure 2-3).

## Effect of competition and predation

During the first 9 days of the experiment, populations with a higher initial population density (and therefore a higher degree of intraspecific competition) remained more abundant but the effect decreased with time (Figure 4 and Table 2). The variance explained by intraspecific competition also decreased from 71% to 22% over this period (SI Table 1). A high initial density resulted in lower future population densities (starting from day 4), although this effect was limited (Table 2). The population with the lowest initial density (10 *Daphnia* per test vessel) reached the highest total *D. magna* abundance (135 individuals). The initial positive effect of a high initial density persisted longer for adult *D. magna* (until day 10; SI Table 4) compared to the other size classes (day 2 and -4 for subadult and juveniles, respectively; SI Table 5-6). High initial densities resulted in a higher and more constant proportion of adults in the second half of the experiment compared to low initial densities (Figure 3).

*B. calyciflorus* population densities decreased sharply after one week and *B. calyciflorus* completely disappeared by day 10 (SI Figure 14). Although *B. calyciflorus* disappeared, significant but limited differences were observed between population densities of the different interspecific competition treatments starting from day 4 until day 15 (Figure 5 and Table 3). At the end of the experimental period, differences in population density were no longer observed between the different degrees of interspecific competition. Abundances of adult *D. magna* were never negatively affected by interspecific competition during the whole experiment (SI Table 7) while abundances of subadult and juvenile individuals were (SI Table 8-9). The effect of interspecific competition on the abundance of juveniles was only significant up to day 10 because almost no juveniles were observed in either of the pyrene exposure treatments the following sample days.

Of all species interactions studied, predation had the largest negative effect on population densities (Figure 3, 6 and Table 4). Predation had a continuous negative effect on total *D. magna* abundance. The explained variance was always higher than 42%, except on day 15 when most variance was

explained by pyrene exposure (Table 4). Because *Chaoborus* sp. larvae were added 3 days after the start of the experiment, predation was not significant at day -4. A negative effect of predation was first observed for adults (at day 0) but the largest effects were observed for the abundances of juveniles and subadults (Figure 3 and SI Table 10-12).

### **Combined effects of pyrene and species interactions**

Significant interactions between pyrene and predation or between pyrene and competition were rare and most of the times changed inconsistently with increasing pyrene exposure. However, on day 15 the interaction between high pyrene exposure and predation and between high pyrene exposure and intraspecific competition positively affected the total *D. magna* abundance, suggesting antagonism between each of these two types of species interaction and chemical toxicity. The variance of the total abundance explained by these two interactions on day 15 was 8.4% and 16.8%, respectively (SI Table 1 and 3). These positive interactions indicated that the negative effect of high pyrene exposure was less pronounced when the population was already exposed to predation or had experienced high intraspecific competition at the start of the experiment.

## **4. Discussion**

### **Pyrene toxicity**

Pyrene has a narcotic mode of action (Di Toro et al. 2000). Phototoxicity of pyrene has been reported (Bellas et al. 2008) but was likely limited in our experimental setup because of the low light conditions (1000-1500 lux). In our study, short-term effects of pyrene were limited and the highest effects occurred 7 days after the second pyrene addition. It is unclear why the first pyrene addition had no observable effects on population densities. The highest concentration measured after the first pyrene addition (71 µg/L) was similar to the  $EC_{50,immobilization}$  determined in the toxicity test performed on juvenile *D. magna* prior to the experiments (68 µg/L).. However, even juvenile *D. magna* – often considered the most sensitive individuals (Muysen and Janssen 2007)- were not

affected by the first pyrene addition (SI Figure 10 and SI Table 6). The results of the pyrene toxicity test did thus not seem applicable to the current experiment. *D. magna* EC<sub>50</sub> values reported in the literature (29 - 55 µg/L in the dark; Nikkilä et al. 1999) were similar to the one found here. Only one study reported a LC<sub>50</sub> value of 136 µg/L (Brausch and Smith 2009). During the second pyrene addition, pyrene concentrations were roughly two times higher, leading to the observed mortality in the highest exposure profile.

It was unclear if the negative effects of pyrene on the abundances of adults after the second pyrene addition resulted from direct mortality or from a combination of direct mortality and reduced survival or growth of smaller life classes. Reduced survival and growth of smaller life classes would lead to a lower amount of individuals that grow to the adult size class over a given time period compared to treatments without pyrene exposure. The negative effect of pyrene was largest on abundances of subadults (SI Table 4-6). Adult *D. magna* were the only size class still affected by pyrene at the end of the experiment (SI Table 4). Reduced survival and growth of earlier life stages will reduce the number of subadults that reach the adult stage (Liess and Foit 2010). Possibly, the negative effect of pyrene on the abundances of adults was thus, at least partly, attributable to effects on earlier life stages. Juveniles were almost absent after the second pyrene addition, even in the control treatment (SI Figure 10), which explains the absence of significant pyrene effects for juveniles. Interestingly, abundances of juveniles were significantly higher on day 22 in the high pyrene exposure profile compared to the control treatment (Figure 3 and SI Table 6). As a result, total population densities were not significantly different between the different pyrene treatments at the end of the experiment (Table 2), leading to the conclusion that total population density recovered. However, it should be noted that the final *D. magna* populations in the high pyrene exposure profile, consisting mainly of juveniles, were probably more susceptible to new chemical stress events compared to those in the other pyrene treatments. This again illustrates that population

structure needs to be accounted for when assessing the response and recovery of a population to (chemical) stress (Stark et al. 2004; Foit et al. 2012).

### **Species interactions**

Of all species interactions studied, predation had the largest effect on total *D. magna* abundance. Effects were visible six days after the addition of *Chaoborus* sp. larvae (starting from day 2) and the highest effects were observed for the abundances of subadults and juveniles (Figure 3 and SI Table 10-12). This indicated a feeding preference: *Chaoborus* sp. larvae preferred to prey on smaller subadult and juvenile *D. magna* than on adult *D. magna*. Size selective feeding by *Chaoborus* sp. larvae has been observed before (Swift 1992). Surprisingly, however, the negative effect of predation was first significant for adults (on day 0) and not for subadults or juveniles. Abundances of subadults and juveniles were very low (subadults) or zero (juveniles) until day 0, so probably the *Chaoborus* larvae were forced to feed on the larger *D. magna* adults. At later time points, juveniles and subadults were more abundant and *Chaoborus* larvae fed on these size classes, leading to a reduced or absent effect of predation on adults. These data show that feeding preferences depend on the ecological context shaped by the prey's population structure.

It is difficult to assess the effects of interspecific competition for the full duration of the experiment because *B. calyciflorus* were reduced to low densities (<10%) after day 7 and completely disappeared after day 10 (SI Figure 14). The effects of interspecific competition on total population densities were therefore limited (Table 2). Posterior tests performed with the same conditions showed that even in the highest pyrene concentration, *B. calyciflorus* was able to survive for at least 24 days (SI Figure 15). The rotifers were thus outcompeted by *D. magna*, as previously observed in interaction experiments between *B. calyciflorus* and *D. pulex* without chemical stress (Gilbert 1985). Gilbert et al. (1985) observed limited to no effects of the competition with *B. calyciflorus* on population densities of *D. pulex*, similar to the results of the current study. Continuous competition

pressure from *B. calyciflorus* could however lead to different results and future efforts should focus on experimental designs promoting prolonged co-existence between these two zooplankton taxa.

Both intraspecific and interspecific competition seemed to result in effects on reproductive output. Negative effects of different initial densities on the abundances of juveniles and subadults were observed starting from day 2 while these were absent for adults (SI Table 4-6). Similarly, negative effects of interspecific competition were observed for subadults and juveniles from day 4 onward while adults were not affected (SI Table 7-9). High initial competition thus mainly affected early life stages at later time points, suggesting competition-induced effects on *D. magna* reproduction over direct competition effects. According to the dynamic energy budget (DEB) theory, the competition with *B. calyciflorus* or other *D. magna* individuals could reduce the amount of energy that could be allocated to reproduction, resulting in less offspring (Kooijman 1986). However, it is probable that direct competition, through starvation, also contributed to the results. Young *D. magna* life stages are more prone to starvation compared to adults (Preuss et al. 2009; Martin et al. 2013). Under high competition conditions, less food is available per capita, possibly leading to starvation of smaller individuals and contributing to the lower proportion of young life stages in the population.

### **Reduced effect of pyrene when combined with predation and competition**

On day 15, when the pyrene effect was largest, predation and intraspecific competition reduced the negative effect of pyrene on population densities (Figure 3). Contrary to the antagonism observed in the current study, synergism between species interactions and chemical stress is often observed. Synergistic effects between predation and chemical stress have been shown for a wide range of organisms e.g. *Artemia* (Beketov and Liess 2006), amphibians (Relyea 2004) and mayflies (Schulz and Dabrowski 2001). The combination of predation by *Notonecta maculata* and exposure to nonylphenol led to loss of resilience in *Daphnia magna* populations (Gergs et al. 2013). Synergistic effects of competition and chemical stress have been reported for *D. magna* (Foit et al. 2012) and other *Daphnia* species (Knillmann et al. 2012a, 2012b). Although synergistic effects have been

reported most frequently, empirical support exists for antagonistic effects as well. For example, exposure to predator kairomones led to antagonistic interactions with carbaryl exposure on reproduction of *Daphnia magna* (Coors and Meester 2008). This was attributed to larger-sized and thus more tolerant offspring when predation cues were present. Two mechanisms are proposed to explain the antagonism we observe in the current study: differences in population structure and pyrene-induced alterations in species interactions. First, the structure of the populations exposed to predation or to high intraspecific competition differed from that of the populations experiencing low intraspecific competition and populations not exposed to predation. On day 7, immediately before the second pyrene addition, a large negative effect of intraspecific competition and predation on the abundances of subadults and juveniles was observed while the abundances of adults were less affected (Figure 3, SI Table 4-6;10-12). Differences in sensitivity for different *D. magna* size classes have been shown before e.g. for four metals (Hoang and Klaine 2007) or carbaryl (Coors and Meester 2008). We argue that because of the lower proportion of small-sized and thus more sensitive life stages in populations with predation or high (initial) intraspecific competition, pyrene effects were smaller. Second, the feeding rate of *Chaoborus* sp. larvae was possibly inhibited by the pyrene exposure, leading to reduced predation losses. Indeed, the estimated effect of predation (Table 4) was lower on day 15. The effect of pyrene on the feeding rates of *Chaoborus* sp. larvae was not tested in the current study but chemicals have been shown to alter feeding behaviour of fish (Weis et al. 2001) and invertebrates (Maltby and Hills 2008).

Contrary to a similar study with *D. magna* populations exposed to fenvalerate (Liess and Foit 2010), we observed no prolonged dominance of smaller-sized organisms after chemical stress in the treatment with predation: after high pyrene exposure, the proportion of small individuals was higher in the populations not exposed to predation (Figure 3). These contradicting results can be explained by how predation was applied in the two studies. While Liess and Foit (2010) simulated predation by removing individuals non-selective on size, *Chaoborus* sp. larvae preferred to prey on smaller

individuals, leading to lower abundances of juveniles in the predation treatments at the end of the experiment. This highlights the complexity of assessing how ecological interactions alter the response of a population to chemical stress and the need for ecologically realistic tools (De Laender and Janssen 2013; Gabsi et al. 2014).

The current study is an example of how species interactions can lead to *a priori* unpredictable effects of chemicals. Predation and intraspecific competition were shown to interact antagonistically with pyrene. The current study also highlights the need to not only consider the effects of a chemical on population density but also on population structure when assessing the risk of chemicals for populations and communities. Alternative, ecologically more realistic approaches such as mechanistic ecological models (De Laender et al. 2008a, 2013; Galic et al. 2010) could be used to integrate species interactions while assessing the long-term ecological risk of a chemical. In addition, such models could help to infer what processes contribute most to the patterns observed in experimental studies.

## **5. Acknowledgements**

The Chimera project is financed by the Long Range Initiative of CEFIC ([www.cefic-lri.org](http://www.cefic-lri.org); project code: LRI-ECO19).

## References

- Beketov M a, Liess M. The influence of predation on the chronic response of *Artemia* sp. populations to a toxicant. *J Appl Ecol*. 2006;43(6):1069–74.
- Bellas J, Saco-Alvarez L, Nieto O, Beiras R. Ecotoxicological evaluation of polycyclic aromatic hydrocarbons using marine invertebrate embryo-larval bioassays. *Mar Pollut Bull*. 2008;57(6-12):493–502.
- Brausch JM, Smith PN. Development of resistance to cyfluthrin and naphthalene among *Daphnia magna*. *Ecotoxicology*. 2009;18(5):600–9.
- Van den Brink PJ, Hattink J, Bransen F, Donk E Van, Brock TCM. Impact of the fungicide carbendazim in freshwater microcosms. II. Zooplankton, primary producers and final conclusions. *Aquat Toxicol*. 2000;48(2-3):251–64.
- Chapman PM. Integrating toxicology and ecology: putting the “eco” into ecotoxicology. *Mar Pollut Bull*. 2002;44(1):7–15.
- Coors A, Meester L De. Synergistic, antagonistic and additive effects of multiple stressors: predation threat, parasitism and pesticide exposure in *Daphnia magna*. *J Appl Ecol*. 2008;45:1820–8.
- De Hoop L, De Troch M, Hendriks a J, De Laender F. Modeling toxic stress by atrazine in a marine consumer-resource system. *Environ Toxicol Chem*. 2013;32(5):1088–95.
- De Laender F, van den Brink PJ, Janssen CR, Di Guardo A. The ChimERA project: coupling mechanistic exposure and effect models into an integrated platform for ecological risk assessment. *Environ Sci Pollut Res Int*. 2014 Feb 16;
- De Laender F, Janssen CR. The ecosystem perspective in ecotoxicology as a way forward for the ecological risk assessment of chemicals. *Integr Environ Assess Manag*. 2013;9(3):e34–8.
- De Laender F, De Schamphelaere KAC, Vanrolleghem P a, Janssen CR. Validation of an ecosystem modelling approach as a tool for ecological effect assessments. *Chemosphere*. 2008a;71(3):529–45.
- De Laender F, De Schamphelaere KAC, Vanrolleghem PA, Janssen CR. Do we have to incorporate ecological interactions in the sensitivity assessment of ecosystems? An examination of a theoretical assumption underlying species sensitivity distribution models. *Environ Int*. 2008b;34(3):390–6.
- De Laender F, Van Sprang P, Janssen CR. A re-evaluation of fifteen years of european risk assessment using effect models. *Environ Toxicol Chem*. 2013;32(3):594–601.
- Dumont HJ, Balvay G. The dry weight estimate of *Chaoborus flavicans* (Meigen) as a function of length and instars. *Hydro*. 1979;64(2):139–45.
- Dumont HJ, Velde I, Dumont S. The dry weight estimate of biomass in a selection of Cladocera, Copepoda and Rotifera from the plankton, periphyton and benthos of continental waters. *Oecologia*. 1975;19(1):75–97.

- Fleeger JW, Carman KR, Nisbet RM. Indirect effects of contaminants in aquatic ecosystems. *Sci Total Environ.* 2003;317(1-3):207–33.
- Foit K, Kaske O, Liess M. Competition increases toxicant sensitivity and delays the recovery of two interacting populations. *Aquat Toxicol.* 2012;106-107:25–31.
- Gabsi F, Schäffer A, Preuss TG. Predicting the sensitivity of populations from individual exposure to chemicals: the role of ecological interactions. *Environ Toxicol Chem.* 2014;33(7):1449–57.
- Galic N, Hommen U, Baveco JMH, van den Brink PJ. Potential application of population models in the European ecological risk assessment of chemicals. II. Review of models and their potential to address environmental protection aims. *Integr Environ Assess Manag.* 2010;6(3):338–60.
- Gergs A, Zenker A, Grimm V, Preuss TG. Chemical and natural stressors combined: from cryptic effects to population extinction. *Sci Rep.* 2013;3(2036).
- Gilbert JJ. Competition between Rotifers and *Daphnia*. *Ecology.* 1985;66(6):1943–50.
- Hanazato T. Response of a zooplankton community to insecticide application in experimental ponds: a review and the implications of the effects of chemicals on the structure and functioning of freshwater communities. *Environ Pollut.* 1998;101:361–73.
- Hanazato T. Pesticide effects on freshwater zooplankton: an ecological perspective. *Environ Pollut.* 2001;112:1–10.
- Hoang TC, Klaine SJ. Influence of organism age on metal toxicity to *Daphnia magna*. *Environ Toxicol Chem.* 2007;26(6):1198–204.
- Knillmann S, Stampfli NC, Beketov M a, Liess M. Intraspecific competition increases toxicant effects in outdoor pond microcosms. *Ecotoxicology.* 2012a;21:1857–66.
- Knillmann S, Stampfli NC, Noskov Y a, Beketov M a, Liess M. Interspecific competition delays recovery of *Daphnia* spp. populations from pesticide stress. *Ecotoxicology.* 2012b;21:1039–49.
- Kooijman SALM. Energy budgets can explain body size relations. *J Theor Biol.* 1986;121(3):269–82.
- Liebig M, Schmidt G, Bontje D, Kooi BW, Streck G, Traunspurger W, et al. Direct and indirect effects of pollutants on algae and algivorous ciliates in an aquatic indoor microcosm. *Aquat Toxicol.* 2008;88(2):102–10.
- Liess M. Population response to toxicants is altered by intraspecific interaction. *Environ Toxicol Chem.* 2002;21(1):138–42.
- Liess M, Foit K. Intraspecific competition delays recovery of population structure. *Aquat Toxicol.* 2010;97(1):15–22.
- Mackay D, Shiu WY, Ma KC. *Illustrated Handbook of Physical chemical properties and environmental fate for organic chemicals.* Chelsea MI, USA: Lewis Publishers; 1992. p. 597.

- Maltby L, Hills L. Spray drift of pesticides and stream macroinvertebrates: experimental evidence of impacts and effectiveness of mitigation measures. *Environ Pollut.* 2008;156(3):1112–20.
- Martin BT, Jager T, Nisbet RM, Preuss TG, Grimm V. Predicting population dynamics from the properties of individuals: a cross-level test of dynamic energy budget theory. *Am Nat.* 2013;181(4):506–19.
- Morselli M, Semplice M, Villa S, Di Guardo A. Evaluating the temporal variability of concentrations of POPs in a glacier-fed stream food chain using a combined modelling approach. *Sci Total Environ.* 2014;493:571-9.
- Muysen BTA, Janssen CR. Age and exposure duration as a factor influencing Cu and Zn toxicity toward *Daphnia magna*. *Ecotoxicol Environ Saf.* 2007;68(3):436–42.
- Nikkilä a, Penttinen S, Kukkonen J V. UV-B-Induced acute toxicity of pyrene to the waterflea *Daphnia magna* in natural freshwaters. *Ecotoxicol Environ Saf.* 1999;44(3):271–9.
- OECD. Test No. 202: *Daphnia* sp. Acute Immobilisation Test. OECD Guidel Test Chem Sect 2. OECD Publishing; 2004.
- Preston BL. Indirect Effects in Aquatic Ecotoxicology: Implications for Ecological Risk Assessment. *Environ Manage.* 2002;29(3):311–23.
- Preuss TG, Hammers-Wirtz M, Hommen U, Rubach MN, Ratte HT. Development and validation of an individual based *Daphnia magna* population model: The influence of crowding on population dynamics. *Ecol Modell.* 2009;220(3):310–29.
- R Core Team. R: A language and environment for statistical computing. Vienna, Austria: R Foundation for Statistical Computing; 2012.
- Relyea R a. Synergistic impacts of malathion and predatory stress on six species of North American tadpoles. *Environ Toxicol Chem.* 2004;23(4):1080–4.
- Rohr JR, Crumrine PW. Effects of an Herbicide and an Insecticide on Pond Community Structure and Processes. *Ecol Appl.* 2005;15(4):1135–47.
- Rohr JR, Kerby JL, Sih A. Community ecology as a framework for predicting contaminant effects. *Trends Ecol Evol.* 2006;21(11):606–13.
- SCHER, SCENIHR, SCCS. Addressing the New Challenges for Risk Assessment. 2013.
- Schmitt-Jansen M, Veit U, Dudel G, Altenburger R. An ecological perspective in aquatic ecotoxicology: Approaches and challenges. *Basic Appl Ecol.* 2008;9(4):337–45.
- Schulz R, Dabrowski JM. Combined effects of predatory fish and sublethal pesticide contamination on the behavior and mortality of mayfly nymphs. *Environ Toxicol Chem.* 2001;20(11):2537–43.
- Stark JD, Banks JE, Acheampong S. Estimating susceptibility of biological control agents to pesticides: influence of life history strategies and population structure. *Biol Control.* 2004;29(3):392–8.

- Swift MC. Prey capture by the four larval instars of *Chaoborus crystallinus*. *Limnol Oceanogr.* 1992;37(1):14–24.
- Tollrian R. Neckteeth formation in *Daphnia pulex* as an example of continuous phenotypic plasticity: morphological effects of *Chaoborus* kairomone concentration and their quantification. *J Plankton Res.* 1993; 15(11):1309–18.
- Di Toro DM, McGrath JA, Hansen DJ. Technical basis for narcotic chemicals and polycyclic aromatic hydrocarbon criteria. I. Water and Tissue. *Environ Toxicol Chem.* 2000;19(8):1951–70.
- Weis JS, Smith G, Zhou T, Santiago-Bass C, Weis P. Effects of Contaminants on Behavior: Biochemical Mechanisms and Ecological Consequences. *Bioscience.* 2001;51(3):209.
- Zuur AF, Elena NI, Walker NJ, Saveliev AA, Smith GM. Mixed effects models and extensions in ecology with R. Gail M, Krickeberg K, Samet JM, Tsiatis A, Wong W, editors. *Stat. Biol. Heal.* New York: Springer Science+Business Media; 2009.

## Tables

**Table 1. Overview of the different species interactions tested. The columns indicate how many of each species were added to the test vessels for the different species interaction treatments. Each of these treatments was exposed to five different pyrene exposure profiles: no pyrene, solvent control, low, medium and high pyrene exposure.**

Treatment	# <i>D. magna</i>	# <i>B. calyciflorus</i>	# <i>Chaoborus</i> sp. larvae
Control	10	0	0
Intraspecific competition: low	20	0	0
Intraspecific competition: high	40	0	0
Interspecific competition: low	10	333	0
Interspecific competition: high	10	999	0
Predation	10	0	1

**Table 2: GLM estimates of pyrene exposure and intraspecific competition for log10-transformed total *D. magna* abundance after backwards model selection. For each time point, the significant estimates of explanatory variables and their interactions are shown. Non-significant predictor variables are not shown (if never significant) or indicated with “/”.**

Time (days)	-4	0	2	4	7	10	15	22
(Intercept)	1.03	1.18	1.64	1.91	2.13	2.03	1.97	1.88
Low pyrene	/	/	/	/	-0.12	/	/	0.10
Medium pyrene	/	0.19	/	/	-0.09	/	/	/
High pyrene	/	/	/	/	/	-0.07	-0.56	/
Low intraspecific	0.26	0.22	/	-0.12	-0.17	-0.09	/	-0.07
High intraspecific	0.50	0.39	0.12	-0.11	-0.11	-0.13	/	-0.11
Low pyrene X Low intraspecific	/	/	/	/	0.17	/	/	/
Medium pyrene X High intraspecific	/	/	/	0.18	/	/	/	/
High pyrene X High intraspecific	/	/	/	/	/	/	0.30	/

**Table 3: GLM estimates of pyrene exposure and interspecific competition for log<sub>10</sub>-transformed total *D. magna* abundance after backwards model selection. For each time point, the significant estimates of explanatory variables and their interactions are shown. Non-significant predictor variables are not shown (if never significant) or indicated with “/”.**

<b>Time (days)</b>	<b>-4</b>	<b>0</b>	<b>2</b>	<b>4</b>	<b>7</b>	<b>10</b>	<b>15</b>	<b>22</b>
(Intercept)	1.06	1.20	1.70	1.90	2.13	2.02	1.97	1.88
Low pyrene	/	/	/	/	-0.12	/	/	/
Medium pyrene	/	0.17	/	/	/	/	/	/
High pyrene	/	/	/	/	/	-0.09	-0.63	/
Low interspecific	/	0.13	/	/	-0.15	-0.12	-0.11	/
High interspecific	/	/	/	-0.16	-0.24	-0.12	-0.13	/
Low pyrene X High interspecific	/	/	/	/	0.17	/	/	-0.18

**Table 4: GLM estimates of pyrene exposure and predation for log<sub>10</sub>-transformed total *D. magna* abundance after backwards model selection. For each time point, the significant estimates of explanatory variables and their interactions are shown. Non-significant predictor variables are not shown (if never significant) or indicated with “/”.**

<b>Time (days)</b>	<b>-4</b>	<b>0</b>	<b>2</b>	<b>4</b>	<b>7</b>	<b>10</b>	<b>15</b>	<b>22</b>
(Intercept)	1.07	1.27	1.69	1.90	2.08	2.01	1.97	1.88
High pyrene	/	/	/	/	/	/	-0.56	/
Predation	/	/	-0.32	-0.40	-0.38	-0.28	-0.25	-0.22
High pyrene X Predation	/	/	/	/	/	/	0.37	/

**Figures**

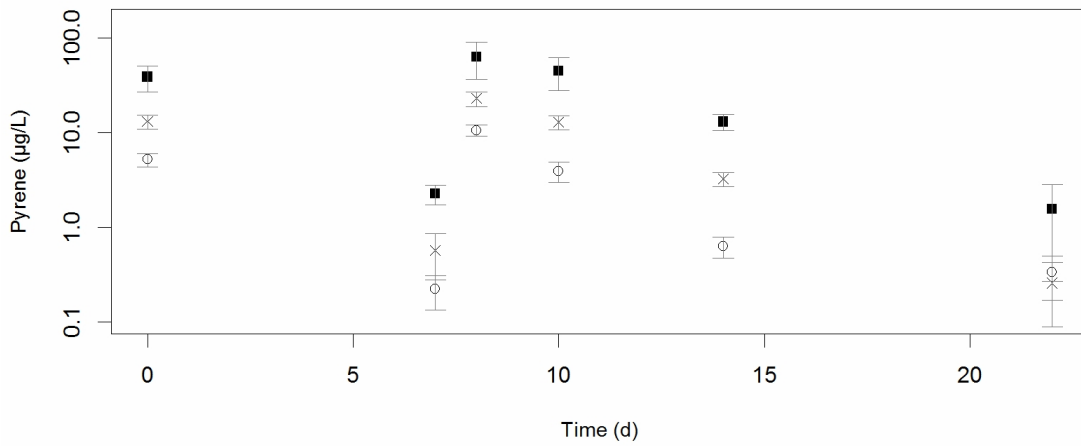


**Figure 1. Measured pyrene concentrations (µg/L) for the low (points), medium (crosses) and high (black squares) pyrene exposure. Average pyrene values with standard deviations (error bars) are depicted.**

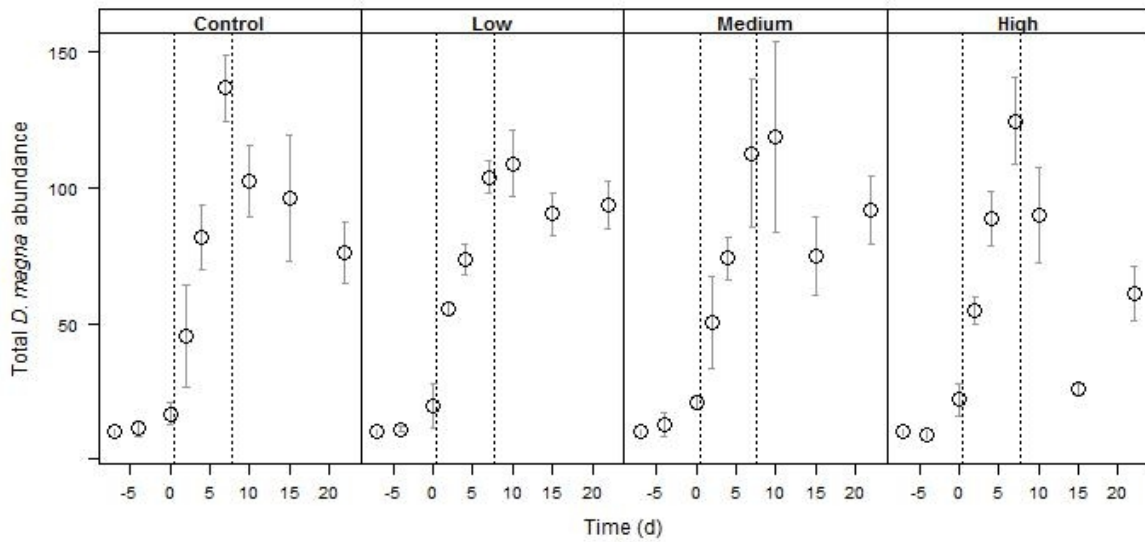


**Figure 2. Total *D. magna* abundances over time for four pyrene exposure profiles: control, low, medium and high pyrene exposure. Data shown are the *D. magna* population densities with no additional species interactions. Average values with standard deviations (error bars) are depicted. Dashed lines indicate the first and the second pyrene application.**

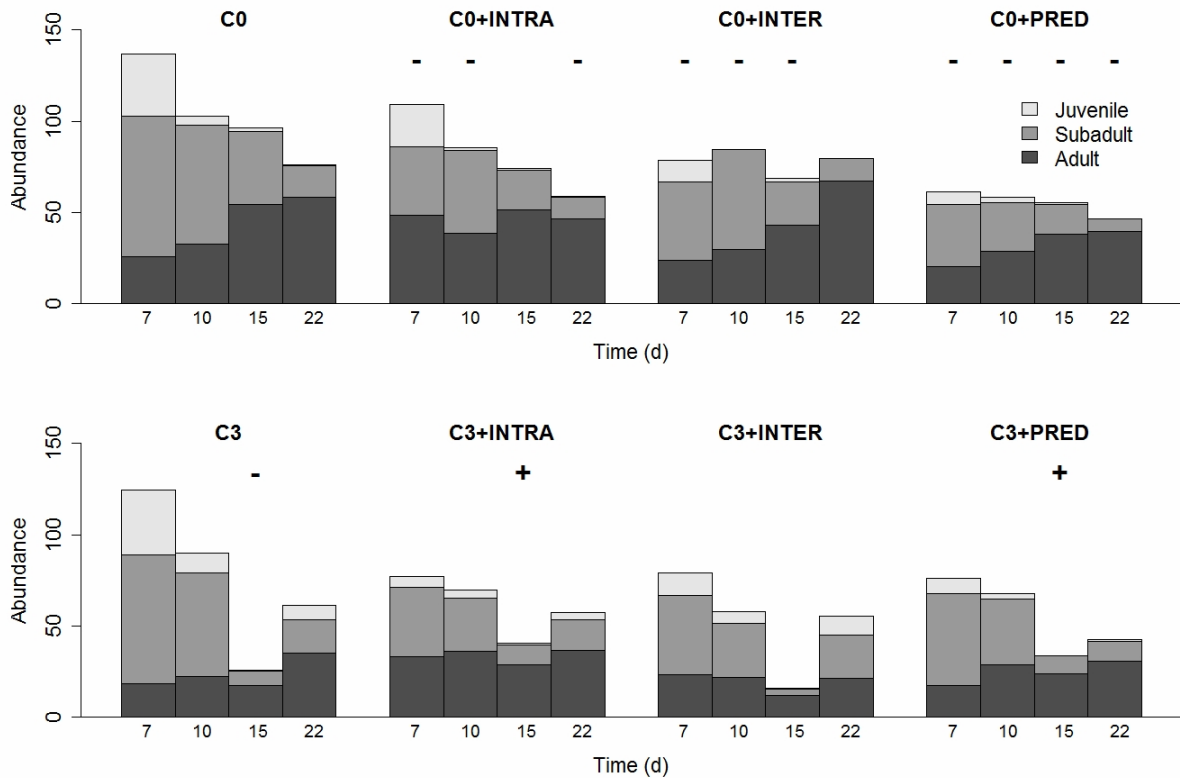


**Figure 3.** Average population structure of *D. magna* just before and after the second pyrene application (day 15) for different treatments. Data shown are the average abundances of adults (dark grey), subadults (medium grey) and juveniles (light grey) of the specific treatments. Error bars are not shown for clarity. “-“ and “+“ indicate a significant negative and positive effect, respectively, of that treatment or interaction of treatments on total population density, compared to the control treatment C0. C0 = no pyrene exposure; C3 = high pyrene exposure; INTRA = high intraspecific competition treatment; INTER = high interspecific competition treatment; PRED= predation treatment.

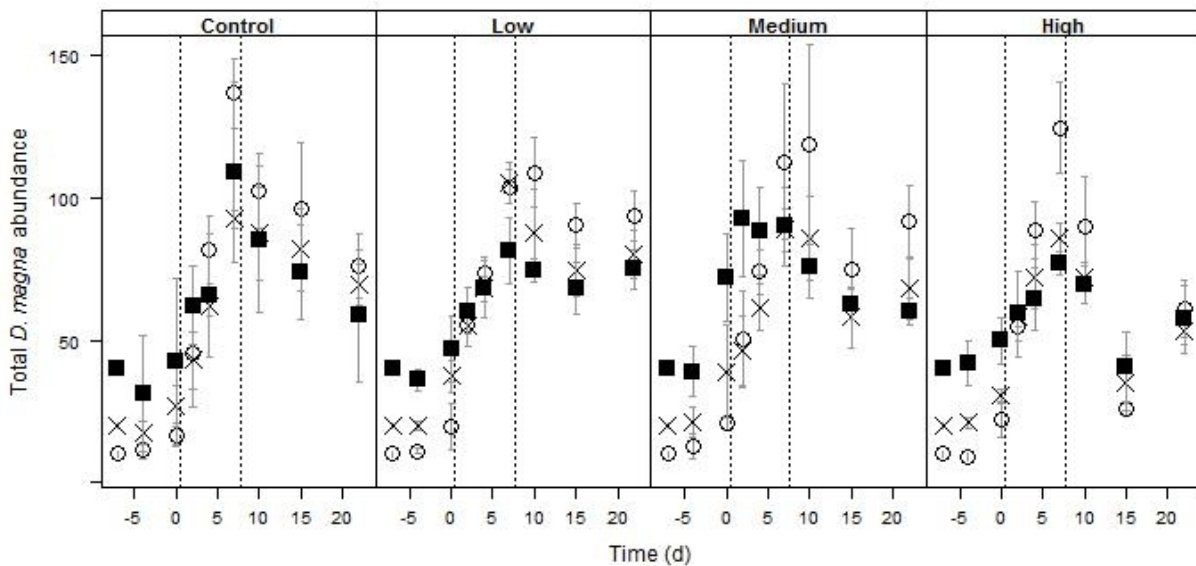


**Figure 4.** Total *D. magna* abundance over time for four pyrene exposure profiles: control, low, medium and high pyrene exposure. Data shown are the *D. magna* population densities for the treatment with no additional species interactions (points), low intraspecific competition (crosses) and high intraspecific competition (black squares). Average values with standard deviations (error bars) are depicted. Dashed lines indicate the first and the second pyrene application.

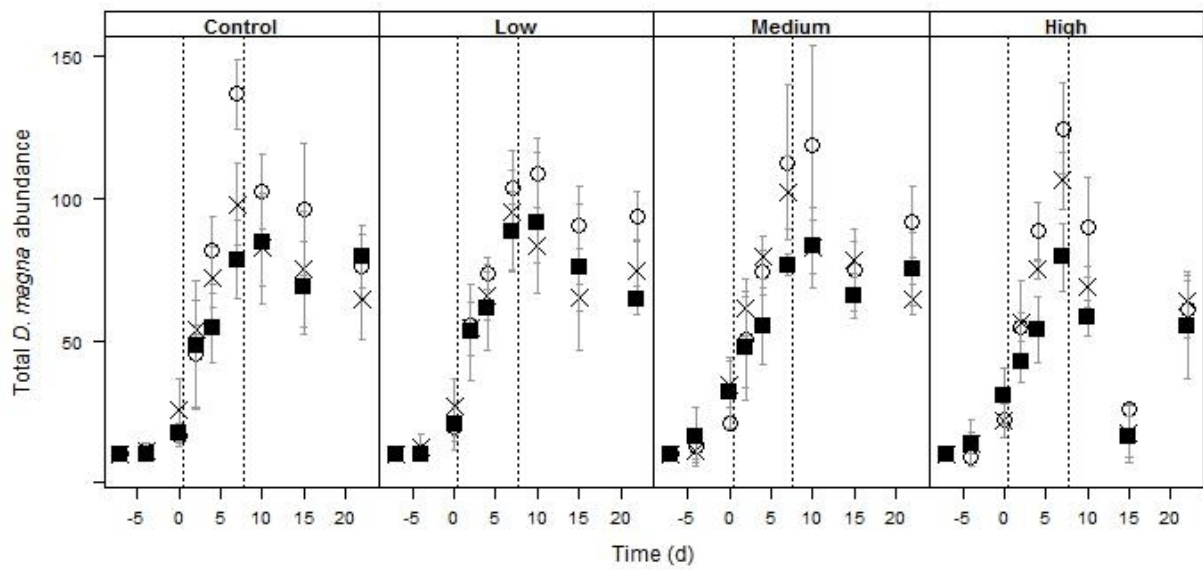


Figure 5. Total *D. magna* abundance over time for four pyrene exposure profiles: control, low, medium and high pyrene exposure. Data shown are the *D. magna* population densities for the treatment with no additional species interactions (points), low interspecific competition (crosses) and high interspecific competition (black squares). Average values with standard deviations (error bars) are depicted. Dashed lines indicate the first and the second pyrene application.

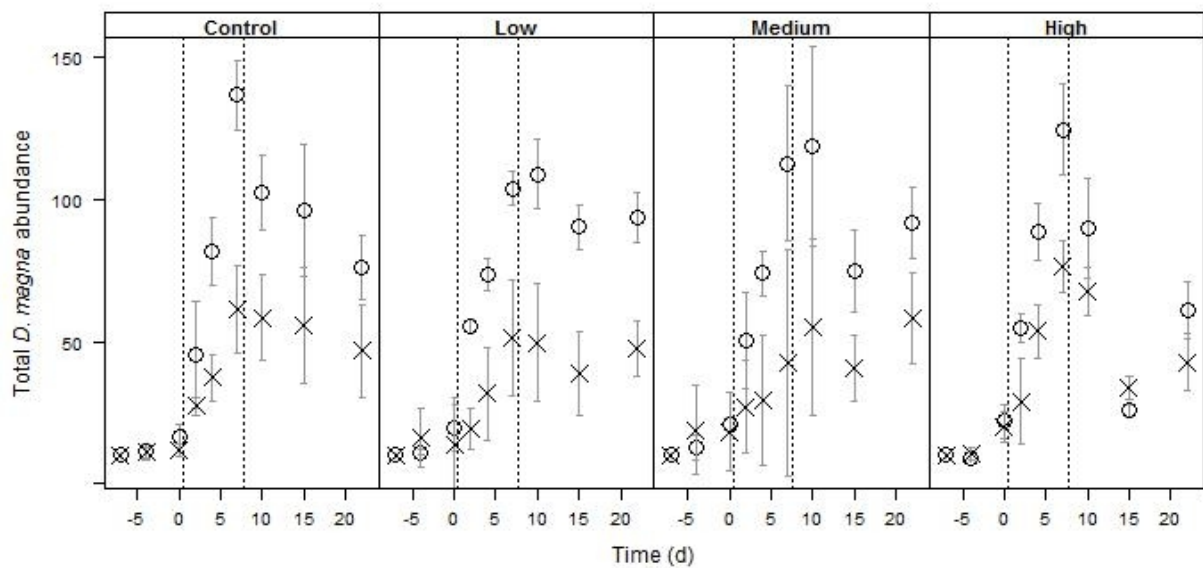


Figure 6. Total *D. magna* abundance over time for four pyrene exposure profiles: control, low, medium and high pyrene exposure. Data shown are the *D. magna* population densities for the treatment without (points) and with predation (crosses). Average values with standard deviations (error bars) are depicted. Dashed lines indicate the first and the second pyrene application.

## Chapter 6. Paper V

### Supporting information for

# Combined effects of intra- and interspecific interactions and pyrene on *Daphnia magna* populations

K. P. J. Viaene<sup>a,\*</sup>, F. De Laender<sup>b</sup>, A. Rico<sup>c,d</sup>, P.J. Van den Brink<sup>c,d</sup>, Antonio Di Guardo<sup>e</sup>, Melissa Morselli<sup>e</sup>, C. R. Janssen<sup>a</sup>

<sup>a</sup>Ghent University (UGent), Laboratory of Environmental Toxicology and Aquatic Ecology, Environmental Toxicology Unit (GhEnToxLab), Plateaustraat 22, 9000 Ghent, Belgium. Tel: +32 (0) 9 264 3779; Fax: +32 (0) 9 264 4199. karel.viaene@ugent.be; colin.janssen@ugent.be.

<sup>b</sup>Namur University, Research Unit in Environmental and Evolutionary Ecology, Rue de Bruxelles 61, 5000 Namur, Belgium. frederik.delaender@unamur.be;

<sup>c</sup>Department of Aquatic Ecology and Water Quality Management, Wageningen University, Wageningen University and Research centre, P.O. Box 47, 6700 AA Wageningen, The Netherlands. Tel: +31-317-481615, Fax: 419000. andreu.rico@wur.nl; paul.vandenbrink@wur.nl.

<sup>d</sup>Alterra, Wageningen University and Research centre, P.O. Box 47, 6700 AA Wageningen, The Netherlands. paul.vandenbrink@wur.nl.

<sup>e</sup>Department of Science and High Technology, University of Insubria, via Valleggio 11, 22100 Como, Italy. antonio.diguardo@uninsubria.it; melissa.morselli@uninsubria.it.

\*Corresponding author

*Submitted to Environmental Toxicology and Chemistry*



## Supporting Information for “The combined effects of intra- and interspecific interactions and pyrene on *Daphnia* populations”.

Authors: K. P. J. Viaene, F. De Laender, A. Rico, P.J. Van den Brink, C. R. Janssen

SI Table 1: Percentage of the total variance explained by pyrene exposure and intraspecific competition. Percentages shown are calculated for the optimal GLM for log<sub>10</sub>-transformed total *D. magna* abundance after backwards model selection on the intraspecific dataset. Non-significant predictor variables are indicated with “/”.

Time (days)	-4	0	2	4	7	10	15	22
Pyrene	/	13.7	10.4	2.1	16.6	12.3	75.4	32.1
Intraspecific	71.0	46.7	21.9	20.4	40.3	38.5	0.9	21.6
Pyrene X Intraspecific	/	/	/	23.2	13.9	/	8.4	/

SI Table 2: Percentage of the total variance explained by of pyrene exposure and interspecific competition. Percentages shown are calculated for the optimal GLM for log<sub>10</sub>-transformed total *D. magna* abundance after backwards model selection on the interspecific dataset. Non-significant predictor variables are indicated with “/”.

Time (days)	-4	0	2	4	7	10	15	22
Pyrene	/	19.5	/	/	5.1	23.1	81.3	24.0
Interspecific	/	12.0	/	51.8	55.8	32.1	4.0	14.0
Pyrene X Interspecific	/	/	/	/	9.6	/	/	18.2

SI Table 3: Percentage of the total variance explained by of pyrene exposure and predation. Percentages shown are calculated for the optimal GLM for log<sub>10</sub>-tra/formed total *D. magna* abundance after backwards model selection on the predation dataset. Non-significant predictor variables are indicated with “/”.

Time (days)	-4	0	2	4	7	10	15	22
Pyrene	/	/	/	/	/	/	45.1	13.3
Predation	/	11.4	51.8	42.4	46.8	54.6	19.5	55.0
Pyrene X Predation	/	/	/	/	/	/	16.8	/

SI Table 4: GLM estimates of pyrene exposure and intraspecific competition for log<sub>10</sub>-transformed adult *D. magna* abundance after backwards model selection. For each time point, the significant estimates of explanatory variables and their interactions are shown. Non-significant predictor variables are not shown (if never significant) or indicated with “/”.

Time (days)	-4	0	2	4	7	10	15	22
(Intercept)	0.57	1.02	1.11	1.22	1.40	1.48	1.69	1.73
Medium pyrene	/	/	/	/	/	0.10	/	/
High pyrene	0.12	/	/	/	-0.12	/	-0.37	-0.18
Low intraspecific	0.30	0.24	0.19	0.16	0.08	/	/	/
High intraspecific	0.46	0.41	0.37	0.32	0.25	0.08	/	/

**SI Table 5: GLM estimates of pyrene exposure and intraspecific competition for log10-transformed subadult *D. magna* abundance after backwards model selection. For each time point, the significant estimates of explanatory variables and their interactions are shown. Non-significant predictor variables are not shown (if never significant) or indicated with “/”.**

<b>Time (days)</b>	<b>-4</b>	<b>0</b>	<b>2</b>	<b>4</b>	<b>7</b>	<b>10</b>	<b>15</b>	<b>22</b>
(Intercept)	0.74	0.56	1.15	1.57	1.89	1.79	1.56	1.08
Low pyrene	/	/	/	/	-0.17	/	/	0.44
High pyrene	/	/	/	/	/	/	-0.70	/
Low intraspecific	0.22	/	/	/	-0.24	-0.14	/	/
High intraspecific	0.49	0.57	0.27	-0.21	-0.33	-0.28	/	/
Low pyrene X Low intraspecific	/	/	/	/	0.32	/	/	/
Medium pyrene X High intraspecific	/	/	/	0.28	/	/	/	-0.63

**SI Table 6: GLM estimates of pyrene exposure and intraspecific competition for log10-transformed juvenile *D. magna* abundance after backwards model selection. For each time point, the significant estimates of explanatory variables and their interactions are shown. Non-significant predictor variables are not shown (if never significant) or indicated with “/”.**

<b>Time (days)</b>	<b>-4</b>	<b>0</b>	<b>2</b>	<b>4</b>	<b>7</b>	<b>10</b>	<b>15</b>	<b>22</b>
(Intercept)	/	/	1.25	1.47	1.47	0.69	/	-0.52
Medium pyrene	/	0.79	/	/	/	0.32	/	/
High pyrene	/	0.87	/	/	/	0.33	/	1.03
Low intraspecific	0.51	/	/	-0.39	-0.34	/	/	/
High intraspecific	0.75	/	-0.71	-0.75	-0.61	-0.55	/	/
High pyrene X Low intraspecific	/	-1.37	/	/	/	/	/	/
High pyrene X High intraspecific	/	-1.02	/	/	/	/	/	/

**SI Table 7: GLM estimates of pyrene exposure and interspecific competition for log10-transformed adult *D. magna* abundance after backwards model selection. For each time point, the significant estimates of explanatory variables and their interactions are shown. Non-significant predictor variables are not shown (if never significant) or indicated with “/”.**

<b>Time (days)</b>	<b>-4</b>	<b>0</b>	<b>2</b>	<b>4</b>	<b>7</b>	<b>10</b>	<b>15</b>	<b>22</b>
(Intercept)	0.61	1.03	1.14	1.20	1.42	1.49	1.72	1.77
Medium pyrene	/	/	/	/	/	0.10	/	/
High pyrene	/	/	/	/	-0.09	-0.10	-0.57	-0.22
Low interspecific	/	/	/	0.13	/	/	/	/
High pyrene X High interspecific	/	/	/	/	/	/	/	-0.29

**SI Table 8: GLM estimates of pyrene exposure and interspecific competition for log10-transformed subadult *D. magna* abundance after backwards model selection. For each time point, the significant estimates of explanatory variables and their interactions are shown. Non-significant predictor variables are not shown (if never significant) or indicated with “/”.**

Time (days)	-4	0	2	4	7	10	15	22
(Intercept)	0.79	0.56	1.21	1.56	1.89	1.83	1.59	1.06
Low pyrene	/	/	/	/	-0.17	/	/	/
High pyrene	/	/	/	/	/	-0.14	-0.81	0.42
Low interspecific	/	0.35	/	/	/	-0.15	-0.32	-0.42
High interspecific	-0.35	0.32	/	-0.14	-0.27	-0.16	-0.23	/
Low pyrene X Low interspecific	/	/	/	/	0.22	/	/	/
Low pyrene X High interspecific	/	/	/	/	0.23	/	/	/
High pyrene X High interspecific	0.59	/	/	/	/	/	/	/

**SI Table 9: GLM estimates of pyrene exposure and interspecific competition for log10-transformed juvenile *D. magna* abundance after backwards model selection. For each time point, the significant estimates of explanatory variables and their interactions are shown. Non-significant predictor variables are not shown (if never significant) or indicated with “/”.**

Time (days)	-4	0	2	4	7	10	15	22
(Intercept)	-0.48	/	1.15	1.44	1.52	0.57	/	-0.81
Medium pyrene	0.56	/	/	/	/	0.56	/	/
High pyrene	/	/	/	/	/	/	/	1.79
Low interspecific	-0.59	/	/	-0.38	-0.49	/	/	/
High interspecific	/	/	/	-0.41	-0.57	-1.22	/	/
High pyrene X Low interspecific	/	-1.58	/	/	/	/	/	/
Low pyrene X High interspecific	/	/	/	/	/	1.21	/	/
High pyrene X High interspecific	/	/	/	-0.44	/	1.00	/	/

**SI Table 10: GLM estimates of pyrene exposure and predation for log10-transformed adult *D. magna* abundance after backwards model selection. For each time point, the significant estimates of explanatory variables and their interactions are shown. Non-significant predictor variables are not shown (if never significant) or indicated with “/”.**

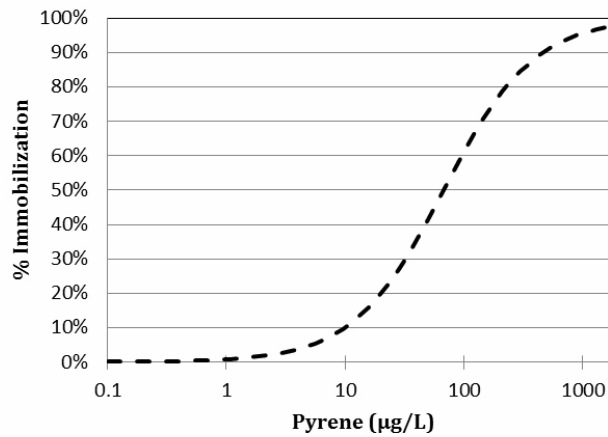
Time (days)	-4	0	2	4	7	10	15	22
(Intercept)	0.67	1.02	1.11	1.22	1.36	1.49	1.67	1.76
High pyrene	/	/	/	/	/	/	-0.36	-0.16
Predation	/	-0.20	-0.22	-0.22	-0.18	/	/	-0.16

**SI Table 11: GLM estimates of pyrene exposure and predation for log10-transformed subadult *D. magna* abundance after backwards model selection. For each time point, the significant estimates of explanatory variables and their interactions are shown. Non-significant predictor variables are not shown (if never significant) or indicated with “/”.**

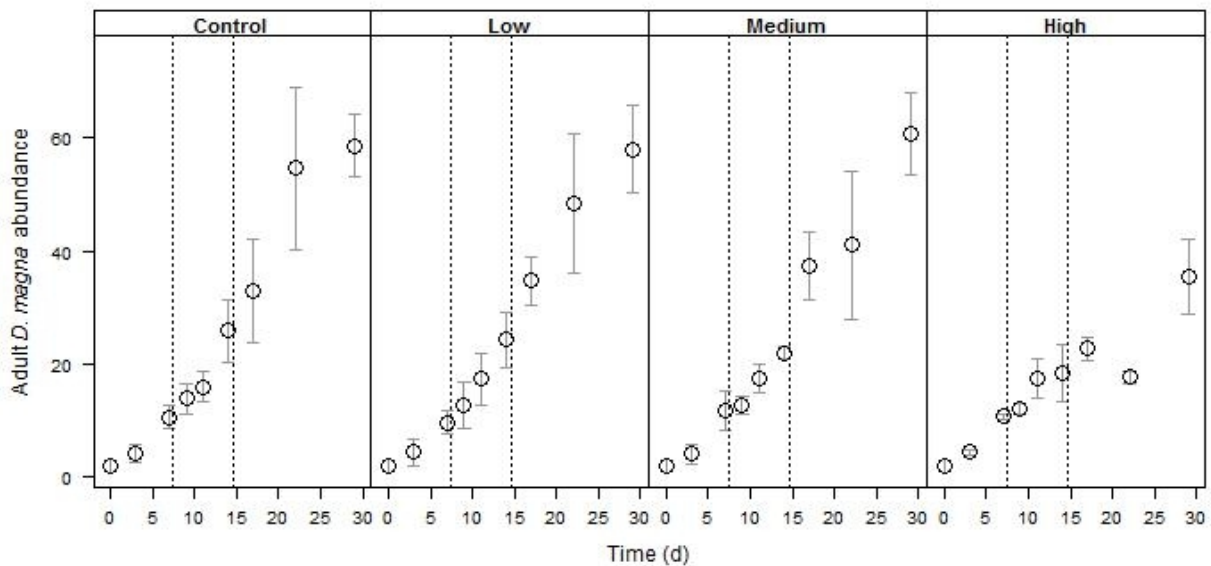
Time (days)	-4	0	2	4	7	10	15	22
(Intercept)	0.67	0.55	1.01	1.56	1.89	1.79	1.56	1.27
Medium pyrene	/	/	/	/	-0.28	/	/	/
High pyrene	/	/	/	/	/	/	-0.70	/
Predation	/	/	/	-0.34	-0.36	-0.37	-0.50	-0.33

SI Table 12: GLM estimates of pyrene exposure and predation for log10-transformed juvenile *D. magna* abundance after backwards model selection. For each time point, the significant estimates of explanatory variables and their interactions are shown. Non-significant predictor variables are not shown (if never significant) or indicated with “/”.

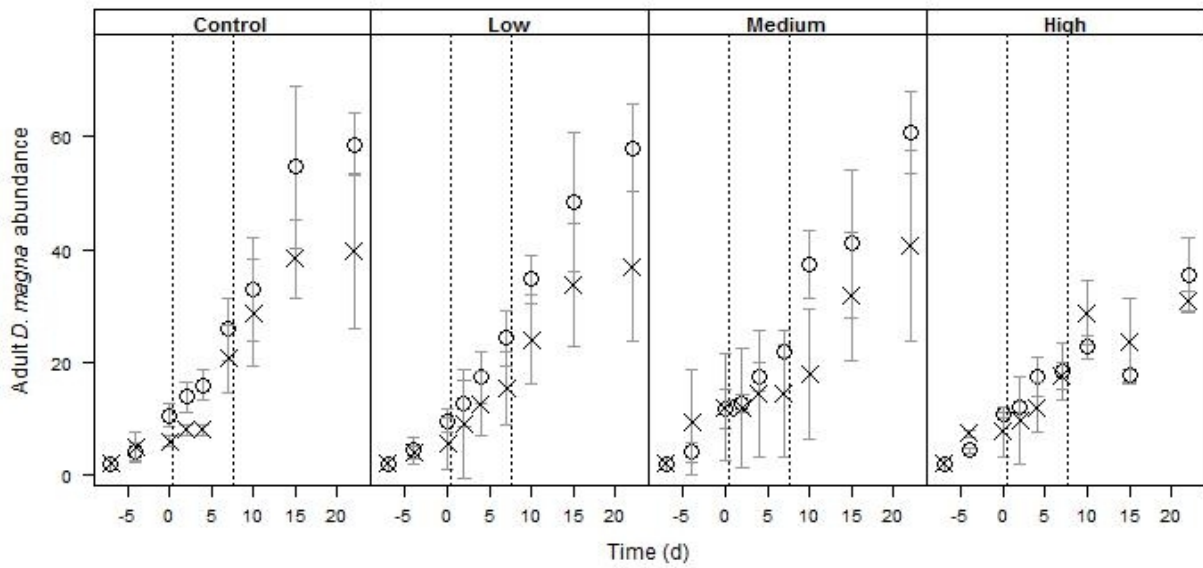
Time (days)	-4	0	2	4	7	10	15	22
(Intercept)	/	/	1.25	1.51	1.47	0.57	-0.42	-0.57
High pyrene	/	0.79	/	/	/	/	/	0.96
Predation	/	/	-0.67	-1.03	-0.80	/	/	/
Low pyrene X Predation	/	/	/	/	/	-1.07	/	/



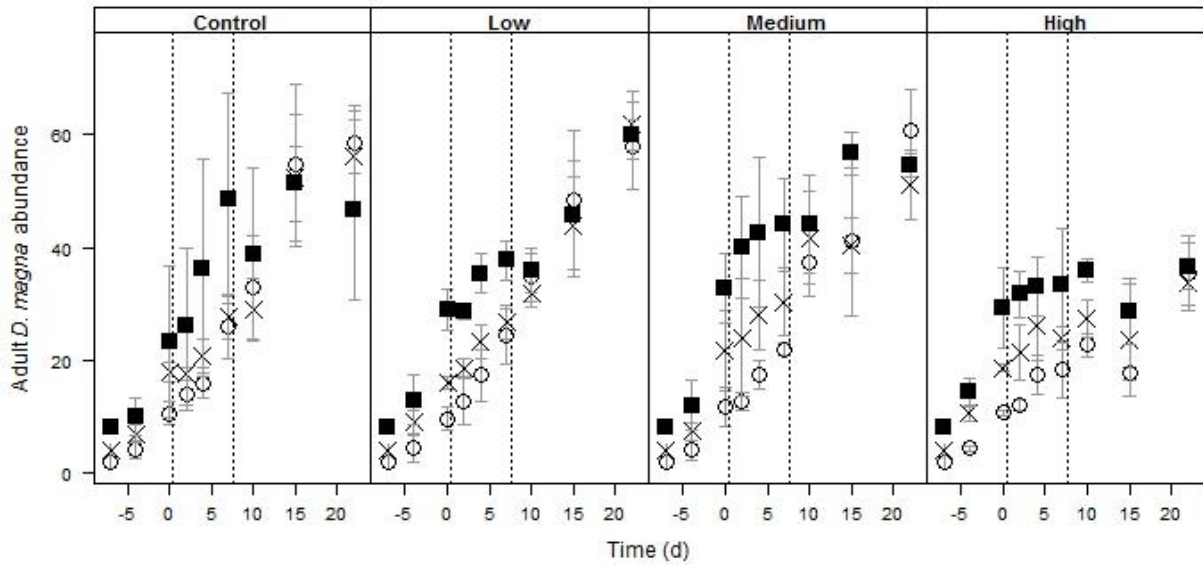
SI Figure 1: Concentration response curve for pyrene based on the results of a 48 hours test with *D. magna*.



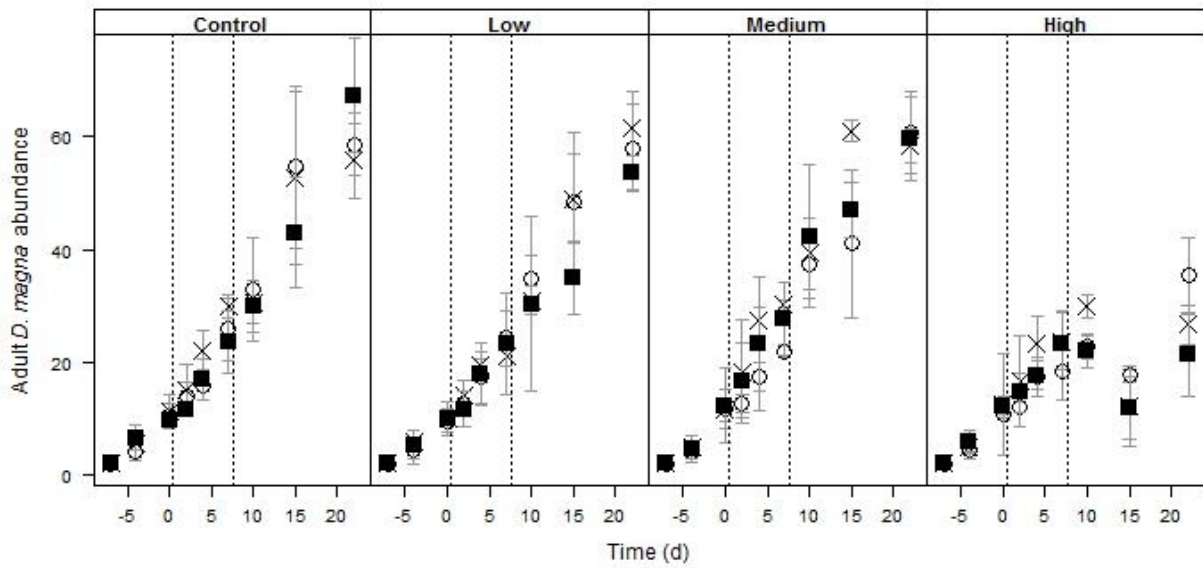
SI Figure 2. Adult *D. magna* abundance over time for four pyrene exposure profiles: control, low, medium and high pyrene exposure. Data shown are the adult *D. magna* abundances with no additional species interactions. Average values with standard deviations (error bars) are depicted. Dashed lines indicate the first and the second pyrene application.



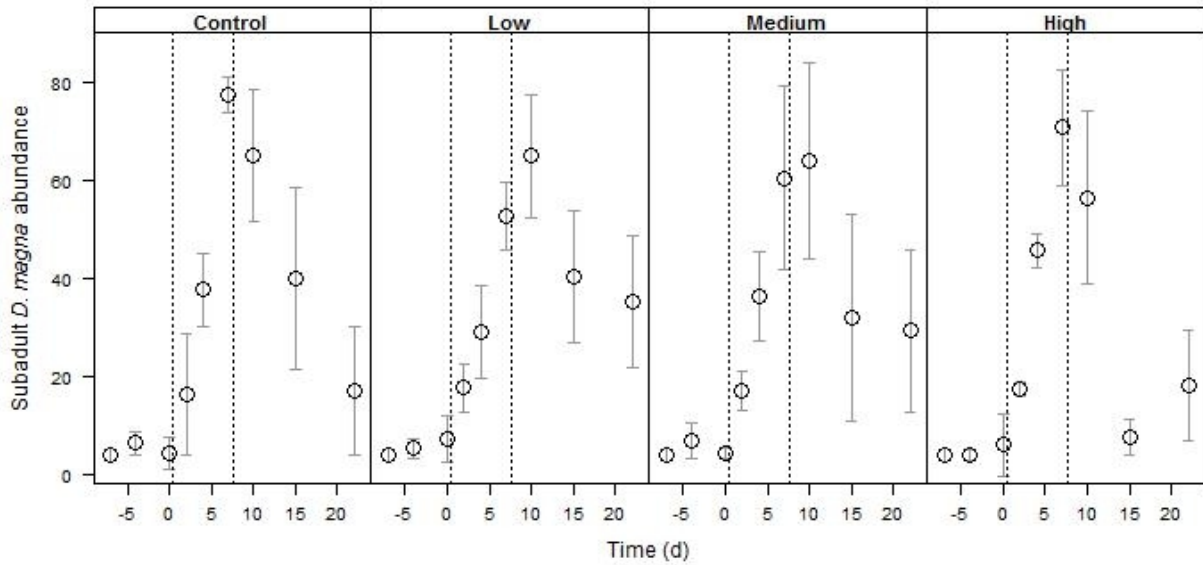
SI Figure 3. Adult *D. magna* abundance over time for four pyrene exposure profiles: control, low, medium and high pyrene exposure. Data shown are the treatments without (points) and with predation (crosses). Average values with standard deviations (error bars) are depicted. Dashed lines indicate the first and the second pyrene application.



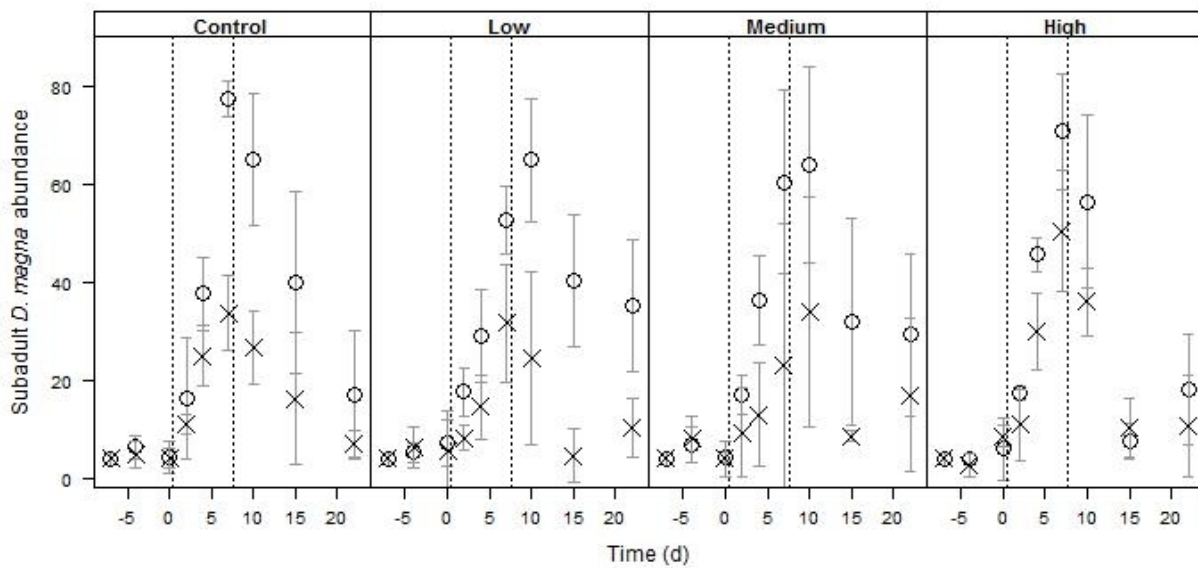
SI Figure 4. Adult *D. magna* abundance over time for four pyrene exposure profiles: control, low, medium and high pyrene exposure. Data shown are the treatments with no additional species interactions (points), low intraspecific competition (crosses) and high intraspecific competition (black squares). Average values with standard deviations (error bars) are depicted. Dashed lines indicate the first and the second pyrene application.



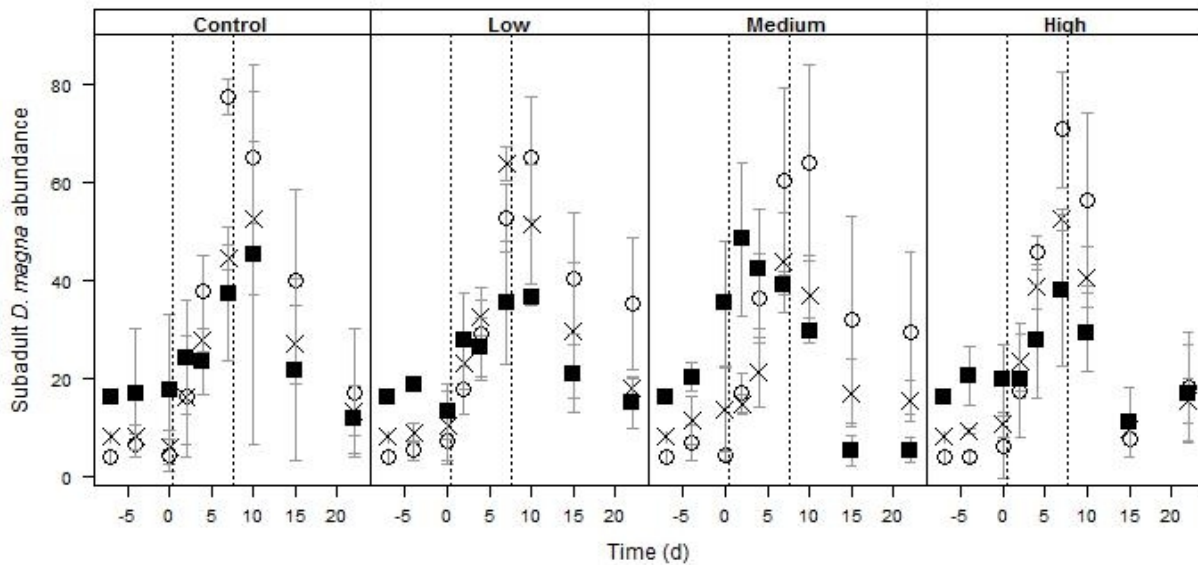
SI Figure 5. Adult *D. magna* abundance over time for four pyrene exposure profiles: control, low, medium and high pyrene exposure. Data shown are the treatments with no additional species interactions (points), low interspecific competition (crosses) and high interspecific competition (black squares). Average values with standard deviations (error bars) are depicted. Dashed lines indicate the first and the second pyrene application.



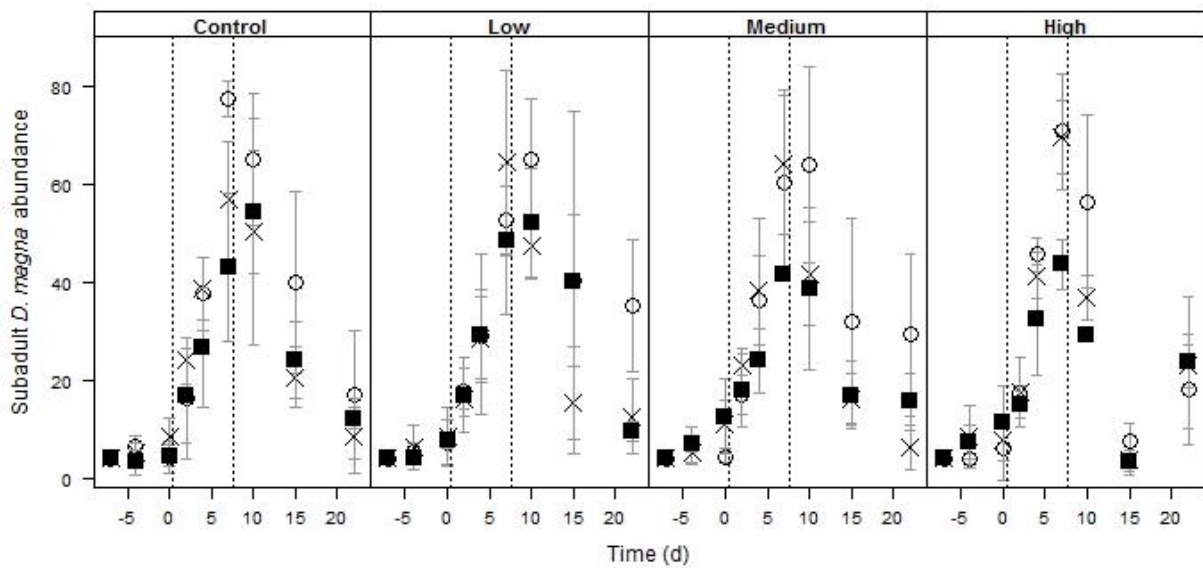
SI Figure 6. Subadult *D. magna* abundance over time for four pyrene exposure profiles: control, low, medium and high pyrene exposure. Data shown are the subadult *D. magna* abundances with no additional species interactions. Average values with standard deviations (error bars) are depicted. Dashed lines indicate the first and the second pyrene application.



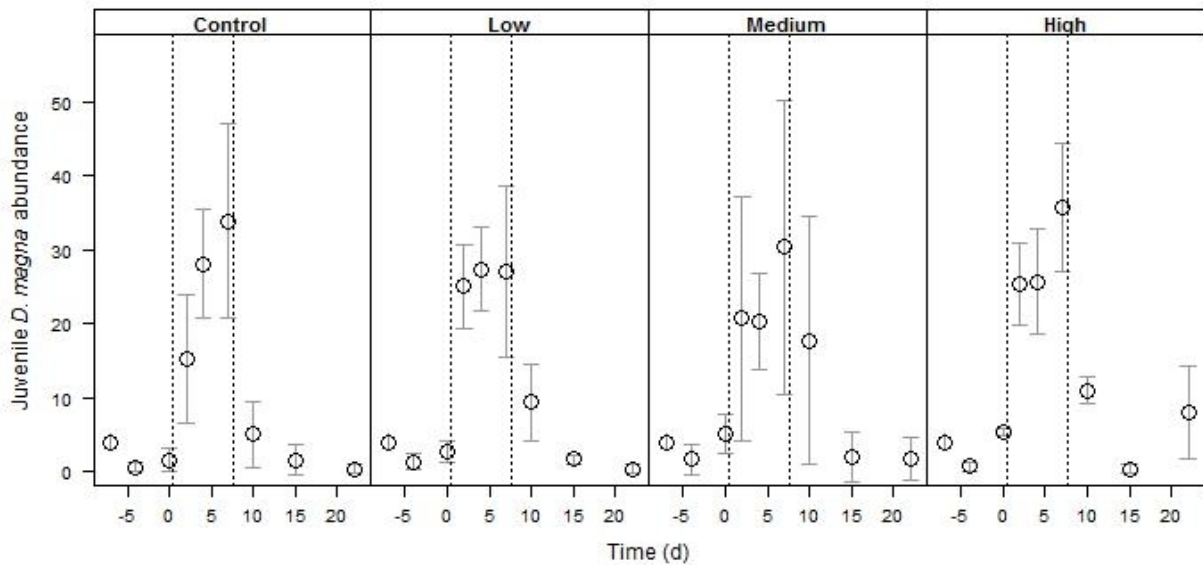
SI Figure 7. Subadult *D. magna* abundance over time for four pyrene exposure profiles: control, low, medium and high pyrene exposure. Data shown are the treatments without (points) and with predation (crosses). Average values with standard deviations (error bars) are depicted. Dashed lines indicate the first and the second pyrene application.



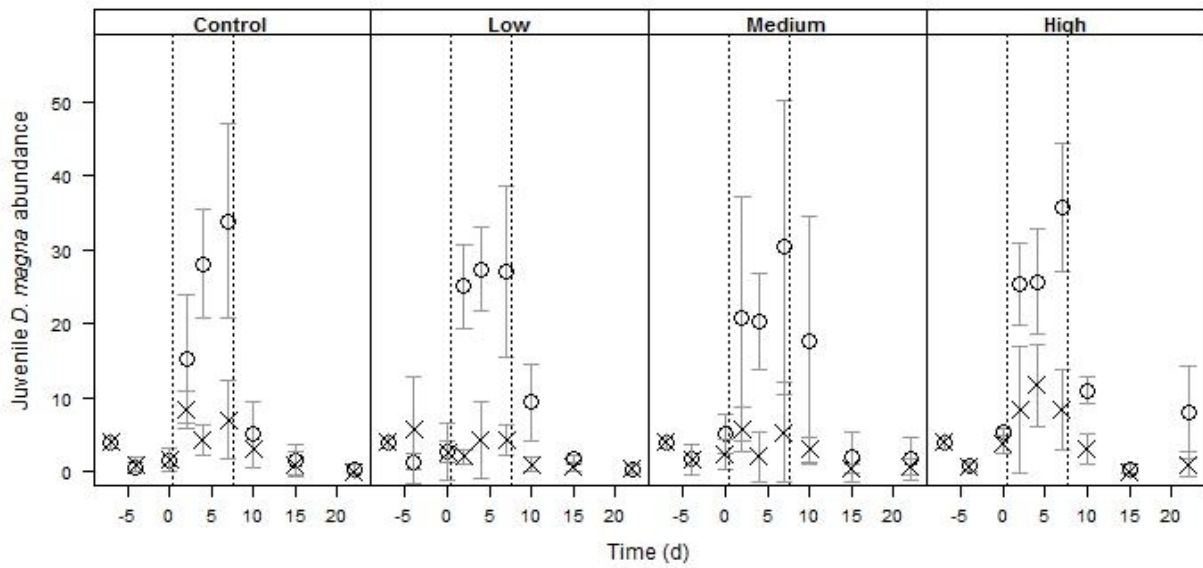
SI Figure 8. Subadult *D. magna* abundance over time for four pyrene exposure profiles: control, low, medium and high pyrene exposure. Data shown are the treatments with no additional species interactions (points), low intraspecific competition (crosses) and high intraspecific competition (black squares). Average values with standard deviations (error bars) are depicted. Dashed lines indicate the first and the second pyrene application.



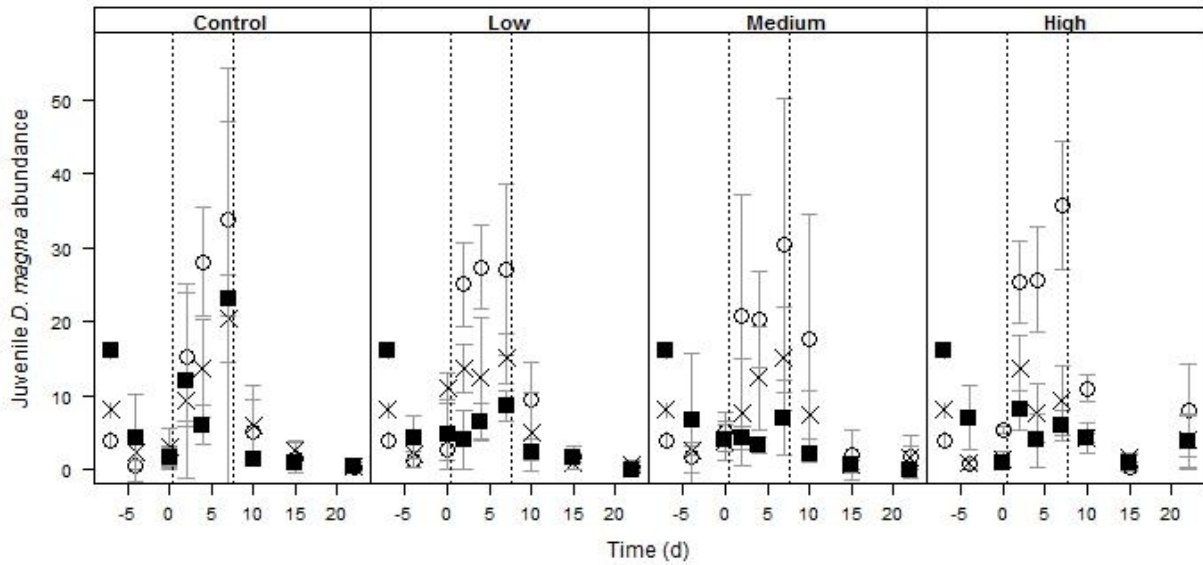
SI Figure 9. Subadult *D. magna* abundance over time for four pyrene exposure profiles: control, low, medium and high pyrene exposure. Data shown are the treatments with no additional species interactions (points), low interspecific competition (crosses) and high interspecific competition (black squares). Average values with standard deviations (error bars) are depicted. Dashed lines indicate the first and the second pyrene application.



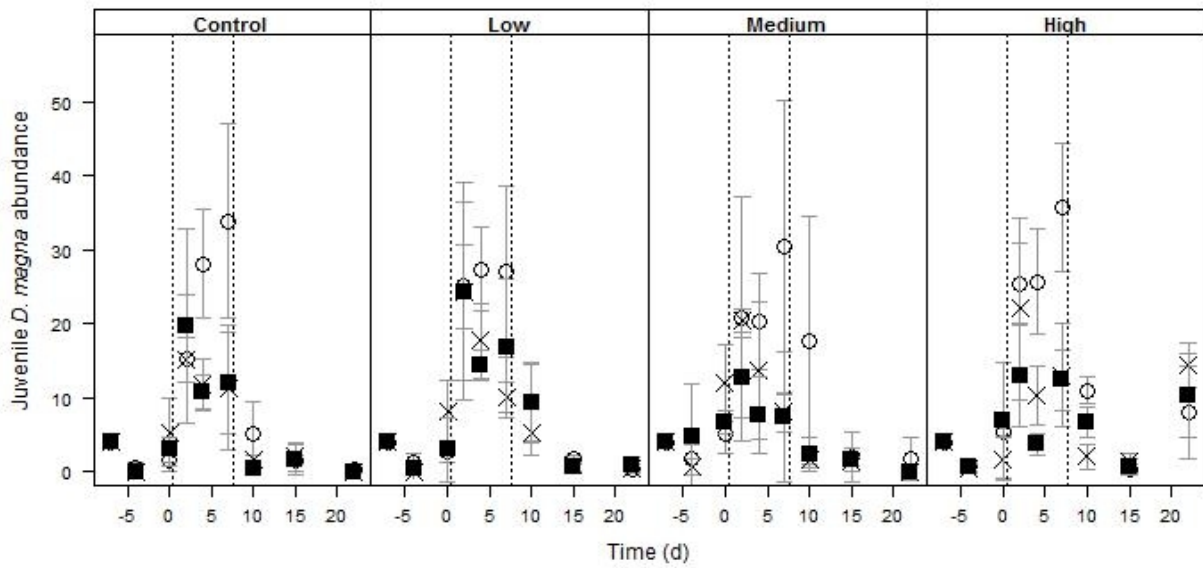
SI Figure 10. Juvenile *D. magna* abundance over time for four pyrene exposure profiles: control, low, medium and high pyrene exposure. Data shown are the juvenile *D. magna* abundances with no additional species interactions. Average values with standard deviations (error bars) are depicted. Dashed lines indicate the first and the second pyrene application.



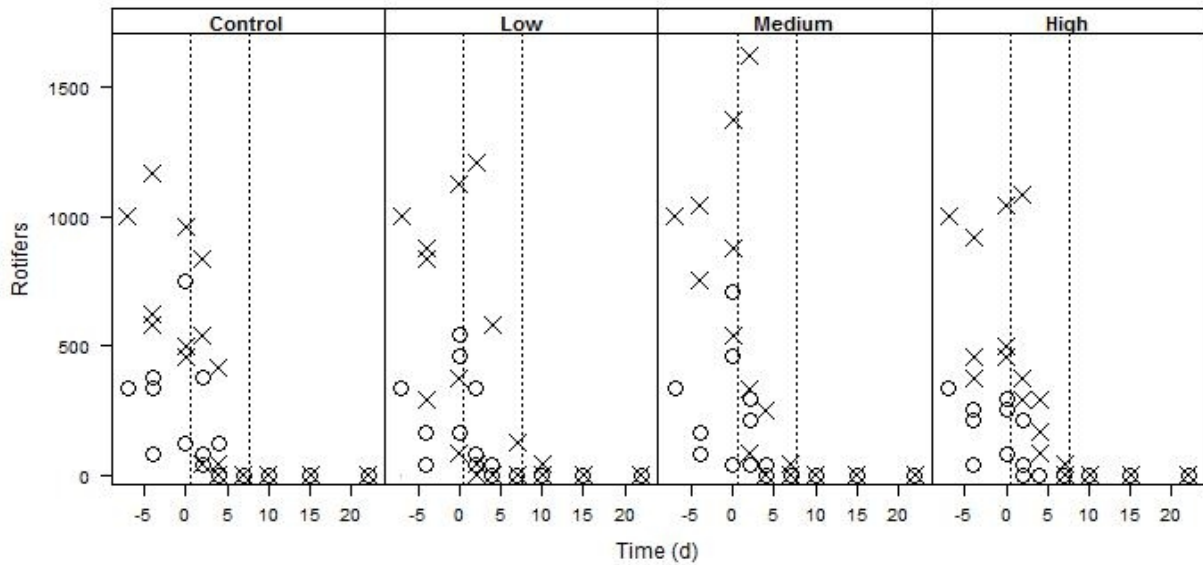
SI Figure 11. Juvenile *D. magna* abundance over time for four pyrene exposure profiles: control, low, medium and high pyrene exposure. Data shown are the treatments without (points) and with predation (crosses). Average values with standard deviations (error bars) are depicted. Dashed lines indicate the first and the second pyrene application.



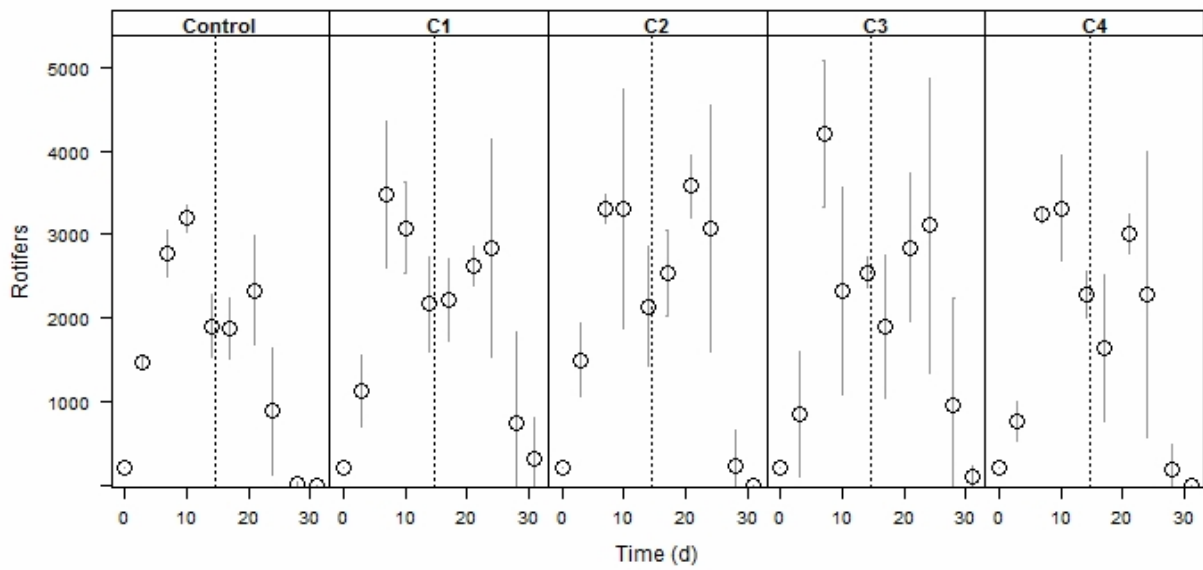
SI Figure 12. Juvenile *D. magna* abundance over time for four pyrene exposure profiles: control, low, medium and high pyrene exposure. Data shown are the treatments with no additional species interactions (points), low intraspecific competition (crosses) and high intraspecific competition (black squares). Average values with standard deviations (error bars) are depicted. Dashed lines indicate the first and the second pyrene application.



SI Figure 13. Juvenile *D. magna* abundance over time for four pyrene exposure profiles: control, low, medium and high pyrene exposure. Data shown are the treatments with no additional species interactions (points), low interspecific competition (crosses) and high interspecific competition (black squares). Average values with standard deviations (error bars) are depicted. Dashed lines indicate the first and the second pyrene application.



SI Figure 14. *B. calyciflorus* population sizes over time with *D. magna* present for four pyrene exposure profiles: control, low, medium and high pyrene exposure. Initial population sizes of 333 rotifers · vessel<sup>-1</sup> (points) and 999 rotifers · vessel<sup>-1</sup> (crosses) are shown. Average values are depicted. Dashed lines indicate first and the second pyrene application.



SI Figure 15. *B. calyciflorus* population sizes over time without *D. magna* for four pyrene exposure profiles: control, low, medium and high pyrene exposure. Initial population sizes of 333 rotifers · vessel<sup>-1</sup> (points) and 999 rotifers · vessel<sup>-1</sup> (crosses) are shown. Average values are depicted. Dashed lines indicate first and the second pyrene application.

### Model validation

The model validation plots were added as a separate zip archive. More details can be found in the word file supplied in the zip archive.



## Chapter 7. Paper VI

# Investigating the need for complex vs. simple scenarios to improve predictions of aquatic ecosystem exposure with the SoilPlus model

Davide Ghirardello<sup>a</sup>, Melissa Morselli<sup>a</sup>, Stefan Otto<sup>b</sup>, Giuseppe Zanin<sup>c</sup> and Antonio di Guardo<sup>a\*</sup>

<sup>a</sup>Environmental Modelling Group, Department of Science and High Technology, University of Insubria, Via Valleggio 11, 22100 Como, CO, Italy

<sup>b</sup>National Research Council (CNR), Institute of Agro-environmental and Forest Biology, Agripolis, Viale dell'Università 16, 35020 Legnaro, PD, Italy

<sup>c</sup>Department of Agronomy, Food, Natural Resources, Animals and Environment (DAFNAE), University of Padova, Agripolis, Viale dell'Università 16, 35020 Legnaro, PD, Italy

\*Corresponding author

*Environmental Pollution* **2014**, *184*, 502–510





## Investigating the need for complex vs. simple scenarios to improve predictions of aquatic ecosystem exposure with the SoilPlus model



Davide Ghirardello<sup>a</sup>, Melissa Morselli<sup>a</sup>, Stefan Otto<sup>b</sup>, Giuseppe Zanin<sup>c</sup>,  
Antonio Di Guardo<sup>a,\*</sup>

<sup>a</sup> Environmental Modelling Group, Department of Science and High Technology, University of Insubria, Via Valleggio 11, 22100 Como, CO, Italy

<sup>b</sup> National Research Council (CNR), Institute of Agro-environmental and Forest Biology, Agripolis, Viale dell'Università 16, 35020 Legnaro, PD, Italy

<sup>c</sup> Department of Agronomy, Food, Natural Resources, Animals and Environment (DAFNAE), University of Padova, Agripolis, Viale dell'Università 16, 35020 Legnaro, PD, Italy

### ARTICLE INFO

#### Article history:

Received 9 February 2013

Received in revised form

19 August 2013

Accepted 4 October 2013

#### Keywords:

Aquatic ecosystem exposure

DynA

Fugacity model

GIS

Sensitivity

SoilPlus

Spatial resolution

### ABSTRACT

A spatially-explicit version of the recent multimedia fate model SoilPlus was developed and applied to predict the runoff of three pesticides in a small agricultural watershed in north-eastern Italy. In order to evaluate model response to increasing spatial resolution, a tiered simulation approach was adopted, also using a dynamic model for surface water (DynA model), to predict the fate of pesticides in runoff water and sediment, and concentrations in river water. Simulation outputs were compared to water concentrations measured in the basin. Results showed that a high spatial resolution and scenario complexity improved model predictions of metolachlor and terbuthylazine in runoff to an acceptable performance ( $R^2 = 0.64$ – $0.70$ ). The importance was also shown of a field-based database of properties (i.e. soil texture and organic carbon, rainfall and water flow, pesticides half-life in soil) in reducing the distance between predicted and measured surface water concentrations and its relevance for risk assessment.

© 2013 Elsevier Ltd. All rights reserved.

### 1. Introduction

The problem of non-point source pollution together with the effects of pesticides on non-target organisms has been one of the most studied environmental issues for almost half-a-century (White et al., 1967), and the need to reduce the risk for non-target terrestrial and aquatic ecosystems is acknowledged in current European Legislation, under Directives 91/414/EC and 2009/128/EC (EC, 1991, 2009). In addition, the EU Water Framework Directive (EC, 2000) specifies that site-specific tools and indicators have to be developed for the management of river basins, in order to promote the protection of surface water ecosystems.

A number of models have been developed to predict soil and surface/ground water pesticides concentrations, like PRZM (Suarez, 2006) or PEARL (Leistra et al., 2000). These models generally treat the soil as a one-dimensional multi-layered compartment, but do not usually account for spatial interactions over a catchment. Instead, one such model is SWAT (Neitsch et al., 2005). While many

of these models can be applied at field level, when evaluating the potential pesticide contamination of surface water at a basin scale, the adoption of average (or prevalent) field properties in basin-wide (one large field scenario) simulations could produce misleading results. This is especially relevant when soil texture, organic carbon, crop, pesticide application etc., heterogeneity is high. To account for spatial variability, a Geographic Information System (GIS) can be coupled to fate models, in order to provide an adequate scenario description, without necessarily realizing a full integration of GIS and model. Barra et al. (2000) is an example of this approach, in which the SoilFug model (Di Guardo et al., 1994) was loosely coupled to a GIS to perform spatially-explicit simulations at a basin scale. More recently, the GeoPEARL model (Tiktak et al., 2003) and EuroPEARL model (Tiktak et al., 2006) were developed to evaluate the risk related to leaching in the Netherlands and Europe on a geographical basis. In another approach, the MACRO model (Jarvis, 1995) was coupled to GIS (Balderacchi et al., 2008) to evaluate the vulnerability of groundwater in the Marche Region, Italy. In addition, the PRZM model was linked to a GIS in California (Luo and Zhang, 2009, 2010) to predict runoff at a large watershed level and to evaluate the leaching of chemicals towards groundwater (Ali Akbar and Lin, 2010). A

\* Corresponding author.

E-mail address: [antonio.diguardo@uninsubria.it](mailto:antonio.diguardo@uninsubria.it) (A. Di Guardo).

relatively simpler procedure based on the approach by Gutsche and Rossberg (1999) was successfully applied on a small watershed to assess the fate of a number of pesticides (Bonzini et al., 2006). Models for runoff potential of stream sites by a spatially explicit calculation are also available at regional scale with a resolution of 10–50 km grid (Schriever and Liess, 2007). A multimedia fate model with spatial resolution, based on a geo-referenced environment in GIS, was also developed and applied to monitoring data of benzene, dioxins, and 1,3-butadiene in Japan (Suzuki et al., 2004). More recently, European wide approaches were published at high resolution (1 km or better) (Pistocchi, 2008; Pistocchi et al., 2010).

While there are many GIS-modelling approaches, a link between a site-specific soil model with layered soil and dynamic air compartments to a GIS capable of performing runoff simulations at catchment scale has not yet been developed. Such an approach could be relevant when evaluating the fate of a chemical in the soil/air at a basin scale, for example when evaluating the fate of pesticides applied to soil or vegetation in the air compartment (or an adjacent field) during application (drift) and after (volatilization from soil and vegetation surfaces and consequent deposition/precipitation). Another possible use is when the impact of sources adjacent to the basin are to be taken into account. An example of the impact of such sources is given in a recent study (Morselli et al., 2012), in which the integration of a physical dispersion model and fugacity-based air/soil model allowed the fate of polycyclic aromatic hydrocarbons in a complex emission scenario to be predicted. The need for enhancing the understanding of the temporal and spatial dynamics of ecosystem exposure within Ecological Risk Assessment procedures has recently been pointed out by Di Guardo and Hermens (2013). This is particularly relevant in order to increase the ecological realism of exposure prediction, for example evaluating the role of a complex environmental scenario in describing pulse exposure concentrations in surface waters receiving runoff from adjacent treated fields.

The aim of this study is to further develop and evaluate the spatially-explicit version of SoilPlus, a dynamic model of the fate of organic chemicals (Ghirardello et al., 2010), applied to a small agricultural catchment, as a case study, at three increasing levels of spatial resolution and complexity (Tier I to III). A full model-GIS integration was realized, which allows the model to directly interact with spatial data without the help of a separate GIS software. SoilPlus was used to calculate the runoff of three pesticides to the receiving ditches and river stretches, while a modified version of the DynA surface water model (Di Guardo et al., 2006) was used to simulate the fate in the hydrographic network of the River Meolo. Predicted environmental concentrations (PECs) calculated on a daily basis in river water during the spring-summer growing season were compared to measured concentrations, and the results are discussed in view of the improved prediction accuracy with increasing spatial resolution.

## 2. Materials and methods

### 2.1. Improved SoilPlus

SoilPlus is a fugacity-based, dynamic and site-specific multimedia model of the fate of organic chemicals in soil and air. It considers two dynamic air compartments, and a number of 0.005 m-thick soil compartments; three mass balance equations are solved for water, organic matter and the simulated chemical. A detailed description of the SoilPlus model is given in Ghirardello et al. (2010). In the present case study, SoilPlus was improved in two ways: (a) the original Runge–Kutta scheme for solving the system of ordinary differential equations was updated with a much more efficient scheme, using an adaptive and implicit method of medium order (ESDIRK 4/5, full details can be found in Semplice et al., 2012), and (b) an open source GIS product, namely the MapWinGIS.ocx Active X control, v. 4.9 (MapWinGIS website, 2010) was implemented, thus realizing a model-driven GIS-integration. When running in the GIS-mode, the simulation scenario must be loaded from a standard shapefile containing spatial data at field level (one polygon), a query engine

then extracts the georeferenced input data from the shapefile attribute table (for example, site specific pedological properties, weather station data, and pesticide application rates) and the calculation is run for each polygon. In the present version, neither drift (or volatilization from soil) nor vegetated buffer strip effects on surface water concentrations were included. In the case of herbicides applied to soil the drift to surface water is of less importance than runoff, generally leading to PECs from 1 to 2 orders of magnitude lower (Verro et al., 2009). For this reason no calculation was performed for drift of metolachlor and terbuthylazine to surface water. For the insecticide fenitrothion, since no measured concentrations in water were available for the dates of application and days immediately following, no drift loadings calculation to surface water was performed; however, it should be noted that for fenitrothion, a contribution could arise from drift during applications to the crop canopy, resulting in PECs in surface water up to 1 order of magnitude higher than runoff-related PECs (Verro et al., 2009).

Given the absence of buffer strips in the area, the present version of the model does not consider the contribution of vegetated buffer strips in reducing chemical runoff loadings to surface water. However, recent approaches (Sabbagh et al., 2010) could be implemented to further refine the calculation, improving the ecological realism, although they might require additional data for their validation. A scheme of the GIS-integration is provided in Fig. 1. The integrated model was coded in Microsoft Visual Basic 6.

### 2.2. DynA model

Chemical dissipation processes occurring in the hydrographic network were modelled with the DynA model (Di Guardo et al., 2006). DynA is a dynamic water/sediment model and was used to simulate both the ditches around the fields and the River Meolo itself. At the current state of development, DynA model was not integrated in the soil model but run separately. However, its full integration with the soil/air model will be the subject of a further development. More details can be found in Text SI-1.

### 2.3. Site description

The investigated site was the basin of the River Meolo (north-eastern Italy), in which a sampling campaign was conducted in 2003–2004 to determine the river water concentrations of some selected pesticides, following their application. A detailed description of the scenario characteristics, sampling and analytical methods used and results for this case study can be found in Bonzini et al. (2006).

*Source of geographical information.* The River Meolo is a 17 km-long resurgence river that drains a 2828 ha basin. Runoff water reaches the outlet within a one-day period, with a mean flow rate at the outlet of approximately  $3 \text{ m}^3 \text{ s}^{-1}$  (Bonzini et al., 2006). Spatially-explicit information about the land use, crop distribution, hydrographic network, and pedological characteristics was provided by Verro et al. (2009, personal communication) collected and stored in the ESRI “shapefile” format. Most of the catchment (86%) is agricultural land, about 95% of which is cultivated. According to the USDA classification, 47% of the soils are loam and silty loam and 53% are silty clay loam and silty clay. The latter are more prone to generate runoff (Rawls et al., 1992). Organic carbon (OC) content ranges from 0.81% to 5.55%. These two extremes only occur loam and silty loam soils and represent 6% and 5% of the basin area, respectively, while the most frequent OC content is around 1.30%. Table SI-1 (a and b) reports additional details of textural and organic carbon distribution as well as air temperature and rainfall in the basin. Field observations showed that transfer of rainwater from fields to river occurs rapidly by runoff, within a few hours to one day according to rainfall pattern (Bonzini et al., 2006). Leaching is very unlikely because of the heavy soil types, watertable depth (0.7–1.0 m) and local rainfall pattern, characterized by storms in May and June and drought in summer. Runoff as preferential or unique transfer pathway has also been observed in field trials in similar conditions (Otto et al., 2008, 2012).

*Pesticide application.* In this case study the fate of the three most applied pesticides in the basin was investigated and simulated: two herbicides (metolachlor and terbuthylazine) and one insecticide (fenitrothion), for which measured concentrations were published (Bonzini et al., 2006). Table SI-2 reports the physical–chemical properties. Application dates and rates were based on those present in Bonzini et al. (2006): metolachlor was applied on maize (163 ha,  $1.34 \text{ kg ha}^{-1}$ ) and soybean (53 ha,  $1.47 \text{ kg ha}^{-1}$ ) around April 9 and May 11 respectively, terbuthylazine was applied on maize (503 ha,  $0.79 \text{ kg ha}^{-1}$ ) from April 8 to 24, and fenitrothion on grapevines (235 ha,  $0.35 \text{ kg ha}^{-1}$ ) around July 2 and 16. Detailed information at field level was available for the type of pesticide applied in each field and application rates, but generally not for exact application dates. When necessary, application dates were therefore attributed following Bonzini et al. (2006) and are discussed later. Measured pesticide concentrations in the River Meolo were available at 4 sampling points (Bonzini et al., 2006): Point 1 (Le Crosero, spring), Point 2 (Rovarè, mid-course), Point 3. (Monastier, autosampler station), Point 4 (Castelletto, outlet) (Fig. 2). Given the partitioning properties of the selected pesticides only water dissolved concentrations were calculated and compared to measured ones.

*Estimated baseflow for ditches and residence time.* Based on the available hydrological information and field observations, a constant baseflow was assumed for ditches, together with an average residence time of water for the whole basin (estimated as about 12 h). A comparison between rainfall data and flow rates

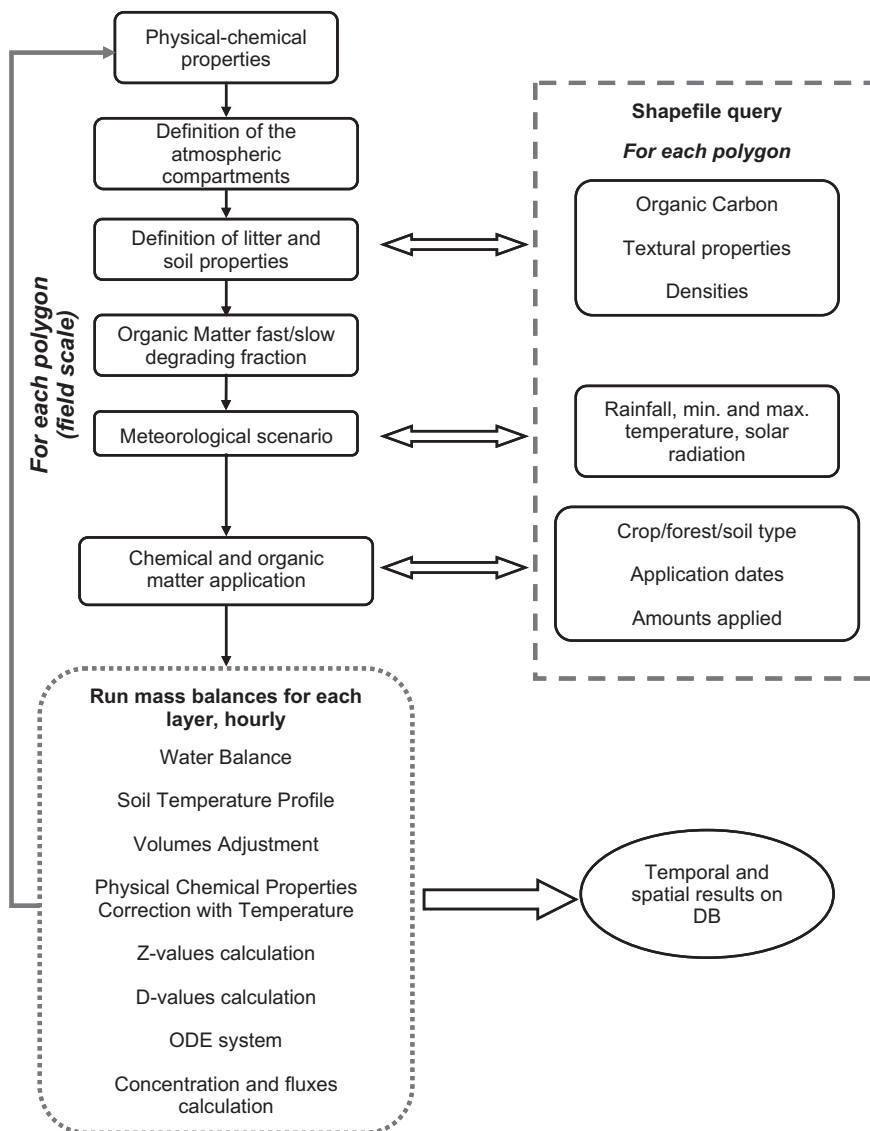


Fig. 1. Flux diagram of the GIS integration logic in SoilPlus. The final database stores output data for further elaborations.

showed that some rainfall events started during the night (May 4–5; May 22–23; June 2–3; June 12–13; August 13–14; September 14–15) and stopped the following day. A fraction of the runoff load was thus considered as part of the runoff for the following day. More details about these assumptions are in Text SI-2, while a precise description of the four-stage modelling approach is in Text SI-3 and Fig. SI-1.

#### 2.4. Simulation design and parameterization of the hydrographic network

Given the details above, the modelling approach can be considered semi-distributed. Spatial heterogeneity (texture, organic matter, rainfall and pesticide applications) was lumped at field level, where each field (simulation unit for SoilPlus) is represented by a polygon in a vector based approach. There was a total of about 2000 simulated polygons for the hydrological-only simulations, whereas the chemical fate simulations were performed for about 500–700 polygons depending on the chemical.

The rationale behind the simulation scheme was to gradually increase the spatial resolution and complexity of the scenarios in order to improve the accuracy of the predictions. In a tiered logic, a more accurate scenario definition should have positive consequences on the accuracy of the PECs compared to measured results (FOCUS, 2001). The availability of detailed information on the agro-environment, i.e. standard shapefile with spatial data at field level (pedological properties, weather station data, and pesticide application rates), allows simulation up to field level on a daily basis. A scheme of the increasing complexity is given in Fig. 3. For each pesticide, the following series of simulations were performed for the period from January 1 to September 30:

*Tier I.* Treated fields were considered as a single basin-wide field, with the most-frequent homogeneous soil properties obtained from the GIS information available (low spatial resolution). In this basin-wide scenario chemical runoff amounts were diluted in the daily water volume obtained from the daily flow rates measured near the basin outlet (Monastier sampling point, Point 3 in Fig. 2). This scenario considered no spatial heterogeneity and no hydrographic network.

*Tier II.* Each field was parameterized and calculated independently, by retrieving spatial data from the GIS. In this field-specific scenario, concentrations were calculated for each field and amounts of chemicals in runoff water were obtained for each day summing the contribution of each field. The predicted concentration in water at the Monastier sampling point was then obtained by simply diluting the daily amounts as in Tier I. This scenario used all the spatial information available but neglected the role of the hydrographic network in the basin in reducing concentrations towards the river.

*Tier III.* Each field was calculated separately as in Tier II, and the runoff water from each field was routed through the DynA model, applied to a series of representative ditches and river segments, in order to account for the loss processes (such as volatilization, degradation, adsorption to sediment, etc.) that could occur between each field and the sampling point. More details can be found in Text SI-4. This scenario used all the spatial information available, and also accounted for the role of the hydrographic network in reducing concentrations towards the sampling point.

#### 2.5. Modelling evaluation

Comparisons between predicted and measured concentrations were performed for the Monastier sampling point (Point 3 in Fig. 2), located 1 km upstream of the

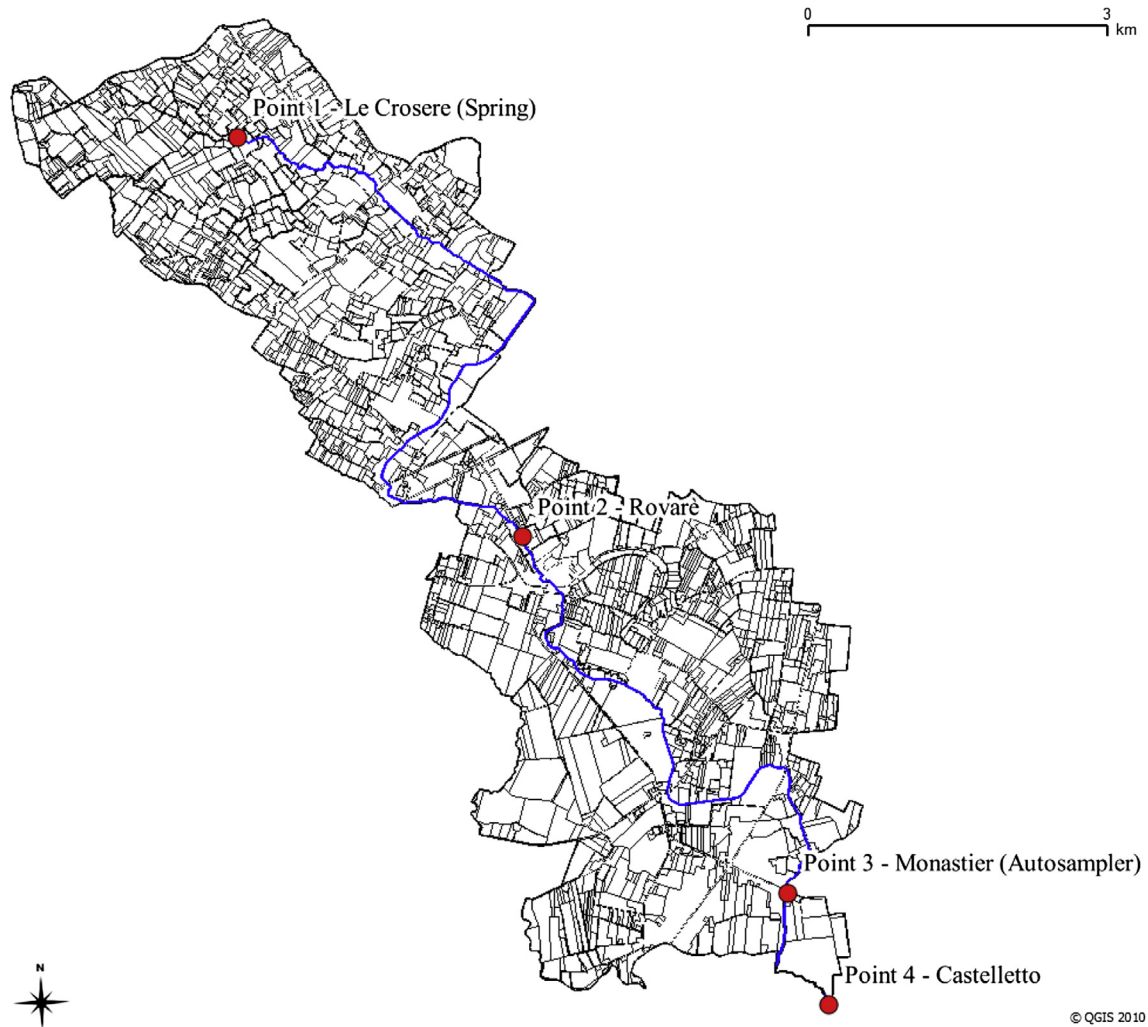


Fig. 2. River Meolo basin. Locations of sampling points and single fields (polygons) are shown. (Verro et al., 2009, personal communication).

basin outlet in Castelletto (Point 4 in Fig. 2), where water samples were continuously taken during rainfall events with an autosampler. This sampler was coupled to a hydrometer to continuously measure the river flow rate, in order to trigger the collection of water samples during rainfall events (Bonzini et al., 2006).

Rainfall, daily minimum, maximum and average temperatures and global radiation data on a 5-min basis were obtained from the local environmental protection agency (ARPAV website, 2012) for three weather stations located near the basin and for the Monastier sampling point. Each of the four rainfall datasets was assigned to a specific section of the basin according to Bonzini et al. (2006).

The overall predictive capacity of the model was evaluated with the Nash–Sutcliffe efficiency (NSE) index (Nash and Sutcliffe, 1970), calculated as:

$$NSE = 1 - \frac{\sum_{i=1}^n (P_i - O_i)^2}{\sum_{i=1}^n (O_i - \bar{O})^2}$$

where  $P_i$  is the predicted value,  $O_i$  the observed value, and  $\bar{O}$  the mean of observed values. NSE can range from 1 downwards to a negative value. An NSE = 1 indicates exact predictions and lower values indicate less agreement between the predicted and observed data. In general, a good model performance is expressed by an NSE higher than 0.4–0.5 (Cho and Mostaghimi, 2009) even if negative values are common in model calibration studies (Akteer and Babel, 2012; Holvoet et al., 2008). For further discussion on these evaluation criteria refer to Krause et al. (2005). For a detailed predicted vs. observed analysis, a linear regression and a correlation analysis (Pearson’s  $r$  and Spearman Correlation) were performed (StatSoft Inc,

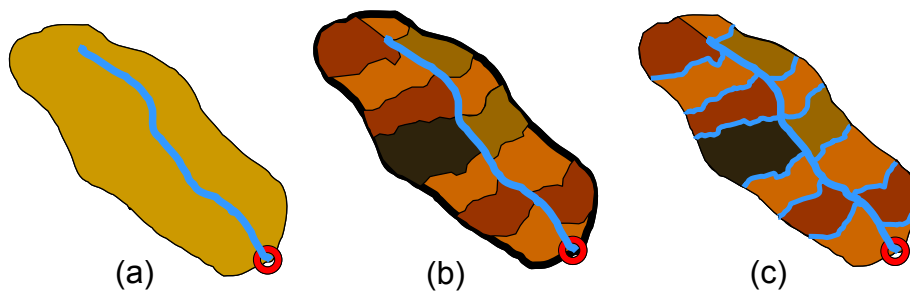


Fig. 3. Scheme of the increasing level of complexity in the simulations. (a) corresponds to Tier I, (b) to Tier II, (c) to Tier III. Brown colours are fields characterized by different properties, light blue is surface water, the red ring is the point in which water concentrations are calculated (see text for details). (For interpretation of the references to colour in this figure legend, the reader is referred to the web version of this article.)

2011) and graphical comparison was also used to identify general agreement and trends.

### 3. Results and discussion

For all simulation Tiers, three general results were relevant (Fig. 4):

- 1) calculated concentrations over the 6-month period were in general agreement with the observed concentrations in the River Meolo (Fig. 4);
- 2) predicted values for metolachlor and terbutylazine generally decreased from Tier I to Tier III and the prediction accuracy improved. Table 1 reports the comparison of the calculated statistical indices while the regression curves of observed/

predicted concentrations and relevant coefficients are shown in Fig. 5.

3) a very low background contamination was calculated for all pesticides before first applications, i.e. terbutylazine <0.011, metolachlor <0.024, fenitrothion <0.016, (all values are  $\mu\text{g/L}$ , see baseline levels in Fig. 4), given the concentrations measured in the spring water at Point 1 during the same period (Bonzini et al., 2006).

#### 3.1. Effect of spatial resolution on PECs in water

*Tier I.* This was the lowest spatial resolution simulation, performed on a hypothetical single basin-wide field with prevalent properties, and showed the general features of the model and its

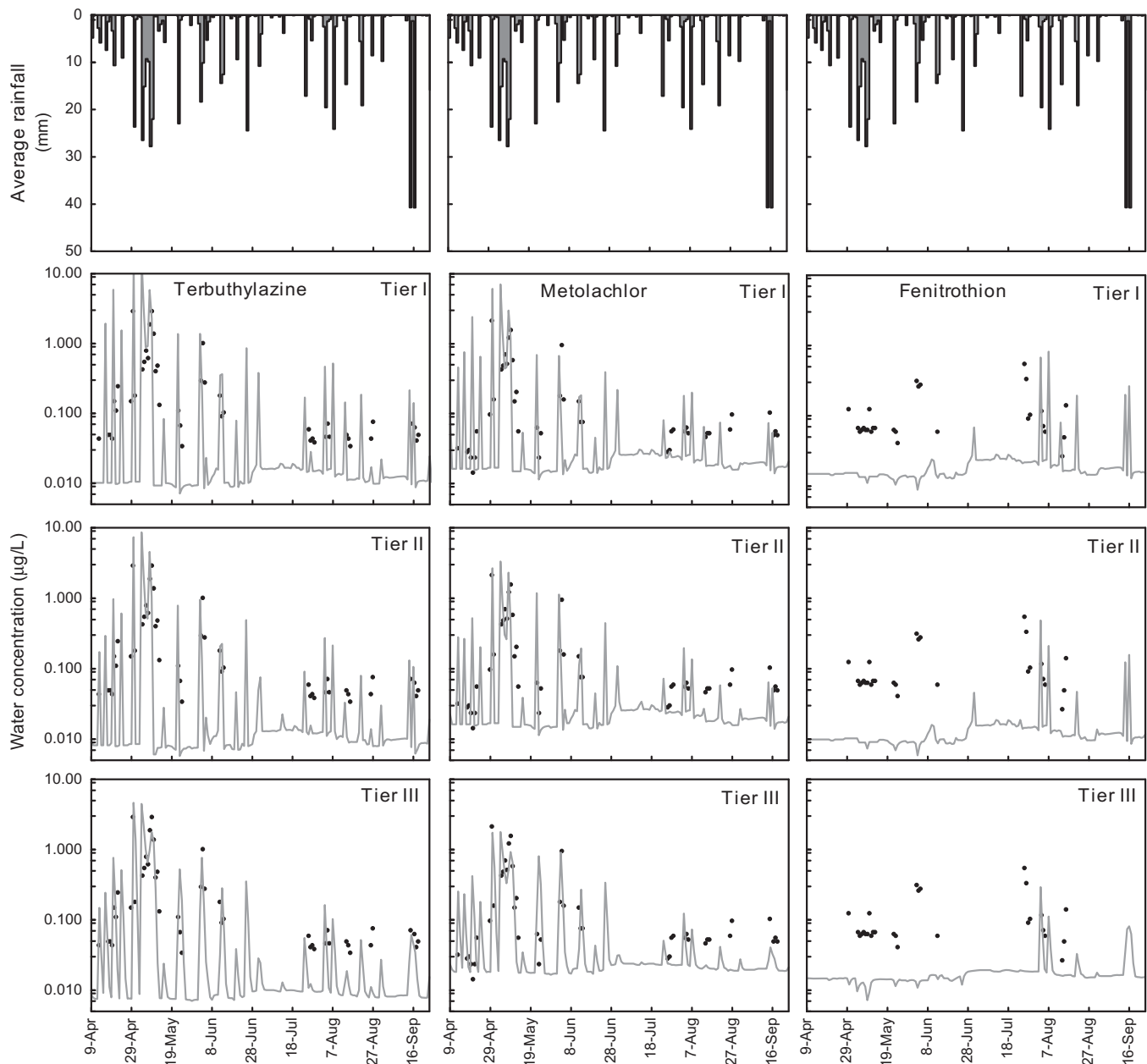


**Fig. 4.** Trends of predicted (grey solid lines) and measured (black dots) pesticides concentrations in River Meolo water during the spring-summer crops growing season, at the Monastier sampling point (Point 3 in Fig. 2). Above is the average rainfall, below the simulations with increasing spatial resolution (Tier I, Tier II and Tier III).

**Table 1**  
Statistical performance of the model.

Statistic*	Dataset	Tier I	Tier II	Tier III	Tier I	Tier II	Tier III
		Terbut	Terbut	Terbut	Metol	Metol	Metol
Mean of Predicted concentration	All data	1.19	0.65	0.51	0.56	0.32	0.28
Mean of Predicted concentration	Without 4th May	0.87	0.46	0.41	0.41	0.26	0.24
NSE	All data	-21.29	-4.57	-0.43	-7.28	-0.78	0.48
NSE	Without 4th May	-9.20	-1.01	0.43	-2.22	0.21	0.70
Pearson's correlation r	All data	0.53	0.55	0.66	0.59	0.61	0.73
Pearson's correlation r	Without 4th May	0.70	0.74	0.80	0.72	0.78	0.83
Coeff. of determ. ( $R^2$ )	All data	0.28	0.31	0.43	0.35	0.37	0.54
Coeff. of determ. ( $R^2$ )	Without 4th May	0.48	0.55	0.64	0.51	0.60	0.70
Spearman Rank Order correlation	All data	0.28	0.31	0.63	0.31	0.32	0.50
Spearman Rank Order correlation	Without 4th May	25 (n.s.)	28 (n.s.)	62	0.27 (n.s.)	0.28 (n.s.)	0.47
Number of paired data	All data	45	45	45	45	45	45
Number of paired data	Without 4th May	44	44	44	44	44	44

\*All correlations are significant at  $p < 0.05$  except those specified (n.s.).

capacity to simulate the driving forces determining the fate of pesticides. The model reproduced the general trend of measured concentrations in the simulated period, particularly for terbuthylazine and metolachlor (Tier I graphs in Fig. 4). The highest concentration peaks in the left part of the graph (from the end of April to early June), representing the so-called “spring flush”, were predicted by the model with a general overestimation of a factor between 3 and 35. Additionally, the model tended to overestimate pesticide concentrations during April, and to miss some events of lower concentration in late summer. April was indicated as the application period for maize, but the uncertainties about the exact application dates (Bonzini et al., 2006) made it difficult to accurately predict concentration peaks in that period. This means, as

stated elsewhere (Luo and Zhang, 2009; Bonzini et al., 2006), that the lack of information about the application dates represents a crucial aspect for the calculation of accurate PECs. The low accuracy of predictions in late summer (e.g. the two points at the end of August) could in turn be related to uncertainties in the water mass balance during irrigation events.

Despite the reasonably good reproduction of the concentration trends at this level of spatial resolution, the overall SoilPlus performance for terbuthylazine and metolachlor resulted in negative NSE for both simulations (-21.3 and -7.3, respectively, Table 1). It should be pointed out that NSEs are greatly affected by the highest values of predicted and measured concentrations. Thus, the few overestimates of concentration peaks can greatly affect the NSE,

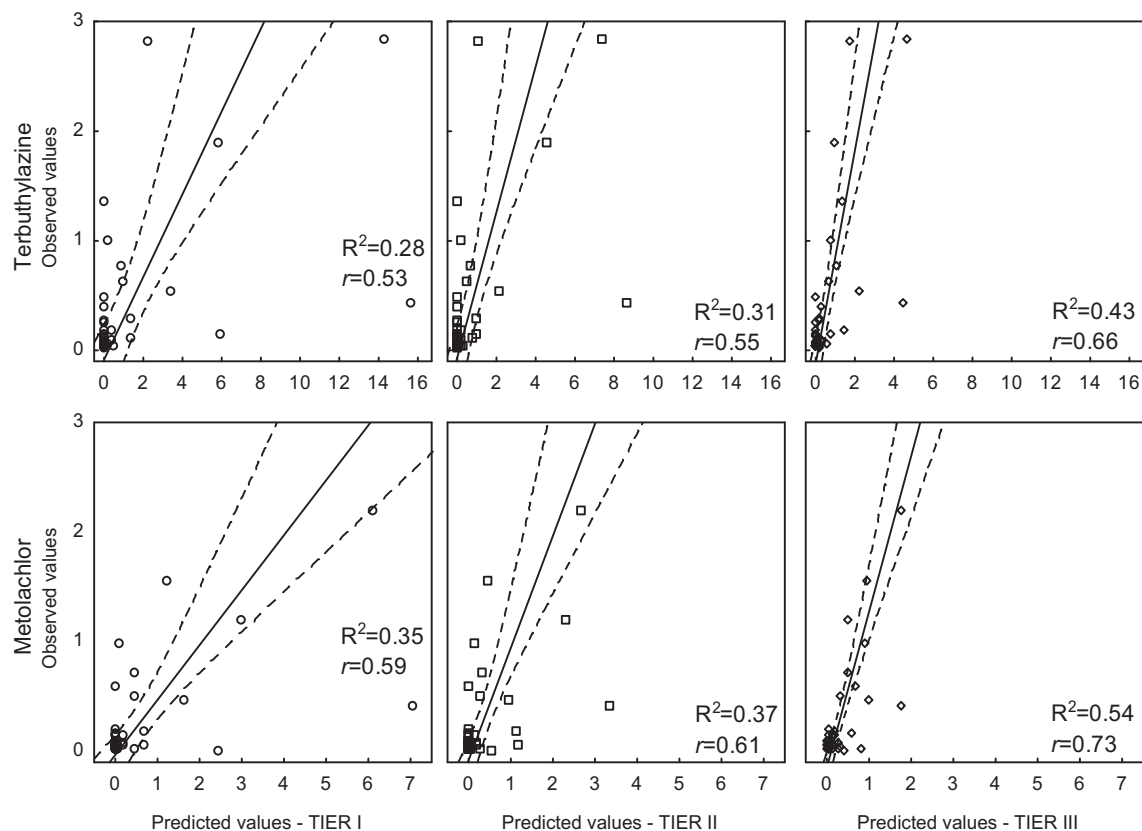


**Fig. 5.** Predicted vs. observed concentration of metolachlor and terbuthylazine for simulations with increasing spatial resolution (Tier I, Tier II and Tier III). Regression line, 95% confidence bands,  $R^2$  and Pearson's  $r$  are indicated. All correlations are significant at  $p < 0.01$ .

although the overall performance of the model is sound. Furthermore, NSE values were strongly affected by the values of May 4, for which large differences between observed and predicted values were calculated (metolachlor: observed = 0.42, predicted = 7.04; terbuthylazine: observed = 0.44, predicted = 15.60, all values in  $\mu\text{g/L}$ ). Those differences exceeded (mean + 3\*standard deviation) and can be considered outliers, and when excluded the NSE improved to  $-2.22$  for metolachlor and  $-9.20$  for terbuthylazine.

Fenitrothion represents a more peculiar case, since concentrations comparable to those measured after the summer application dates were also detected during spring. Local observations and interviews with local dealers suggested that this was very likely due to applications in private gardens and small orchards in the spring. Nonetheless, calculated PECs in summer are generally in the same order of magnitude as measured results.

**Tier II.** This field-specific scenario represented a detailed spatially-specific (GIS-based) simulation, where the properties of each field (such as organic carbon and texture, etc.) were used.

This increased spatial resolution resulted in appreciable effects on prediction accuracy, and this was clear by comparing Tier I to Tier II simulations. The three Tier II graphs in Fig. 4 show that PECs calculated for terbuthylazine and metolachlor more closely followed the measured concentrations than in Tier I, and the higher peaks were predicted within a factor of 7–19. Also the over-predictions in April were smaller compared to those calculated in the Tier I simulation, within a factor of 5; the fenitrothion PECs were similarly reduced.

The increased spatial resolution (i.e. real vs. average basin data) and field-specific simulations resulted in improved model predictions (Table 1). This was reached by reducing the variability of the pedological characteristics of each field, which can greatly affect chemical partitioning (which, for non-polar organic chemicals, is essentially dominated by the OC fraction) and runoff generation (Rawls et al., 1992). It is worth noting that the better performance of Tier II vs. Tier I depends on the fact that soil and environmental property values are not normally distributed and therefore the arithmetical mean is not the best estimator. As an example, Maize field distribution in the basin, as well as of texture classes and organic carbon are shown in Fig. SI-2. This issue is discussed later with a series of *ad hoc* worst case simulations.

Tier II simulation is comparable, in principle, to the one depicted in Bonzini et al. (2006), in which PECs were calculated for the same scenario. While the two spatial approaches are similar, the models differ in that the present model calculates the overall fate of chemicals in soil and water, while the approach in Bonzini et al. (2006) was built upon a simple relationship that required additional factors to be described and assumed, such as the presence of buffer strips and their role in the prediction. However, buffer strips are almost absent in the Meolo river basin and cannot be used to justify a pesticide water concentration reduction during runoff events.

Also for Tier II the NSE values were strongly affected by the values of May 4, and when excluded the NSE improved to 0.22 for metolachlor and to  $-1.01$  for terbuthylazine.

**Tier III.** This last Tier represented the highest degree of realism investigated in this case study, since not only a field-specific scenario parameterization was used, but also the contribution of the hydrographic network to the overall fate of pesticides was included. Tier III simulations showed a further improvement in model predictions, if compared to Tiers I and II. This was true particularly for the highest peaks after the late April–June applications, which can be considered the most important events from a risk assessment point of view, since this is the period in which the aquatic ecosystem can be exposed to the highest concentrations. Metolachlor predictions consistently improved; the number of concentration peaks

overestimated by the model was reduced, and the highest peaks were generally predicted within a factor of 8. Although an over-estimation of a factor of 33 was calculated for May 23, an NSE = 0.48 was obtained for the whole simulation period, confirming the improvement of the predictive capacity of the approach. However, the model still overestimated concentrations during April by a factor of 2–30, likely because of the uncertainty of application dates. In order to evaluate a different pattern of application dates, an additional simulation was run for metolachlor, which was supposed to be applied on maize and soybean within a wider application period (from April 9 to 29) instead of on two single days. This scenario/hypothesis reduced the amount available for runoff in early April and, consequently, the runoff peaks up to one order of magnitude (event of April 13). The overall model performance again gave a slightly negative NSE ( $-0.14$ ) for the whole dataset, which improved to a positive value of 0.59 when the outlier of May 4 was excluded. It is worth noting that the range of observed concentrations of metolachlor (0.01–2.19  $\mu\text{g/L}$ ) was similar to that found in a similar research performed in an agricultural catchment in France (Boithias et al., 2011), but in the present study the model agreement was about double ( $R^2 = 0.54$ , see Fig. 5).

Model performance also improved for terbuthylazine, concentrations of which were overestimated within a factor of 5 for April. Higher measured concentrations were generally overestimated within a factor of 8 and an NSE = 0.43 was calculated for the whole period when the outlier of May 4 was excluded.

The overestimation calculated on May 4 was common to all the simulations performed, and seems to be related to the hydrological response of the basin during the whole rainfall event, resulting in a rapid increase only by the end of the event.

The ditches contribution to water balance was reflected in the water fluxes calculated by the model at point 3 (Monastier), which were in satisfying agreement with the measured ones, resulting in an NSE = 0.6 for the whole period. The Tier III level of simulation, with the highest spatial resolution and complexity, greatly improved the precision of predictions for metolachlor and terbuthylazine, as indicated by the close linear relationship between predicted and measured concentrations and as only 4–6 values out of 45 can be considered of low precision (i.e. outside a 95% confidence interval, Fig. 5). The response in the case of fenitrothion improved even if inconsistencies existed for peaks that did not correspond to rainfall events, which seemed to be related to its use in private gardens in the basin, as reported earlier. A similar lack of obvious relationship between flow and load transported off-site during individual events was found in other studies for chlorpyrifos (Oliver et al., 2012).

**Evaluation of dissipation in the hydrographic network.** The dissipation processes occurring within the hydrographic network calculated with the DynA model add a significant but relatively small influence on the overall mass balance of the investigated pesticides from the edge-of-field to the basin outlet. For example, in the ditches of sub-basin 1, of the three tracers investigated, fenitrothion losses were the highest (about 4% in water throughout the simulation), while for terbuthylazine and metolachlor the degradation losses were lower (2% and 0.25% respectively). The net transfer to the sediment compartment throughout the simulation was less than 1% of the total runoff amount, which led to maximum sediment concentrations around 0.05 ng/g (fenitrothion), 1.4 ng/g (metolachlor), and 1.5 ng/g (terbuthylazine), at the basin outlet. However, if a more hydrophobic chemical was run, the effect of the ditch system was relatively more appreciable (Text SI-5). This can also be more effective when highly productive (because of algal or macrophyte biomass) ditches are encountered (Gobas et al., 1991; Poissant et al., 2008). More details on the dissipation processes can be found in Text SI-5.

The choice of the treated fields when simulating a small catchment at such detailed scale is crucial for the response of the model, at least for the chemicals simulated in this study, which appreciably partition to water. Considering these results in the context of Tier II simulations, in a field-specific scenario the lack of information on the actually treated fields could result in an appreciable source of uncertainty. This information is generally difficult to obtain, as are the exact application dates, but is nonetheless another crucial aspect affecting the final model response. However, given the general availability of land use GIS data, most of the data needed for a spatially-explicit simulation can be obtained and used, as in this case study, to considerably improve the prediction of runoff trend and peaks and the related risk assessment for aquatic ecosystems.

*Worst case simulations and preliminary uncertainty analysis.* While a comprehensive analysis of input and SoilPlus model uncertainty will be the subject of a subsequent *ad hoc* paper, some preliminary observations can be made on the key factors affecting the model predictions.

In Tier I, a number of worst-case scenario simulations were performed considering hypothetical treated areas characterized by extreme soil textures and OC content, based on the data available for the Meolo scenario. The daily amount of chemical runoff was compared with the output of the Tier II GIS-based simulations. Results were very variable, and the Tier I worst-case scenario simulations calculated daily runoff loads up to 2 orders of magnitude larger than those of the GIS-based simulations. The huge variation observed in these worst-case scenario simulations stresses the importance of the uncertainty in soil data collection, pesticide properties and model parameterization. When a model is used in a deterministic way, these sources of uncertainty should be taken into account, as discussed in Dubus et al. (2003). Without taking spatial resolution into account and running hypothetical pesticides, Heuvelink et al. (2010) analysed how uncertainties in soil and pesticide properties propagate using GeoPearl, and showed that the parameters which contribute most to the uncertainty are the transformation half-life in soil and, to a lesser extent, the coefficient of sorption on organic matter. Indeed, the half-life of pesticides is very variable at field and catchment scale (Ghafoor et al., 2011); a recent Italian research highlighted, for example, that terbutylazine half-life in soil ranges from 10 to 50 days (Bottoni et al., 2013). An additional cause of uncertainty is related to the lack of precise dates for the application of pesticides. Given the relatively long (compared to the possible range of application dates) half-lives in soil of the simulated pesticides (20–45 days), we preliminarily estimate that the uncertainty in water concentration prediction would range between 10 and 20%. Compared to the other source of uncertainty these values should be considered negligible.

#### 4. Conclusions

Increasing spatial resolution and introducing a hydrographic network improved the prediction of temporal variations of PECs: with the pesticides compared in this exercise the overprediction significantly decreased from non-spatial to spatial simulation. The inclusion of ditch and river processes did not greatly enhance the predictions, but it was shown that with higher Kow chemicals and/or presence of vegetation their contribution could be substantial. Results presented in this study show that SoilPlus can calculate the pulse-exposure concentrations occurring at a small-catchment scale with a reasonably satisfying degree of accuracy. The comparison among the three different tiers suggests that a higher spatial resolution is useful especially when environmental properties are not normally distributed, and the main part of the

exposure is in a few large emission events, as is usual in an agricultural watershed. This is relevant in the procedure of risk evaluation as prescribed by the WFD (EC, 2000), along with experimental evidence in recent studies on ecotoxicological response to pulse exposure concentrations (Reinert et al., 2002; Ashauer et al., 2007; Vallotton et al., 2008). The increased accuracy on PEC calculation deriving from considering a spatially-explicit scenario could be significantly used to evaluate the impact of such pulse exposure scenarios in an updated ecological risk assessment framework. To further enhance the predicting ability in such dynamically changing environments, an hourly prediction of surface water concentrations should be performed, supported by the collection of monitoring data at the same temporal resolution for model verification, as suggested by Di Guardo and Hermens (2013).

#### Acknowledgements

The Italian Ministry of University and Research provided the financial support for this research (Project: Ecotoxicological risk of plant protection products: ecological effects and mitigation measures, PRIN 2008). The PhD course in Environmental Science of the University of Insubria funded the scholarship of Davide Ghirardello. Dr. Roberto Verro is kindly acknowledged for providing the GIS files for the GIS simulations. Dr. Matteo Semplice is kindly acknowledged for the help provided during implementation of the numerical method.

#### Appendix A. Supplementary data

Supplementary data related to this article can be found at <http://dx.doi.org/10.1016/j.envpol.2013.10.002>.

#### References

- Akter, A., Babel, M.S., 2012. Hydrological modeling of the Mun River basin in Thailand. *J. Hydrol.* 452–453, 232–246.
- Ali Akbar, T., Lin, H., 2010. GIS based ArcPRZM-3 model for bentazon leaching towards groundwater. *J. Environ. Sci.-China* 22, 1854–1859.
- ARPAV website, 2012. Regional Agency for the Protection of the Environment, Veneto Region, Northern Italy. Official website: <http://www.arpa.veneto.it/home2/htm/home.asp>.
- Ashauer, R., Boxall, A.B.A., Brown, C.D., 2007. New ecotoxicological model to simulate survival of aquatic invertebrates after exposure to fluctuating and sequential pulses of pesticides. *Environ. Sci. Technol.* 41, 1480–1486.
- Balderacchi, M., Di Guardo, A., Vischetti, C., Trevisan, M., 2008. The effect of crop rotation on pesticide leaching in a regional pesticide risk assessment. *Environ. Sci. Technol.* 42, 8000–8006.
- Barra, R., Vighi, M., Maffioli, G., Di Guardo, A., Ferrario, P., 2000. Coupling SoilFug model and GIS for predicting pesticide pollution of surface water at watershed level. *Environ. Sci. Technol.* 34, 4425–4433.
- Boithias, L., Sauvage, S., Taghavi, L., Merlina, G., Probst, J.-L., Sánchez Pérez, J.M., 2011. Occurrence of metolachlor and trifluralin losses in the Save river agricultural catchment during floods. *J. Hazard. Mater.* 196, 210–219.
- Bonzini, S., Verro, R., Otto, S., Lazzaro, L., Finizio, A., Zanin, G., Vighi, M., 2006. Experimental validation of a geographical information systems-based procedure for predicting pesticide exposure in surface water. *Environ. Sci. Technol.* 40, 7561–7569.
- Bottoni, P., Grenni, P., Lucentini, L., Barra Caracciolo, A., 2013. Terbutylazine and other triazines in Italian water resources. *Microchem. J.* 107, 136–142.
- Cho, J., Mostaghimi, S., 2009. Evaluating cell-based components of DANTSAT for predicting surface and subsurface transport of pesticides. *Biosyst. Eng.* 102, 473–485.
- Di Guardo, A., Hermens, J.L.M., 2013. Challenges for exposure prediction in ecological risk assessment. *Integr. Environ. Assess. Manag.* 9, e4–e14. <http://dx.doi.org/10.1002/ieam.1442>.
- Di Guardo, A., Calamari, D., Zanin, G., Consalter, A., Mackay, D., 1994. A fugacity model of pesticide runoff to surface water: development and validation. *Chemosphere* 28, 511–531.
- Di Guardo, A., Ferrari, C., Infantino, A., 2006. Development of a dynamic aquatic model (DynA Model): estimating temporal emissions of DDT to Lake Maggiore (N. Italy). *Environ. Sci. Pollut. Res.* 13, 50–58.
- Dubus, I.G., Brown, C.D., Beulke, S., 2003. Sources of uncertainty in pesticide fate modelling. *Sci. Total Environ.* 317, 53–72.

- EC, 1991. Council Directive 91/414/EEC of 15 July 1991 Concerning the Placing of Plant Protection Products on the Market.
- EC, 2000. EU Water Framework Directive, Directive 2000/60/EC of the European Parliament and of the Council of 23 October 2000 Establishing a Framework for Community Action in the Field of Water Policy.
- EC, 2009. Council Directive 2009/128/EC Establishing a Framework for Community Action to Achieve the Sustainable Use of Pesticides.
- FOCUS, 2001. Focus Surface Water Scenarios in the EU Evaluation Process Under 91/414/EEC. Report prepared by the FOCUS Working Group on Surface Water Scenarios, EC Document Reference SANCO/4802/2001-rev.2, p. 245 <http://focus.jrc.ec.europa.eu/sw/index.html>.
- Ghirardello, D., Morselli, M., Semplice, M., Di Guardo, A., 2010. A dynamic model of the fate of organic chemicals in a multilayered air/soil system: development and illustrative application. *Environ. Sci. Technol.* 44, 9010–9017.
- Ghafoor, A., Moeys, J., Stenström, J., Tranter, G., Jarvis, N.J., 2011. Modeling spatial variation in microbial degradation of pesticides in soil. *Environ. Sci. Technol.* 45, 6411–6419.
- Gobas, F.A.P.C., McNeil, E.J., Lovett-Doust, L., Haffner, G.D., 1991. Bioconcentration of chlorinated aromatic hydrocarbons in aquatic macrophytes. *Environ. Sci. Technol.* 25, 924–929.
- Gutsche, V., Rossberg, D., 1999. Comparing Environmental Risk Indicators for Pesticides. The Results of the European CAPER Project. Centre for Agriculture and Environment, Utrecht, The Netherlands. CLM 426-1999, 69–83 (184).
- Heuvelink, G.B.M., Burgers, S.L.G.E., Tiktak, A., Van den Berg, F., 2010. Uncertainty and stochastic sensitivity analysis of the GeoPEARL pesticide leaching model. *Geoderma* 155, 186–192.
- Holvoet, K., van Griensven, A., Gevaert, V., Seuntjens, P., Vanrolleghem, P.A., 2008. Modifications to the SWAT code for modelling direct pesticide losses. *Environ. Model. Softw.* 23, 72–81.
- Jarvis, N.J., 1995. Simulation of soil water dynamics and herbicide persistence in a silt loam soil using the MACRO model. *Ecol. Model.* 81, 97–109.
- Krause, P., Boyle, D.P., Båse, F., 2005. Comparison of different efficiency criteria for hydrological model assessment. *Adv. Geosci.* 5, 89–97.
- Leistra, M., van der Linden, A.M.A., Boesten, J.J.T.I., Tiktak, A., van den Berg, F., 2000. PEARL Model for Pesticide Behaviour and Emissions in Soil-plant Systems. Description of Processes. Alterra Report 013. Alterra, Wageningen, The Netherlands.
- Luo, Y., Zhang, M., 2009. A geo-referenced modeling environment for ecosystem risk assessment: organophosphate pesticides in an agriculturally dominated watershed. *J. Environ. Qual.* 38, 664–674.
- Luo, Y., Zhang, M., 2010. Spatially distributed pesticide exposure assessment in the Central Valley, California, USA. *Environ. Pollut.* 158, 1629–1637.
- MapWinGis website, 2010. MapWindow GIS Development Group official website <http://www.mapwindow.org>.
- Morselli, M., Ghirardello, D., Semplice, M., Raspa, G., Di Guardo, A., 2012. Integration of an atmospheric dispersion model with a dynamic multimedia fate model: development and illustration. *Environ. Pollut.* 164, 182–187.
- Nash, J.E., Sutcliffe, J.V., 1970. River flow forecasting through conceptual models. Part 1. A discussion of principles. *J. Hydrol.* 10, 282–290.
- Neitsch, S.L., Arnold, J.G., Kiniry, J.R., Williams, J., 2005. Soil Water Assessment Tool Theoretical Documentation. <http://www.brc.tamus.edu/swat/index.html>.
- Oliver, D.P., Kookana, R.S., Anderson, J.S., Cox, J., Waller, N., Smith, L., 2012. The off-site transport of pesticide loads from two land uses in relation to hydrological events in the Mt. Lofty Ranges, South Australia. *Agr. Water Manag.* 106, 70–77.
- Otto, S., Cardinali, A., Marotta, E., Paradisi, C., Zanin, G., 2012. Effect of vegetative filter strips on herbicide runoff under various types of rainfall. *Chemosphere* 88, 113–119.
- Otto, S., Vianello, M., Infantino, A., Zanin, G., Di Guardo, A., 2008. Effect of a full-grown vegetative filter strip on herbicide runoff. Maintaining of filter capacity over time. *Chemosphere* 71, 74–82.
- Pistocchi, A., Sarigiannis, D.A., Vizzaino, P., 2010. Spatially explicit multimedia fate models for pollutants in Europe: state of the art and perspectives. *Sci. Total Environ.* 408, 3817–3830.
- Pistocchi, A., 2008. A GIS-based approach for modeling the fate and transport of pollutants in Europe. *Environ. Sci. Technol.* 42, 3640–3647.
- Poissant, L., Beauvais, C., Lafrance, P., Deblois, C., 2008. Pesticides in fluvial wetlands catchments under intensive agricultural activities. *Sci. Total Environ.* 404, 182–195.
- Rawls, W.J., Ahuja, L.R., Brakensiek, D.L., Shirmohammadi, A., 1992. Infiltration and soil water movement. In: Maidment, D.R. (Ed.), *Handbook of Hydrology*. McGraw-Hill Inc., New York, pp. 5.1–5.51.
- Reinert, K.H., Giddings, J.M., Judd, L., 2002. Effect analysis of time varying or repeated exposures in aquatic ecological risk assessment of agrochemicals. *Environ. Toxicol. Chem.* 21, 1977–1992.
- Sabbagh, G.J., Fox, G., Muñoz-Carpena, R., Lenz, M., 2010. Revised framework for pesticide aquatic environmental exposure assessment that accounts for vegetative filter strips. *Environ. Sci. Technol.* 44, 3839–3845.
- Schriever, C.A., Liess, M., 2007. Mapping ecological risk of agricultural pesticide runoff. *Sci. Total Environ.* 384, 264–279.
- Semplice, M., Ghirardello, D., Morselli, M., Di Guardo, A., 2012. Guidance on the selection of efficient computational methods for multimedia fate models. *Environ. Sci. Technol.* 46, 1616–1623.
- StatSoft Inc, 2011. STATISTICA (Data Analysis Software System), Version 10. StatSoft, Inc., Tulsa, OK, 74104, USA. [www.statsoft.com](http://www.statsoft.com).
- Suarez, L.A., 2006. PRZM-3. A Model for Predicting Pesticide and Nitrogen Fate in the Crop Root and Unsaturated Soil Zones: Users Manual for Release 3.12.2. National Exposure Research Laboratory, U.S. Environmental Protection Agency, Athens, GA.
- Suzuki, N., Murasawa, K., Sakurai, T., Nansai, K., Matsuhashi, K., Moriguchi, Y., Tanabe, K., Nakasugi, O., Morita, M., 2004. Geo-referenced multimedia environmental fate model (G-CIEMS): model formulation and comparison to the generic model and monitoring approaches. *Environ. Sci. Technol.* 38, 5682–5693.
- Tiktak, A., Boesten, J.J.T.I., van der Linden, A.M.A., Vanclouster, M., 2006. Mapping ground water vulnerability to pesticide leaching with a process-based meta-model of EuroPEARL. *J. Environ. Qual.* 35, 1213–1226.
- Tiktak, A., van der Linden, A.M.A., Boesten, J.J.T.I., 2003. The GeoPEARL Model. Model Description, Applications and Manual. RIVM Report 716601007. RIVM, Bilthoven, The Netherlands.
- Verro, R., Finizio, A., Otto, S., Vighi, M., 2009. Predicting pesticide environmental risk in intensive agricultural areas. I: screening level risk assessment of individual chemicals in surface waters. *Environ. Sci. Technol.* 43, 522–529.
- Vallotton, N., Eggen, R.L.L., Escher, B.I., Krayenbuhl, J., Chèvre, N., 2008. Effect of pulse herbicidal exposure on *Scenedesmus vacuolatus*: a comparison of two photosystem II inhibitors. *Environ. Toxicol. Chem.* 27, 1399–1407.
- White, A.W., Barnett, A.P., Wright, B.G., Holladay, J.H., 1967. Atrazine losses from fallow land caused by runoff and erosion. *Environ. Sci. Technol.* 1, 740–744.



## Chapter 7. Paper VI

Supporting information for

### **Investigating the need for complex vs. simple scenarios to improve predictions of aquatic ecosystem exposure with the SoilPlus model**

Davide Ghirardello<sup>a</sup>, Melissa Morselli<sup>a</sup>, Stefan Otto<sup>b</sup>, Giuseppe Zanin<sup>c</sup> and Antonio di Guardo<sup>a\*</sup>

<sup>a</sup>Environmental Modelling Group, Department of Science and High Technology, University of Insubria, Via Valleggio 11, 22100 Como, CO, Italy

<sup>b</sup>National Research Council (CNR), Institute of Agro-environmental and Forest Biology, Agripolis, Viale dell'Università 16, 35020 Legnaro, PD, Italy

<sup>c</sup>Department of Agronomy, Food, Natural Resources, Animals and Environment (DAFNAE), University of Padova, Agripolis, Viale dell'Università 16, 35020 Legnaro, PD, Italy

\*Corresponding author

*Environmental Pollution* **2014**, *184*, 502–510



## Supporting information to:

### Investigating the need for complex vs. simple scenarios to improve predictions of aquatic ecosystem exposure with the SoilPlus model

Davide Ghirardello<sup>1</sup>, Melissa Morselli<sup>1</sup>, Stefan Otto<sup>2</sup>, Giuseppe Zanin<sup>3</sup> and Antonio Di Guardo<sup>1\*</sup>

1. Environmental Modelling Group, Department of Science and High Technology, University of Insubria, Via Valleggio 11, 22100 Como, Italy.

2. National Research Council (CNR), Institute of Agro-Environmental and Forest Biology, Viale dell'Università 16, 35020 Legnaro PD, Italy

3. Department of Environmental Agronomy and Crop Science, University of Padova, Agripolis, Viale dell'Università 16, 35020 Legnaro PD, Italy

#### **Table of contents**

Text SI-1: Modified DynA model.....	233
Text SI-2: Estimated baseflow for ditches and residence time.....	233
Text SI-3: Four-stage modelling approach details.....	234
Text SI-4: Details on Tier 1-2-3 parameterization.....	235
Text SI-5: Details on dissipation processes in the hydrographic network.....	236
Tables and Figures .....	237
Figure SI-1 .....	240
Figure SI-2 .....	<b>Error! Bookmark not defined.</b>
References.....	242

---

\* Corresponding author e-mail: [antonio.diguardo@uninsubria.it](mailto:antonio.diguardo@uninsubria.it) phone: +39-031-2386480; fax +39-031-2386449

### ***Text SI-1: Modified DynA model***

In order to account for the rapid changes in water volumes due to runoff events, the “variable storage method” was implemented according to the formulation adopted in the SWAT model (Neitsch et al., 2005). The modified model also includes the numerical method implemented in SoilPlus. Lastly, the biodegradation rate in water and sediment was adjusted for daily water temperature with an Arrhenius equation, using the same formulation adopted in the TOXWA model (Beltman et al., 2006); average daily water temperatures were calculated from the average daily air temperature using the approach by Stefan and Preud’homme (1993), also implemented in the SWAT model (Neitsch et al., 2005).

### ***Text SI-2: Estimated baseflow for ditches and residence time***

An analysis of the rainfall and river flow rate datasets showed that an almost constant difference in the flow rate was measured between Points 1 and 2, and between Points 2 and 3 (with reference to Figure 2 in the manuscript), also during days with no (or scarce) rainfall. An average flow rate difference was thus calculated for sub-basins 1 and 2, and assumed to be the baseflow for the ditches. The same analysis, conducted on 5-minute rainfall and flow rate data, allowed estimation of the time elapsed from the beginning of a rainfall event and the appearance of the peak in the river flow rate at Point 3. On average, river flow peaks occurred within 12 hours after the beginning of a rain event. Given the daily runoff calculation in SoilPlus, when rain fell at night the chemical and water runoff outputs were redistributed between the previous and the following day before running the DynA model. This procedure was necessary for the 6 following significant rain events: May 4-10; May 22-23; June 2-3; June 12-13; August 13-14; September 14-17. During these events, 10% to 65% of the runoff loads were assigned to the current day, and the remainder as input for the following day.

### **Text SI-3: Four-stage modelling approach details**

The four-stage modelling approach presented in Figure SI-1 was designed to perform Tier III simulations, and could be briefly described as follows:

*Stage 1.* The SoilPlus model was used to simulate the “emission scenario”, that is the daily runoff loadings (water + chemical) entering the ditches. The field-specific SoilPlus outputs were summed for each sub-basin, and divided by the number of ditches considered, in order to assign the same daily runoff load to each ditch. The overall runoff water contribution was calculated by running only the water balance sub-routine of SoilPlus for the shapefile representing the complete Land Use, which comprises more than 2,000 polygons to be simulated at once. The chemical runoff loads were in turn simulated by running the SoilPlus model only for treated fields; this was necessary for time-saving reasons, since each field-specific (polygon) simulation for the chemical fate is considerably slower than the same simulation run for the water balance alone.

*Stage 2.* Based on the above assumptions, the ditches of sub-basin 1 and 2 were simulated, resulting in daily water and chemical input for each sub-basin.

*Stage 3.* River Meolo sub-basin 1 was simulated considering a dynamic-baseflow, using the daily flows measured at the spring (Le Crosere, Point 1 in Figure 2 in the manuscript); the average daily water flow rates and chemical loadings of the ditches of sub-basin 1 were considered as inputs. Average daily outflowing water volumes (converted into flow rates,  $L s^{-1}$ ) and outflowing chemical amounts ( $\mu g h^{-1}$ ) were then calculated and used as input for sub-basin 2.

*Stage 4.* River Meolo sub-basin 2 was simulated as above and the resulting pesticide concentrations in water were compared to experimental concentrations measured at the autosampler station (Monastier, Point 3 in Figure 2 in the manuscript).

This integrated four-stage procedure also allowed the contamination of the sediment compartment to be simulated, along with loss and transport processes occurring in both water and sediments. Details on the parameterization of the DynA model for the ditches and River Meolo sub-basins are given in Table SI-2.

#### ***Text SI-4: Details on Tier 1-2-3 parameterization***

In Tier I the treated area is simulated as a whole, parameterized with the most frequent OC content (1.282 % and set at 1.30% in the scenario), average rainfall and weather data and the most frequent soil texture (silty clay loam). The most treated crops and date were also selected on the basis of the indications provided in the main text. Metolachlor was thus applied on maize and soybean, on April 9 (216 ha, 1.37 kg ha<sup>-1</sup>), terbuthylazine on maize on April 16 (503 ha, 0.79 kg ha<sup>-1</sup>), and fenitrothion on grapevines on July 9 (235 ha, 0.35 kg ha<sup>-1</sup>).

In Tiers II and III, spatially-explicit information for the scenario description was retrieved directly from the simulation shapefile, obtained by overlapping layers containing landscape information consisting of pedological properties, area of influence for each weather station, land use, reference sub-basin. This information was obtained by Verro (2009, personal communication). The GIS-analysis was performed with the open-source GIS software Quantum GIS 1.8.0 (QGIS, 2013)). The treated fields (polygons of the shapefile) were selected in order to represent each texture and OC content proportionally to the covered basin area. For all the metolachlor and terbuthylazine simulations, the application depth was assumed to be the 0-5 cm soil layer, while for fenitrothion (applied directly to leaves), a more surficial worst case assumption was used and the depth was set at 2 cm.

While in Tiers I and II the dissipation processes occurring in the ditches and river were not considered, the step-by-step procedure depicted in Figure SI-1 was followed in Tier III. The Meolo river basin was divided into two sub-basins, namely “sub-basin 1” (sub-basin outlet located at Point 2 in Figure 2 in the manuscript) and “sub-basin 2” (sub-basin outlet located at Point 3 in Figure 2 in the manuscript). The overall length of the network of ditches was measured for both sub-basins with Quantum GIS (QGIS, 2013). A “parsimonious” approach was then applied, which consisted of dividing the network length of each sub-basin into a number of 5,000 m long and 1 m wide ditches merging into the River Meolo in parallel. Based on the measurement performed with Quantum GIS, the network of sub-basin 1 was represented by 10 parallel ditches, while that of sub-basin 2 was

represented by 8 parallel ditches. Accordingly, the River Meolo was subdivided into two main stretches, called Meolo 1 (9,000 m long, 7 m wide, from Point 1 to Point 2 in Figure 2 in the manuscript) and Meolo 2 (7,000 m long, 7 m wide, from Point 2 to Point 3). The final portion (1,000 m long) was the portion not monitored by the autosampler and was not further considered. This rather simplified approach is on an intermediate level of complexity between the simulation of the River Meolo as a single water body (without considering the ditch network) and a full GIS-based integration between each edge-of-field simulation and the receiving, georeferenced ditch.

Text SI-6:

***Text SI-5: Details on dissipation processes in the hydrographic network***

Running the modified DynA model for the ditches and river segments showed that the dissipation processes occurring within the hydrographic network scarcely influence the overall mass balance of the three investigated pesticides once they exit the fields with runoff. The system seems to be largely dominated by advective processes; the overall water and pesticide residence time is quite short and this is explained by the partitioning properties of the chemicals, with relatively low  $K_{OW}$  ( $\text{Log } K_{OW} \cong 3$ ) and relatively long half-lives (4 to 60 days, see Table SI-1). However, when a more hydrophobic chemical was run, the effect of the ditch system became relatively more appreciable. Simulations performed with pendimethalin ( $\text{Log } K_{OW} = 5.18$ ; (7)) showed that a 10% reduction can occur between in/out of the chemical entering the ditches. The net transfer to the sediment deposition accounted for 1.5%, whilst the rest of the dissipation occurred mainly by volatilization and degradation in almost equal proportions.

## Tables and Figures

Table SI-1a – Textural and Organic carbon for maize fields in Meolo basin.

Soil Type	Type (%)	Subtype	Subtype (%)	Organic carbon (%)
Loam	10.96		10.96	0.81
Silt Loam	24.34	SL1	7.96	1.98
		SL2	8.35	0.9
		SL 3	8.02	5.55
Clay Loam	25.09		25.09	1.15
Silty Clay Loam	33.75	SCL 1	9.85	1.57
		SCL 2	20.93	1.28
		SCL 3	2.97	1.86
Silty Clay	5.86		5.86	1.66

Note: Type (%) represents the percentage of the maize area in each soil type; Subtype represents the percentage of each type characterized by a specific organic carbon average value.

Table SI-1b – Selected descriptive parameters for minimum, maximum and daily average temperatures and rainfall in Meolo basin. Total rainfall in the simulation period was 861 mm.

	min T (°C)	max T (°C)	Average T (°C)	Rain mm
Average	8.35	18.89	13.47	3.14
Standard Deviation	7.12	9.06	8.00	7.69
Median	9.05	21.05	14.89	0.00

Table SI-2: Physical-chemical properties of the simulated chemicals at 25 °C.

	<b>Metolachlor</b>	<b>Terbuthylazine</b>	<b>Fenitrothion</b>	<b>Pendimethalin</b>
Molecular Weight (g mol <sup>-1</sup> )	283.8 <sup>1</sup>	229.7 <sup>1</sup>	277.25 <sup>1</sup>	281.3 <sup>1</sup>
Water Solubility (g m <sup>-3</sup> )	530 <sup>2</sup>	8.5 <sup>3</sup>	30 <sup>2</sup>	0.3 <sup>1</sup> (at 20°C)
Molar enthalpy of dissolution (J mol <sup>-1</sup> )	27000 <sup>4</sup>	27000 <sup>4</sup>	27000 <sup>4</sup>	27000 <sup>4</sup>
Vapor Pressure (Pa)	0.00418 <sup>2</sup>	0.00015 <sup>3</sup>	0.00013 <sup>2</sup>	0.004 <sup>1</sup>
Molar enthalpy of vaporization (J mol <sup>-1</sup> )	95000 <sup>4</sup>	95000 <sup>4</sup>	95000 <sup>4</sup>	95000 <sup>4</sup>
Log Kow	3.13 <sup>2</sup>	3.04 <sup>3</sup>	3.4 <sup>2</sup>	5.18 <sup>1</sup>
Melting point (°C)	-62.8 <sup>1</sup>	176 <sup>5</sup>	3.4 <sup>1</sup>	58 <sup>5</sup>
Half-life soil (days)	23 <sup>3</sup>	45 <sup>3</sup>	20 <sup>2</sup>	35 <sup>6</sup>
Half-life sediment (days)	240 <sup>2</sup>	70 <sup>5</sup>	12 <sup>2</sup>	16 <sup>5</sup>
Half-life water (days)	60 <sup>2</sup>	6 <sup>5</sup>	4 <sup>2</sup>	4 <sup>5</sup>

References:

<sup>1</sup> (7); <sup>2</sup> (8); <sup>3</sup> (9); <sup>4</sup> Default value from the FOCUS Working Group (10); <sup>5</sup> Based on the Footprint Database (11); <sup>6</sup> (12).

Table SI-3: Parameterization of the DynA model for the ditches and Meolo sub-basins.

Parameter required by DynA	Ditches	Notes	River Meolo	Notes
Length (m)	5,000	<i>a</i>	Meolo 1: 9,000 Meolo 2: 7,000	<i>a</i>
Width (m)	1		7	
Average residence time (h)	Ditch 1: 5 Ditch 2: 2.5	<i>b</i>	Meolo 1: 3 Meolo 2: 3	<i>b</i>
Average baseflow water depth (m)	Ditch 1: 0.09 Ditch 2: 0.23	<i>c</i>	Meolo 1: 0.34 Meolo 2: 0.44	<i>c</i>
Average water baseflow (L s <sup>-1</sup> )	Ditch 1: 24 Ditch 2: 130	<i>d</i>	Meolo 1: dynamic Meolo 2: dynamic	<i>e</i> <i>f</i>
Water outflow (L s <sup>-1</sup> )	dynamic	<i>g</i>	dynamic	<i>g</i>
Sediment active layer depth (m)	0.05	<i>h</i>	0.05	<i>h</i>
Concentration of particles in water column (mg L <sup>-1</sup> )	15	<i>h</i>	15	<i>h</i>
Concentration of particles in inflow water (mg L <sup>-1</sup> )	15	<i>h</i>	15	<i>h</i>
Density of particles in water (kg m <sup>-3</sup> )	2.400	<i>i</i>	2.400	<i>i</i>
Density of particles in sediment (kg m <sup>-3</sup> )	2.400	<i>i</i>	2.400	<i>i</i>
Density of aerosol particles (kg m <sup>-3</sup> )	1.500	<i>i</i>	1.500	<i>i</i>
Fraction of OC in ditch/river water particles	0.05	<i>h</i>	0.05	<i>h</i>
Fraction of OC in sediment particles	0.05	<i>h</i>	0.05	<i>h</i>
Fraction of OC in resuspended sediment particles	0.05	<i>h</i>	0.05	<i>h</i>
Fraction of OC in inflow suspended sediment solids	0.05	<i>h</i>	0.05	<i>h</i>
Yearly rainfall (m)	1.250	<i>l</i>	1.250	<i>l</i>
Volatilization MTC (air side) (m h <sup>-1</sup> ) (MTCa)	5	<i>i</i>	5	<i>i</i>
Volatilization MTC (water side) (m h <sup>-1</sup> ) (MTCw)	0.05	<i>i</i>	0.05	<i>i</i>
Burial rate of solids (g m <sup>-2</sup> day <sup>-1</sup> )	0.1	<i>m</i>	0.1	<i>m</i>
Resuspension rate of solids (g m <sup>-2</sup> day <sup>-1</sup> )	6.4	<i>m</i>	6.4	<i>m</i>
Deposition rate of solids (g m <sup>-2</sup> day <sup>-1</sup> )	6.5	<i>m</i>	6.5	<i>m</i>
Sediment – water diffusion MTC (m h <sup>-1</sup> ) MTCws	0.00015	<i>n</i>	0.00015	<i>n</i>
Volume fraction of particles in surface sediment	0.4	<i>h</i>	0.4	<i>h</i>

Notes:

*a*: based on the spatial analysis performed on the GIS files

*b*: average values assumed in order to match the observed time of runoff (see text SI-1)

*c*: obtained in relation to the average residence time

*d*: based on the flow rates analysis (see manuscript)

*e*: based on measured flow rates at Point 1 (Figure 2 in the manuscript)

*f*: calculated (see description of Tier III and Figure 3 in the manuscript)

*g*: calculated on the basis of daily runoff water outputs (see description of Tier III and Figure 3 in the manuscript)

*h*: based on recommendations by the FOCUS Working Group (10)

*i*: based on Mackay (2001)

*l*: yearly average obtained from daily rainfall data

*m*: based on Warren and Mackay (2004)

*n*: calculated, based on (Mackay (2001)

**Figure SI-1**

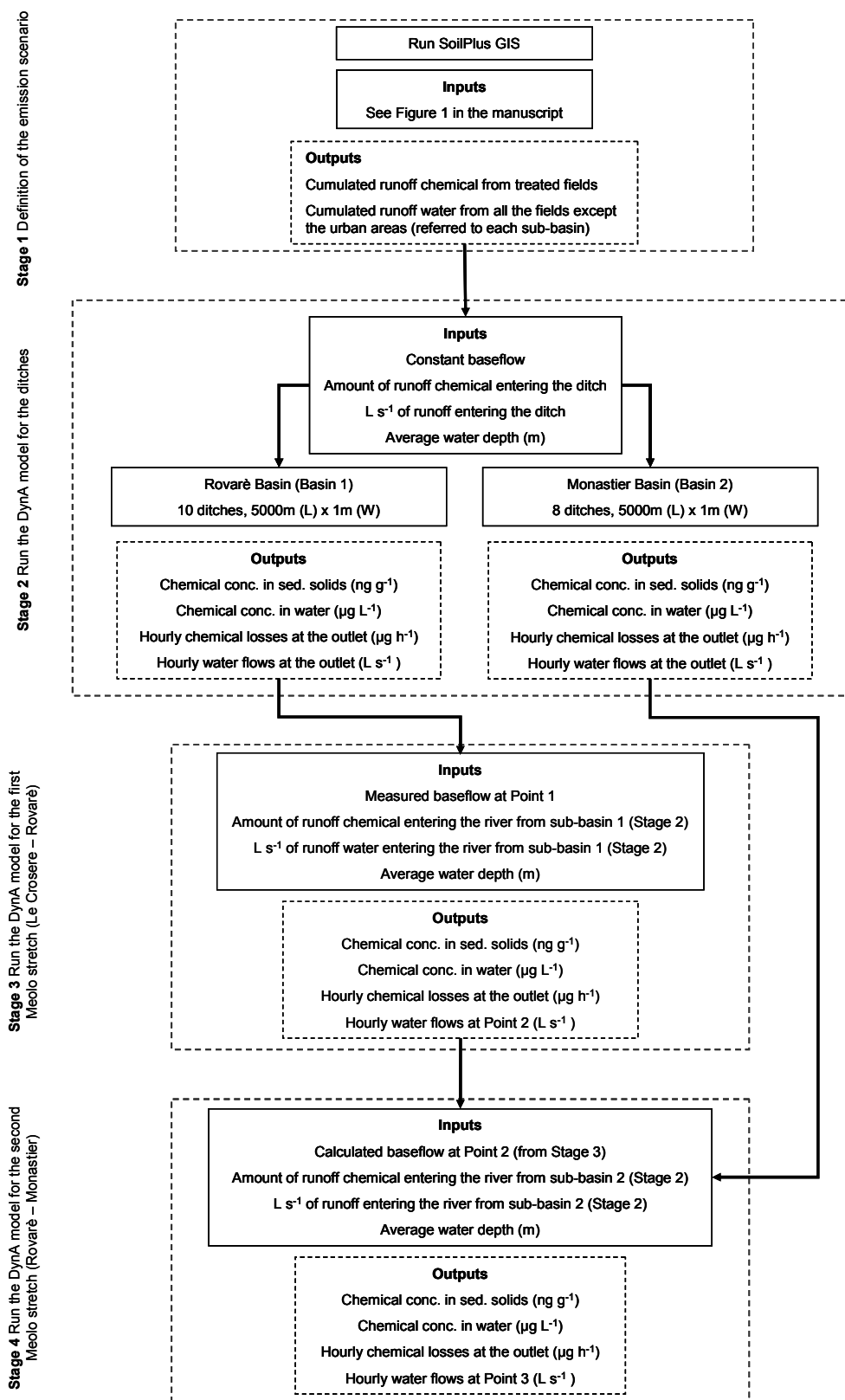


Figure SI-1: Scheme of the modelling approach for simulations of Tier III, with reference to sampling points (Point 1, 2 and 3 as in Figure 2 in the manuscript).

**Figure SI-2**

(A)

(B)

(C)

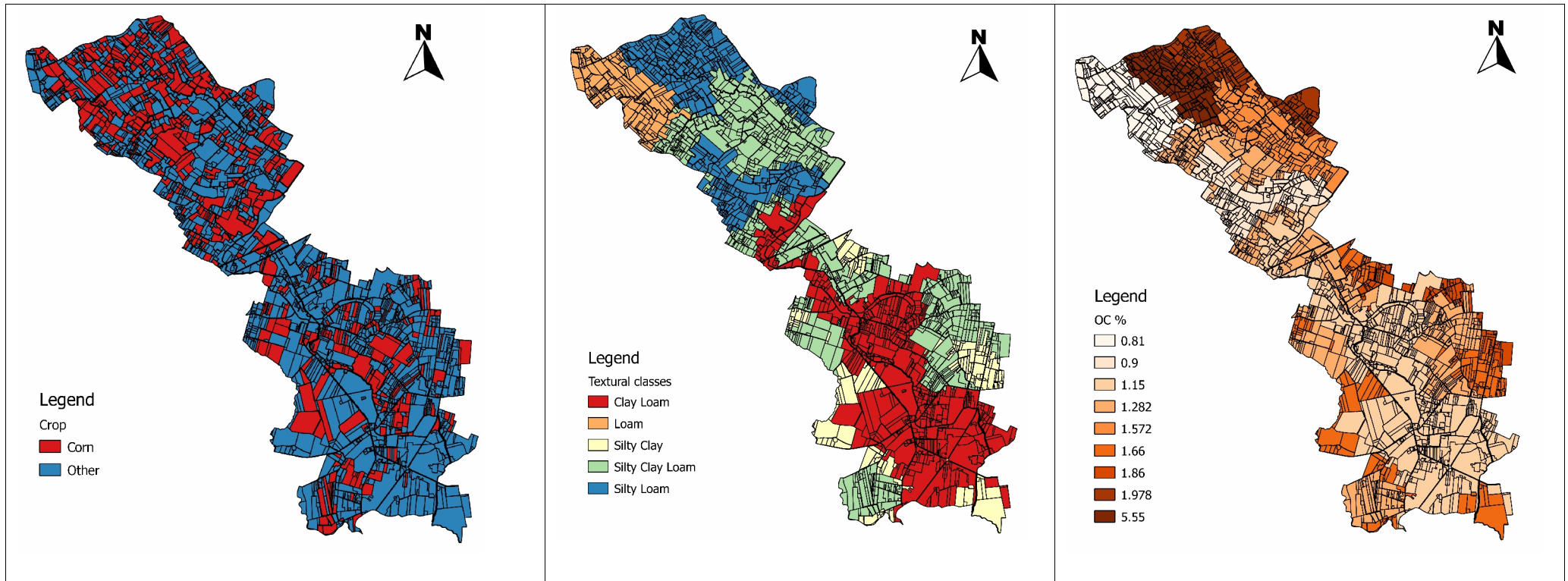


**Figure SI2 – Meolo Basin: (A) Maize fields vs. the rest of the area; (B) Distribution of textural classes; (C) Distribution of organic carbon percentages**

## References

- Alister, C. A., Gomez, P. A., Rojas, S., Kogan, M. 2009. Pendimethalin and oxyfluorfen degradation under two irrigation conditions over four years application. *J. Environ. Sci. Health B*. 44, 337-343.
- Beltman, W. H. J., Ter Horst, M. M. S., Adriaanse P. I., De Jong, A. 2006. Manual of FOCUS\_TOXSWA version 2.2.1. Wageningen, Alterra, Alterra-rapport 586. 198 pp.
- Di Guardo, A., Calamari, D., Zanin, G., Consalter, A., Mackay, D. 1994. A fugacity model of pesticide runoff to surface water: Development and validation. *Chemosphere* 28, 511–531.
- FOCUS 2001. Focus surface water scenarios in the EU evaluation process under 91/414/EEC. Report prepared by the FOCUS Working Group on Surface Water Scenarios, EC Document Reference SANCO/4802/2001-rev.2. 245 pp, <http://focus.jrc.ec.europa.eu/sw/index.html>
- Footprint Database. Available at <http://sitem.herts.ac.uk/aeru/iupac/index.htm>
- Mackay, D. 2001. *Multimedia Environmental Models: The Fugacity Approach*, 2nd Ed., Lewis Publishers: Boca Raton, FL, USA,
- Mackay, D., Shiu, W. Y., Ma, K. C. 1997. *Illustrated Handbook of Physical-chemical Properties and Environmental Fate for Organic Chemicals. Volume V: Pesticide Chemicals*. Lewis Publisher, Boca Raton, FL, USA,
- Neitsch, S. L., Arnold, J. G., Kiniry, J. R., Williams, J. 2005. *Soil Water Assessment Tool Theoretical Documentation*, <http://www.brc.tamus.edu/swat/index.html>.
- QGIS website 2013. The Quantum GIS Project official website, <http://www.qgis.org/>
- Stefan, H. G., Preud'homme, E. B. 1993. Stream temperature estimation from air temperature. *Wat. Res. Bull.* 29, 27-45.
- Tomlin, C. D. S. 1997. (Ed.) *The Pesticide Manual*, 11<sup>th</sup> ed., British Crop Protection Council: Farnham, Surrey, UK.
- Verro, R., Finizio, A., Otto, S., Vighi, M. 2009. Predicting pesticide environmental risk in intensive agricultural areas. I: screening level risk assessment of individual chemicals in surface waters. *Environ. Sci. Technol.* 43, 522-529.
- Warren, C., Mackay, D. A. 2004. Screening level mass balance model of sediment remediation options. *Soil Sed. Cont.* 13, 283-297.



## Chapter 8. Paper VII

# Modelling the temporal uptake of semi-volatile organic chemicals in plants using an ecologically realistic scenario

Elisa Terzaghi<sup>a</sup>, Melissa Morselli<sup>a</sup>, Matteo Semplice<sup>b</sup>, Bruno Cerabolini<sup>c</sup>, Kevin C. Jones<sup>d</sup> and Antonio di Guardo<sup>a\*</sup>

<sup>a</sup>Department of Science and High Technology, University of Insubria, Via Valleggio 11, 22100 Como, Italy

<sup>b</sup>Department of Mathematics, University of Turin, Via C. Alberto 10, 10123 Torino TO, Italy

<sup>c</sup>Department of Theoretical and Applied Sciences, University of Insubria, Via J. H. Dunant 3, 21100 Varese, Italy

<sup>d</sup>Lancaster Environment Centre, Lancaster University, Lancaster LA1 4YQ, UK

\*Corresponding author

*Draft to be submitted to Environmental Science & Technology*



## **ABSTRACT**

A new dynamic vegetation model was developed to simulate the fate of organic compounds in the air/plant/litter/soil system. Key features of the model are the double-layered air compartment (planet boundary layer, PBL and residual layer) interacting dynamically with vegetation and multilayered litter/soil compartments. Vegetation can represent both monospecific and multispecific forest. Leaf biomass is dynamically calculated employing two important ecological parameters (LAI and SLA), while stem and root biomass are assumed constant over time. The model was used to investigate the air compartment structure and meteorological variability in influencing PAH air-leaf exchanges, simulating a broadleaf wood located in Northern Italy (Como). Modelled leaf concentrations showed a satisfying agreement with measured one. Leaves appeared to act as a “filter” but also as a “dispenser” of air contaminants in response to meteorological parameters and emission changes. A preliminary sensitivity analysis showed that air concentrations are most affected by emission, PBL height and wind speed, while for leaf concentrations  $K_{OW}$ , air temperature and SLA are also important. Illustrative simulations were then performed for PCB 52 and PCB 153 to show the influence of leaves biomass on air concentrations in realistic forest conditions in terms of air residence time, wind speed and domain size.

## **1. INTRODUCTION**

Most of the multimedia fate models developed in the past did not generally include vegetation compartment. The reason was that modellers had enormous difficulty calculating the partitioning of chemicals into plants rather than plants were considered unimportant (Mackay, 2001). The introduction of the vegetation compartment in multimedia fate models had received more attention as a result of the realization that (1) consumption of contaminated vegetation was a major route for

the transfer of some toxic chemicals along the food chain and (2) that plants played an important role in influencing contaminant concentrations in the surrounding compartments i.e. air and soil. Since the late 1980s, a number of models with different degree of complexity have been developed. Plants were also included in the European Union System for the Evaluation of Substances (EUSES) (EC, 2004) which is recommended in European Union for risk assessment of organic chemicals.

Many of the bioaccumulation models described in the literature are steady state models: they assumed that chemical concentrations in plant and other compartments, as well as, meteorological and ecological scenario are constant over time. On the contrary unsteady state models can account for the changes in environmental conditions, chemical emission and plant parameters and allow predicting plant concentration at different times during the growing season (Undeman et al., 2009). However most of these models consider only the variability in exposure concentrations and assume that many plant and environmental parameters are constant over time, lacking of ecological realism. Therefore this approach, even if required less input data, may lead to erroneous results when comparing predictions to measured values. This drawback was recently highlighted by the European Community (EC, 2013), which has reported that the approach currently employed for environmental risk assessment need to be improved in the coming years since it lacks of ecological realism both in the exposure and effect evaluation. Concerning the exposure assessment, this goal can be achieved through the development of a number of more realistic scenarios which consider temporal and spatial variability of environmental parameters and their adoption in dynamic multimedia fate model capable to predict time and space variable concentrations.

Recently, an ecologically realistic and full dynamic scenario (Terzaghi et al., 2015) was developed in order to investigate in detail how the variability of a number of meteorological and ecological parameters can influence the uptake/release of polycyclic aromatic hydrocarbon (PAHs) by plants and therefore air concentrations. Since different factors could influence PAH air and leaf

concentrations, it was highlighted that the assistance of a full dynamic multimedia fate model is required if data are to be interpreted reliably.

In the present work, a dynamic vegetation model that accounts for the variability of meteorological and ecological parameters was developed and integrated in an existing air/soil model (SoilPlus) which includes a double layered air compartment and a multilayered litter/soil compartment (Ghirardello et al., 2010). More specifically the air compartments represent the residual layer and the planet boundary layer (PBL) and could change in height and wind speed on an hourly basis. PBL height is one of the key parameters in determining the diurnal variability of contaminants air concentrations. Recently, Morselli et al., 2011 showed that air concentrations could be predicted including PBL variability in multimedia fate models; however they did not take into account vegetation. Generally, when vegetation is considered in model that include PBL dynamics, it is kept constant for the whole growing season (McLeod et al., 2001) or both vegetation and PBL height are assumed not to change with time (Zhang et al., 2003).

Here, for the first time the role of air compartment structure and meteorological variability in influencing PAH air-leaf exchanges was investigated, adopting the scenario developed by Terzaghi et al., 2015 in the resulting vegetation model (SoilPlusVeg). Further specific simulations will be provided in a later publication to show the importance of ecological parameters such Leaf Area Index (LAI) and Specific Leaf Area (SLA), the timing of budburst and production of new leaves during the growing season in determining the influence of each plant species that composed the wood on contaminant air concentrations.

## 2. MATERIAL AND METHODS

**2.1 Development of the vegetation model.** A new dynamic vegetation model based on the fugacity approach (Mackay, 2001) was developed. The vegetation model simulates a forest/wood composed of plants composed of roots, stem and foliage. While foliage biomass and volume varies over time, root and stem volumes are assumed to be constant. The processes considered in the vegetation model are represented in **Figure 1**. The arrows indicate the transfer, degradation and growth processes. In this model formulated in term of fugacity, compartment capacities are expressed in terms of  $Z$  values (**Table 1**) while transport, transformation and growth processes are computed by means of  $D$  values (**Table 2**). Both  $D$  and  $Z$  values are drawn upon on different modelling published paper. Organic chemicals can reach the vegetation compartment through dry gaseous deposition (absorption), dry particle deposition, rain dissolution of dissolved chemical, wet particle deposition and root uptake from soil, while they can leave it through volatilization, wash off, wax erosion, litter fall, growth dilution, degradation and transfer from roots to soil; moreover translocation through the xylem and phloem allows the chemical movement from roots to leaves and vice versa.

**Table 1 - Fugacity capacity,  $Z$  values ( $\text{mol/Pa}\cdot\text{m}^3$ ) in the vegetation model**

<b>Plant compartment</b>	<b><math>Z</math> values (<math>\text{mol/Pa}\cdot\text{m}^3</math>)</b>
Roots	$Z_R = RCF \cdot \rho_R / H$
Stem	$Z_{St} = SCF \cdot \rho_{St} / H$
Foliage	$Z_F = K_{PA} \cdot \rho_F / RT$

$Z_R$ ,  $Z_{St}$ ,  $Z_F$  are the fugacity capacity of roots, stem and foliage ( $\text{mol/Pa}\cdot\text{m}^3$ ),  $RCF$  is the Root Concentration factor ( $\text{L/kg}$ ),  $SCF$  is the Stem Concentration Factor ( $\text{L/kg}$ ),  $K_{PA}$  is the plant/air partition coefficient ( $\text{m}^3/\text{g}$ ),  $\rho_R$  ( $\text{kg/L}$ ),  $\rho_{St}$  ( $\text{kg/L}$ ),  $\rho_F$  ( $\text{g/m}^3$ ) are the densities of roots, stem and foliage,  $H$  is the Henry's Law Constant ( $\text{Pa}\cdot\text{m}^3/\text{mol}$ ),  $R$  is the gas constant ( $\text{Pa}\cdot\text{m}^3/\text{mol}\cdot\text{K}$ ),  $T$  is the temperature ( $\text{K}$ )

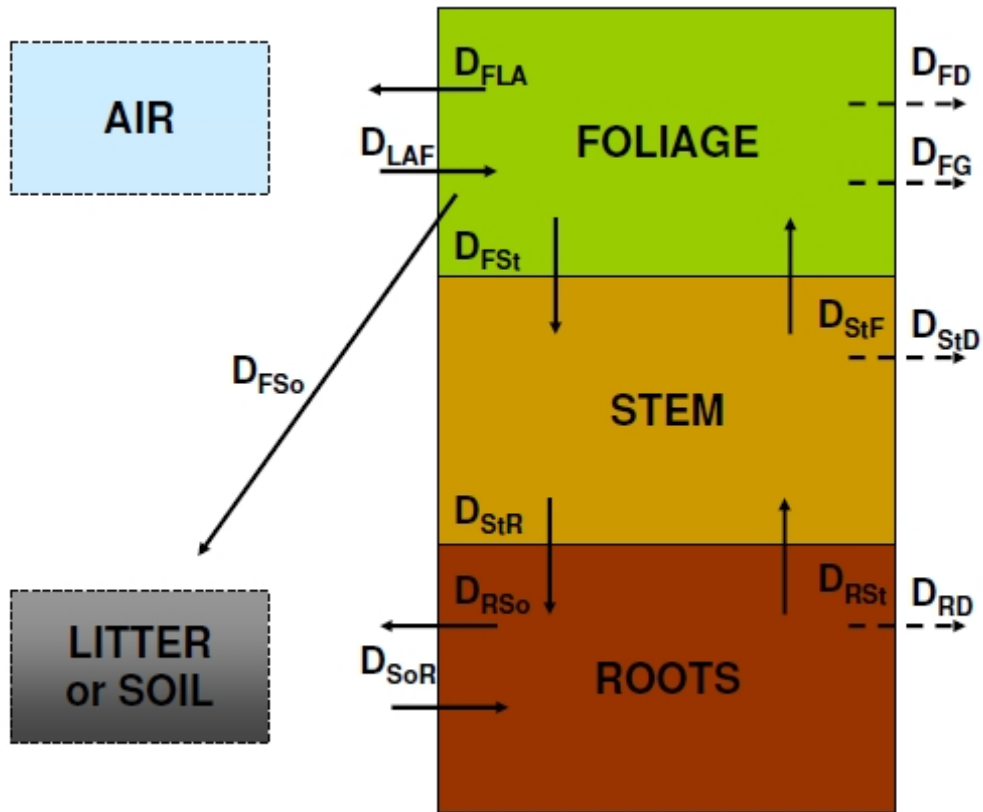


**Figure 1 - Schematic representation of the plant compartments and processes considered in the vegetation model**

In the model presented here, each compartment is described by a time dependent mass-balance equation written in differential form (for the steady-state form of the mass balance equation see SI-2) in which the amount (mol) is the unknown parameter:

$$\mathbf{Roots: } \frac{dmol_{ROOTS}}{dt} = a + b \cdot mol_{SOIL} + c \cdot mol_{STEM} - d \cdot mol_{ROOTS} \quad \mathbf{Eq.1}$$

$$\mathbf{Stem: } \frac{dmol_{STEM}}{dt} = e + f \cdot mol_{ROOTS} + g \cdot mol_{FOLIAGE} - h \cdot mol_{STEM} \quad \mathbf{Eq.2}$$

$$\mathbf{Foliage: } \frac{dmol_{FOLIAGE}}{dt} = i + l \cdot mol_{LOWERAIR} + m \cdot mol_{STEM} - n \cdot mol_{FOLIAGE} \quad \mathbf{Eq.3}$$

The left-hand terms represent the variation of the chemical amount (mol) in roots, stem, and foliage with time. The letters **a-n** include the terms involved in the mass balance (**Table 3**).

Table 2 - Time dependent D values (mol/h· Pa) in the vegetation model

Process	D values (mol/h· Pa)	
Soil-Root transfer	$D_{SoR} = \phi \cdot D_X + D_X / 20$	
Root-Soil transfer	$D_{RSO} = D_X / 20$	
Root-Stem transfer	$D_{RSI} = D_X$	
Stem-Root transfer	$D_{SIR} = D_P$	
Stem-Foliage transfer	$D_{SIF} = D_X$	
Foliage-Stem transfer	$D_{FSI} = D_P$	
Absorption to foliage	$D_{LAF}$	$D_{AF-G} = 1 / (1/D_{AB-F} + 1/D_C)$
Dry particle deposition to foliage		$D_{AF-P} = U_{AF-P} \cdot v_{AQ} \cdot Z_Q \cdot A_S \cdot LAI$
Rain dissolution to foliage		$D_{AF-R} = U_R \cdot Z_W \cdot A_S \cdot FrUF$
Wet particle deposition to foliage		$D_{AF-Q} = U_R \cdot v_{AQ} \cdot Z_Q \cdot Q \cdot A_S \cdot FrUF$
Volatilization from foliage	$D_{FLA} = D_{AF-G}$	
Wash off	$D_{FSO}$	$D_{FS-R} = (1 - FrUF) \cdot (D_{AF-R} + D_{AF-Q})$
Wax erosion		$D_{CUT} = (0.01 \cdot V_F) \cdot k_{CUT} \cdot Z_F$
Litter fall		$D_{FB} = G_{FB} \cdot Z_F$
Foliage growth	$D_{FG} = V_F \cdot k_{FG} \cdot Z_F$	
Degradation in foliage	$D_{FD} = V_F \cdot k_{FD} \cdot Z_F$	
Degradation in stem	$D_{SID} = V_{SI} \cdot k_{SID} \cdot Z_{SI}$	
Degradation in roots	$D_{RD} = V_R \cdot k_{RD} \cdot Z_R$	

$D_X$  is the D value for the bulk flow in the xylem (mol/h· Pa),  $D_P$  is the D value for the bulk flow in the phloem (mol/h· Pa),  $\phi$  is a factor that considers the delay caused by a membrane barrier (-), TSCF is the Transpiration Stream Concentration Factor (-),  $D_{LAF}$  is the overall D value for air to foliage transfer (mol/h· Pa),  $D_C$  is the D value for diffusion into cutin (mol/h· Pa),  $D_{AB-F}$  is D value for the transport across the air boundary layer (mol/h· Pa),  $U_{AF-P}$  is the dry deposition particle velocity to the vegetation canopy (m/h),  $v_{AQ}$  is the volume fraction of particle in air (-),  $Z_Q$  is the fugacity capacity of atmospheric particles (mol/Pa·m<sup>3</sup>),  $A_S$  is the area of the land surface (m<sup>2</sup>), LAI is the Leaf Area Index (m<sup>2</sup>/m<sup>2</sup>),  $U_R$  is the rain rate (m<sup>3</sup>rain/m<sup>2</sup>area·h),  $Z_W$  is the fugacity capacity of water (mol/Pa·m<sup>3</sup>), FrUF is the fraction of precipitation that is intercepted by the canopy and evaporates (-), Q is the scavenging ratio (-),  $D_{FSO}$  is the overall D value for foliage to litter or soil transfer (mol/h· Pa)  $k_{CUT}$  is the cuticle erosion rate constant (1/h),  $G_{FB}$  is the litter fall rate (m<sup>3</sup>/h),  $k_{FG}$  is the leaf growth rate (1/h),  $k_{FD}$ ,  $k_{RD}$ ,  $k_{SID}$  are the degradation rate constant in foliage, roots and stem (1/h)

**Table 3 – Groups of variables involved in the mass-balance equations in the vegetation model**

<b>a</b>	$E_R$
<b>b</b>	$D_{SoR}/V \cdot Z_T$
<b>c</b>	$D_{StR}/V_{St} \cdot Z_{St}$
<b>d</b>	$(D_{RSO} + D_{RSSt} + D_{RD})/V_R \cdot Z_R$
<b>e</b>	$E_{St}$
<b>f</b>	$D_{RSSt}/V_R \cdot Z_R$
<b>g</b>	$D_{FSF}/V_F \cdot Z_F$
<b>h</b>	$(D_{StR} + D_{StF} + D_{StD})/V_{St} \cdot Z_{St}$
<b>i</b>	$E_F$
<b>l</b>	$D_{LAF}/V_{LA} \cdot Z_{LA}$
<b>m</b>	$D_{StF}/V_{St} \cdot Z_{St}$
<b>n</b>	$D_{FLA} + D_{FSO} + D_{FSSt} + D_{FD} + D_{FG}/V_F \cdot Z_F$

$E_R$  is the direct emission in roots (mol),  $E_{St}$  is the direct emission in stem (mol),  $E_F$  is the direct emission in foliage (mol),  $D_{SoR}$  is the soil to roots D value (mol/Pa·h),  $D_{StR}$  is the stem to roots D value (mol/Pa·h),  $D_{RSO}$  is the roots to soil D value (mol/Pa·h),  $D_{RSSt}$  is the roots to stem D value (mol/Pa·h),  $D_{RD}$  is the root degradation D value (mol/Pa·h),  $D_{FSSt}$  is the foliage to stem D value (mol/Pa·h),  $D_{StF}$  is the stem to foliage D value (mol/Pa·h),  $D_{StD}$  is the stem degradation D value (mol/Pa·h),  $D_{LAF}$  is the total lower air to foliage D value (mol/Pa·h),  $D_{FLA}$  is the foliage to lower air D-value (mol/Pa·h),  $D_{FSO}$  is the total foliage to soil D value (mol/Pa·h),  $D_{FD}$  is the foliage degradation D-value (mol/Pa h),  $D_{FG}$  is the foliage growth D value (mol/Pa·h),  $V_R$  is the root volume (m<sup>3</sup>),  $V_{St}$  is the stem volume (m<sup>3</sup>),  $V_F$  is the foliage volume (m<sup>3</sup>),  $V_{LA}$  is the lower air volume (m<sup>3</sup>),  $VZ_T$  is the total of the products of volumes and Z values for each soil phase (mol/Pa),  $Z_R$  is the root fugacity capacity (mol/Pa·m<sup>3</sup>),  $Z_{St}$  is the stem fugacity capacity (mol/Pa·m<sup>3</sup>),  $Z_F$  is the foliage fugacity capacity (mol/Pa·m<sup>3</sup>),  $Z_{LA}$  is the lower air fugacity capacity (mol/Pa·m<sup>3</sup>).

Equations 1-3 are 1st-order ordinary differential equations (ODEs), and the system is solved numerically using a 5th-order accurate, diagonally implicit Runge-Kutta method with adaptive time stepping (ESDIRK; Semplice et al., 2012).

For more details about model parameterization see the Supporting information where Z-values (SI1-A), compartment densities (SI1-B), wood composition (SI1-C), compartement biomass and volume (SI1-D and SI1-E), index of root distribution in soil (SI1-F), ecological parameters (SI1-G) and D values (SI1-H) are reported.

**2.2 Vegetation model integration with SoilPlus.** The assembled vegetation model was integrated in an existing dynamic air/soil model (SoilPlus) described in detail in Ghirardello et al., 2010. **Figure 2** shows a schematic representation of the vegetation sub- compartments and their relationships with the air and the litter/soil compartments of the SoilPlus model. The resulting model (SoilPlusVeg) includes: 1) two-layered dynamic atmosphere, namely lower air (LA) and upper air (UA) representing the planet boundary layer (PBL) and the residual layer respectively, which vary in height and wind speed on an hourly basis; 2) a multi-layered soil, bare or covered by up to three litter horizons; 3) a vegetation compartment which can be composed of a mono-specific or a multi-specific forest/wood which includes roots, stem, leaves. When the vegetation model was integrated in SoilPlus it was assumed that the new compartments (foliage, stem, roots) did not change the volume of the other compartments (upper air, lower air, litter and mineral soil) and in order to distribute root volume in each soil layers, considering the rooting distribution in soil, the Gale and Grigal (1987) model was chosen. More details are given in **SI-1F**.

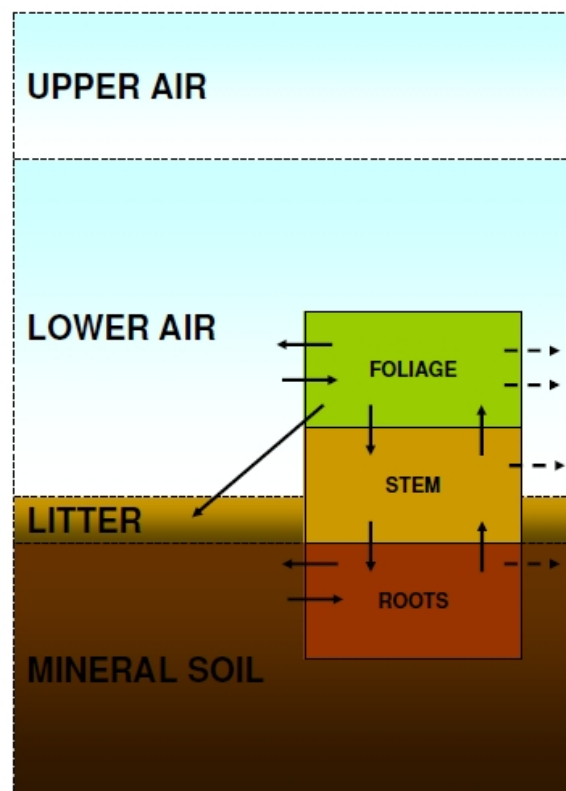


**Figure 2 - Schematic representation of SoilPlusVeg**

**2.3 Simulation scenario for the model evaluation.** An evaluation of the SoilPlusVeg model performance was carried out for 3 PAHs of different physical-chemical properties, phenanthrene, pyrene and chrysene (for physical–chemical properties see **SI-3**) comparing model output with a dataset of leaf concentrations measured in a small broadleaf wood located in Northern Italy (Como) (Terzaghi et al., 2015). The vegetation compartment was parameterized as reported in **SI-1**. Simulations were performed for a mixed broadleaf wood located in Como (Northern Italy), composed of *Cornus mas* (cornel), *Corylus avellana* (hazelnut) and *Acer pseudoplatanus* (maple). Bud burst occurred on March, 15 for the two understorey species (cornel and hazelnut), while maple leaves appeared about 3 weeks later on April, 7. The growing season ended on December, 5 but comparison between predicted and measured results was performed for a shorter period (March, 15 – June, 7) and for only two species (cornel and maple). The air compartments were parameterized as reported in Morselli et al., 2011. Upper air height ranged between 10 m to 2267 m while that of lower air between 100 m and 3000 m, depending on the season and the period of the day (day or night). Wind speed in upper air ranged between 0.2 m/s and 43 m/s, while in lower air between 0.2 m/s and 33 m/s. Such data were calculated with the help of a meteorological preprocessor (for details, see Morselli et al., 2012) starting from upper air soundings and standard meteorological observations collected during 2007 for a semi-urban site located in the proximity of Milan, about 50-km away from Como. Despite the topographical setting of Como (surrounded by 800 to 1000-m mountains) could determine differences in PBL height and dynamics with respect to the Milan site (substantially flat), we decided to resort to this meteorological dataset because of its completeness and given the lack of an upper air sounding station in the surroundings of Como.

Soil/litter compartments were parameterized as reported in Ghirardello et al., 2010. The total thickness of the litter/soil system was 15 cm. A single litter horizon (Oe) of 2 cm depth and a loamy sand soil of 13 cm were simulated. The litter/soil horizons were subdivided into a number (30) of 0.005-m thick layers. OC fractions were set to 40% and 2% in litter and soil compartment

respectively. Other meteorological parameters such as temperature, precipitation and solar radiation and PM<sub>10</sub> concentrations were provided by the Regional Environmental Protection Agency (ARPA, 2014) on an hourly or daily basis for 2007 for Como city. In order to run the model, an estimate of the emission conditions was needed. The PAHs sources were calibrated to reflect the observed range of variability in measured concentrations (Terzaghi et al., 2015). More specifically the direct chemical and PM<sub>10</sub> emission to lower air was calibrated in order to obtain the best possible fit to the range of measured concentrations (average of the week), while a PM<sub>10</sub> background concentration equal to the lowest measured concentration ( $7 \mu\text{g}/\text{m}^3$ ) was assumed. No background concentration for chemical was considered. More details about PAH and particulate matter emission to the system are reported in SI-4.

## 2.4 Sensitivity analysis

A preliminary sensitivity analysis was conducted simulating the fate of pyrene in a 1-ha wide vegetation-air-litter-soil system. 1-year simulations were performed, for a static environmental scenario characterized by a fixed-height atmospheric compartment (LA height = 686 m, UA height = 957 m), with constant wind speed (3.5 m/s in LA and 4.35 m/s in UA), overlaying a 2-cm deep layered litter and a 13-cm deep layered loamy sand soil (layer depth = 5 mm). A constant foliage compartment volume of  $2.7 \text{ m}^3$  was simulated, resulting from static LAI, SLA and leaf density values ( $2.4 \text{ m}^2/\text{m}^2$ ,  $0.032 \text{ m}^2/\text{g}$  and  $282747.2 \text{ g}/\text{m}^3$ , respectively). A constant chemical discharge to the LA compartment ( $1.53 \cdot 10^{-10} \text{ mol}/\text{h}$ ) was adopted, while PM background concentration and emission to LA were kept fixed in order to obtain a constant PM level in LA of  $15.77 \mu\text{g}/\text{m}^3$ . All the static input values listed above were calculated as averages of the dynamic ones described in the parameterization for model evaluation. Tested parameters included chemical emission, physical-chemical properties and, environmental half-lives, meteorological parameters (LA height and wind speed, air temperature, precipitations), vegetation characteristics (LAI, SLA, and leaf density), partition and mass-transfer coefficients, and litter/soil organic carbon fractions. A local sensitivity

analysis (Augusiak et al., 2014) was performed by varying each parameter by 0.1% and calculating the influence of such variations on two target parameters, namely the steady-state concentrations in LA ( $\text{ng}/\text{m}^3$ ) and leaves ( $\mu\text{g}/\text{g}$  d.w.), by assessing the index  $S$  (MacLeod et al., 2002):

$$|S| = \left| \frac{\Delta O / O}{\Delta I / I} \right| \quad \text{Eq.4}$$

where  $I$  is the input variable,  $O$  is the output of interest, and  $\Delta I$  and  $\Delta O$  are the variations in input and output parameters, respectively.

### 3. RESULTS AND DISCUSSION

#### 3.1 Sensitivity analysis

In **Figure 3** the influence of the key parameters ( $S > 10^{-2}$ ) on the two targets (chemical concentrations in LA and leaves) is depicted, while a complete list of results can be found in **Table SI-10**. Pyrene concentrations in LA were mostly affected by emission, LA height and wind speed ( $S \sim 1$ ), while only a slight contribution of parameters such as  $K_{OW}$  and  $K_{OA}$ , precipitations,  $LAI$  and  $Kpa$  was observed ( $S \sim 10^{-4}$ ). The reduced influence of vegetation biomass on atmospheric concentrations was ascribed to the extremely low residence time of air ( $\sim 30$  s), which caused advective air movement to be the dominant flux for pyrene removal in LA. However, the influence of vegetation in sequestering chemicals from air at different wind velocities was thoroughly investigated in Model illustration section. For pyrene concentrations in leaves, the most influential parameter was  $K_{OW}$  ( $S = 2.7$ ), followed by emission, LA height and wind speed, air temperature, and  $SLA$  ( $S \sim 1$ ). Other significant parameters were octanol-air partition coefficient ( $\text{Log } K_{OA}$ ), enthalpy of phase change between plant and air ( $Enth$ ), chemical half-life in air ( $HL_{air}$ ), mass transfer coefficient for transport across the air-boundary layer ( $U_{ABL}$ ) and  $Kpa$  ( $0.22 < S < 0.83$ ). Being a local sensitivity analysis (i.e., one parameter varied a little at a time), the effort presented here did not allow capturing, for example, the effect of the interactions between parameters (Augusiak et al., 2014); however, it helped in the identification of the crucial input parameters (e.g., emission, LA compartment characteristics, physical-chemical properties) to which particular attention should be paid in order to obtain accurate results.

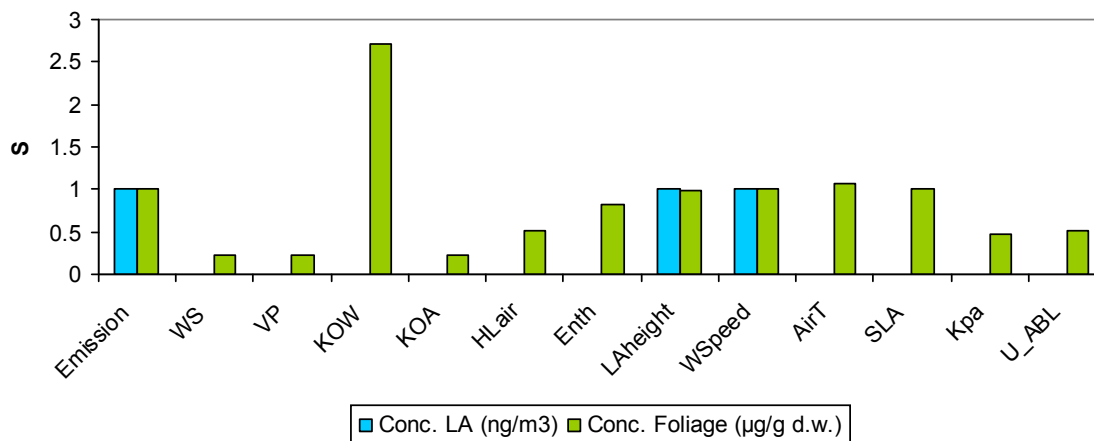


**Figure 3 - Results of the sensitivity analysis for the two target parameters (pyrene concentrations in LA,  $\text{ng/m}^3$ , and leaves,  $\mu\text{g/g d.w.}$ ). Only the most influential input parameters ( $S > 10^{-2}$ ) were reported in the chart: emission ( $\text{mol/h}$ ), water solubility ( $WS$ ,  $\text{g/m}^3$ ), vapour pressure ( $VP$ ,  $\text{Pa}$ ), octanol-water partition coefficient ( $K_{OW}$ ), octanol-air partition coefficient ( $K_{OA}$ ), half-life in air and foliage, ( $HLair$ ,  $\text{d}$ ), enthalpy of phase change between plant and air ( $Enth$ ,  $\text{J/mol}$ ), LA height (m) and wind speed ( $\text{m/s}$ ), air temperature ( $AirT$ ,  $^{\circ}\text{C}$ ), SLA ( $\text{m}^2/\text{g}$ ), plant-air partition coefficient ( $Kpa$ ,  $\text{m}^3/\text{g}$ ), and mass transfer coefficient for transport across the air-boundary layer ( $U_{ABL}$ ,  $\text{m/h}$ ). For all other parameters and corresponding  $S$  values see Table SI-10.**

### 3.2 Model evaluation

The SoilPlusVeg evaluation was performed running whole year simulation for phenanthrene, pyrene and chrysene, using the meteorological and emission scenario described in section 2.3. The results of the comparison for a three-month period (March, 15 - June, 7) in which measured concentrations were available are shown in **Figure 4**. **Figure SI-7** shows the comparison between measured and predicted concentrations at the time of sampling (h 11).

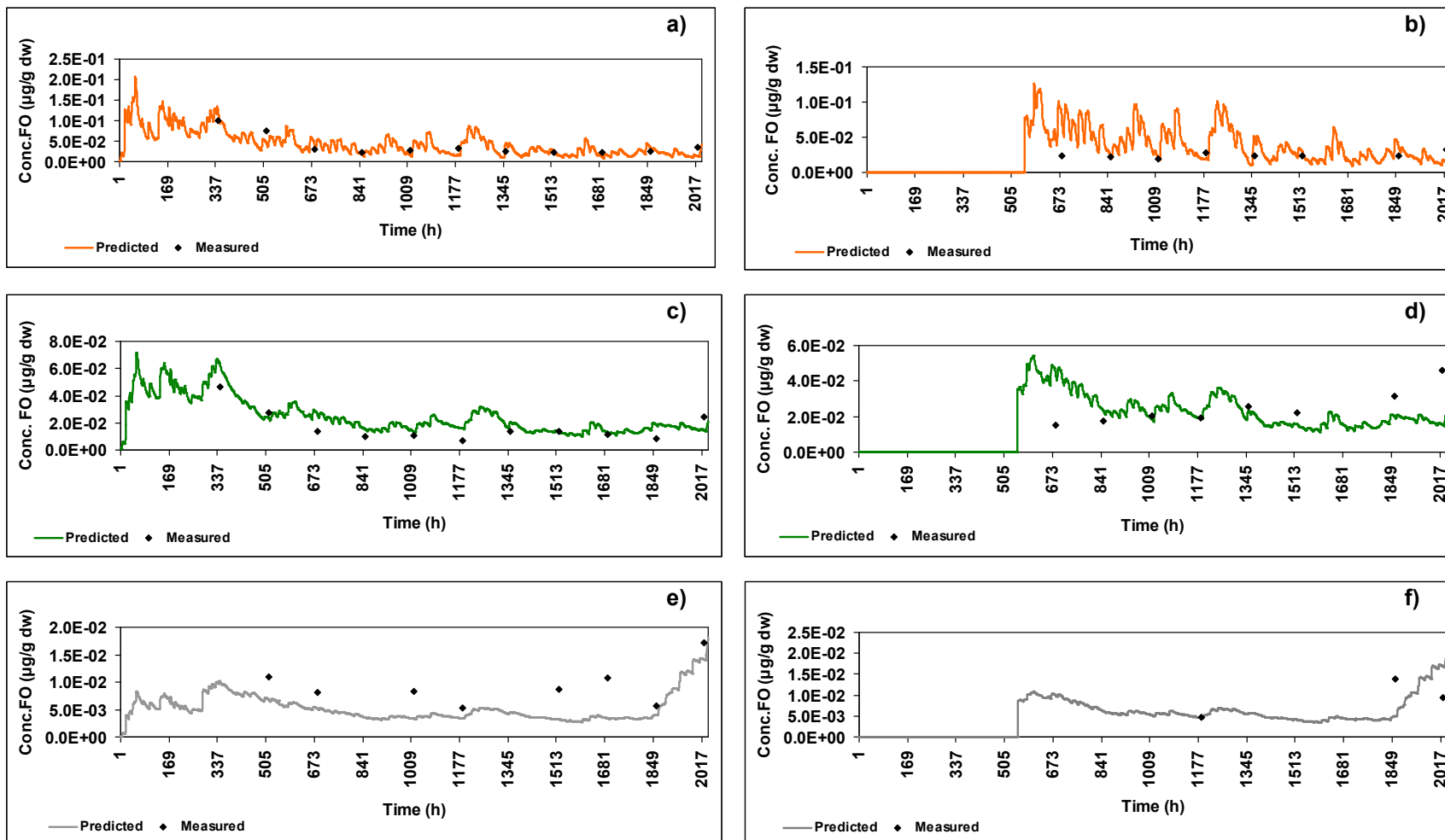


Figure 4 - Comparison between predicted (solid line) and measured (marker) concentrations ( $\mu\text{g/g dw}$ ) in leaves of cornel (a,c,e) and maple (b,d,f) of phenanthrene (orange), pyrene (green) and chrysene (grey)

Modelled concentrations in leaves (solid line) seem to reproduce the seasonal pattern of the measured one in which leaf concentrations decrease with time, oscillating within a small range according to air concentration trend which is influenced by chemical emission and meteorological parameters (high PBL height and solar radiation which cause chemical dilution and photo degradation). A similar trend was shown for PAHs measured in oak, ash and hazel leaves (Howsam et al., 2001) which remained within a small range during the whole growing season, deviating significantly only when air concentrations increase (due to uncontrolled burning of garden and domestic refuse). In Terzaghi et al., 2015 this leaf concentration trend was ascribed to the collection of different aged leaves and PAH volatilization/degradation from/on leaf surface enhanced by temperature increase. At the moment, SoilPlusVeg does not consider the possibility of production of new leaves during the growing season. However, the performed simulations show that the role of the timing of budburst and production of new leaves during the growing season is less relevant with respect to PAH source and meteorological parameters in influencing leaf concentrations.

Model results show a satisfying agreement (within a factor about 3) with measured data, considering both plant species (cornel and maple) and all three chemicals. Over- and underestimation of measured data could be ascribed to local oscillation in chemical emission and meteorological scenario (PBL height and wind speed). Other factors that could be taken into account are: 1) the presence of other species in the wood that were not considered in model parameterization; 2) the species fraction which was assumed constant over time; 3) chemical half life in leaves does not vary between day and night even if photolysis is one of the major transformation processes for PAHs in the environment (Wang et al., 2005); 4) the temperature data used to update plant/air partition coefficient are those of air and not of leaf surface.

In general predicted concentrations for cornel better reproduce the measured concentration trend, as demonstrated by the calculated efficiency factors (EF) (**Table SI-11**). This probably depends to species-specific features that are not considered in SoilPlusVeg. Cornel measured concentrations (phe and pyr) do not show an increasing trend with time as for maple. Maple behavior might be better described by a two-compartment uptake model: a thin surface that rapidly reaches equilibrium and exchange contaminants with air, and a larger internal compartment that slowly accumulates the contaminant with time. Although in SoilPlusVeg model the D value for absorption to leaves consider both the transport across the air-boundary layer and the diffusion into the cutin, leaves are still considered a single compartment.

The largest discrepancy where observed for chrysene in cornel leaves. This is probably due to the fact that particle phase chrysene predicted in air by SoilPlusVeg is a factor of 2 to 5 higher with respect to the measured value, causing an underestimation of leaf concentrations. In the present version, SoilPlusVeg does not include a mass balance for air particles, but particulate matter is considered an air sub-compartment having equal fugacity. This might be responsible of the overestimation of air particle associated chrysene. Furthermore a simplistic description of particle-leaf interaction is adopted, without considering, for example, the processes of particle encapsulation in leaves and particle erosion (Terzaghi et al., 2013).

**Table SI-12** summarizes min, max, mean and median input and output fluxes to/from leaves for the three selected chemicals. Absorption followed by volatilization and degradation are the most important fluxes when considering phenanthrene and pyrene. Dry particle and wet particle deposition are relevant for chrysene being a particle associated PAH. In order to evaluate how the variability of meteorological parameters can influence the uptake/release of PAHs by plants and therefore air concentrations, a three-day period (April, 11 – April, 13) was chosen. Air and leaf concentrations (of phenanthrene and

chrysene), PBL height and chemical emission trend during the selected period are depicted in **Figure SI-8**, while input/output fluxes in/from leaves are reported in **Figure 5**.

Predicted concentrations in leaves follow air concentration changes caused by the variability of PBL height and chemical emission. In general air concentrations are higher during nighttime hours when PBL is low and chemical emission is still high (e.g. from 17 to 22 h of 11 April). On the contrary, during nighttime hours characterized by lower emission (e.g. from 1 to 6 h of 12 April) PBL influence is less evident. During daytime hours, despite the elevated chemical emission, the higher PBL height causes a dilution of chemical in air resulting in lower concentrations.

Phenanthrene modeled concentrations show larger oscillations in leaves than chrysene due to their different physical and chemical properties. Phenanthrene in leaves was shown to take only few hours to reach equilibrium with air, while chrysene needs more time (days) (Terzaghi et al., submitted). This depends on its higher Log  $K_{OA}$  which reduces its uptake rate. Leaves were shown to behave as a dynamic compartment contributing to the diurnal variation of organic contaminant concentrations, which deposit or volatilize from their surface in response to environmental conditions changes (Hornbuckle et al., 1996; Hung et al., 2001; Gouin et al., 2002). The air-leaf surface exchange is believed to be the major short-term source and sink of many persistent organic compounds (Hornbuckle et al., 1996).

In general, for both simulated chemicals, a higher air-foilage flux (absorption) can be observed during hours characterized by low PBL height (which increases air concentrations) and low temperature (which increases plant-air partition coefficient,  $K_{PA}$ ). As appears from **Figure 5**, during some hours, volatilization flux exceeds absorption indicating that leaves can act not only as a "filter" but also as "dispenser" of air contaminants, depending on meteorological conditions. Chemical release from leaves could happen both during daytime hours (driven by temperature mediated volatilization together with

chemical gradient inversion caused by the increase of PBL height) and during some nighttime hours (caused by the emission reduction and therefore chemical gradient inversion). **Table SI-13** and **Table SI-14** summarize hourly values (of April, 11 and April, 12) of absorption and volatilization fluxes, temperature, PBL height, emission and air and leaf concentrations for phenanthrene and chrysene.

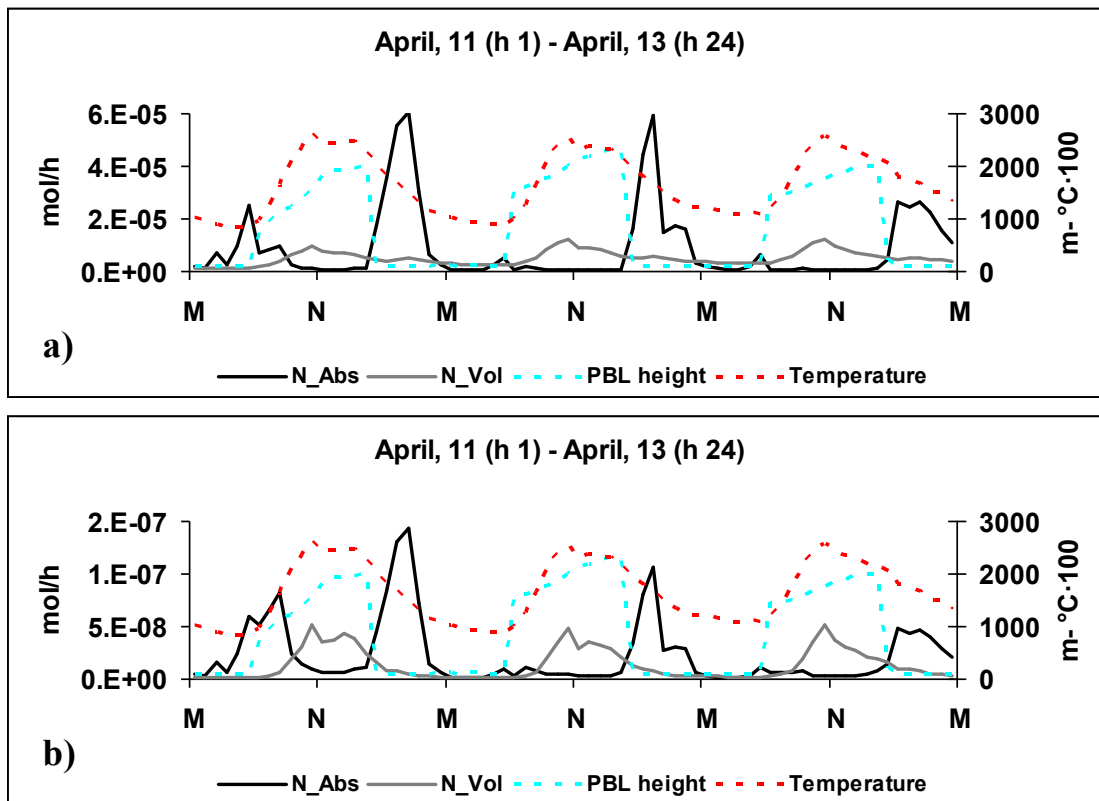


Figure 5 - Absorption (solid black line) and volatilization (solid grey line) fluxes, temperature (dotted red line) and PBL height (dotted light blue line) trend during a three-day period (April, 11 – April, 13) for phenanthrene (a) and chrysene (b). Please not that for illustration purposes temperature values was multiplied for a factor of 100. “M” means midnight while “N” stands for noon.

A comparison between air concentrations predicted without (“ConcLANoVeg”) and with vegetation compartment (“ConcLAVeg”) was made in order to evaluate the influence of the simulated wood in reducing/increasing air concentration through chemical absorption and volatilization. Vegetation biomass, as already highlighted in the sensitivity analysis section, shows a low influence on atmospheric concentration with delta between “ConcLANoVeg” and “ConcLAVeg” ranging from -2.86 to 2.96 for phenanthrene, from -1.69 to 2.90 for pyrene and from -0.32 to 2.08 for chrysene. In the following section the causes of this low vegetation effect in sequestering chemicals from air is investigated.

### 3.3 Model illustration

In and around forest canopy, wind velocity is reduced and the profile is altered, therefore “wind attenuation factors” should be adopted when performing simulations with models that include a vegetation compartment. Larcher, 2003 shows that on a surface covered by tree, wind can be 20% to 80% of the wind measured over a tree less area.

In order to show the influence of the vegetation in filtering chemicals from air at different wind velocities, an illustration was performed for two polychlorinated biphenyls of different physical and chemical properties (**Table SI-15**): PCB 52 and PCB 153. The dynamic simulations in low-wind conditions were performed assuming the same LA and UA heights adopted in the reference scenario described in section 2.3, but decreasing wind speed by a factor of 2 and 5, according to the average and minimum wind attenuation factors reported in Larcher, 2003. Despite such low wind speed values are not related to the computed UA and LA heights, they were adopted with the only aim of investigating the role of air residence time and vegetation biomass in determining chemical atmospheric concentrations. Chemical and PM sources to the system were assumed in order to obtain realistic PCB air concentrations.

The difference ( $\Delta\%$ ) of PCB air concentrations predicted without vegetation and considering this compartment, adopting different wind speed (reference wind, “WindRef”; wind attenuated of a factor of 2, “Wind50%”; wind attenuated of a factor of 5, “Wind20%”) are depicted in **Figure 6**. Positive  $\Delta\%$  represent hours when vegetation uptakes contaminants from air, while negative  $\Delta\%$  represent hours when vegetation releases contaminants to air.

For both chemicals, wind reduction resulted in a higher capability of plant to reduce air concentrations. Maximum positive  $\Delta\%$  increases from 3% to 12% for PCBs 52 and, from 3% to 11% for PCB 153. Maximum negative  $\Delta\%$  increases from -1.2% to -6% for PCBs 52 and, from -1.6% to -7% for PCB 153. This is mainly due to the increase of average air residence time from  $\sim 65$  sec with the “RefWind” scenario to  $\sim 6$  min with “Wind20%” scenario.

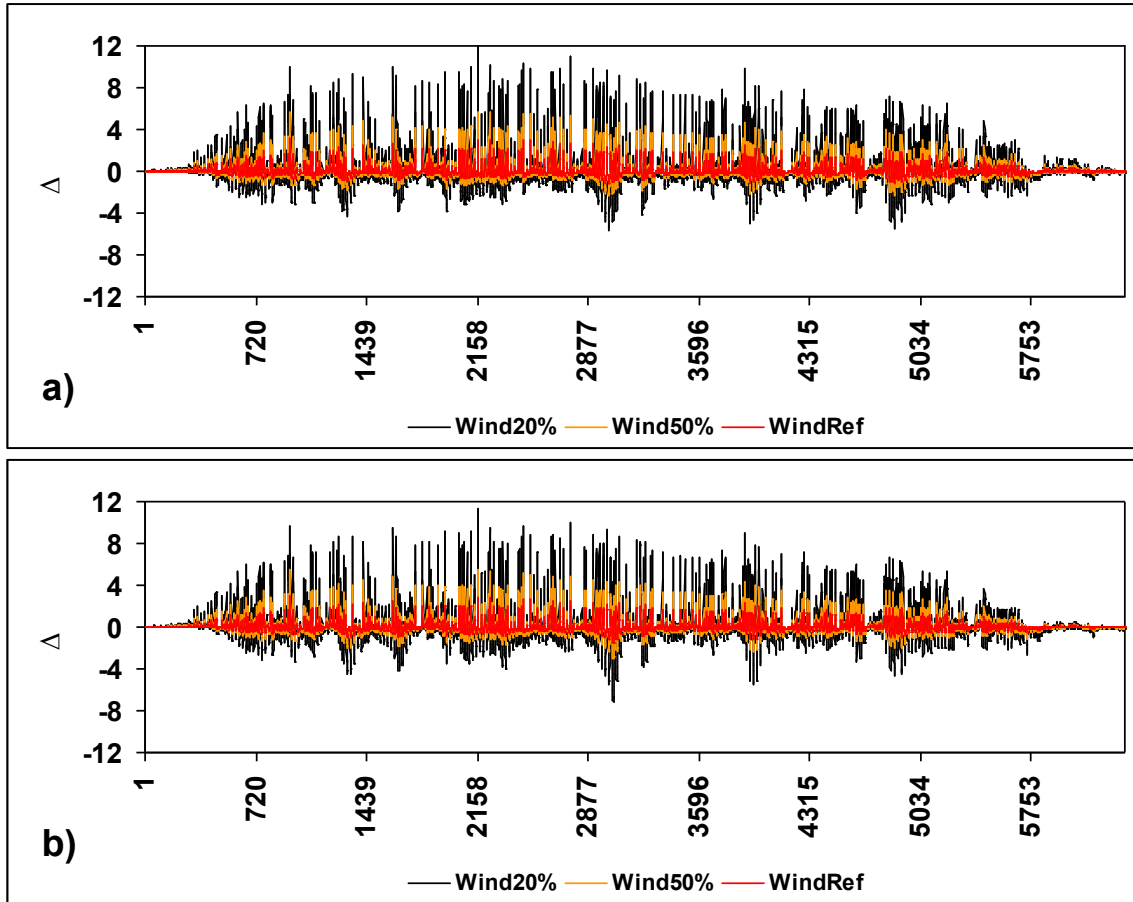


**Figure 6- Difference ( $\Delta\%$ ) of PCB (a, PCB52; b) PCB 153) air concentrations predicted without vegetation and considering this compartment, adopting different wind speed (reference wind, “WindRef”; wind attenuated of a factor of 2, “Wind50%”; wind attenuated of a factor of 5, “Wind20%”).**

However, results obtained with the higher wind speed, underestimate that reported in Jaward et al., 2005, in which the forest filter effect was evaluated measuring PCB air concentrations in forest and in the near clearing employing PUF disk. In the broadleaf forest located at 1100 m, comparable in composition to that simulated here, PUF sequestered amount (and therefore air concentrations) experienced a reduction of 34% and 47% for PCB 52 and PCB 153 respectively, with respect to the clearing site.

Another important factor that could influence air residence time is the model domain. Previously simulations (included those of model evaluation) were performed considering a soil surface of 1 ha, since the modeled vegetation was more representative of an “urban small wood” rather than a forest. Using this type of domain resulted in lower air residence time again. Therefore in order to show the influence of the vegetation in filtering chemicals from air considering different model domain (1 ha, “urban wood” and 100 ha, “forest”) an illustration was performed for PCB 52 and PCB 153 using the “Wind20%” scenario. The difference ( $\Delta\%$ ) of PCB air concentrations predicted without vegetation and considering this compartment, adopting a different model domain and wind speed attenuated of a factor of 5 are depicted in **Figure 7**. For both chemicals, model domain increase resulted in a higher capability of plant to reduce air concentrations. Maximum positive  $\Delta\%$  increases from 12% to 40% for PCBs 52 and, from 11% to 42% for PCB 153. Maximum negative  $\Delta\%$  increases from -6 % to - 37% for PCBs 52 and, from -7% to -47% for PCB 153. This is mainly due to the increase of average air residence time from ~ 6 min with the “1ha” scenario to 1 h with the “100 ha” scenario.

This illustration provides information on vegetation influence on air concentrations both changing wind conditions and model domain in order to increase air residence time. Vegetation resulted more important when wind was reduced to 20% and model domain was increased of one order of magnitude.

This suggests that in the future SoilPlusVeg has to be improved considering an “air canopy layer” in addition to upper air and lower air compartments, in order to take into account the influence of the presence of the vegetation on air structure and meteorological parameters.

Performed simulations helped in understanding that, during low air residence time situations, air concentrations are more influenced by chemical emission and meteorological parameters rather than by vegetation biomass.

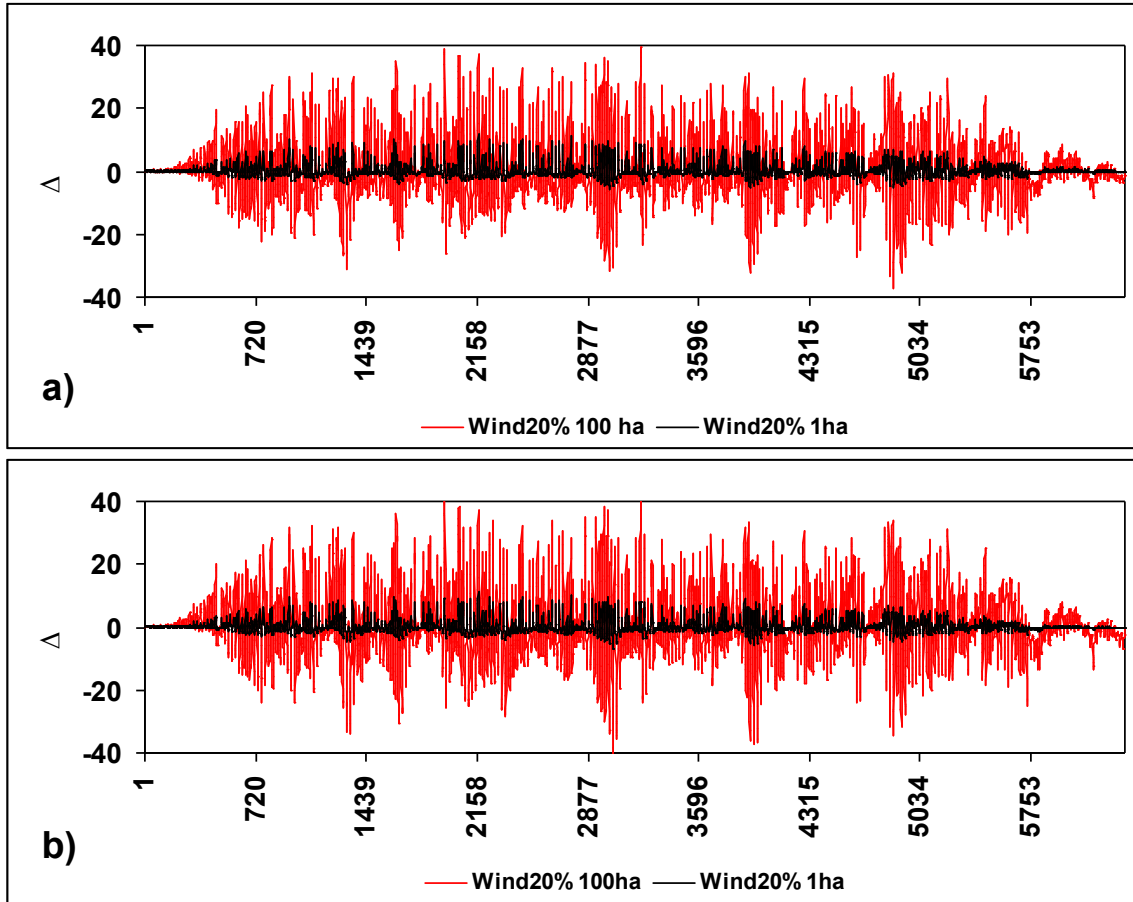


Figure 7- Difference ( $\Delta\%$ ) of PCB (a, PCB52; b) PCB 153) air concentrations predicted without vegetation and considering this compartment, adopting a different model domain (100 ha) and wind speed attenuated of a factor of 5

#### 4. ACKNOWLEDGEMENTS

Prof. Alberto Vianelli is acknowledged for its contribution about the ecophysiological aspect of this work.

## 5. REFERENCES

- ARPA, 2014. Regional Environmental Protection Agency official web site: [http://ita.arpalombardia.it/ITA/qaria/doc\\_RichiestaDati.asp](http://ita.arpalombardia.it/ITA/qaria/doc_RichiestaDati.asp). Last access on April, 2014.
- Augusiak, J., Van den Brink, P. J., Grimm, V. Merging validation and evaluation of ecological models to 'evaluation': A review of terminology and a practical approach. *Ecological Modeling* (2014), 280, 117–128
- EC, 2004. European Union System for the Evaluation of Substances 2.0 (EUSES 2.0). Prepared for the European Chemicals Bureau by the National Institute of Public Health and the Environment (RIVM), Bilthoven, The Netherlands (RIVM Report no. 601900005). Available via the European Chemicals Bureau, <http://ecb.jrc.it>.
- EC, 2013. SCHER (Scientific Committee on Health and Environmental Risks), SCENIHR (Scientific Committee on Emerging and Newly Identified Health Risks), SCCS (Scientific Committee on Consumer Safety), Addressing the New Challenges for Risk Assessment, March 2013, European Commission.
- Gale, M. R., and D. F. Grigal. Vertical root distribution of northern tree species in relation to successional status. *Canadian Journal of Forest Research* (1987), 17:829-834.
- Ghirardello D., Morselli M., Semplice M. and Di Guardo A., 2010. Dynamic model of the fate of organic chemicals in a multilayered air/soil system: development and illustrative application. *Environmental Science & Technology* (2010), 44: 9010–9017.
- Gouin, T., Thomas, G. O., Cousins, I., Barber, J., Mackay, D., Jones, K. C. Air-surface exchange of polybrominated diphenyl ethers and polychlorinated biphenyls. *Environmental Science & Technology* (2002), 36, 1426-1434.
- Hornbuckle, K. C.; Eisenreich, S. J. Dynamics of gaseous semivolatile organic compounds in a terrestrial ecosystem-effects of diurnal and seasonal climate variations. *Atmospheric Environment* (1996), 30: 3935-3945.
- Howsam M., Jones K.C., Ineson P. PAHs associated with the leaves of three deciduous tree species. *Chemosphere* (2001), 44: 155-164.

- Hung. H., Thomas, G. O., Jones, K. C., Mackay, D. Grass-air exchange of Polychlorinated Biphenyls. *Environmental Science & Technology* (2001), 35: 4066-4073.
- Jaward F.M., Di Guardo A., Nizzetto L., Cassani C., Raffaele F., Ferretti R. and Jones K. PCBs and Selected Organochlorine Compounds in Italian Mountain Air: the Influence of Altitude and Forest Ecosystem Type. *Environmental Science & Technology* (2005), 39: 3455-3463.
- Larcher W. Physiological plant ecology. 4<sup>th</sup> ed. Berlin: Springer; 2003.
- Mackay D., 2001. Multimedia environmental models: the fugacity approach (second edition). Lewis publisher, Boca Raton.
- MacLeod M., Woodfine D.G., Mackay D., McKone T., Bennet D.; Maddalena R. BETR North America: A regionally segmented multimedia contaminant fate model for North America. *Environmental Science & Pollution Research* (2001), 8: 156 – 163.
- MacLeod, M., Fraser, A.J., Mackay, D. Evaluating and expressing the propagation of uncertainty in chemical fate and bioaccumulation models. *Environmental Toxicology and Chemistry* (2002), 21: 700–709.
- Morselli M., Ghirardello D., Semplice M. and Di Guardo A. Modeling short-term variability of semivolatile organic chemicals in air at a local scale: an integrated modeling approach. *Environmental pollution* (2011), 159:1406-1412.
- Morselli M., Ghirardello D., Semplice M., Raspa G. and Di Guardo. Integration of an atmospheric dispersion model with a dynamic multimedia fate model: development and illustration. *Environmental Pollution* (2012), 164: 182 -187.
- Semplice M., Ghirardello D., Morselli M, Di Guardo A., 2011. Guidance on the selection of efficient computational methods for multimedia fate models. *Environmental Science & Technology* (2012), 46: 1616–1623.
- Terzaghi E., Wild E., Zacchello G., Cerabolini B., Jones K.C. and Di Guardo A. Forest Filter Effect: Role of leaves in capturing/releasing air particulate matter and its associated PAHs. *Atmospheric Environment* (2013), 74: 378-384.

- Terzaghi E., Zacchello G., Scacchi M., Raspa G., Jones K.C., Cerabolini B., Di Guardo A. Towards more ecologically realistic scenarios of plant uptake modelling for chemicals: PAHs in a small forest. *Science of the Total Environment* (2015), 505: 329-337.
- Terzaghi E., Scacchi M., Cerabolini B., Jones K.C., Di Guardo A. Estimation of PAH variability in air using high volume, film and vegetation as samplers. Submitted to *Science of the Total Environment*.
- Udemann E, Czub G, McLachlan MS. Addressing temporal variability when modeling bioaccumulation in plants. *Environmental Science & Technology* (2009); 43: 3751-3756.
- Wang D., Chen J., Xu Z., Qiao X., Huang L. Disappearance of polycyclic aromatic hydrocarbons sorbed on surfaces of pine [*Pinus thunbergii*] needles under irradiation of sunlight: volatilization and photolysis. *Atmospheric Environment* (2005), 39: 4583 – 4591.
- Zhang Q., Crittenden J. C., Shonnard D., Mihelcic J. R. Development and evaluation of an environmental multimedia fate model CHEMGL for the Great Lakes region. *Chemosphere* (2003), 50: 1377-1397.

## Chapter 8. Paper VII

Supporting information for

# Modelling the temporal uptake of semi-volatile organic chemicals in plants using an ecologically realistic scenario

Elisa Terzaghi<sup>a</sup>, Melissa Morselli<sup>a</sup>, Matteo Semplice<sup>b</sup>, Bruno Cerabolini<sup>c</sup>, Kevin C. Jones<sup>d</sup> and Antonio di Guardo<sup>a\*</sup>

<sup>a</sup>Department of Science and High Technology, University of Insubria, Via Valleggio 11, 22100 Como, Italy

<sup>b</sup>Department of Mathematics, University of Turin, Via C. Alberto 10, 10123 Torino TO, Italy

<sup>c</sup>Department of Theoretical and Applied Sciences, University of Insubria, Via J. H. Dunant 3, 21100 Varese, Italy

<sup>d</sup>Lancaster Environment Centre, Lancaster University, Lancaster LA1 4YQ, UK

\*Corresponding author

*Draft to be submitted to Environmental Science & Technology*



# Modelling the temporal uptake of semi-volatile organic chemicals in plants using an ecologically realistic scenario

Terzaghi Elisa<sup>a</sup>, Morselli Melissa<sup>a</sup>, Matteo Semplice<sup>b</sup>, Cerabolini Bruno<sup>c</sup>, Kevin Jones<sup>d</sup>, Di Guardo Antonio<sup>a\*</sup>

<sup>a</sup>Department of Science and High Technology, University of Insubria, Via Valleggio 11, 22100 Como, Italy

<sup>b</sup>Department of Mathematics, University of Turin, Via C. Alberto 10, 10123 Torino TO, Italy

<sup>c</sup>Department of Theoretical and Applied Sciences, University of Insubria, Via J. H. Dunant 3, 21100 Varese, Italy

<sup>d</sup>Lancaster Environment Centre, Lancaster University, Lancaster LA1 4YQ, UK

<b>Text SI-1 MODEL PARAMETERIZATION.....</b>	<b>3</b>
A) Z values.....	3
B) Density.....	7
C) Wood composition.....	8
D) Biomass.....	9
E) Volume.....	11
F) Index of rooting distribution.....	13
G) Ecological parameters.....	14
H) D values.....	16
<b>Text SI-2 MASS BALANCE EQUATIONS.....</b>	<b>26</b>
<b>Text SI-3 PHYSICAL-CHEMICAL PROPERTIES OF SELECTED PAHs.....</b>	<b>27</b>
<b>Text SI-4 EMISSION SCENARIO FOR THE SoilPlusVeg EVALUATION.....</b>	<b>28</b>
<b>Text SI-5 SENSITIVITY ANALYSIS RESULTS.....</b>	<b>30</b>
<b>Text SI-6 MODEL EVALUATION RESULTS.....</b>	<b>31</b>

---

\* Corresponding author: Department of Science and High Technology, University of Insubria, Via Valleggio 11, 22100 Como, Italy; Tel.: +39 031 238 6480; Fax: +39 031 2386449; E-mail address [antonio.diguardo@uninsubria.it](mailto:antonio.diguardo@uninsubria.it) (A. Di Guardo)

A) Concentrations.....	31
B) Efficiency Factors.....	32
B) Fluxes.....	33
C) Short-term variability.....	34
<b>Text SI-7 PHYSICAL-CHEMICAL PROPERTIES OF SELECTED PCBs.....</b>	<b>37</b>

## SI-1 MODEL PARAMETERIZATION

### SI-1A) Z values

This section reported the equations employed to calculate Z values for roots, stem and leaves.

#### Roots

Fugacity capacity of roots ( $Z_R$ ) was calculated as reported in Calamari et al., 1987:

$$Z_R = RCF \cdot \rho_R / H \quad \text{Eq.S1}$$

where RCF is the Root Concentration Factor (L/kg),  $\rho_R$  is the root density (kg/L) and H is the Henry's law Constant ( $\text{Pa} \cdot \text{m}^3/\text{mol}$ ).

Density of roots is assumed being equal to 0.180 kg/L and RCF was calculated according to Briggs et al., 1982:

$$\text{Log}(RCF - 0.82) = 0.77 \cdot \text{Log} K_{OW} - 1.52 \quad \text{Eq.S2}$$

$$RCF = \left(10^{[0.77 \cdot \text{Log} K_{OW} - 1.52]} + 0.82\right) \quad \text{Eq.S3}$$

#### Stem

Fugacity capacity of stem ( $Z_{St}$ ) was calculated as reported in Calamari et al., 1987:

$$Z_{St} = SCF \cdot \rho_{St} / H \quad \text{Eq.S4}$$

where SCF is the Stem Concentration Factor (L/kg),  $\rho_{St}$  is the stem density (kg/L), H is the Henry Law Constant ( $\text{Pa} \cdot \text{m}^3/\text{mol}$ ).

Density of stem was assumed being equal to 0.590 kg/L and SCF was calculated according to Briggs et al., 1983:

$$SCF = K_{stem / xylem\_sap} \cdot TSCF \quad \text{Eq.S5}$$

where  $K_{stem/xylem\_sap}$  is the stem/xylem sap partition coefficient (SCXF) and TSCF is the transpiration stream concentration factor. Considering that:

$$\text{Log} (K_{stem / xylem\_sap} - 0.82) = 0.95 \cdot \text{Log} K_{OW} - 2.05 \quad \text{Eq.S6}$$

$$TSCF = 0.784 \cdot \text{Exp} - \left[ \frac{(\text{Log} K_{OW} - 1.78)^2}{2.44} \right] \quad \text{Eq.S7}$$

SCF resulted in:

$$SCF = \left( 10^{[0.95 \cdot \text{Log} K_{OW} - 2.05]} + 0.82 \right) \cdot 0.784 \cdot \text{Exp} - \left[ \frac{(\text{Log} K_{OW} - 1.78)^2}{2.44} \right] \quad \text{Eq.S8}$$

## Foliage

Fugacity capacity of foliage ( $Z_F$ ) was calculated as reported in Wania and McLachlan, 2001 :

$$Z_F = K_{PA} \cdot Z_A \quad \text{Eq.S9}$$

Where  $K_{PA}$  is the dimensionless plant/air partition coefficient on a volume/volume basis ( $\text{mol} \cdot \text{m}^3 / \text{mol} \cdot \text{m}^3$ ) and  $Z_A$  is the fugacity capacity of air ( $\text{mol} / \text{m}^3 \cdot \text{Pa}$ ).

Considering that  $Z_A = 1/RT$ , where R is the gas constant ( $\text{Pa} \cdot \text{m}^3 / \text{mol} \cdot \text{K}$ ) and T is the temperature (K):

$$Z_F = K_{PA} / RT \quad \text{Eq.S10}$$

The plant/ air partition coefficient (25°C) was determined for each species that composed the wood (cornel, hazelnut, maple), using the relationship reported in Nizzetto et al, 2008:

$$\text{Log } K_{PA} = y_0 + a \cdot \text{Log } K_{OA} \quad \text{Eq.S11}$$

where  $\text{Log } K_{PA}$  is the plant/air partition coefficient on a mass/volume basis ((pg g<sup>-1</sup> of dry leaf)/(pg m<sup>-3</sup> of air)),  $\text{Log } K_{OA}$  is the octanol/air partition coefficient (25°C),  $y_0$  and  $a$  are the regression parameters (**Table SI-1**).

In order to obtain a dimensionless plant/air partition coefficient as in Wania and McLachlan, 2001, it was necessary to include foliage leaf density  $\rho_F$  (g/m<sup>3</sup>):

$$Z_F = K_{PA} \cdot \rho_F / RT \quad \text{Eq.S12}$$

In order to obtain a bulk  $Z$  values for the whole canopy it was necessary to determine a canopy/air partition coefficient  $K_{CA}$  as follows:

$$K_{CA} = \sum_{i=1}^n f_i \cdot K_{PAi} \quad \text{Eq.S13}$$

where  $K_{PAi}$  is the plant/air partition coefficient for the  $i$ -species and  $f_i$  is the volume contribution of the  $i$ -species to the volume of the total canopy (see **SI-1C** for more details).

The bulk  $Z$  value for the whole canopy was given by:

$$Z_{F\_bulk} = K_{CA} \cdot \rho_C / RT \quad \text{Eq.S14}$$

where  $\rho_C$  is the density of the foliage of the whole canopy calculated as reported in **SI-1B**.

Since  $K_{PA}$  is influenced by the temperature, it was updated with the air temperature following the approach of Komp and McLachlan, 1997:

$$\frac{K_{PA}}{K_{PA0}} = \text{Exp} \left[ \left( \frac{1}{T} - \frac{1}{T_0} \right) \cdot \frac{\Delta H_{PA}}{R} \right] \quad \text{Eq.S15}$$

where  $T_0$  is the ambient temperature (273.15 K),  $T$  is a reference temperature (K),  $R$  is the gas constant (kJ/mol K), and  $\Delta H_{PA}$  is the enthalpy of phase change between the plant and the air (kJ/ mol),  $K_{PA0}$  is the plant /air partition coefficient at the ambient temperature and  $K_{PA}$  is the plant /air partition coefficient at the reference temperature.

**Table SI-1 Parameters of the  $K_{PA}$  equation**

<b>Plant species</b>	<b><math>y_0</math></b>	<b><math>a</math></b>
<b>Cornel</b>	-3.10	0.49
<b>Hazelnut</b>	-2.12	0.38
<b>Maple</b>	-3.08	0.49

Please note that since values for cornel were not available, those of white ash reported in Nizzetto et al., 2008 were used.

## SI-1B) Density

**Table SI-2** summarizes density values of roots and stem used to parameterized the wood.

**Table SI-2 Root and stem density values**

Compartment	Density (kg/L dw)	References	Notes
Roots	0.180	Comas and Eissenstat, 2004	Mean of 25 woody-species
Stem	0.590	Gabauer et al., 2008	<i>Acer pseudoplatanus</i>

For leaves, values reported in Terzaghi et al., 2015 were used to calculate the canopy density as follows:

$$\rho_C = \sum_{i=1}^n f_i \cdot \rho_i \quad \text{Eq.S16}$$

where  $\rho_i$  is the density for the  $i$ -species and  $f_i$  is the volume contribution of the  $i$ -species to the volume of the total canopy (see **SI-1C** for more details). As shown by Terzaghi et al., 2015, leaf density increases with time. **Table SI-3** summarizes min and max leaf density value for each species and for the canopy. Max values are in agreement with those shown in Castro-Diez et al., 2000).

**Table SI-3 Leaf density values**

<b>Compartment</b>	<b>Min <math>\rho</math> (kg/L dw)</b>	<b>Max <math>\rho</math> (kg/L dw)</b>
Cornel	0.201	0.255
Hazelnut	0.236	0.320
Maple	0.155	0.285
Canopy	0.222	0.286

### SI-1C) Wood composition

The fraction of each plant species that composed the wood at each time during the growing season are summarized in **Table SI-4** and are calculated as reported in Terzaghi et al., 2015. Bud burst occurs on March, 15 for the two under storey species (cornel and hazelnut), while maple leaves appear about 3 weeks later on April, 7.

**Table SI-4 Wood composition during the simulation period (March, 15 – June, 07)**

<b>Period</b>	<b>frac cornel</b>	<b>frac hazelnut</b>	<b>frac maple</b>
<b>15 March-06 April</b>	41%	59%	0%
<b>07 April – 07 June</b>	16%	36%	48%

### SI-1D) Biomass

Root biomass of the simulated wood was assumed to be equal to the root biomass of a temperate deciduous forest reported in Jackson et al., (1997): 42000 kg/ha.

In order to estimate a stem biomass value to be used to simulate the broadleaf wood, root biomass value was divided by the root/shoot ratio reported in Jackson et al. (1996) equal to 0.23, obtaining a stem biomass of about 183000 kg/ha. As shoot includes both stem and leaves, in order to obtain stem biomass values, leaf biomass (max: 1185 kg/ha) has to be subtracted to shoot biomass resulting in 181424 kg/ha.

Roots and stem biomass were assumed not to change during the simulation period but they were considered constant over time.

Foliage biomass was calculated as the ratio of two ecological parameters (see SI-1G), LAI (Leaf Area Index) and SLA (Specific Leaf Area) reported in Terzaghi et al., 2015:

$$B = \frac{LAI}{SLA_C} \quad \text{Eq.S17}$$

where B is the leaf biomass (g/m<sup>2</sup>), LAI is the Leaf Area Index (m<sup>2</sup>/m<sup>2</sup>) and SLA<sub>C</sub> is the mean Specific Leaf Area of the canopy (m<sup>2</sup>/g).

SLA of the canopy was calculated as follows:

$$SLA_C = \sum_{i=1}^n f_i SLA_i \quad \text{Eq.S18}$$

where SLA<sub>i</sub> is the SLA for the *i*-species and *f<sub>i</sub>* is the volume contribution of the *i*-species to the volume of the total canopy (see SI-1C for more details).

While root and stem biomass for a standing forest can be considered relatively constant, foliage biomass varied during the simulation period. The trend of the foliage biomass obtained is reported in **Figure SI-1**.

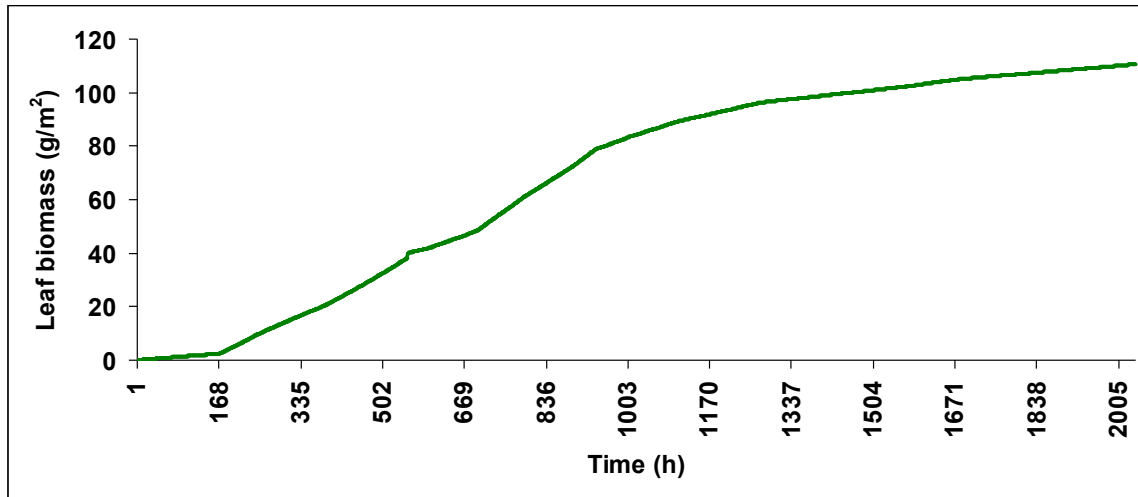


**Figure SI-1** Leaf biomass temporal trend during the simulation period (March, 15 – June, 07)

**Table SI-5** summarizes biomass values for each plant compartment.

**Table SI-5** Root, stem, leaf biomass values

<b>Compartment</b>	<b>Biomass (kg/ha dw)</b>
Roots	42000
Stem	181424
Leaves	dynamic

### SI-1E) Volume

Foliage volume was calculated according to Cousins and Mackay, 2000 as follows:

$$V_F = \frac{B_F}{\rho_F} \cdot A_S \quad \text{Eq.S19}$$

where  $V_F$  is the foliage volume ( $\text{m}^3$ ),  $B_F$  is the foliage biomass ( $\text{g}/\text{m}^2$ ),  $A_S$  is the soil surface ( $\text{m}^2$ ) and  $\rho_F$  is the foliage density ( $\text{g}/\text{m}^3$ ).

**Figure SI-2** shows foliage volume calculated considering a soil surface of  $10000 \text{ m}^2$ , the dynamic leaf density (**SI1-B**) and the trend of foliage biomass shown in **Figure SI-1**.

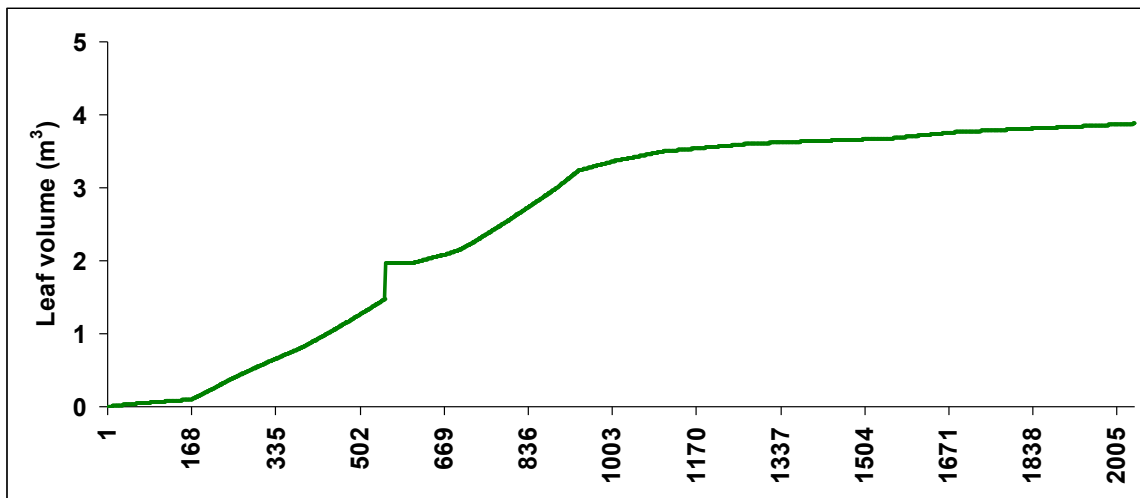


**Figure SI-2** Leaf volume temporal trend during the simulation period (March, 15 – June, 07)

Root and stem volume was calculated using the same equation. Table **SI-6** shows the results of the root and stem volume calculated assuming a root and a stem density of  $180 \text{ kg}/\text{m}^3$  and  $590 \text{ kg}/\text{m}^3$  respectively, soil surface of  $10000 \text{ m}^2$  and a root and a stem biomass of  $4.2 \text{ kg}/\text{m}^2$  and  $18.14 \text{ kg}/\text{m}^2$  respectively.

**Table SI-6 Root, stem and leaf volume**

<b>Compartment</b>	<b>Volume (m<sup>3</sup>)</b>
<b>Roots</b>	233
<b>Stem</b>	308
<b>Foliage</b>	Dynamic

### SI-1F) Index of rooting distribution

In order to distribute root volume in each soil layers, considering the rooting distribution in soil, the Gale and Grigal (1987) model was chosen. This is a model of vertical root distribution based on the following asymptotic equation:

$$y = 1 - \beta^d \quad \text{Eq.S20}$$

where  $y$  is the cumulative root fraction (a proportion between 0 and 1), from the soil surface to depth  $d$  (cm), and  $\beta$  is extinction coefficient which provides a simple numerical index of rooting distribution. High  $\beta$  values (e.g. 0.98) correspond to greater proportion of roots at depth and low  $\beta$  values (e.g. 0.92) imply a greater proportional of roots near the soil surface. Jackson et al. (1996) suggested a  $\beta$  values and a percentage of roots in the upper 30 cm of soil for a temperate deciduous forest equal to 0.966 and 65% respectively. **Figure SI-3** shows cumulative proportion root distribution as a function of soil depth for a temperate deciduous forest (Jackson et al., 1996).

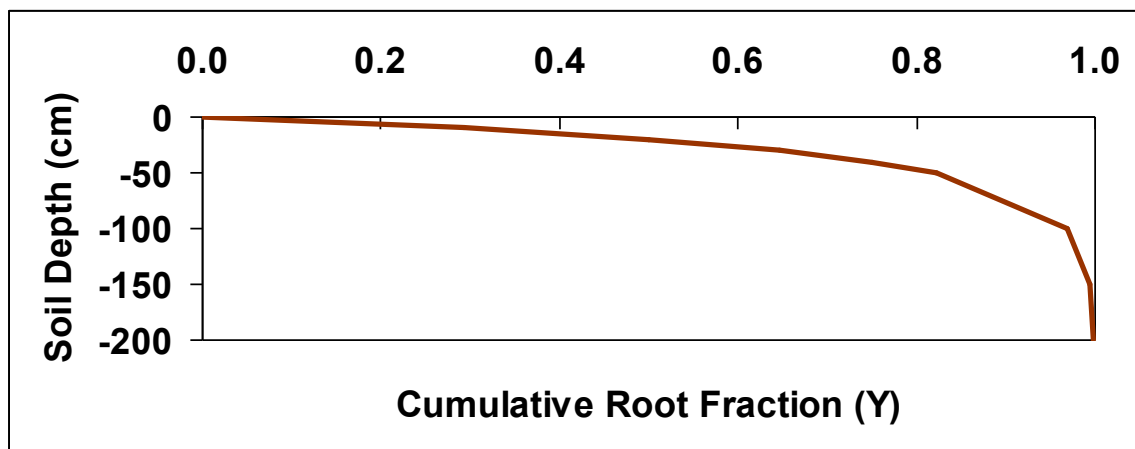


Figure SI-3 Cumulative proportion root distribution as a function of soil depth for a temperate deciduous forest (Redrawn from Jackson et al., 1996)

## SI-1G) Ecological parameters

Two ecological parameters, LAI and SLA, were used to parameterize the vegetation model. LAI is defined as the amount of leaf area ( $m^2$ ) in a canopy per unit ground area ( $m^2$ ) and can be regarded as an index of the total foliar biomass accumulating organic contaminants from the air and a measure of the density of surface available for exchange with the atmosphere. SLA expresses the amount of leaf surface per unit of dry weight ( $cm^2/g$ ) and can be considered as a measure of the surface available for organic contaminants exchange with air per units of leaf mass. These two parameters allow to calculate a dynamic foliar biomass and to predict the accumulation of organic chemicals in forests rather than in single plants. **Figure SI-4** show  $SLA_C$  and LAI trend.  $SLA_C$  was calculated as shown in **SI-1D** employing SLA of cornel, hazelnut and maple reported in Terzaghi et al., 2015. Since SoilPlusVeg requires hourly input parameters, two hourly databases (one for LAI and one for SLA) were created linearly interpolating measured data. LAI values were corrected by subtracting the first measured value relative to wood. The last measured SLA value of each species was kept constant until the end of the growing season. The hourly values of LAI and  $SLA_C$  were employed to calculate leaf hourly biomass as described in **SI-1D**. Moreover  $SLA_C$  and  $SLA_{stable}$  (SLA values at full development of leaves equal to  $\sim 291 cm^2/g$ ) were used to correct the  $K_{CA}$  in order to take into account the different capability of leaves to uptake contaminants from air depending to their SLA value which change over the growing season (Terzaghi et al., 2015):

$$K_{CA_{SLA}} = K_{CA} \cdot \frac{SLA_C}{SLA_{stable}} \quad \text{Eq.S21}$$

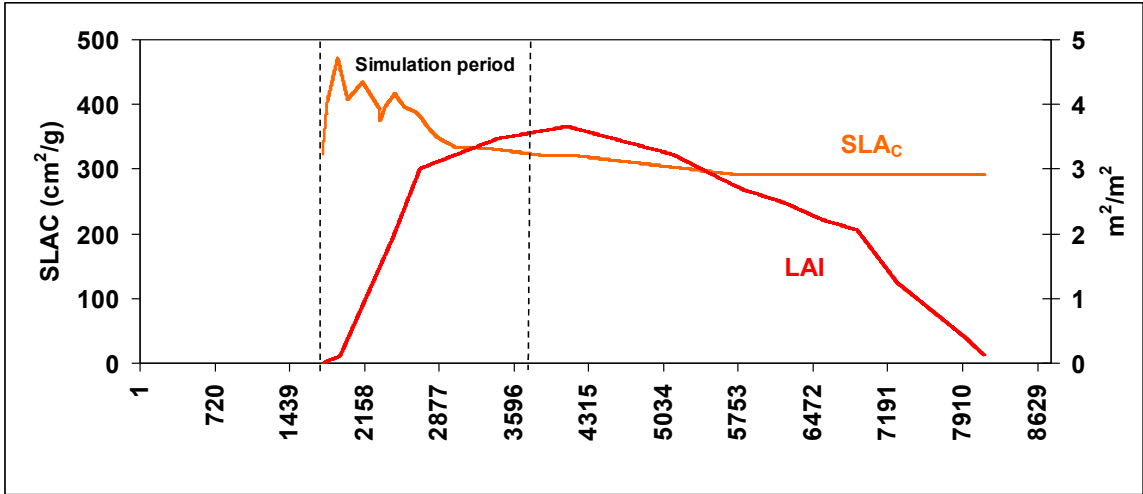


Figure SI-4 SLAC and LAI trend. Dots lines represent the period of the year considered to perform simulation

## SI-1H) D values

In this subchapter, equations for D value determination for all the processes listed in Table SI-7 are reported.

**Table SI-7 Plant uptake model processes**

<b>Plant uptake model processes</b>	
<b>1</b>	Dry gaseous deposition to foliage (absorption)
<b>2</b>	Volatilization from foliage
<b>3</b>	Dry particle deposition to foliage
<b>4</b>	Wet particle deposition to foliage
<b>5</b>	Wet deposition of dissolved chemical to foliage
<b>6</b>	Wash off
<b>7</b>	Wax erosion
<b>8</b>	Litter fall
<b>9</b>	Leaf growth
<b>10</b>	Degradation in foliage
<b>11</b>	Degradation in stem
<b>12</b>	Degradation in roots
<b>13</b>	Soil to roots transfer
<b>14</b>	Roots to soil transfer
<b>15</b>	Roots to stem transfer
<b>16</b>	Stem to roots transfer
<b>17</b>	Stem to foliage transfer
<b>18</b>	Foliage to stem transfer

## 1. Dry gaseous deposition to foliage (**absorption**): $D_{AF-G}$

The overall D value for air-foliage gaseous exchange  $D_{AF-G}$  was defined as reported in Cousins and Mackay, 2001:

$$D_{AF-G} = \frac{1}{\frac{1}{D_C} + \frac{1}{D_{AB-F}}} \quad \text{Eq.S22}$$

where  $D_C$  is the D value for diffusion into the cutin (mol/Pa·h) and  $D_{AB-F}$  is the D value for the transport across the air boundary layer (mol/Pa·h).

$D_{AB-F}$  was defined as:

$$D_{AB-F} = U_{AB-F} \cdot Z_A \cdot A_S \cdot LAI \quad \text{Eq.S23}$$

where  $U_{AB-F}$  is the mass transfer coefficient for transport across the air-boundary layer (9 m/h) and  $Z_A$  is the fugacity capacity of air (mol/Pa·m<sup>3</sup>) ( $Z_A=1/RT$ ),  $A_S$  is the area of land surface (m<sup>2</sup>), LAI is the Leaf Area Index (m<sup>2</sup>/m<sup>2</sup>).

$D_C$  was defined as:

$$D_C = U_C \cdot Z_F \cdot A_S \cdot LAI \quad \text{Eq.S24}$$

where  $U_C$  is the mass transfer coefficients for transport through the cuticle (m/h) and  $Z_F$  is the fugacity capacities of foliage (mol/Pa·m<sup>3</sup>),

The mass transfer coefficient for transport through the cuticle ( $U_C$ ) was calculated as follows:

$$U_C = 3600 \cdot P_C \cdot \left( \frac{1}{K_{AW}} \right) \quad \text{Eq.S25}$$

where  $P_C$  is the permeance (m/s) and  $K_{AW}$  is the air-water partition coefficient.

$P_C$  of *Citrus aurantium* (Riederer, 1995) (Eq. S26) and *Capsicum annuum* (Trapp, 1995) (Eq. S27) leaf cuticles was calculated as follows:

$$\text{Log } P_C = 0.704 \cdot \text{Log } K_{ow} - 11.2 \quad \text{Eq.S26}$$

$$\text{Log } P_C = -3.47 - 2.79 \cdot \text{Log } MW + 0.970 \cdot \text{Log } K_{ow} \quad \text{Eq.S27}$$

An average permeance for use in the model was given by:

$$P_C(\text{average}) = \left[ \frac{P_C(\text{Citrus aurantium}) + P_C(\text{Capsicum annuum})}{2} \right] \quad \text{Eq.S28}$$

## 2. Volatilization from foliage: $D_{FLA}$

D value for volatilization from foliage  $D_{FA-G}$  was defined as reported in Cousins and Mackay, 2001:

$$D_{FA-G} = D_{AF-G} \quad \text{Eq.S29}$$

## 3. Dry particle deposition to foliage: $D_{AF-P}$

The D value for dry particle deposition  $D_{AF-P}$  was estimated as follows (Cousins and Mackay, 2001):

$$D_{AF-P} = U_{AF-P} \cdot v_{AQ} \cdot Z_Q \cdot A_S \cdot LAI \quad \text{Eq.S30}$$

Where  $U_{AF-P}$  is the dry deposition particle velocity to the vegetation canopy (5 m/h),  $v_{AQ}$  is the volume fraction of particle in air, and  $Z_Q$  is the fugacity capacity of atmospheric particles ( $\text{mol/Pa} \cdot \text{m}^3$ ) ( $Z_Q = K_{QA} Z_A$  where  $K_{QA}$  is the aerosol particle/air partition coefficient).

#### 4. Wet particle deposition to foliage: $D_{AF-Q}$

The D value for wet particle deposition to foliage  $D_{AF-Q}$  was estimated as follows (Cousins and Mackay, 2001):

$$D_{AF-Q} = U_R \cdot v_{AQ} \cdot Z_Q \cdot Q \cdot A_S \cdot FrUF \quad \text{Eq.S31}$$

where  $U_R$  is the rain rate ( $m^3/m^2 \cdot h$ ),  $Q$  is the scavenging ratio (200000) and  $FrUF$  is the fraction of precipitation that is intercepted by the canopy and evaporates.

In Cousins and Mackay, 2001 it is assumed that 90% of the precipitation falling on vegetation is washed of to the soil (i.e.  $FrUF=0.1$  for  $LAI=3$ ), therefore for the present study, a time dependent  $FrUF$  was calculated solving this proportion:

$$3:0.1 = LAI_t : X \quad \text{Eq.S32}$$

$$X = FrUF = \frac{0.1 LAI_t}{3} \quad \text{Eq.S33}$$

**Figure SI-5** shows the time dependent trend of  $FrUF$  for the simulated wood.

#### 5. Rain dissolution of dissolved chemical: $D_{AF-R}$

The D value for wet deposition of dissolved chemical to foliage  $D_{AF-R}$  was estimated as follows (Cousins and Mackay, 2001):

$$D_{AF-R} = U_R \cdot Z_W \cdot A_S \cdot FrUF \quad \text{Eq.S34}$$

where  $Z_W$  is the is the fugacity capacity of water ( $mol/Pa \cdot m^3$ ) ( $Z_W=1/H$ ).

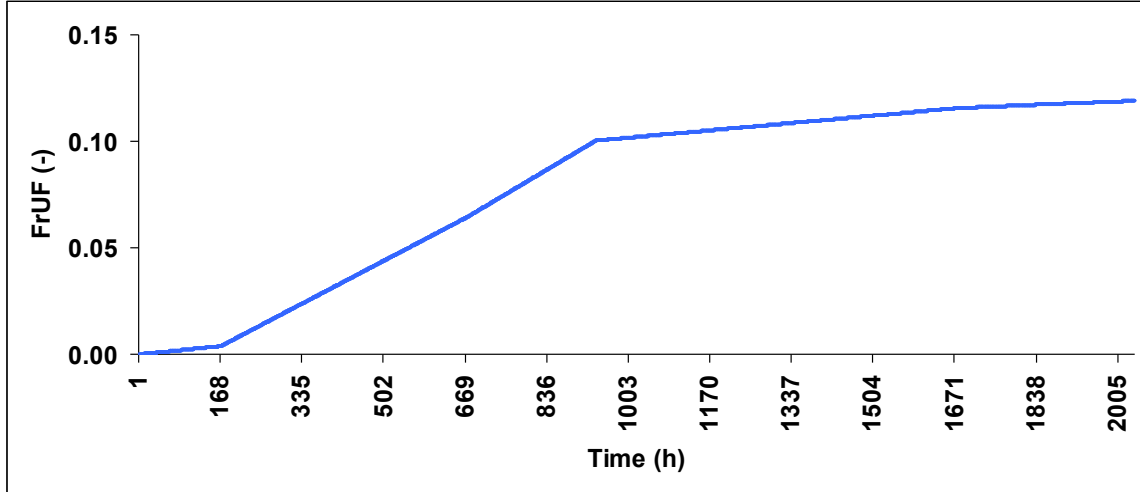


Figure SI-5 Time dependent trend of FrUF during the simulation period (March, 15 – June, 07)

## 6. Wash off: $D_{FS-R}$

The D value for the wash off  $D_{FS-R}$  was calculated as (Cousins and Mackay, 2001):

$$D_{FS-R} = (1 - FrUF) \cdot (D_{AF-R} + D_{AF-Q}) \quad \text{Eq.S35}$$

## 7. Wax erosion: $D_{CUT}$

The D value for the wax erosion  $D_{CUT}$  was calculated as reported in Komprda et al., 2009:

$$D_{CUT} = V_{CUT} \cdot k_{CUT} \cdot Z_F \quad \text{Eq.S36}$$

$V_C$  is the cuticle volume ( $m^3$ ),  $Z_C$  is the cuticle fugacity capacity ( $mol/Pa \cdot m^3$ ) and  $k_{CUT}$  is the cuticle erosion rate constant ( $h^{-1}$ ).

As this process is not well quantified, in this study it was assumed that the cuticle represents the 1% of the total volume of the foliage and that the cuticle erosion rate constant is equal to 0.01, therefore:

$$D_{CUT} = (0.01 \cdot V_F) \cdot k_{CUT} \cdot Z_F \quad \text{Eq.S37}$$

### 8. Litter fall: $D_{FB}$

The D value for litter fall  $D_{FB}$  was calculated as follows (Wania and McLachlan, 2001):

$$D_{FB} = G_{FB} \cdot Z_F \quad \text{Eq.S38}$$

where  $G_{FB}$  is the litter fall rate ( $m^3$  leaves/h).

In the present work the litter fall rate was calculated from the differences in canopy volume between June, 21 (h 4105) and December, 05 (h 8113) resulting in a  $G_{FB}$  of  $0.00095738 m^3$  leaves/h:

$$G_{FB} = \frac{V_{4105} - V_{8113}}{t_{8113} - t_{4105}} \quad \text{Eq.S39}$$

Please note that this process was not considered for model evaluation since the simulation period ended before that litter fall began.

### 9. Leaf growth: $D_{FG}$

D value for leaf growth  $D_{FG}$  is calculated as reported in Cousins and Mackay, 2001:

$$D_{FG} = V_F \cdot k_{FG} \cdot Z_F \quad \text{Eq.S40}$$

where  $k_{FG}$  is the leaf growth rate (1/d).

According to Nizzetto et al., 2007 the rate constant for growth can be calculated as follows:

$$k_{FG} = \frac{dB}{dt} \frac{1}{B} \quad \text{Eq.S41}$$

$$k_{FG} = \frac{dLAI/SLA}{dt} \frac{1}{LAI/SLA} \quad \text{Eq.S42}$$

$$k_{FG} = \frac{B_{n+1}-B_n}{h_{n+1}-h_n} \frac{1}{B_{n+1}} \quad \text{Eq.S43}$$

where  $B_n$  is the foliage biomass ( $\text{g/m}^2$ ) at the hour  $n$  and  $B_{n+1}$  is the foliage biomass ( $\text{g/m}^2$ ) at the hour  $n+1$ , LAI is the Leaf Area Index ( $\text{m}^2/\text{m}^2$ ), SLA is the Specific Leaf Area ( $\text{m}^2/\text{g}$ ).

### 10. Degradation in foliage: $D_{FD}$

D value for degradation in foliage  $D_{FD}$  is calculated as reported in Paterson et al., 1991:

$$D_{FD} = V_F \cdot k_{FD} \cdot Z_F \quad \text{Eq.S44}$$

where  $k_{FD}$  is the first order rate constant (1/h).

Cousins and Mackay, 2001 expected high degradation rates in the canopy, because the leaves try to maximize their exposure to solar radiation. According to this assumption, the main degradation path in the canopy is photolysis. Therefore they assumed that degradation in the canopy can be described using the same rate constant as for degradation in the air.

### 11. Degradation in stem: $D_{StD}$

D value for degradation in stem  $D_{StD}$  is calculated as reported in Paterson et al., 1991.

$$D_{StD} = V_{St} \cdot k_{StD} \cdot Z_{St} \quad \text{Eq.S45}$$

where  $k_{StD}$  is the first order rate constant (1/h). As no value of  $k_{StD}$  was found in the literature, in this work  $k_{StD}$  was assumed to be equal to the degradation rate in soil (first layer).

## 12. Degradation in roots: $D_{RD}$

D value for degradation in roots  $D_{RD}$  is calculated as reported in Paterson et al., 1991.

$$D_{RD} = V_R \cdot k_{RD} \cdot Z_R \quad \text{Eq.S46}$$

where  $k_{RD}$  is the first order rate constant (1/h). As no value of  $k_{RD}$  was found in the literature, in this work  $k_{RD}$  was assumed to be equal to the degradation rate in soil (first layer).

## 13. Soil to roots and root to soil transfer: $D_{SoR}$ and $D_{RSo}$

The D value for exchange between soil and roots was calculated as reported in Paterson et al., 1991:

$$D_{SoR} = \phi \cdot D_X + \frac{D_X}{20} \text{ (xylem flow and diffusion)} \quad \text{Eq.S47}$$

$$D_{RSo} = \frac{D_X}{20} \text{ (diffusion only)} \quad \text{Eq.S48}$$

Where  $\phi$  is a factor that considers the delay caused by a membrane barrier (0.82),  $D_X$  is the D value for the bulk flow in the xylem (mol/Pa·h). The magnitude of the diffusive flow from root to soil is assumed to be 5% of the xylem flow ( $D_X/20$ ).

D value for the bulk flow in the xylem ( $D_X$ ) was defined as:

$$D_X = G_X \cdot Z_W \quad \text{Eq.S49}$$

Where  $Z_W$  is the fugacity capacity of water (mol/Pa·m<sup>3</sup>) and  $G_X$  is the flow rate (m<sup>3</sup>/h) in the xylem.

In the present study  $G_X$  was defined as:

$$G_X = Tr \cdot A_S \cdot LAI \quad \text{Eq.S50}$$

Where  $Tr$  is the transpiration flow rate ( $m^3/h$  per  $m^2$  of foliage).

A transpiration flow rate of  $0.000009 m^3/h$  per  $m^2$  of foliage was used (Tang et al., 2006). As reported in Tang et al., 2006 and Kramer and Boyer, 1995, canopy transpiration varies during the day and during the growing season. Different factors such as solar radiation, vapour pressure deficit of the canopy air and plant species, leaf temperature, wind velocity, leaf area or LAI, root/shoot ratio, leaf size and shape, leaf orientation, leaf surfaces, leaf anatomy influence the transpiration flow rate, but in the present work only the variation with LAI is considered.

#### 14. Roots to stem and stem to roots transfer

The  $D$  value for exchange between roots and stem was calculated as reported in Paterson et al., 1991, considering that chemical transport occurs in association with sap flow in the xylem:

$$D_{RSI} = D_X \quad \text{Eq.S51}$$

The reverse process from stem to roots occurs in the phloem. Flow rate in the phloem  $G_p$  is slow compared to those of the xylem (Windt et al., 2006). In the present work, phloem flow was assumed to be 5% of the xylem flow. Consequently bulk flow in the phloem can be described by  $D$  value as follows (Paterson et al., 1991):

$$D_p = G_p Z_w = \frac{G_x}{20} Z_w \quad \text{Eq.S52}$$

Where  $G_p$  is the flow rate ( $m^3/h$ ) in the phloem.

Therefore  $D$  value for stem to roots transfer results in:

$$D_{RSI} = D_p \quad \text{Eq.S53}$$

## 15. Stem to foliage and foliage to stem transfer

Transfer of chemical between stem and foliage is assumed to take place by means of the xylem and phloem resulting in the following D values (Paterson et al., 1991):

$$D_{St F} = D_X \qquad \text{Eq.S54}$$

$$D_{F St} = D_P \qquad \text{Eq.S55}$$

## SI-2 MASS BALANCE EQUATIONS

The plant model is a dynamic mass balance compartmental model and requires to solve the differential form of three mass balance equations which describe the mass balance of the chemical in each plant compartment (mol/h):

### Roots

$$V_R Z_R df_R / dt = E_R + f_{So} \cdot D_{SoR} + f_{St} \cdot D_{StR} - f_R \cdot (D_{RSO} + D_{RSt} + D_{RD}) \quad \text{Eq.S56}$$

### Stem

$$V_{St} Z_{St} df_{St} / dt = E_{St} + f_R \cdot D_{RSt} + f_F \cdot D_{FSt} - f_{St} \cdot (D_{StR} + D_{StF} + D_{StD}) \quad \text{Eq.S57}$$

### Foliage:

$$V_F Z_F df_F / dt = E_F + f_{LA} \cdot D_{LAF} + f_{St} \cdot D_{StF} - f_F \cdot (D_{FLA} + D_{FSo} + D_{FSt} + D_{FD} + D_{FG}) \quad \text{Eq.S58}$$

Where  $f_R$  is the root fugacity (Pa),  $f_{St}$  is the stem fugacity (Pa).  $f_F$  is the foliage fugacity (Pa),  $V_R$  is the root volume ( $m^3$ ),  $V_{St}$  is the stem volume ( $m^3$ ),  $V_F$  is the foliage volume ( $m^3$ ),  $Z_R$  is the root fugacity capacity ( $mol/Pa \cdot m^3$ ),  $Z_{St}$  is the stem fugacity capacity ( $mol/Pa \cdot m^3$ ),  $Z_F$  is the foliage fugacity capacity ( $mol/Pa \cdot m^3$ ),  $E_R$  is the direct emission in roots (mol),  $E_{St}$  is the direct emission in stem (mol),  $E_F$  is the direct emission in foliage (mol).  $D_{SoR}$  is the soil to roots D value ( $mol/Pa \cdot h$ ),  $D_{StR}$  is the stem to roots D value ( $mol/Pa \cdot h$ ),  $D_{RSO}$  is the roots to soil D value ( $mol/Pa \cdot h$ ),  $D_{RSt}$  is the roots to stem D value ( $mol/Pa \cdot h$ ),  $D_{RD}$  is the root degradation D value ( $mol/Pa \cdot h$ ),  $D_{FSt}$  is the foliage to stem D value ( $mol/Pa \cdot h$ ),  $D_{StF}$  is the stem to foliage D value ( $mol/Pa \cdot h$ ),  $D_{StD}$  is the stem degradation D value ( $mol/Pa \cdot h$ ),  $D_{LAF}$  is the total lower air to foliage D value ( $mol/Pa \cdot h$ ),  $D_{FLA}$  is the foliage to lower air D-value ( $mol/Pa \cdot h$ ),  $D_{FSo}$  is the total foliage to soil/litter D value ( $mol/Pa \cdot h$ ),  $D_{FD}$  is the foliage degradation D-value ( $mol/Pa \cdot h$ ),  $D_{FG}$  is the foliage growth D value ( $mol/Pa \cdot h$ ).

### TEXT SI-3 PHYSICAL-CHEMICAL PROPERTIES OF SELECTED PAHs

Simulations were performed for three chemical of contrasting physical and chemical properties: phenanthrene, pyrene and chrysene (**Table SI-8**).

**Table SI-8 Physical and chemical properties of phenanthrene, pyrene and chrysene**

<b>Properties</b>	<b>Phenanthrene</b>	<b>Pyrene</b>	<b>Chrysene</b>
<b>MW (mg/L)</b>	178.20	202.250	228.3
<b>WS (mg/L)</b>	1.10	0.132	0.002
<b>VP (Pa)</b>	0.02	0.0006	0.000000570
<b>Log K<sub>OW</sub></b>	4.57	5.18	5.86
<b>Log K<sub>OA</sub></b>	7.45	8.61	10.44
<b><math>\Delta H_{VAP}</math> (J/mol)</b>	78.3	89.4	106.2
<b><math>\Delta H_{PA}</math> (J/mol)</b>	78985	111595	153409
<b>HL soil (h)</b>	5500	17000	17000
<b>HL air (h)</b>	55	170	170
<b>HL leaves (h)</b>	as air	as air	as air
<b>HL stem (h)</b>	as soil	as soil	as soil
<b>HL roots (h)</b>	as soil	as soil	as soil

Data from Mackay et al., 1992

$\Delta H_{VAP}$  from Roux et al., 2008

$\Delta H_{PA}$  calculated as reported in Kömp and McLachlan, 1997

LogK<sub>OA</sub> calculated from LogK<sub>OA</sub> and LogK<sub>AW</sub>

## TEXT SI-4 EMISSION SCENARIO FOR THE SoilPlusVeg EVALUATION

PAH atmospheric origin is very different: by-products from incomplete combustion of fossil fuels and wood, residential heating, coke production and vehicular traffic (Morville et al., 2011). Residential heating and vehicular traffic can be considered as a major source of PAHs in Como air (ARPA, 2007), in particular at the suburban site selected for SoilPlusVeg evaluation. In order to perform simulation, chemical emissions in lower air were calibrated to reflect the observed range of variability in measured concentration (Terzaghi et al., 2015) and corrected employing hourly traffic emission factor (**Table SI-9**) reported in Menut et al., 2012 in order to consider a more realistic time profile of traffic emissions. Residential heating was not taken into account for emission correction, since model evaluation was performed for three months (March, 15- June, 7) which could consider mainly a non-heating period (residential heating stopped on April, 15 in Como). PM<sub>10</sub> emission was calibrated in order to match the average weekly concentrations for Como city (ARPA, 2014). Chemical and PM<sub>10</sub> emission trend are shown in **Figure SI-6**.

**Table SI-9 Traffic emission factor (from Menut et al., 2012)**

<b>Hours</b>	<b>Emission factor</b>	<b>Hours</b>	<b>Emission factor</b>
1	0.2	13	1.3
2	0.12	14	1.4
3	0.1	15	1.45
4	0.08	16	1.55
5	0.12	17	2
6	0.23	18	2.1
7	0.9	19	1.7
8	1.7	20	1.1
9	1.8	21	0.7
10	1.5	22	0.6
11	1.25	23	0.55
12	1.2	24	0.4

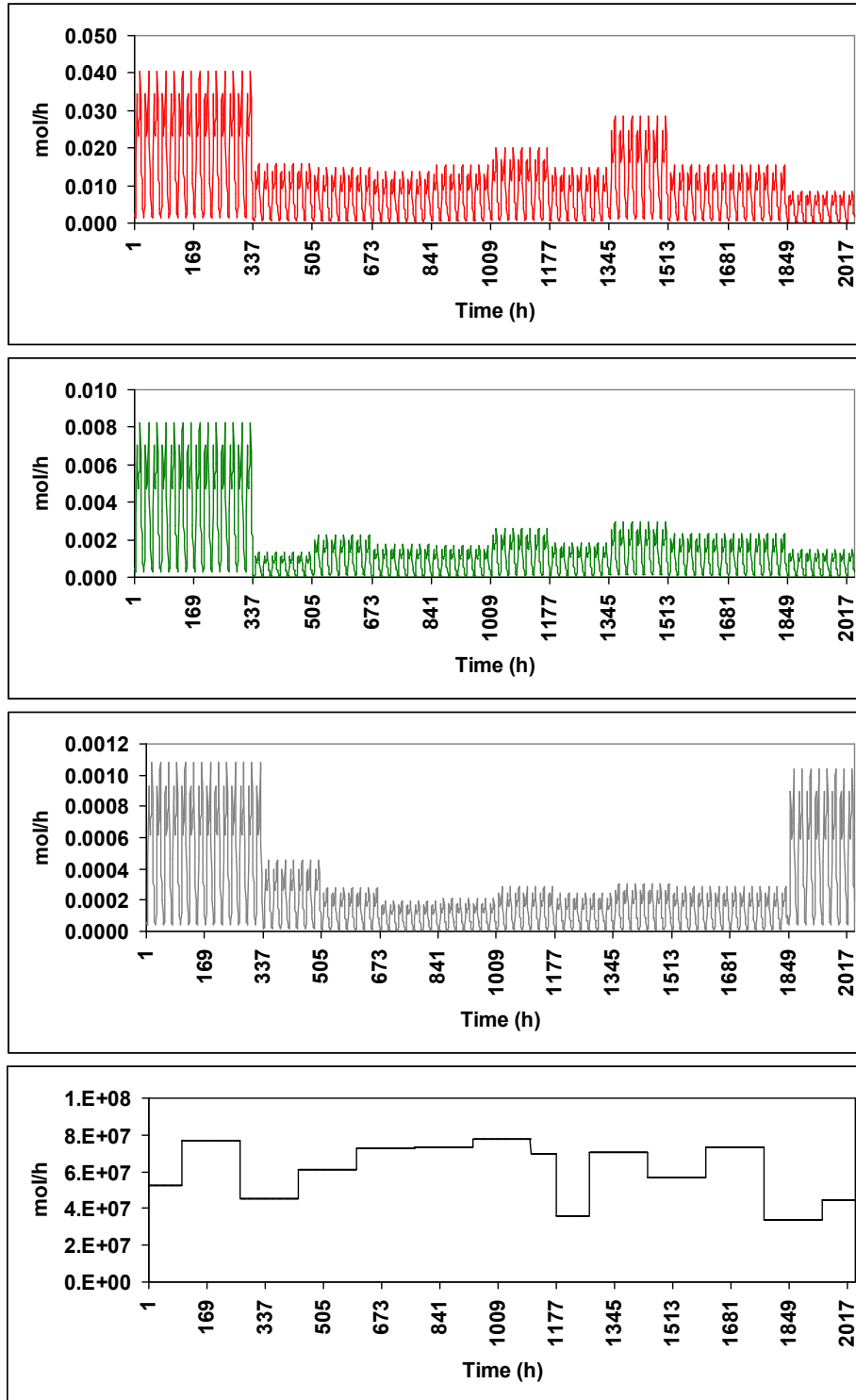


Figure SI-6 Chemical and PM<sub>10</sub> emission trend during the simulation period (March, 15 – June, 07): phenanthrene (in red), pyrene (in green), chrysene (in grey), PM<sub>10</sub> (in black)

## TEXT SI-5 SENSITIVITY ANALYSIS RESULTS

Table SI-10 Results of the sensitivity analysis for the two target parameters (pyrene concentrations in LA, ng/m<sup>3</sup>, and leaves, µg/g d.w.)

Parameters	Conc. LA (ng/m <sup>3</sup> )	Conc. Foliage (µg/g d.w.)
<i>Emission</i>	1.00E+00	1.00E+00
<i>WS</i>	2.76E-04	2.29E-01
<i>VP</i>	0.00E+00	2.29E-01
<i>KOW</i>	5.52E-04	2.71E+00
<i>KOA</i>	2.76E-04	2.27E-01
<i>HLsoil</i>	0.00E+00	6.59E-06
<i>HLair</i>	0.00E+00	5.22E-01
<i>Enth</i>	2.76E-04	8.29E-01
<i>PMback</i>	0.00E+00	3.59E-03
<i>PMem</i>	0.00E+00	4.50E-03
<i>PMDepVel</i>	0.00E+00	2.52E-06
<i>PMDepVelFO</i>	0.00E+00	1.14E-02
<i>LAheight</i>	9.99E-01	9.94E-01
<i>WSpeed</i>	9.99E-01	9.99E-01
<i>AirT</i>	0.00E+00	1.08E+00
<i>Precip</i>	2.76E-04	2.61E-03
<i>LAI</i>	2.76E-04	9.34E-05
<i>SLA</i>	0.00E+00	1.00E+00
<i>DensFO</i>	0.00E+00	1.22E-09
<i>Kpa</i>	2.76E-04	4.77E-01
<i>OCfrSoil</i>	0.00E+00	8.14E-10
<i>OCfrLitter</i>	0.00E+00	1.07E-07
<i>KEA</i>	0.00E+00	0.00E+00
<i>QRain</i>	0.00E+00	9.69E-04
<i>MTC_UA_FA</i>	0.00E+00	0.00E+00
<i>MTC_LA_UA</i>	0.00E+00	1.15E-06
<i>MTC_UA_LA</i>	0.00E+00	1.49E-09
<i>U_Cut</i>	0.00E+00	1.22E-09
<i>U_ABL</i>	2.76E-04	5.08E-01
<i>Kcut</i>	0.00E+00	1.28E-04

All the 30 tested input parameters were reported: emission (mol/h), water solubility (*WS*, g/m<sup>3</sup>), vapour pressure (*VP*, Pa), octanol-water partition coefficient (*K<sub>OW</sub>*), octanol-air partition coefficient (*K<sub>OA</sub>*), half-life in soil (*HLsoil*, d) and air (and foliage, *HLair*, d), enthalpy of phase change between plant and air (*Enth*, J/mol), PM background concentration (*PMback*, µg/m<sup>3</sup>) and emission to LA (*PMem*, µg/h), dry particle deposition velocity to soil (*PMDepVel*, m/h) and foliage (*PMDepVelFO*, m/h), LA height (m) and wind speed (m/s), air temperature (*AirT*, °C), LAI (m<sup>2</sup>/m<sup>2</sup>), SLA (m<sup>2</sup>/g), leaf density (*DensFO*, g/m<sup>3</sup>), plant-air partition coefficient (*K<sub>pa</sub>*, m<sup>3</sup>/g), OC fraction in soil (*OCfrSoil*) and litter (*OCfrLitter*), air-side volatilization MTC (*KEA*, m/h), scavenging ratio for rain (*QRain*), MTCs for transfer to free atmosphere (*MTC\_UA\_FA*, m/h), from LA to UA (*MTC\_LA\_UA*, m/h) and from UA to LA (*MTC\_UA\_LA*, m/h), MTCs for transport through leaf cuticle (*U\_Cut*, m/h) and across the air-boundary layer (*U\_ABL*, m/h), and cuticle erosion rate constant (*Kcut*, 1/h).

# TEXT SI-6 MODEL EVALUATION RESULTS

## SI-6A) Concentrations

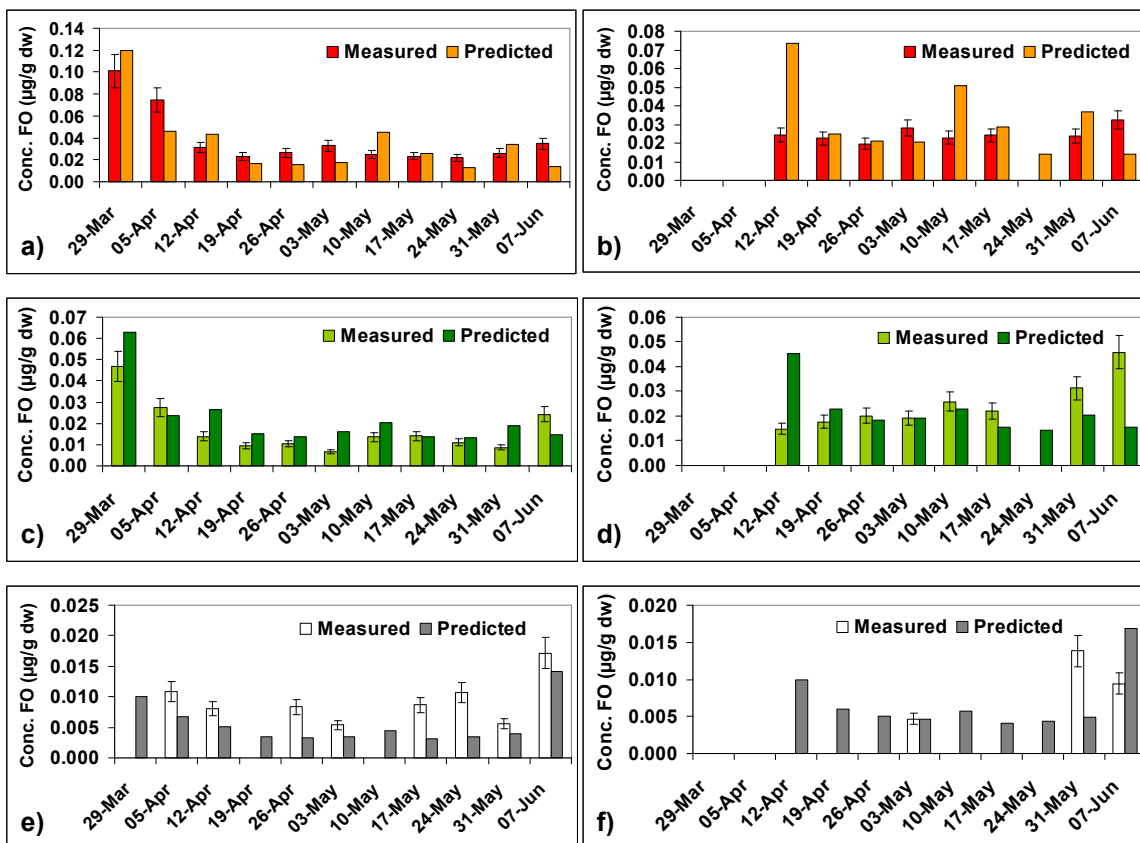


Figure SI-7 - Comparison between predicted and measured concentrations (µg/g dw) in leaves of cornel (a,c,e) and maple (b,d,f) of phenanthrene (red and orange), pyrene (light green and dark green) and chr (white and grey) during the hour of sampling (h 11). Bars represent the analytical error assumed equal to 15%.

### SI-6B) Efficiency factors

The use of efficiency factor (EF) (Mayer and Buttler, 1993) is a way to quantify the adequacy of model predictions compared to experimental observations. Good model performances are obtained when EF ranges from 0 to 1. The calculated EFs for the SoilPlusVeg model, considering leaf concentrations, are reported in **Table SI-11**.

**Table SI-11 – Efficiency factors for leaf concentration prediction**

<b>Chemical</b>	<b>Cornel</b>	<b>Maple</b>
<b>Phenanthrene</b>	0.58	-33.66
<b>Pyrene</b>	0.42	-1.96
<b>Chysene</b>	-0.50	-2.33

## SI-5C) Fluxes

Table SI-12 Input/Output fluxes to/from leaves of phenanthrene, pyrene and chrysene

Phenanthrene Fluxes (mol/h)				
Fluxes	Min	Max	Mean	Median
<b>N_Abs</b>	2.43E-09	1.50E-04	6.98E-06	1.75E-06
N_DryPart	1.45E-11	2.43E-06	9.09E-08	7.43E-09
N_WetPart	1.03E-10	3.08E-06	6.97E-08	8.95E-09
N_RainDiss	1.93E-10	1.16E-06	5.15E-08	1.24E-08
<b>N_Vol</b>	2.60E-11	2.25E-05	4.52E-06	3.75E-06
N_WashOff	2.40E-09	9.67E-07	6.76E-08	2.04E-08
N_WaxEr	2.43E-15	6.72E-10	1.84E-10	1.64E-10
N_LitterFall	0.00E+00	0.00E+00	0.00E+00	0.00E+00
N_FO_St	3.56E-15	2.02E-09	3.88E-10	3.12E-10
N_St_FO	9.36E-23	1.66E-10	7.49E-11	7.48E-11
<b>N_Dr</b>	3.06E-11	8.47E-06	2.32E-06	2.06E-06
Pyrene Fluxes (mol/h)				
Fluxes	Min	Max	Mean	Median
<b>N_Abs</b>	4.22E-10	1.66E-05	8.12E-07	2.20E-07
N_DryPart	2.35E-11	2.13E-06	8.37E-08	7.75E-09
N_WetPart	1.23E-10	3.73E-06	8.29E-08	9.85E-09
N_RainDiss	9.86E-11	6.04E-07	2.64E-08	6.22E-09
<b>N_Vol</b>	8.14E-13	3.23E-06	4.93E-07	3.61E-07
N_WashOff	7.44E-10	1.24E-06	4.15E-08	1.15E-08
N_WaxEr	4.66E-16	1.85E-10	8.20E-11	8.51E-11
N_LitterFall	0.00E+00	0.00E+00	0.00E+00	0.00E+00
N_FO_St	3.92E-16	9.71E-10	1.46E-10	1.02E-10
N_St_FO	1.28E-23	7.74E-11	3.27E-11	3.20E-11
<b>N_Dr</b>	1.90E-12	7.56E-07	3.34E-07	3.47E-07
Chrysene Fluxes (mol/h)				
Fluxes	Min	Max	Mean	Median
N_Abs	1.03E-11	1.93E-06	3.83E-08	1.14E-08
N_DryPart	3.12E-11	5.07E-06	7.90E-08	1.28E-08
N_WetPart	2.07E-10	1.20E-05	2.14E-07	3.61E-08
N_RainDiss	8.21E-11	9.83E-07	3.75E-08	8.24E-09
N_Vol	4.84E-15	1.56E-07	1.21E-08	5.49E-09
N_WashOff	9.10E-11	2.16E-06	3.55E-08	5.76E-09
N_WaxEr	4.14E-17	9.99E-11	1.80E-11	1.63E-11
N_LitterFall	0.00E+00	0.00E+00	0.00E+00	0.00E+00
N_FO_St	3.29E-17	6.77E-10	4.93E-11	2.22E-11
N_St_FO	1.95E-24	4.25E-11	1.49E-11	1.52E-11
<b>N_Dr</b>	1.69E-13	4.07E-07	7.33E-08	6.64E-08

### SI-6D) Short term variability

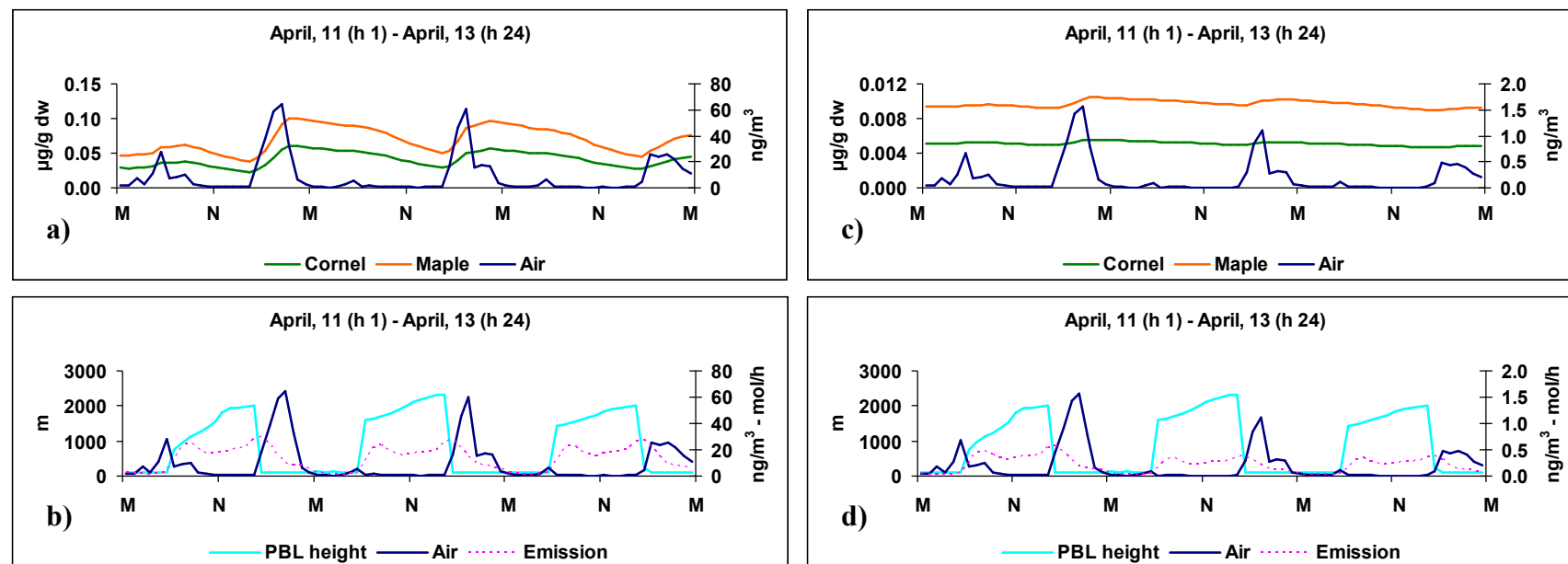


Figure SI-8 Trend of concentration in leaves of cornel (solid green line) and maple (solid orange line) and in air (solid blue line), emission (dotted pink line) and PBL height (solid light blue line), during a three-day period (April, 11 – April, 13): phenanthrene (a,b) and chrysene (c,d). Please note that for illustration purposes emission values was multiplied for a factor of 2000. “M” means midnight while “N” stands for noon.

Table SI-13- Hourly values (of April, 11 and April, 12) of absorption and volatilization fluxes (N\_Abs and N\_Vol, mol/h), temperature (T, °C), PBL height (PBL, m), emission (mol/h) and air (ConcLA, ng/m<sup>3</sup>) and leaf concentrations (ConcFO C, cornel and ConcFO M, maple, µg/g dw) for phenanthrene. Hours during which Nabs>Nvol are shown in green, while those during which Nvol>Nabs are shown in light blue.

Day	Hour	N_Abs	N_Vol	Δ%	N	T	PBL	Emission	ConLA	ConcFo	ConcFo
11-Apr	1	1.71E-06	1.49E-06	13	10	100	1.42E-03	1.63	0.0288	0.0466	
	2	1.47E-06	1.35E-06	8	10	100	8.50E-04	7.60	0.0284	0.0461	
	3	6.89E-06	1.30E-06	81	9	100	7.08E-04	3.04	0.0292	0.0475	
	4	2.76E-06	1.22E-06	56	9	100	5.66E-04	10.92	0.0292	0.0475	
	5	9.93E-06	1.29E-06	87	9	100	8.50E-04	27.79	0.0307	0.0500	
	6	2.53E-05	1.51E-06	94	9	100	1.63E-03	7.41	0.0354	0.0578	
	7	6.93E-06	1.75E-06	75	10	737	6.37E-03	8.67	0.0360	0.0589	
	8	8.14E-06	2.49E-06	69	13	948	1.20E-02	10.29	0.0368	0.0602	
	9	9.68E-06	4.08E-06	58	17	1112	1.27E-02	2.85	0.0375	0.0615	
	10	2.69E-06	6.57E-06	-144	21	1230	1.06E-02	1.71	0.0361	0.0593	
	11	1.61E-06	7.98E-06	-395	24	1352	8.85E-03	1.19	0.0341	0.0561	
	12	1.12E-06	9.79E-06	-772	26	1544	8.50E-03	0.74	0.0316	0.0520	
	13	7.05E-07	7.57E-06	-973	24	1811	9.20E-03	0.70	0.0296	0.0488	
	14	6.67E-07	7.31E-06	-995	25	1929	9.91E-03	0.72	0.0276	0.0456	
	15	6.85E-07	7.34E-06	-972	25	1947	1.03E-02	1.08	0.0257	0.0425	
	16	1.03E-06	6.53E-06	-536	25	1967	1.10E-02	1.23	0.0241	0.0398	
	17	1.18E-06	4.95E-06	-320	23	1997	1.42E-02	18.30	0.0228	0.0379	
	18	1.71E-05	4.35E-06	75	21	117	1.49E-02	37.79	0.0255	0.0423	
	19	3.53E-05	4.03E-06	89	18	100	1.20E-02	59.22	0.0322	0.0535	
	20	5.54E-05	4.82E-06	91	17	100	7.79E-03	64.54	0.0431	0.0717	
	21	6.05E-05	4.97E-06	92	15	100	4.96E-03	32.32	0.0550	0.0917	
	22	3.04E-05	4.39E-06	86	13	100	4.25E-03	6.51	0.0604	0.1009	
	23	6.13E-06	3.80E-06	38	12	100	3.89E-03	2.40	0.0601	0.1005	
	24	2.27E-06	3.40E-06	-50	11	119	2.83E-03	0.79	0.0590	0.0989	
12-Apr	1	7.52E-07	3.10E-06	-313	10	142	1.30E-03	0.80	0.0577	0.0967	
	2	7.55E-07	2.86E-06	-280	10	108	7.78E-04	0.39	0.0564	0.0947	
	3	3.78E-07	2.67E-06	-608	9	142	6.48E-04	0.62	0.0551	0.0926	
	4	5.93E-07	2.50E-06	-321	9	100	5.18E-04	2.47	0.0539	0.0907	
	5	2.35E-06	2.46E-06	-5	9	100	7.78E-04	5.22	0.0531	0.0895	
	6	4.99E-06	2.37E-06	52	9	100	1.49E-03	0.46	0.0529	0.0893	
	7	4.56E-07	2.68E-06	-488	10	1593	5.83E-03	1.71	0.0516	0.0873	
	8	1.69E-06	3.56E-06	-111	13	1624	1.10E-02	1.06	0.0505	0.0855	
	9	1.05E-06	5.34E-06	-410	16	1688	1.17E-02	0.74	0.0488	0.0828	
	10	7.35E-07	8.60E-06	-1070	21	1781	9.72E-03	0.59	0.0464	0.0787	
	11	5.82E-07	1.10E-05	-1797	24	1873	8.10E-03	0.57	0.0434	0.0738	
	12	5.63E-07	1.23E-05	-2080	26	1986	7.78E-03	0.54	0.0401	0.0683	
	13	5.39E-07	8.93E-06	-1556	23	2112	8.42E-03	0.40	0.0377	0.0643	
	14	3.97E-07	9.12E-06	-2198	24	2189	9.07E-03	0.46	0.0352	0.0601	
	15	4.62E-07	8.28E-06	-1691	24	2263	9.40E-03	0.47	0.0330	0.0564	
	16	4.73E-07	7.31E-06	-1446	23	2308	1.00E-02	0.86	0.0310	0.0531	
	17	8.61E-07	6.03E-06	-601	22	2330	1.30E-02	16.59	0.0295	0.0505	
	18	1.63E-05	4.91E-06	70	19	118	1.36E-02	45.63	0.0315	0.0541	
	19	4.48E-05	5.40E-06	88	18	100	1.10E-02	60.28	0.0396	0.0681	
	20	5.93E-05	5.97E-06	90	17	100	7.13E-03	15.25	0.0505	0.0870	
	21	1.50E-05	4.86E-06	68	15	100	4.54E-03	17.64	0.0522	0.0900	
	22	1.74E-05	4.41E-06	75	14	100	3.89E-03	16.17	0.0543	0.0937	
	23	1.60E-05	4.11E-06	74	13	100	3.56E-03	3.39	0.0561	0.0969	
	24	3.36E-06	3.83E-06	-14	12	100	2.59E-03	2.13	0.0552	0.0955	

Table SI-14- Hourly values (of April, 11 and April, 12) of absorption and volatilization fluxes (N\_Abs and N\_Vol, mol/h), temperature (T, °C), PBL height (PBL, m), emission (mol/h) and air (ConcLA, ng/m<sup>3</sup>) and leaf concentrations (ConcFO C, cornel and ConcFO M, maple, µg/g dw) for chrysene. Hours during which Nabs>Nvol are shown in green, while those during which Nvol>Nabs are shown in light blue.

Day	Hour	N_Abs	N_Vol	Δ%	N	T	PBL	Emisison	ConLA	ConcFo	ConcFo
11-Apr	1	4.04E-09	1.64E-09	59	10	100	9.41E-03	3.71	0.0052	0.0094	
	2	3.48E-09	1.39E-09	60	10	100	9.38E-03	2.58	0.0051	0.0094	
	3	1.63E-08	1.21E-09	93	9	100	9.38E-03	0.46	0.0051	0.0094	
	4	6.52E-09	1.08E-09	84	9	100	9.36E-03	0.92	0.0051	0.0094	
	5	2.35E-08	1.08E-09	95	9	100	9.39E-03	0.38	0.0051	0.0094	
	6	5.99E-08	1.12E-09	98	9	100	9.53E-03	0.28	0.0052	0.0095	
	7	5.21E-08	1.45E-09	97	10	737	9.54E-03	0.58	0.0052	0.0095	
	8	6.63E-08	2.76E-09	96	13	948	9.57E-03	0.72	0.0052	0.0096	
	9	8.25E-08	6.92E-09	92	17	1112	9.61E-03	0.55	0.0052	0.0096	
	10	2.35E-08	1.87E-08	20	21	1230	9.58E-03	1.50	0.0052	0.0096	
	11	1.44E-08	3.03E-08	-110	24	1352	9.53E-03	1.90	0.0051	0.0095	
	12	1.03E-08	5.17E-08	-401	26	1544	9.47E-03	2.30	0.0051	0.0095	
	13	6.69E-09	3.54E-08	-429	24	1811	9.41E-03	3.39	0.0051	0.0094	
	14	6.40E-09	3.74E-08	-485	25	1929	9.35E-03	3.63	0.0050	0.0093	
	15	6.58E-09	4.30E-08	-554	25	1947	9.28E-03	3.63	0.0050	0.0093	
	16	9.88E-09	3.85E-08	-290	25	1967	9.23E-03	2.57	0.0049	0.0092	
	17	1.14E-08	2.47E-08	-117	23	1997	9.18E-03	2.85	0.0049	0.0092	
	18	4.57E-08	1.56E-08	66	21	117	9.26E-03	3.43	0.0049	0.0093	
	19	8.36E-08	8.73E-09	90	18	100	9.48E-03	1.57	0.0051	0.0095	
	20	1.31E-07	7.29E-09	94	17	100	9.84E-03	0.65	0.0052	0.0098	
	21	1.43E-07	4.99E-09	97	15	100	1.02E-02	0.37	0.0055	0.0102	
	22	7.18E-08	3.32E-09	95	13	100	1.04E-02	0.65	0.0055	0.0104	
	23	1.45E-08	2.53E-09	83	12	100	1.04E-02	2.96	0.0055	0.0104	
	24	6.14E-09	2.10E-09	66	11	119	1.04E-02	4.91	0.0055	0.0104	
12-Apr	1	1.76E-09	1.82E-09	-4	10	142	1.04E-02	5.74	0.0055	0.0104	
	2	1.44E-09	1.62E-09	-12	10	108	1.03E-02	4.49	0.0055	0.0103	
	3	8.82E-10	1.47E-09	-67	9	142	1.03E-02	5.75	0.0054	0.0103	
	4	1.06E-09	1.34E-09	-25	9	100	1.02E-02	4.13	0.0054	0.0102	
	5	4.23E-09	1.33E-09	68	9	100	1.02E-02	1.56	0.0054	0.0102	
	6	8.99E-09	1.24E-09	86	9	100	1.02E-02	1.41	0.0053	0.0102	
	7	3.22E-09	1.63E-09	49	10	1593	1.01E-02	3.91	0.0053	0.0101	
	8	1.19E-08	2.95E-09	75	13	1624	1.01E-02	1.96	0.0053	0.0101	
	9	7.48E-09	6.86E-09	8	16	1688	1.00E-02	3.22	0.0052	0.0100	
	10	5.29E-09	1.89E-08	-257	21	1781	9.98E-03	3.64	0.0052	0.0100	
	11	4.23E-09	3.47E-08	-720	24	1873	9.91E-03	3.65	0.0052	0.0099	
	12	4.14E-09	4.91E-08	-1087	26	1986	9.84E-03	3.42	0.0051	0.0098	
	13	4.00E-09	2.96E-08	-640	23	2112	9.78E-03	3.65	0.0051	0.0098	
	14	2.96E-09	3.48E-08	-1076	24	2189	9.71E-03	5.16	0.0050	0.0097	
	15	3.47E-09	3.25E-08	-837	24	2263	9.65E-03	4.45	0.0050	0.0096	
	16	3.56E-09	2.85E-08	-701	23	2308	9.59E-03	4.57	0.0050	0.0096	
	17	6.49E-09	2.15E-08	-232	22	2330	9.53E-03	3.21	0.0049	0.0095	
	18	3.34E-08	1.27E-08	62	19	118	9.57E-03	3.44	0.0049	0.0096	
	19	8.08E-08	9.98E-09	88	18	100	9.77E-03	1.19	0.0050	0.0098	
	20	1.07E-07	7.73E-09	93	17	100	1.01E-02	0.58	0.0052	0.0101	
	21	2.71E-08	4.88E-09	82	15	100	1.01E-02	1.47	0.0052	0.0101	
	22	3.14E-08	3.75E-09	88	14	100	1.01E-02	1.09	0.0052	0.0101	
	23	2.88E-08	3.08E-09	89	13	100	1.02E-02	1.09	0.0052	0.0102	
	24	6.06E-09	2.74E-09	55	12	100	1.02E-02	3.78	0.0052	0.0102	

**Text SI-7 PHYSICAL-CHEMICAL PROPERTIES OF SELECTED PCBs**

**Table SI-15 Physical and chemical properties of**

<b>Properties</b>	<b>PCB 52</b>	<b>PCB 153</b>
<b>MW (mg/L)</b>	291.99	360.88
<b>WS (mg/L)</b>	0.03	0.001
<b>VP (Pa)</b>	0.0049	0.000119
<b>Log K<sub>OW</sub></b>	6.10	6.90
<b>Log K<sub>OA</sub></b>	7.81	8.66
<b>ΔH<sub>VAP</sub> (J/mol)</b>	80800	91400
<b>ΔH<sub>PA</sub>* (J/mol)</b>	86600	116700
<b>HL soil (h)</b>	55000	5500
<b>HL air (h)</b>	1700	550
<b>HL leaves (h)</b>	as air	as air
<b>HL stem (h)</b>	as soil	as soil
<b>HL roots (h)</b>	as soil	as soil

Data from Mackay et al., 1992

ΔH<sub>VAP</sub> and ΔH<sub>PA</sub> calculated as reported in Kömp and McLachlan, 1997

LogK<sub>OA</sub> calculated from LogK<sub>OA</sub> and LogK<sub>AW</sub>

## REFERENCES

- ARPA, 2007. Rapporto sulla qualità dell' aria di Como e provincia.
- ARPA, 2014. Regional Environmental Protection Agency official web site: [http://ita.arpalombardia.it/ITA/qaria/doc\\_RichiestaDati.asp](http://ita.arpalombardia.it/ITA/qaria/doc_RichiestaDati.asp). Last access on April, 2014.
- Briggs G. G., Bromilow R. H., Evans A. A. and Williams M. Relationship between lipophilicity and the distribution of non-ionised chemicals in barley shoots following uptake by roots. *Pesticide Science* (1983), 14: 492-500.
- Briggs G.G., Bromilow R.H. and Evans A.A. Relationship between lipophilicity and root uptake and translocation of non-ionized chemicals by barley. *Pesticide Science* (1982), 13: 495-504.
- Calamari D., Vighi M. and Bacci E., 1987. The use of terrestrial plant biomass as a parameter in the fugacity model. *Chemosphere* (1987), 16: 2359-2364.
- Castro-Diez P., Puyravaud J.P. and Cornelissens J.H.C. Leaf structure and anatomy as related to leaf mass per area variation in seedlings of a wide range of woody plant species and types. *Oecologia* (2008), 124: 476-486.
- Comas L.H. and Eissnstat D.M. Linking fine root traits to maximum potential growth rate among 11 mature temperate tree species. *Functional Ecology* (2004), 18: 388-397.
- Cousin I.T. and Mackay D. Strategies for including vegetation compartments in multimedia models. *Chemosphere* (2001), 44: 643-654.
- Cousins I.T. and Mackay D., 2000. Transport parameters and mass balance equation for vegetation in a Level III fugacity model. Report.
- Gabauer T., Horna V. and Lauschner C. Variability in radial sap flux density patterns and sapwood area among seven co-occurring temperate broad-leaved tree species. *Tree Physiology* (2008), 28: 1821–1830.

- Gale, M. R., and D. F. Grigal. 1987. Vertical root distribution of northern tree species in relation to successional status. *Canadian Journal of Forest Research*, (1987), 17: 829-834.
- Jackson R.B., Mooney H.A., and Schulze E.D. A global budget for fine root biomass, surface area and nutrient contents. *Proceedings of the National Academic of Sciences* (1997), 94: 7362-7366.
- Jackson, R. B., J. Canadell, J. R. Ehleringer, H. A. Mooney, O. E. Sala, and E. D. Schulze. A global analysis of root distributions for terrestrial biomes. *Oecologia* (1996), 108: 389-411
- Kömp P. and McLachlan M. Influence of Temperature on the Plant/Air Partitioning of Semivolatile Organic Compounds. *Environmental Science & Technology* (1997), 31: 886-890.
- Komprda J., Kubosova K., Dvorska A., Scheringer M., Klanova J. and Holoubek I. Application of an unsteady state environmental distribution model to a decal time series of PAHs concentrations in Central Europe. *Journal of Environmental Monitoring* (2009), 11: 269-276.
- Kramer Paul J. and Boyer John S. (1995). Water relations of plant and soil. Elsevier Science (USA).
- Mackay D., Shiu W.Y., Ma K.C., 1992. Illustrated handbook of physical-chemical properties and environmental fate for organic chemicals. Lewis Publisher, Chelsea, USA.
- Mayer D.G. and Buttler D.G. Statistical validation. *Ecological modelling* (1993), 68: 21 -32.
- Menut, L., Goussebaile, A., Bessagnet, B., Khvorostiyarov, D.; Ung, A. Impact of realistic hourly emissions profiles on air pollutant concentrations modelled with CHIMERE. *Atmospheric Environment* (2012), 49, 233-244-
- Morville S, Delhomme O, Millet M. Seasonal and diurnal variations of atmospheric PAH concentrations between rural, suburban and urban areas. *Atmospheric Pollution Research* (2011), 2: 363-373.
- Nizzetto, L., Pastore, C., Liu, X., Camporini, P., Sroppiana, D., Herbert, B., Boschetti, M., Zhang, G., Brivio, P. A., Jones, K. C., Di Guardo, A. Accumulation parameters and seasonal

trends for PCBs in temperate and boreal forest plant species. *Environmental Science & Technology* (2008), 42: 5911–5916.

- Paterson S., Mackay D. and Gladman A. A fugacity model of chemical uptake by plants from soil and air. *Chemosphere* (1991), 23: 539-565,
- Riederer M. 1995. In *Plant contamination: modeling and simulation of organic chemical processes*. Lewis publishers, Boca Raton, FL.
- Roux M. V., Temprado M., Chickos J.S., Nagano Y. Critically evaluated thermochemical properties of polycyclic aromatic hydrocarbons. *Journal of Physical and Chemical Reference Data*, (2008), 37: 1855 – 1996.
- Tang J., Bolstad P.V., Ewers B.E., Desai A. R., Davis K. J. and Carey E.V. Sap flux-upscaled canopy transpiration, stomatal conductance and water use efficiency in a old growth forest in the Great Lakes region of United States. *Journal of Geophysical research* (2006), 11: 1-12.
- Terzaghi E., Zacchello G., Scacchi M., Raspa G., Jones K.C., Cerabolini B., Di Guardo A. Towards more ecologically realistic scenarios of plant uptake modelling for chemicals: PAHs in a small forest. *Science of the Total Environment* (2015), 505: 329-337.
- Trapp S. 1995. In *Plant contamination: modeling and simulation of organic chemical processes*. Lewis publishers, Boca Raton, FL.
- Wania F. and McLachlan M. Estimating the influence of forest on the overall fate of SOCs using a multimedia fate model. *Environmental Science & Technology* (2001), 35: 582-590.
- Windt C.W., Vergeldt F.J., De Jager P.A. and Van As H. MRI of long-distance water transport: a comparison of the phloem and xylem flow characteristics and dynamics in poplar, castor bean, tomato and tobacco. *Plant, Cell and Environment* (2006), 29: 1715-1729.